

APPLICATIONS OF CO₂ IN HOMOGENEOUS CATALYSIS

Philip G. Jessop

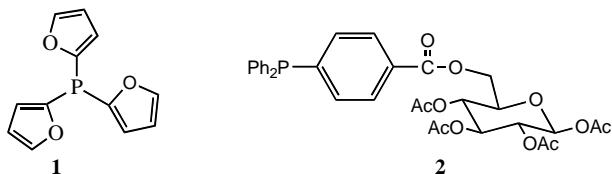
Department of Chemistry, Queen's University, Kingston, ON, Canada

Introduction

Carbon dioxide can serve as a solvent for homogeneous catalysis but it is capable of much more. Over the past 4 years, we and others have shown that it can be used as an extractant for the removal of products from ionic or polymeric liquid solvents after homogeneous catalysis, as a modifier of liquid phase solvent properties, as an agent for accelerating solventless reactions of some solids, and as a trigger for partitioning and miscibility changes. All of these capabilities of CO₂ can be used to modify the selectivity, increase the turnover frequency, or achieve the recycling of homogeneous catalysts. In addition, of course, CO₂ can serve as a reagent. Our recent results in these areas will be presented.

Homogeneous Catalysis in Supercritical CO₂

Homogeneous catalysis has been performed in supercritical CO₂ (scCO₂)¹ since Kramer and Leder's isomerization experiments in the 1970's,² although most work in this area has been done since the mid 1990's.³ Examples of increased rates^{4,5} or selectivities⁶ compared to those in liquid solvents have been observed. In many cases, catalyst solubility in scCO₂ was found to be insufficient, especially when triarylphosphine ligands were employed. This problem has been addressed by switching to trialkylphosphines⁴ or by putting fluorinated groups on the meta or para positions of the triarylphosphines.⁷ New data, obtained in collaboration with Beckman's group, will be presented showing that incorporation of ether or ester groups into the phosphines increases the solubility of the ligand in scCO₂. Solubility data comparing PPh₃ with electronically similar ligands containing heteroaromatic rings (e.g. structure **1**) or ester-containing substituents (e.g. structure **2**) will be presented.⁸ On a weight fraction basis, both are significantly more soluble than PPh₃, while on a mole fraction basis ligand **1** has by far the greater solubility.



Biphasic Catalysis

Homogeneous catalysts are too expensive and often too toxic to be allowed to be lost in the product stream. Traditional methods for recovering the catalyst usually involve destroying the catalyst, but newer techniques including biphasic catalysis make it possible to recover the catalyst without damage. Biphasic catalysis involves two mutually immiscible fluids and relies on the catalyst partitioning exclusively into one phase (the catalyst-bearing phase) while the product partitions primarily into the other phase. Many systems of this type suffer from nonexclusive partitioning of the catalyst, leading to catalyst losses, and partial miscibility of the two fluid phases, leading to loss of one solvent in the other.

CO₂/Ionic Liquid Mixtures. Blanchard et al.⁹ showed that a common ionic liquid, N,N-butylmethylimidazolium hexafluorophosphate ([bmim]PF₆) is completely insoluble in scCO₂. The Jessop group showed that this fact, combined with the

observation that heavy aromatic compounds (in analogy to asymmetric ligands of the BINAP type) partition essentially exclusively into the ionic liquid (IL) phase rather than the scCO₂ phase. This was the basis for a catalyst successful recycling scheme,¹⁰ in which homogeneous catalysis was performed in an IL following which product was extracted by scCO₂, leaving behind a reusable catalyst solution in IL. The product could thus be obtained free of solvent or catalyst.

CO₂/Liquid Polymer Mixtures. The excellent performance of the CO₂/IL biphasic catalysis method encouraged further research in this area in the Jessop group, but it became obvious that the method could be improved by finding a cheaper replacement for the IL. The ideal replacement would be cheaper, halide-free and entirely nontoxic. PEG (poly(ethylene glycol)) was chosen, even though at room temperature it is a solid. PEG is nontoxic, very inexpensive, and able to dissolve catalyst precursors and organic substrates. The solubility of PEG in scCO₂ is very low, especially at molecular weights over 1000 g/mol. The fact that it is a solid at room temperature is less problematic than it sounds because a) the melting point is only 20-40°C above room temperature, and b) the melting point of PEG is significantly lower in the presence of scCO₂. Early tests with a simple homogeneous hydrogenation showed that biphasic catalysis could be performed in the PEG/scCO₂ mixture, that the product could be easily extracted by the scCO₂, and that the catalyst solution could then be recycled multiple times.¹¹

Continued work in this area involves the evaluation of several possible liquid polymers and other nonvolatile solvents. Some, such as glycerol and polyols, have been rejected because they are incapable of dissolving catalyst precursors and substrates. Others such as poly(dimethylsiloxane) and eicosane have been rejected because they are too soluble in scCO₂. Liquids that are currently being considered are shown in Figure 1. Their polarities are illustrated in Figure 2.

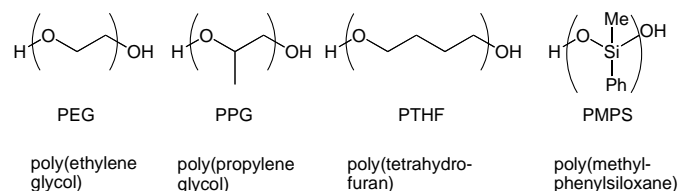


Figure 1. The structures of liquid polymers being considered as potential solvents for biphasic homogeneous catalysis.

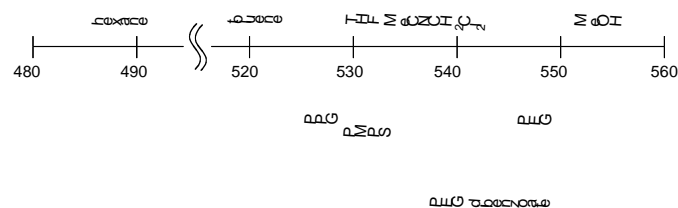


Figure 2. The polarity of liquid polymers compared to traditional liquid solvents, shown on a scale of Nile Red absorption maxima.

Obedient Catalysts and Solvents

Bergbreiter¹² introduced the idea of “smart” ligands or catalysts, meaning ligands or catalysts that change their nature or solubility when circumstances require it, without need for a signal from the human operator. In his work, the ligands formed complexes that had lower solubility at higher temperatures, so that if an exothermic reaction got carried away and the temperature rose as a result, the catalyst would automatically precipitate and thereby slow down the reaction.

In a collaboration between the Jessop group and the Eckert and Liotta groups at Georgia Tech., we have been exploring the possibility of designing “obedient” ligands and solvents, which reversibly change their nature upon receiving a signal or input from the human operator. For example, cyclohexane is fluorophobic (meaning that it can not dissolve highly fluorinated compounds) but cyclohexane with CO₂ dissolved therein (at >30 bar CO₂) is fluorophilic and therefore capable of dissolving fluorinated compounds¹³ or being miscible with fluorinated liquids.¹⁴ Thus cyclohexane is a very simple example of an obedient solvent with CO₂ dissolution as the trigger for the change. This fact was used as the basis for a method that causes an “obedient” catalyst to switch back and forth between being homogeneous and being heterogeneous. Powdered fluorosilica with a highly fluorinated catalyst precursor complex adsorbed on its surface is placed in a solution of substrate in cyclohexane. Dissolution of CO₂ into the cyclohexane triggers the extraction into solution of the catalyst from the silica, thereby allowing homogeneous catalysis to take place. After the reaction, the CO₂ pressure is released, triggering the redeposition of the catalyst back onto the silica, so that the catalyst becomes heterogeneous for the purposes of catalyst/product separation.

CO₂ as a Reagent or Substrate

Research by many groups has been directed at increasing the rate of reactions of CO₂ and increasing the range of reactions in which CO₂ acts as a reagent or substrate. Recent results in the Jessop group include the development of a facile method for combinatorial catalyst discovery for CO₂ fixation at high pressure,¹⁵ and new or improved syntheses of formic acid,¹⁵⁻¹⁸ formanilide,¹⁹ carbanilide,¹⁹ tetraalkylureas,²⁰ and carboxylic acids (in progress).

CO₂ in Other Roles

Carbon dioxide can assist homogeneous catalysis in many other ways. CO₂ dissolved in organic solvents lowers the melting point, viscosity, and polarity of the liquid phase and increases mass transfer rates and the solubility of reagent gases. These changes can directly affect rates and selectivities of catalysis.^{16,21-26}

Carbon dioxide can also be used to accelerate solventless reactions of some solids,²⁷ by taking advantage of the melting-point lowering that occurs in the presence of CO₂. In a similar manner, the final yields of some reactions can be increased.

Carbon dioxide can also serve as an in-situ temporary protecting group, as reported by Leitner.²⁸

Concluding Remarks

Although it is considered a waste material, CO₂ can be useful for the promotion of homogeneous catalysis in a wide variety of ways, not all of which have been presented here. In similar ways, CO₂ can promote other kinds of reactions; research in other groups continues along those lines. While it is not claimed that use of CO₂ in this manner will have any significant effect on the global warming problem, it is precisely the fact that CO₂ is a waste product that makes it inexpensive enough to be considered for some of these roles.

Acknowledgement. The author acknowledges the great assistance of his students, postdoctoral fellows, and collaborators (whose names appear in the references) and support from the Division of Chemical Sciences, Office of Basic Energy Sciences, U. S. Department of Energy (grant number DE-FG02-99ER14986) and from the Natural Sciences and Engineering Research Council, Canada. The author, Canada Research Chair in Green Chemistry, also acknowledges the support of the Canada Research Chairs program.

References

- (1) Jessop, P. G.; Leitner, W., Eds. *Chemical Synthesis using Supercritical Fluids*; VCH/Wiley: Weinheim, 1999.
- (2) Kramer, G. M.; Leder, F.; Exxon Research and Engineering Co.: U. S., 1975, p 5.
- (3) Jessop, P. G.; Ikariya, T.; Noyori, R. *Chem. Rev.* **1999**, *99*, 475-493.
- (4) Jessop, P. G.; Ikariya, T.; Noyori, R. *Nature* **1994**, *368*, 231-233.
- (5) Kainz, S.; Brinkmann, A.; Leitner, W.; Pfaltz, A. *J. Am. Chem. Soc.* **1999**, *121*, 6421-6429.
- (6) Burk, M. J.; Feng, S.; Gross, M. F.; Tumas, W. *J. Am. Chem. Soc.* **1995**, *117*, 8277-8278.
- (7) Kainz, S.; Koch, D.; Baumann, W.; Leitner, W. *Angew. Chem., Int. Ed. Engl.* **1997**, *36*, 1628-1630.
- (8) Ablan, C. D.; Jessop, P. G.; Beckman, E. *in preparation* **2003**.
- (9) Blanchard, L. A.; Hancu, D.; Beckman, E. J.; Brennecke, J. F. *Nature* **1999**, *399*, 28-29.
- (10) Brown, R. A.; Pollet, P.; McKoon, E.; Eckert, C. A.; Liotta, C. L.; Jessop, P. G. *J. Am. Chem. Soc.* **2001**, *123*, 1254-1255.
- (11) Heldebrant, D. J.; Jessop, P. G. *J. Am. Chem. Soc.* **2003**, *125*, 5600-5601.
- (12) Bergbreiter, D. E.; Zhang, L.; Mariagnanam, W. M. *J. Am. Chem. Soc.* **1993**, *115*, 9295-9296.
- (13) Jessop, P. G.; Olmstead, M. M.; Ablan, C. D.; Grabenauer, M.; Sheppard, D.; Eckert, C. A.; Liotta, C. L. *Inorg. Chem.* **2002**, *41*, 3463-3468.
- (14) West, K. N.; Bush, D.; Hallett, J. P.; Brown, J. S.; Liotta, C. L.; Eckert, C. A. In *Proceedings of the 2nd International Meeting on High Pressure Chemical Engineering*; Brunner, G., Ed.; Hamburg, Germany, 2001.
- (15) Tai, C. C.; Chang, T.; Roller, B.; Jessop, P. G. *Inorg. Chem.* **2003**, *42*, 7340-7341.
- (16) Thomas, C. A.; Bonilla, R. J.; Huang, Y.; Jessop, P. G. *Can. J. Chem.* **2001**, *79*, 719-724.
- (17) Munshi, P.; Main, A. D.; Linehan, J.; Tai, C. C.; Jessop, P. G. *J. Am. Chem. Soc.* **2002**, *124*, 7963-7971.
- (18) Tai, C. C.; Pitts, J.; Main, A. D.; Linehan, J.; Munshi, P.; Jessop, P. G. *Inorg. Chem.* **2002**, *41*, 1606-1614.
- (19) Munshi, P.; Heldebrant, D.; McKoon, E.; Kelly, P. A.; Tai, C.-C.; Jessop, P. G. *Tetrahedron Lett.* **2003**, *44*, 2725-2727.
- (20) Tai, C. C.; Huck, M. J.; McKoon, E. P.; Woo, T.; Jessop, P. G. *J. Org. Chem.* **2002**, *67*, 9070-9072.
- (21) Combes, G. B.; Dehghani, F.; Lucien, F. P.; Dillow, A. K.; Foster, N. R. In *Reaction Engineering for Pollution Prevention*; Abraham, M. A., Hesketh, R. P., Eds.; Elsevier: Amsterdam, 2000, pp 173-181.
- (22) Musie, G.; Wei, M.; Subramaniam, B.; Busch, D. H. *Coord. Chem. Rev.* **2001**, *219*, 789-820.
- (23) Subramaniam, B.; Busch, D. H. In *Carbon Dioxide Conversion and Utilization*; Song, C., Gaffney, A. F., Fujimoto, K., Eds.; ACS: Washington, 2002, pp 364-386.
- (24) Wei, M.; Musie, G. T.; Busch, D. H.; Subramaniam, B. *J. Am. Chem. Soc.* **2002**, *124*, 2513-2517.
- (25) Sellin, M. F.; Webb, P. B.; Cole-Hamilton, D. J. *Chem. Commun.* **2001**, 781-782.
- (26) Jessop, P. G.; Stanley, R.; Brown, R. A.; Eckert, C. A.; Liotta, C. L.; Ngo, T. T.; Pollet, P. *Green Chem.* **2003**, *5*, 123-128.
- (27) Jessop, P. G.; DeHaai, S.; Wynne, D. C.; Nakawatase, D. *Chem. Commun.* **2000**, 693-694.
- (28) Wittmann, K.; Wisniewski, W.; Mynott, R.; Leitner, W.; Kranemann, C. L.; Rische, T.; Eilbracht, P.; Kluwer, S.; Ernsting, J. M.; Elsevier, C. L. *Chem. Eur. J.* **2001**, *7*, 4584-4589.

Carbon dioxide as a solvent for synthesis and processing

Andrew B Holmes, Wilhelm T. S. Huck, Klaus Kahle, Connie K. Y. Lee, and Christine K. Luscombe

Melville Laboratory, Department of Chemistry, University of Cambridge, Lensfield Road, Cambridge CB2 1EW, United Kingdom

Abstract

Supercritical carbon dioxide is emerging as a potentially interesting solvent for synthesis and processing under environmentally benign conditions. In this paper we address three features of the use of carbon dioxide where the particular benefits of the solvent realise different consequences from those observed in conventional organic solvents.

We first examined the dipolar cycloaddition of nitrile oxides to alkenes and alkynes and show that the regiocontrol obtained can be tuned according to the solvent density. We then address the applications of the Suzuki cross-coupling reaction using a solid phase supported palladium catalyst to make conjugated aromatic materials. Extension to the use of conventional solvents allows the synthesis of CO₂-philic oligomeric fluorene derivatives. Finally, we demonstrate the patterned deposition of a fluorinated polymer onto a patterned silicon wafer substrate.

Nitrile Oxide Cycloadditions in Supercritical Carbon Dioxide

Apart from the Diels-Alder reaction,^{1, 2} there has been little reported on cycloaddition chemistry in scCO₂. 1,3-Dipolar cycloadditions are an important class of cycloadditions, typically giving rise to 5-membered heterocycles, many of which are of pharmaceutical interest. In the present study, reactions of nitrile oxides and olefins were examined in scCO₂. The scope of nitrile oxide cycloadditions in scCO₂ was exemplified in high yielding reactions of mesitonitrile oxide with numerous alkenes and alkynes bearing various functional groups.

Synthesis of fluorine-containing polyfluorenes

Many factors determine whether or not a polymer shows solubility in liquid or supercritical CO₂. Amongst them are the polymer backbone architecture, the amount and the nature of CO₂-philic groups and the distribution of such groups within the polymer. In order to find the optimal structure of a CO₂ soluble polyfluorene and its content of CO₂-philic fluorine, the first aim was to synthesise a range of homo- and copolymers with various degrees of fluorination and then carry out solubility tests in supercritical carbon dioxide. While one possibility of varying the fluorine content is altering the length of the fluorinated side chain, another approach is the synthesis of copolymers containing fluorinated as well as non-fluorinated units (Fig. 2).

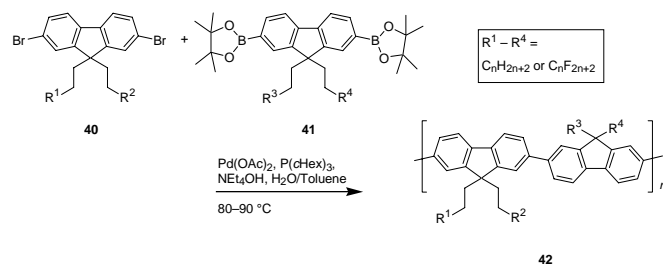


Fig. 1: Synthesis of partially fluorinated polyfluorenes **42** by Suzuki polymerization.

The polymerization reactions were carried out under the conditions optimized for the synthesis of alkyl substituted polyfluorenes. The polymers produced in this way were quite soluble under the reaction conditions if they contained at least 25% of non-fluorinated alkyl substituents. Any higher degree of fluorination led to the precipitation of polymer that then proved insoluble in all common solvent. A possible reason for the lack of solubility of the polymers is a high degree of crystallinity caused by interactions of the fluorinated side chains as well as the stiffness of the polymer. In order to make the polymers more flexible, a series of linkers was introduced into the backbone. Since these linkers break down the conjugation of the resulting polymers, it is important that a minimum conjugation length is maintained to allow efficient electroluminescence. This work shows sufficient promises to justify further research.

Patterned Deposition in sc Carbon Dioxide

Considerable progress has been made in recent years in using compressed CO₂ for deposition of fluorinated coatings on surfaces. One particularly attractive application is in advanced photolithography where there has been much interest in submicron feature sizes using fluoropolymers which are transparent at 157 nm. A preliminary study into the potential use of compressed CO₂ as an alternative solvent for inkjet printing is presented. This technique should have many applications in the deposition of organic and polymeric materials for optoelectronic devices. Preliminary results were carried out using a 10 cm³ stainless steel high pressure reaction vessel equipped with a sapphire window.

Typical procedure for deposition of a polymer in CO₂ onto a patterned Si wafer

A solution of fluorolink® in compressed CO₂ was prepared in a 500 cm³ reaction vessel as follows. Fluorolink® (0.5 g) was charged into the vessel and then sealed. Liquid carbon dioxide was withdrawn from a supply cylinder (BOC, CP grade; 99.995%), passed through the chiller (2) and compressed by the air driven liquid piston pump (Haskell MCPV-71). The chiller was required to avoid cavitation of the pump. The CO₂ stream was then heated to the desired conditions by the use of heat exchanger and directed to the reaction vessel.

The pressure was raised by the pump to 100 bar and maintained at this condition by the back pressure regulator (Go Products, Model PR-57). The vessel was located within an insulated air bath, which was maintained at a constant temperature of 35°C (± 0.1 °C) during the process. The temperature was recorded using type K thermocouples (RS Electronics) encased in 316 stainless steel and displayed on a temperature indicator (T200, RS Electronics). The pressure was measured by a pre-calibrated pressure transducer and a dedicated indicator (Druck PTX 52100 and DPI 262, respectively), which had an accuracy of ± 0.3 %. After a short equilibration time (10 mins) in which the polymer became solubilized in the CO₂, the cell was vented via a heated nozzle (length 10 cm; diameter 127 μ m) and the contents were delivered onto a patterned Si wafer which was held at a distance (d) 3 cm away from the nozzle outlet for a period of 30 s. Pressure drop within the vessel during spraying was minimized by increasing the stroke rate of the piston pump to maintain the pressure within the system. The patterned Si wafer was prepared using UV mask lithography on alkyltrichlorosilane self-assembled monolayers (SAMs) at the Base Technology Centre, Seiko-Epson, Suwa, Japan.

The following parameters were altered in order to obtain the best results for deposition: the polymer {poly(1*H*,1*H*,2*H*,2*H*-perfluorooctyl acrylate), poly(1*H*,1*H*,2*H*,2*H*-perfluorooctyl methacrylate) and Fluorolink®}, the solution concentration (0.02 - 0.1 wt%), temperature within the reaction vessel (25 - 35 °C), time for deposition (5 - 30 s), the nozzle temperature during deposition (25 - 35 °C), nozzle dimensions (length 5 - 10 cm; diameter 127 μ m) and finally the distance (d) from nozzle outlet to wafer (3 - 10 cm).

Our results suggest that better patterns are observed after deposition by using more concentrated solutions at 35 °C, lowest possible nozzle diameter and nozzle lengths of 10 cm. Under these conditions we were able to obtain good resolution with 5 μ m dot sizes. Improved deposition also occurred when the distance between the Si wafer and the nozzle was reduced. At lower temperatures precipitation of the polymer occurred at the tip of the nozzle. Increasing the nozzle temperature reduced the amount of precipitation. When nozzles with a larger capillary diameter were used, the polymer was deposited unevenly leading to poor pattern replication. Similarly when the distance between the wafer and nozzle was increased, poor pattern replication was observed. Improved deposition was achieved when the duration of the experiment was extended to 30 s. This is presumably due to the improved mass transfer from the solution onto the wafer allowing a more even distribution of the polymer solution.

References

- (1) Renslo, A. R.; Weinstein, R. D.; Tester, J. W.; Danheiser, R. L. *J. Org. Chem.*, **1997**, *62*, 4530. (b) Weinstein, R. D.; Renslo, A. R.; Danheiser, R. L.; Harris, J. G.; Tester, J. W. *J. Phys. Chem.*, **1996**, *100*, 12337. (c) Weinstein, R. D.; Renslo, A. R.; Danheiser, R. L.; Tester, J. W. *J. Phys. Chem. B*, **1999**, *103*, 2878.
- (2) Clifford, A. A.; Pople, K.; Gaskill, W. J.; Bartle, K. D.; Rayner, C. M. *J. Chem. Soc., Chem. Commun.*, **1997**, 595. (b) Clifford, A. A.; Pople, K.; Gaskill, W. J.; Bartle, K. D.; Rayner, C. M. *J. Chem. Soc., Faraday Trans.*, 1998, **94**, 1451.

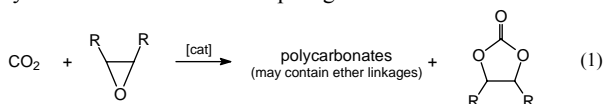
THE COUPLING OF EPOXIDES AND CARBON DIOXIDE IN THE PRESENCE OF HOMOGENEOUS TRANSITION-METAL CATALYSTS. PRODUCTION OF POLYCARBONATES VS CYCLIC CARBONATES

Donald J. Darensbourg, Ryan M. Mackiewicz, Andrea L. Phelps, and Jody L. Rodgers

Texas A&M University, Department of Chemistry,
College Station, TX 77843

Introduction

Over the past decade a variety of efficient homogeneous catalysts or catalyst precursors have been developed to couple the thermodynamically stable carbon dioxide molecule with highly reactive substrates. One of the most promising processes involves the coupling of carbon dioxide and epoxides to afford cyclic carbonates or polycarbonates (eq. 1).¹ The production of polycarbonates from carbon dioxide and epoxides represents an environmentally benign synthetic route to these biodegradable thermoplastics which are mostly prepared by the interfacial polycondensation of diols and phosgene.²



Although we and others have made significant advances in the synthesis of these useful thermoplastics from carbon dioxide and epoxides much of the fundamental knowledge concerning the reaction kinetics of these processes is lacking, due in part to the practical challenges associated with sampling and analyzing systems at elevated temperatures and pressures. This information is needed for making this process applicable to the synthesis of a variety of copolymers possessing a range of properties and uses. Here, studies examining in detail the mechanistic aspects of metal catalyzed carbon dioxide/epoxide coupling reactions employing *in situ* infrared spectroscopic methods will be presented.³ In addition, we have attempted to establish a clear mechanistic view of carbon-oxygen bond forming processes resulting from carbon dioxide insertion into M–O bonds using model organometallic derivatives.⁴

Experimental

Methods and Materials. All syntheses and manipulations were carried out on a double manifold Schlenk vacuum line under an argon atmosphere or in an argon filled glovebox. Glassware was flame dried before use. All solvents were freshly distilled prior to being used. Epoxides were purchased from Lancaster Synthesis and were distilled from calcium hydride. Catalysts were prepared by literature methods. Infrared spectra and kinetic measurements were monitored on ASI's ReactIR 1000 system equipped with a MCT detector and a 30 bounce SiCOMP *in situ* probe. ¹H and ¹³C NMR spectra were recorded on Unity + 300 MHz or VXR 300 MHz superconducting high resolution spectrometers.

Copolymerization of Cyclohexene Oxide/Propylene Oxide and Carbon Dioxide. A weighed sample of the catalyst complex was dissolved in 20 ml of the appropriate epoxide. The solution was rapidly loaded *via* an injection port into a 300 mL stainless steel Parr autoclave that had been previously dried overnight at 80°C under vacuum. The reactor was pressurized to 700 psi with CO₂, heated to the desired temperature and stirred for the required time period. After that time, the autoclave was cooled and the CO₂ vented into a fume hood. The reactor was opened and the polymer was isolated

from the viscous/solid mixture by dissolution in small amounts of methylene chloride followed by precipitation from methanol.

High Pressure *in situ* Kinetic Measurements. High pressure reaction kinetics were carried out using a stainless steel Parr autoclave modified with a silicon probe to connect to the ASI ReactIR 1000 system (see Figure 1). The formation rates of the polycarbonate and the cyclic carbonate were monitored by following the $\nu(\text{C}=\text{O})$ of the polycarbonate at $\sim 1750 \text{ cm}^{-1}$ and of the cyclic carbonate at $\sim 1825 \text{ cm}^{-1}$ (see Figure 2).

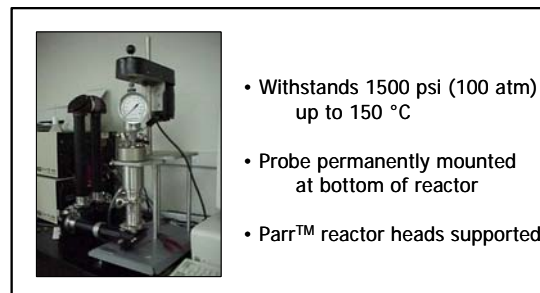


Figure 1. ASI ReactIR™ 1000 with high pressure probe.

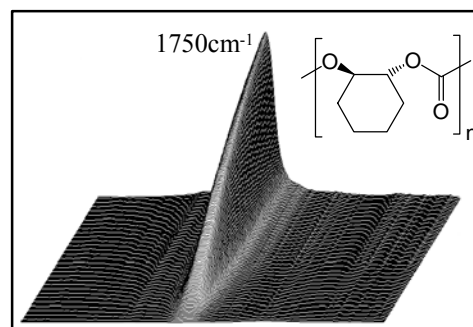


Figure 2. *In situ* infrared monitoring in the $\nu(\text{CO}_2)$ region for polymer formation from CO₂/cyclohexene oxide.

Polymer Characterization. Polymer samples were first characterized by ¹H NMR and IR spectroscopy. The amount of ether linkages were determined *via* ¹H NMR by integrating the peaks corresponding to the methine protons of the polyether at ~ 3.45 ppm and the polycarbonate at ~ 4.6 ppm. The presence or absence of the corresponding cyclic carbonate was investigated by monitoring the presence or absence of the $\nu(\text{C}=\text{O})$ of the cyclic carbonate at $\sim 1825 \text{ cm}^{-1}$. Finally, M_w and M_n measurements were carried out using GPC.

Results and Discussion

We have examined a wide variety of zinc and chromium based derivatives as catalysts for the coupling of carbon dioxide and propylene oxide or cyclohexene oxide. In these studies, as well as those reported by other researchers, the reaction of carbon dioxide and propylene oxide favors production of cyclic carbonate, whereas, the analogous process involving cyclohexene oxide affords mostly polycarbonates. We have ascribed this difference in product selectivity to the ring strain placed on the five-membered carbonate ring in order to accommodate the conformational requirements of the alicyclic cyclohexyl ring. This is evident from a comparison of the crystal structures of cyclic propylene carbonate and cyclic cyclohexylene carbonate (see Figure 3).⁵

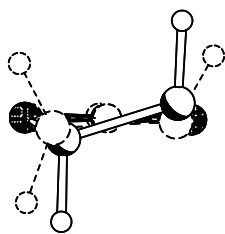


Figure 3. Overlay of the carbonate groups from propylene carbonate (dotted) and cyclohexene carbonate (solid).

Indeed, we have quantified the product selectivity for cyclic carbonate vs polycarbonate production in processes catalyzed by (salen)Cr^{III}Cl derivatives. Comparative kinetic measurements were performed as a function of reaction temperature to assess the activation barrier for production of cyclic carbonates and polycarbonates for the two different classes of epoxides, i.e., alicyclic(cyclohexene oxide) and aliphatic(propylene oxide).⁶ As anticipated in both instances the unimolecular pathway for cyclic carbonate formation has a larger energy of activation than the bimolecular enchainment pathway. That is, the energies of activation determined for cyclic propylene carbonate and polypropylene carbonate formation were 100.5 kJ·mol⁻¹ and 67.6 kJ·mol⁻¹ respectively, as compared with the corresponding values for cyclic cyclohexyl carbonate and polycyclohexylene carbonate production of 133 kJ·mol⁻¹ and 46.9 kJ·mol⁻¹. The small energy difference in the two concurrent reactions for the propylene oxide/CO₂ process (33 kJ·mol⁻¹) accounts for the large quantity of cyclic carbonate produced at elevated temperatures in this instance.

We have examined a wide variety of (salen)CrNu, where Nu = nucleophile, derivatives as catalysts for the copolymerization of epoxides and carbon dioxide, however at this time we will focus on one of the more active derivatives thus far investigated, complex **1** (see Figure 4). The presence of a cocatalyst which can bind to the axial vacant site at the chromium center has been shown to improve the activity of complex **1** (see Table 1).

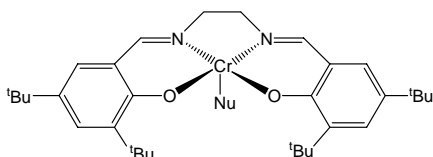


Figure 4. Typical (salen)Cr^{III}Nu (**1**), Nu = Cl(**1a**), N₃(**1b**), catalyst for the copolymerization of epoxides and carbon dioxide.

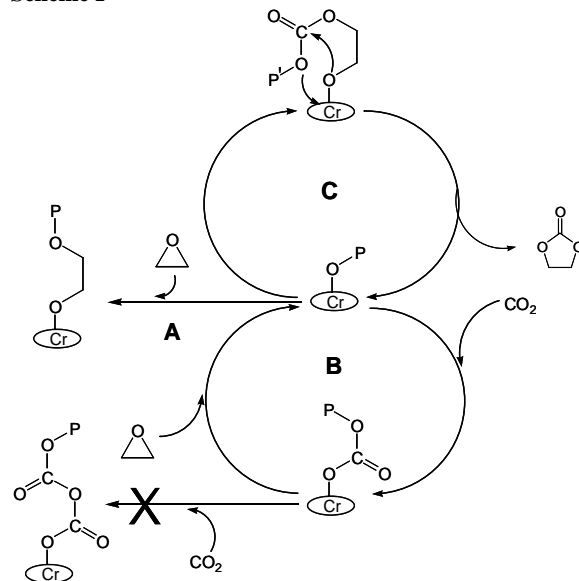
Table 1. Copolymerization Data Using Different Cocatalysts.^a

Complex	Cocatalyst (eq)	TON ^b	TOF ^c	% carbonate
1a	N-methylimidazole (5)	95	24	69%
	PPh ₃ (3) ^d	157	39	96%
	PCy ₃ (3)	578	145	99%
	PPNCl (1) ^e	1004	251	>99%
1b	N-methylimidazole (5)	189	47	90%
	PPh ₃ (3)	284	71	96%
	PCy ₃ (3) ^f	391	98	97%
	PPNCl (1)	1022	255	>99%

^a 50 mg of catalyst dissolved in 20 mL of cyclohexene oxide and injected into a 300 mL Parr autoclave. The reactor was charged to 55 bar CO₂ pressure and heated to 80°C for 4 hours. ^b moles of epoxide consumed / mol. of Cr. ^c moles of epoxide consumed / mol. of Cr / hour. ^d For a 24 hr run, M_n = 22,700 and PDI = 1.55. ^e For a 4 hr run, M_n = 5980 and PDI = 2.05, whereas for a 12 hr run, M_n = 16,800 and PDI = 1.92. ^f For a 10 hr run, M_n = 10,800 and PDI = 1.54.

Scheme 1 summarizes the reaction operative during the CO₂/epoxide coupling process. The relative importance of end pathway is closely linked to the nature of the salen ligand, the cocatalyst, and the epoxide. For example, while a more electron donating salen increases the rate of polymerization with cyclohexene oxide, this seems to have the opposite effect for propylene oxide and tends to decrease the rate of conversion for both cyclic and polymer. A similar situation was observed when changing the cocatalyst, where triphenylphosphine has been shown to produce polymer with no cyclic carbonate, while tricyclohexylphosphine produced mostly polyether and a small amount of polymer. This is to be contrasted with the data in Table 1 for cyclohexene oxide and carbon dioxide copolymerization. Furthermore, as previously demonstrated, copolymerization using cyclohexene oxide is further enhanced through the use of anionic cocatalysts. However, when using a PPN⁺Cl⁻ cocatalyst, this was not the case for propylene oxide as cyclic carbonate was the major product.

Scheme I



Finally, the use of other epoxide substrates based on the cyclohexyl backbone in the copolymerization with carbon dioxide, such as [2-(3,4-epoxycyclohexyl)ethyl]trimethoxysilane, offers the opportunity of affording industrially useful thermoplastics via crosslinking of the silane units.⁷

References

- (1) Darensbourg, D. J.; Holtcamp, M. W.; Struck, G. E.; Zimmer, M. S.; Niezgod, S. A.; Rainey, P.; Robertson, J. B.; Draper, J. D.; Reibenspies, J. H. *J. Amer. Chem. Soc.*, **1999**, *121*, 107.
- (2) Koning, C.; Wildeson, J.; Parton, R.; Plum, B.; Steeman, P.; Darensbourg, D. J. *Polymer* **2001**, *42*, 3995.
- (3) Darensbourg, D. J.; Yarbrough, J. C. *J. Am. Chem. Soc.* **2002**, *124*, 6335.
- (4) Darensbourg, D. J.; Lee, W.-Z.; Phelps, A. L.; Guidry, E. *Organometallics* **2003**, *ACS ASAP*
- (5) Darensbourg, D. J.; Lewis, S. J.; Rodgers, J. L.; Yarbrough, J. C. *Inorg. Chem.* **2003**, *42*, 581.
- (6) Darensbourg, D. J.; Yarbrough, J. C.; Ortiz, C. G.; Fang, C. *J. Am. Chem. Soc.* **2003**, *125*, 7586.
- (7) Darensbourg, D. J.; Rodgers, J. L.; Fang, C. *Inorg. Chem.* **2003**, *42*, 4498.

SYNTHESIS OF CARBONATE BY REACTION OF CARBON DIOXIDE WITH PGE

Sang-Wook Park^a, Dae-Won Park, Tae-Young Kim, Mi-Young Park, and Kwang-Joung Oh

^aDivision of Chemical Engineering, Pusan National University, Pusan 609-735, Korea

Introduction

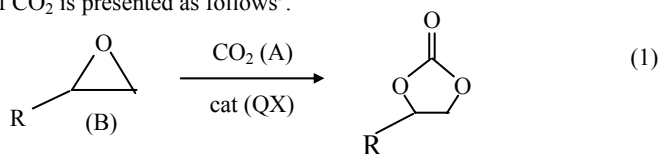
Recently, the chemistry of carbon dioxide has received much attention¹, and its reaction with oxiranes leading to five-membered cyclic carbonate (oxirane-CO₂ reaction) is well-known among many examples^{2,3}. These carbonates can be used as aprotic polar solvent and sources for polymer synthesis⁴. In the oxirane-CO₂ reaction, high pressure (5-50 atm) of CO₂ has been thought to be necessary². The oxirane-CO₂ reactions under atmospheric pressure have been reported⁴ only recently. Many organic and inorganic compounds including amines, phosphines, quaternary ammonium salts, and alkali metal salts are known to catalyze the oxirane-CO₂ reaction³. Most purpose of these papers have been to show the reaction mechanism, the pseudo-first-order reaction rate constant with respect to the concentration of oxirane, and the catalyst dependence of its conversion.

In the mass transfer accompanied by a chemical reaction, the diffusion may have an effect on the reaction kinetics. It is considered worthwhile to investigate the reaction kinetics of the gas-liquid heterogeneous reaction such as the oxirane-CO₂ reaction.

In this study, a chemical absorption mechanism of carbon dioxide into the toluene solution of phenyl glycidyl ether (PGE) and Aliquat 336 (QX), and the experimental value of the equilibrium reaction constant between PGE and Aliquat 336 were presented, from which the reaction rate constant of reaction of CO₂ was obtained using the measured molar flux and liquid-side mass transfer coefficient of CO₂ at 85°C and 1 atm.

Theory

The overall reaction between PGE and CO₂ at atmospheric pressure of CO₂ is presented as follows⁵.



The overall reaction (1) in this study is assumed to consist of three steps as follows⁵;

The three steps are (i) a reversible reaction of PGE and QX to form complex, C₁, (ii) reaction of C₁ and carbon dioxide to form complex, C₂, and (iii) dissociation reversible reaction of C₂ to form QX and five-membered cyclic carbonate.



The mass balances accompanied by the overall reaction (A + B $\xrightarrow{k_c}$ P), which consists of reaction(i)-(iii), and initial and boundary conditions are presented as follows,

$$D_A \frac{\partial^2 [A]}{\partial z^2} = \frac{\partial [A]}{\partial t} + k_c [A][B] \quad (2)$$

$$D_{Cl} \frac{\partial^2 [B]}{\partial z^2} = \frac{\partial [B]}{\partial t} + v k_c [A][B] \quad (3)$$

$$t = 0, z > 0; [A] = 0, [B] = [B]_0 \quad (4)$$

$$t > 0, z = 0; [A] = [A]_i, \frac{\partial [B]}{\partial z} = 0 \quad (5)$$

$$t > 0, z = \infty; [A] = 0, [B] = [B]_0 \quad (6)$$

The mass balances, (2) and (3), and the conditions, (4)-(6) are rearranged the dimensionless forms as follows;

$$\frac{\partial^2 a}{\partial x^2} = \frac{\pi}{4} \frac{\partial a}{\partial \theta} + m a b \quad (7)$$

$$\frac{\partial^2 b}{\partial x^2} = \frac{\pi}{4} r \frac{\partial b}{\partial \theta} + v r q m a b \quad (8)$$

$$\theta = 0, x > 0; a = 0, b = 1 \quad (9)$$

$$\theta > 0, x = 0; a = 1, \frac{\partial b}{\partial x} = 0 \quad (10)$$

$$\theta > 0, x = \infty; a = 0, b = 1 \quad (11)$$

where,

$$a = \frac{[A]}{[A]_i}, b = \frac{[B]}{[B]_0}, x = \frac{z}{\delta}, \theta = \frac{t}{t_o}, \delta = \frac{D_A}{k_L}, q = \frac{[A]_i}{[B]_0}$$

$$t_o = \frac{4D_A}{\pi k_L^2}, m = \frac{k_c [B]_0 D_A}{k_L^2}, r = \frac{D_A}{D_{B1}}$$

The enhancement factor(β), which is defined as ratio of absorption rate of CO₂ with chemical reaction to that without the chemical reaction, is presented as follow;

$$\beta = - \left. \frac{\partial a}{\partial x} \right|_{x=0} \quad (12)$$

The measured enhancement factor, which is obtained under the given experimental condition such as concentration of PGE, Aliquat336, and the agitation speed of the impeller, is used to get the reaction rate constant by the comparison of its value with the value estimated from Eq.(12).

Experimental

Absorption experiments were carried out in a semi-batch flat-stirred agitated vessel constructed of pyrex glass of 0.075 m inside diameter and of 0.13 m in height. Four equally spaced vertical baffles, each one-tenth of the vessel diameter in width, were attached to the internal wall of the vessel. A straight impeller with 0.034 m in length, 0.017 m in width and 0.005 m in thickness was used as the liquid phase agitator and located at the middle position of the liquid phase of 0.3 dm³. The absorption rates of CO₂ were obtained from the difference of the flow rate of CO₂ between inlet and outlet of the vessel at 85°C. The molar flux of CO₂ absorbed into the liquid was obtained from the measured rate of absorption.

Results and Discussion

The concentration profiles of components A and B can be obtained by the numerical analysis (FEMLAB) of the equations (7) and (8). The estimated values concentration of component A and B are shown in **Fig.1** under the typical reaction condition such as [PGE]= 0.1 kmol/m³, [QX]= 0.05 kmol/m³, T= 85°C. As shown in **Fig.1**, the concentration of CO₂ decreases and that of B increases as the depth of the liquid increases. Using the measured molar flux of CO₂ according to the change of fed concentrations of component, PGE and QX, the reaction rate constant of the reaction (1), which can be obtained under the boundary condition such as [A]=0 at z=0, is 0.53 m³/kmol.s at 85°C.

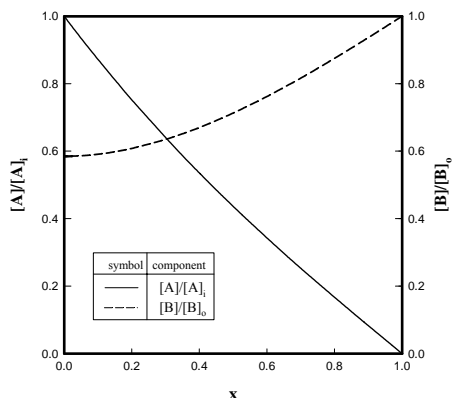


Figure.1. Concentration profile of A and C1. ($[B]_0=0.1 \text{ kmol/m}^3$, $[QX]_0=0.05 \text{ kmol/m}^3$, $T=85^\circ\text{C}$)

The measured value of absorption rate of CO_2 at the concentration of PGE in the range of $0.1\text{--}2.0 \text{ kmol/m}^3$, that of Aliquat336 of 0.05 kmol/m^3 , and the agitation speed of impeller of 50 rev/min are plotted against the concentration of PGE in **Fig. 2**. As shown in **Fig.2**, the absorption rate of CO_2 increased as increasing of PGE concentrations. The reaction rate constant (k_2) was estimated by comparison of enhancement factor obtained from the measured absorption rate of CO_2 in **Fig.2** with the value in Eq.(12).

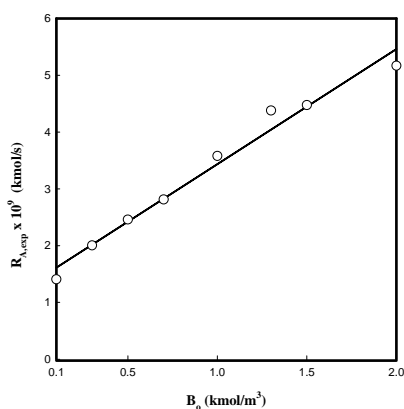


Figure. 2. Effect of PGE concentration on flux of CO_2 .

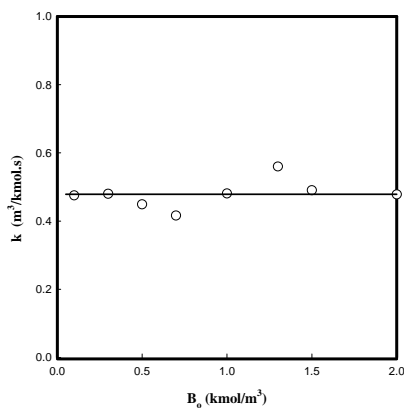


Figure. 3. Effect of PGE concentration on reaction rate constant.

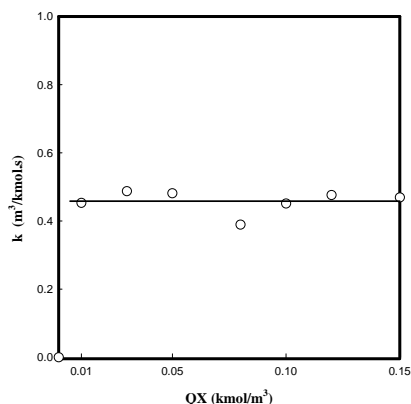


Figure. 4. Effect of QCl concentration on reaction rate constant.

The values of k_2 are plotted against the concentration of PGE in **Fig.3**. As shown in **Fig.3**, the reaction rate constants are constant as $0.434\text{--}0.592 \text{ m}^3/\text{kmol.s}$ at the PGE concentration in the range of $0.5\text{--}2.0 \text{ kmol/m}^3$. Also the values of k_2 , which are estimated by using the experiments at the concentration of PGE of 1.0 kmol/m^3 and those of Aliquat336 in the range of $0.01\text{--}0.15 \text{ kmol/m}^3$, are plotted against the concentration of Aliquat336 in **Fig.4**. As shown in **Fig.4**, the reaction rate constants were constant in the range of Aliquat 336 concentrations.

Conclusion

Carbon dioxide was absorbed into the toluene solution of phenyl glycidyl ether(PGE) as a oxirane and tricaprylylmethylammonium chloride (Aliquat 336, QX) as a catalyst using a semi-batch flat-stirred absorber at 85°C and 1 atm to obtain a five-membered cyclic carbonate, phenoxy methyl ethylene carbonate. The reaction mechanism of oxirane – CO_2 reaction divided into three steps was used to obtain the reaction kinetics using the mass balance equations. The reaction rate constant in the overall reaction between CO_2 and PGE was obtained by the numerical solution of the mass balance equation using the measured molar flux of CO_2 and the liquid-side mass transfer coefficient of CO_2 at given concentration of PGE and QX.

Acknowledgement

This work was supported by KOSEF (Grant No : R01-2003-000-100200-0), the Brain Korea 21 project in 2003, and Brain Busan 21 program.

References

1. Inoue, S., In organic and bioorganic chemistry of carbon dioxide ; Inoue, S., N. Yamazaki, Eds., Kodansha Ltd., Tokyo, 1982.
2. Peppel, W.J., *Ind. Eng. Chem.*, 50(5), 767-770 (1958).
3. Kihara, N., Hara, N., and Endo, T., *J. Org. Chem.*, 58, 6198-6202 (1993).
4. Rokicki, G., *Makromol. Chem.* 186, 331-337 (1985).
5. Aida, T. and S. Inoue, *J. Am. Chem. Soc.*, 105, 1304-1309 (1983).

A Novel Biomimetic Catalyst for Electrochemical Hydrogen Production

Licheng Sun,^{1*} Sascha Ott,¹ Mikael Kritikos,² Björn Åkermark,¹
Reiner Lomoth³

¹ Department of Organic Chemistry, Arrhenius Laboratory,
Stockholm University, S-10691 Stockholm, Sweden,
licheng.sun@organ.su.se

² Department of Structural Chemistry, Arrhenius Laboratory,
Stockholm University, S-10691 Stockholm, Sweden

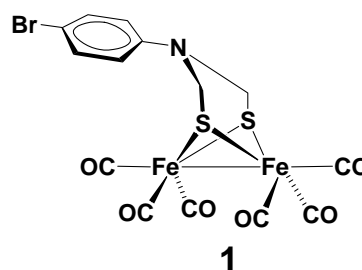
³ Department of Physical Chemistry, BMC, Uppsala University,
BOX 579, S-75123, Uppsala, Sweden

Introduction

To totally solve the problems of pollution and green house effects, the ultimate mean is to use renewable energy source such as solar energy which has been used by nature through photosynthesis for billion years. Hydrogenases are a class of natural enzymes which catalyse the metabolism of hydrogen in cyanobacteria and other microorganisms. They can thereby function either as sinks for energy-rich electrons or provide the organisms with reducing power from hydrogen oxidation.¹⁻³ Hydrogenases are generally divided into two families, the nickel-iron (Ni-Fe) hydrogenases and the iron only (Fe-Fe) hydrogenases, reflecting the different base metals present in the active site. Biologically, the two families differ from each other. The Ni-Fe hydrogenases seem to be more involved in hydrogen oxidation, whereas the iron only hydrogenases tend to catalyse preferentially the production of hydrogen.⁴⁻⁵ It is this remarkable ability of the iron only hydrogenases which has inspired chemists of the bioinorganic community to synthesize close mimics to the active site of the natural system in the search for active hydrogen production catalysts.⁶⁻⁸ From crystallographic as well as theoretical studies of the enzyme, the active site is known to consist of two iron nuclei, which are in bonding distance.^{9,10} They are linked by a dithiolate bridge, recently suggested to possess the structure S-CH₂-NH-CH₂-S (azadithiolate = ADT).^{11,12} Apart from a cysteine-linked [Fe₄S₄] cluster which is part

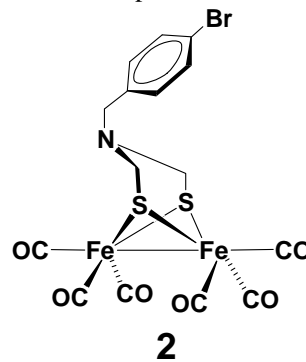
of the electron transfer chain to and from the active site, diatomic ligands carbonyl and cyanide occupy the remaining coordination sites around the iron nuclei.

As biomimetic models for the active sites of Fe-only Hydrogenases, numerous reports have emerged in the bioinorganic literature.¹³⁻²² We have recently described the concept of light-driven proton reduction, using a ruthenium polypyridine complex as the light-harvesting component and a biomimetic model of the iron hydrogenase as proton activation catalyst.²³⁻²⁴ This projected process commences with the absorption of a photon by the ruthenium



photosensitizer. The photo-excited ruthenium complex is oxidatively quenched by the dinuclear iron site, giving rise to a reduced iron species.

After regeneration of the photosensitizer (by an external electron donor), this process is repeated to afford a doubly reduced diiron species which could then drive the reduction of protons.



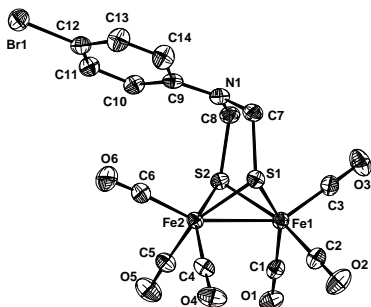
In this paper two biomimetic systems **1** and **2** where a 2-aza-1,3-dithiol bridged Fe-dimer complexes have been synthesized and characterized. The catalytic electrochemical hydrogen evolution of these two

complexes have been investigated.

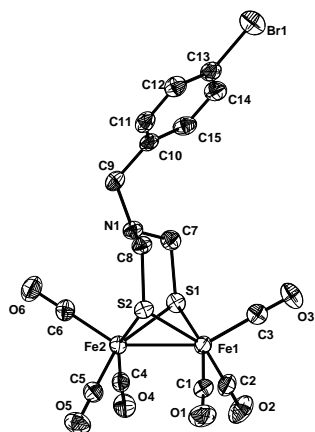
Results and discussion

The bromo-substituted iron complexes **1** and **2** were synthesized by applying a recently published procedure for the preparation of some related complexes.²⁵ Thus, the lithium salt of diironhexacarbonyldisulfide was reacted with the respective *N,N*-di(chloromethyl)-4-bromoaniline and *N,N*-di(chloromethyl)-4-bromobenzylamine, which in

turn were synthesized from the *p*-bromoaniline and *p*-bromobenzylamine in two steps.

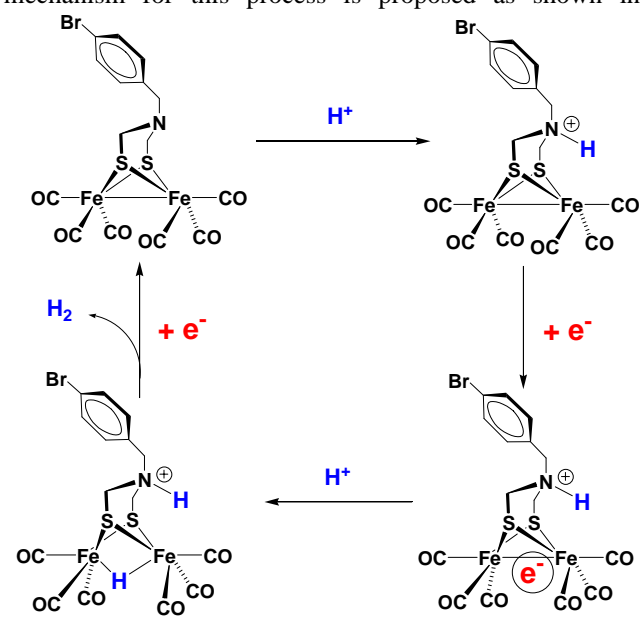


From the X-ray crystal structure it is shown that the $[(\mu\text{-S})_2\text{Fe}_2(\text{CO})_6]$ unit of **1** is very similar to those found in other $[(\mu\text{-S})_2\text{Fe}_2(\text{CO})_6]$ structures reported.²⁶ In the central $[(\mu\text{-SR})_2\text{Fe}_2(\text{CO})_6]$ unit the two Fe atoms and the two S atoms form a butterfly conformation in which the metal



atoms are connected to each other through a Fe-Fe single bond (2.494 Å). In contrast to the Fe-Fe distances the S...S contacts vary slightly more, 3.075 Å. The Fe-C and C-O distances and Fe-C-O angles are all normal with one exception. The Fe-C-O angles for the carbonyls closest to the amine functionality (i.e. trans to the Fe-Fe bond) in **1** deviate significantly from the expected 180° linear arrangements with value of 175.6(7)°. The non-bonding C...N distance between the amine and the closest carbonyl carbon atom in **1** is 3.578 Å. Moreover, the nitrogen atom deviates from the plane defined by C7, C8 and C9 by 0.174(5) Å. This non-planarity ruptures the potential π -conjugation between the phenyl ring and the nitrogen p-orbital.

In contrast to the structure features of **1**, the benzyl moiety in complex **2** resides in a pseudo-equatorial position of the mettaloheterocycle with the nitrogen lone-pair pointing towards an iron nucleus. In the crystal structure, the non-bonding C...N distance between the amine nitrogen and the nearest carbonyl carbon atom in **2** is significantly shorter than that in **1** (3.0 Å vs. 3.5 Å). After protonation of **2**, a close proximity of the proton to the diiron active site can therefore be anticipated. In acetonitrile solution of **2** in the presence of HClO₄, an acidic form **2H⁺** has been observed by ¹HNMR. The UV-Vis absorption maximum is shifted from 328 nm to 332 nm. Two isobestic points at 325 and 362 nm are preserved during the titration, indicating the formation of a single protonation product. Electrochemical hydrogen evolution has been observed in case of **2** at the reduction potential of -1.5 V vs. Fc⁰/Fc⁺. The turnover numbers of this catalysis have been determined as 25. No hydrogen production was found without the complex **2** at the same condition. The catalytic mechanism for this process is proposed as shown in



Scheme-1. This is the first example of electrochemical hydrogen production catalysed by a novel biomimetic model of hydrogenase active site, where a 2-aza-1,3-dithiol bridged Fe-dimer complex has been used.

Acknowledgements

Financial support for this work was provided by the Swedish Energy Agency, the Knut and Alice Wallenberg Foundation and the Swedish Research Council (VR).

References

- (1) Nicolet, Y.; Lemon, B. J.; Fontecilla-Camps, J. C.; Peters, J. W. *Trends Biochem. Sci.* **2000**, *25*, 138-143.
- (2) Peters, J. W. *Curr. Opin. Struct. Biol.*, **1999**, *9*, 670-676.
- (3) Frey, M. *ChemBioChem* **2002**, *3*, 152-160.
- (4) Adams, M. W. W. *Biochim Biophys Acta* **1990**, *1020*, 115-145.
- (5) Cammack, R. *Nature* **1999**, *397*, 214-215.
- (6) Alper, J. *Science* **2003**, *299*, 1686-1687.
- (7) Darensbourg, M. Y.; Lyon, E. J.; Smee, J. J. *Coord. Chem. Rev.* **2000**, *206-207*, 533-561.
- (8) Evans, D. J.; Pickett, C. J. *Chem. Soc. Rev.* **2003**, *32*, 268-275.
- (9) Peters, J. W.; Lanzilotta, W. N.; Lemon, B. J.; Seefeldt, L. C. *Science* **1998**, *282*, 1853-1858.
- (10) Nicolet, Y.; Piras, C.; Legrand, P.; Hatchikian, E. C.; Fontecilla-Camps, J. C. *Structure* **1999**, *7*, 13-23.
- (11) Nicolet, Y.; de Lacey, A. L.; Vernede, X.; Fernandez, V. M.; Hatchikian, E. C.; Fontecilla-Camps, J. C. *J. Am. Chem. Soc.* **2001**, *123*, 1596-1602.
- (12) Fan, H.-J.; Hall, M. B. *J. Am. Chem. Soc.* **2001**, *123*, 3828-3829.
- (13) Winter, A.; Zsolnai, L.; Huttner, G. *Z. Naturforsch.* **1982**, *37b*, 1430-1436.
- (14) Lawrence, J. D.; Rauchfuss, T. B.; Wilson, S. R. *Inorg. Chem.* **2002**, *41*, 6193-6195.
- (15) Lyon, E. J.; Georgakaki, I. P.; Reibenspies, J. H.; Darensbourg, M. Y. *Angew. Chem. Int. Ed.* **1999**, *38*, 3178-3180.
- (16) Lyon, E. J.; Georgakaki, I. P.; Reibenspies, J. H.; Darensbourg, M. Y. *J. Am. Chem. Soc.* **2001**, *123*, 3268-3278.
- (17) Razavet, M.; Davies, S. C.; Hughes, D. L.; Pickett, C. J. *Chem. Commun.* **2001**, 847-848.
- (18) Razavet, M.; Borg, S. J.; George, S. J.; Best, S. P.; Fairhurst, S. A.; Pickett, C. J. *Chem. Commun.* **2002**, 700-701.
- (19) George, S. J.; Cui, Z.; Razavet, M.; Pickett, C. J. *Chem. Eur. J.* **2002**, *8*, 4037-4046.
- (20) Zhao, X.; Georgakaki, I. P.; Miller, M. L.; Mejia-Rodriguez, R.; Chiang, C.-Y.; Darensbourg, M. Y. *Inorg. Chem.* **2002**, *41*, 3917-3928.
- (21) Gloaguen, F.; Lawrence, J. D.; Rauchfuss, T. B.; *J. Am. Chem. Soc.* **2001**, 9476-9477.
- (22) Gloaguen, F.; Lawrence, J. D.; Rauchfuss, T. B.; Benard, M.; Rohmer, M.-M. *Inorg. Chem.* **2002**, *41*, 6573-6582.
- (23) S. Salyi, M. Kritikos, B. Åkermark, L. Sun, *Chem. Eur. J.* **2003**, *9*, 557-560.
- (24) Ott, S.; Kritikos, M.; Åkermark, B.; Sun, L. *Angew. Chem. Int. Ed.* **2003**, 3285-3288.
- (25) Lawrence, J. D.; Li, H.; Rauchfuss, T. B. *Chem. Commun.* **2001**, 1482-1483.
- (26) Lawrence, J. D.; Li, H.; Rauchfuss, T. B.; Benard, M.; Rohmer, M.-M. *Angew. Chem. Int. Ed.* **2001**, *40*, 1768-1771.

Effective Fixation of Carbon Dioxide and Its Application to Polymer Synthesis

Takeshi Endo

Department of Polymer Science and Engineering, Faculty of Engineering, Yamagata University, 4-3-16 Jonan, Yonezawa, Yamagata 992-8510, Japan

Introduction

Recently, the chemistry of carbon dioxide has much attention, since carbon dioxide is the most inexpensive and infinite carbon resources. Furthermore, greenhouse effect due to carbon dioxide has gained much attention and decreasing atmospheric carbon dioxide is a critical problem.¹ From these viewpoints, many chemists have studied on development of efficient methods for CO₂ recovery. Among them, chemical CO₂ fixation by primary or secondary amines have been most intensively studied and have become one of the most promising methods for CO₂ recovery.² However, detailed study concerning CO₂ fixation by tertiary amines. Reaction of epoxide with CO₂ is also attractive candidate for efficient CO₂ fixation; however, high pressure of CO₂ has been generally necessary.³ In the course of our works on chemical CO₂ fixation, we present the reversible CO₂ fixation by amidine derivatives and the reaction of epoxides with CO₂ under atmospheric pressure leading to the cyclic carbonate.

Experimental

Materials. *N*-Methyltetrahydropyrimidine (MTHP) was synthesized according to the reported procedure.⁴ Epoxides were distilled from CaH₂ and stored under nitrogen. *N,N*-dimethylformamide (DMF) and *N*-methylpyrrolidone (NMP) were dried and distilled from CaH₂.

Instruments. ¹H-NMR and ¹³C-NMR spectra were recorded with JEOL JNM-270EX or JEOL JNM-GX500 spectrometer with tetramethylsilane (TMS) as an internal standard. IR spectra were recorded with a Jasco FT/IR-5300 spectrometer. Size exclusion chromatography (SEC) was used to determine number average molecular weight (*M*_n) and molecular weight distribution (*M*_w/*M*_n) of polymer samples with respect to polystyrene standards (Tosoh).

Reversible CO₂ fixation by MTHP. CO₂ was bubbled into anhydrous DMF solution (10 mL) of MTHP (982 mg, 10 mmol) at 25 °C for 3 h to afford MTHP-CO₂ in quantitative fixing efficiency (weight increase in the reaction mixture was 440 mg). Subsequently, a DMF solution of MTHP-CO₂ was heated to 65 °C for 2 h to regenerate MTHP quantitatively. The cycle was repeated two times. The structure of MTHP-CO₂ was confirmed by ¹H NMR, ¹³C NMR, and IR spectra.

Reaction of epoxide with CO₂. A mixture of epoxide (10 mmol), catalyst (5.0 mmol), and naphthalene (0.128 g) was introduced in a two-necked flask equipped with a rubber septum. After the atmosphere was replaced with CO₂, 10.0 mL of NMP was introduced using a syringe through a rubber septum to dissolve the mixture. The solution was allowed to stand at 100 °C with continuous stirring. Periodically, a small portion of the reaction mixture was removed out through rubber septum, diluted with dichloromethane, and washed with water. The organic extract was analyzed by HPLC to estimate the conversion of epoxide and yield of carbonate using naphthalene as an internal standard.

Results and Discussion

1. Reversible CO₂ Fixation by Amidines

The CO₂ fixation by primary or secondary amines to afford the corresponding ammonium carbamates have been already reported,² however, detailed study concerning CO₂ fixation by tertiary amines have not been carried out. Recently, we have found

that *N,N,N'*-trialkylamidines, such as *N*-methyltetrahydropyrimidine (MTHP) can construct reversible CO₂ fixation, where CO₂ was fixed at 25 °C and was released at 65 °C quantitatively (Figure 1).⁵

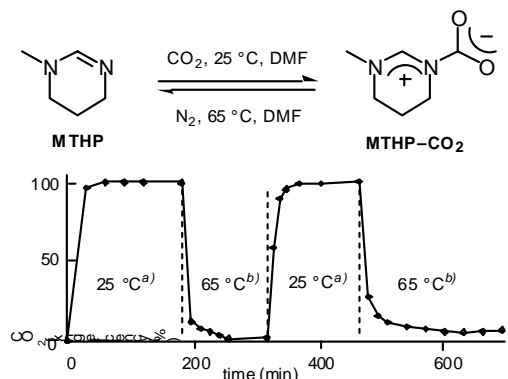
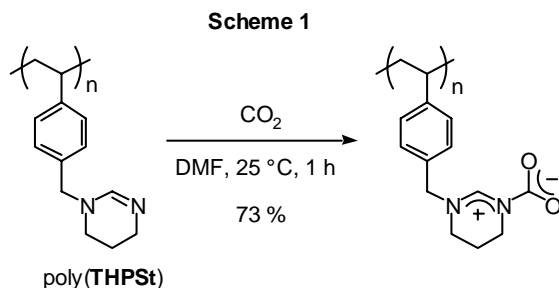


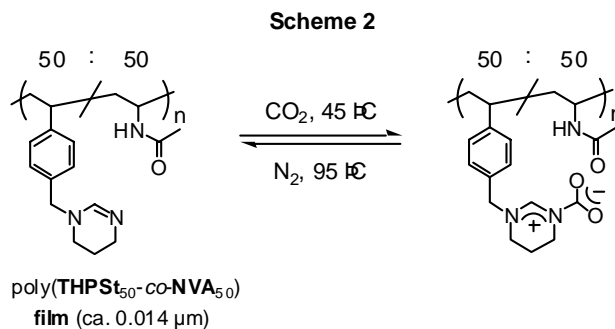
Figure 1. Reversible CO₂ fixation and release by MTHP in DMF. Conditions: *a*) under CO₂ flow (200 mL/min). *b*) under N₂ flow (200 mL/min).

2. Reversible CO₂ Fixation by Polymer Bearing Amidine Moiety

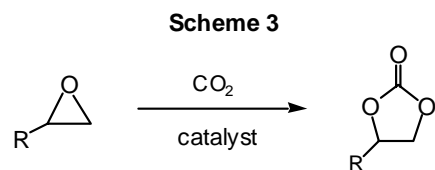
The polymer bearing amidine moiety (poly(THPSt)) was prepared by the synthesis of 4-(1,4,5,6-tetrahydropyrimidine-1-yl)methylstyrene (THPSt) and its radical polymerization. Poly(THPSt) could fix CO₂ in *N,N*-dimethylformamide (DMF) at 25 °C in 73 % fixing efficiency (Scheme 1).



The CO₂ fixation in the solid state using polymer bearing amidine moiety may be one of the most simple, economical, and effective methods for CO₂ recovery. Poly(THPSt) was found to fix CO₂ in the solid state (30 %). The copolymer of THPSt with *N*-vinylacetamide (NVA), poly(THPSt_{50-co-NVA}₅₀) exhibited the higher fixing ability (48 %) than poly(THPSt), presumably due to the decrease in steric hindrance between the adjacent pendant groups. Poly(THPSt_{50-co-NVA}₅₀) was cast from its MeOH solution to form a film that could fix CO₂ at 45 °C in 34 % fixing efficiency. As shown in Scheme 2, the film could conduct the reversible CO₂ fixation, where CO₂ was fixed at 45 °C and was released at 95 °C.

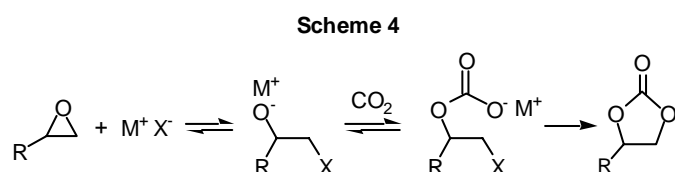


3. Reaction of Epoxide with CO₂



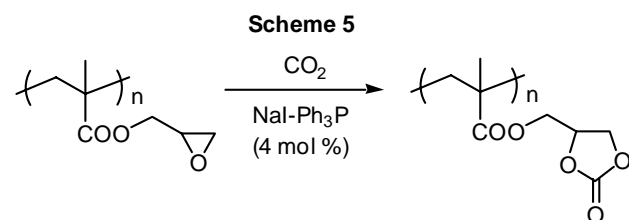
The reaction of epoxides with CO₂ have been already reported. However, high pressure of CO₂ is generally necessary.³ We have

found that alkali metal halides such as lithium bromide show high catalytic activity for this reaction to afford the five-membered cyclic carbonates under atmospheric pressure in excellent yield.⁶ The order of intrinsic activity is following order: chloride > bromide > iodide, which is the order of nucleophilicity of the anion, and lithium salt > sodium salt > benzylammonium salt, which is in accord with the order of Lewis acidity of the cation. The reaction may proceed via nucleophilic attack of halide to epoxide to form β-haloalkoxide which reacts with CO₂ followed by cyclization (Scheme 4).



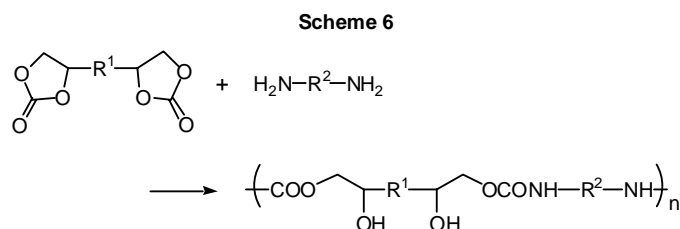
4. Polymer Reaction of Polymer Bearing Epoxide Moiety with CO₂

The incorporation of CO₂ into the polymers bearing epoxide moiety under atmospheric pressure is useful from the viewpoint of CO₂ fixation and the functionality of produced cyclic carbonate. Quantitative incorporation of CO₂ into poly(glycidyl methacrylate) was accomplished in the presence of NaI and Ph₃P as catalyst under atmospheric pressure of CO₂ (Scheme 5).⁷ The polymer could react with primary amines selectively at room temperature to afford the corresponding polymer containing 2-hydroxyethylurethane moiety quantitatively.



5. Synthesis of Bis(cyclic carbonate)s and Their Polyaddition with Diamines

Bis(cyclic carbonate)s were prepared by the reaction of the corresponding bis(epoxide)s with CO₂. Polyaddition of bis(cyclic carbonate)s and diamines afforded the corresponding poly(hydroxyurethane)s with *M_n* 20,000–30,000 in excellent yields (Scheme 6). The presence of water, methanol, or ethyl acetate in the solvent had little effect on *M_n* of the resulting polymer, indicating the high chemoselectivity of the polyaddition reaction.⁸



Conclusion

In this paper, we described several examples for the CO₂ fixation by amidines and epoxides. The reversible fixation–release system of CO₂ by amidine and the polystyrene derivatives having amidine moiety were accomplished. The reaction of epoxide with CO₂ in the presence of alkali metal halides proceeded under atmospheric pressure to afford the corresponding five-membered cyclic carbonate in excellent yield. Further, this reaction was applied to polymer system, i.e., quantitative incorporation of CO₂ into poly(glycidyl methacrylate) and polyaddition of bis(cyclic carbonate)s and diamines to afford the poly(hydroxyurethane)s.

References

- [1] For example, Braustein, P.; Matt, D.; Nobel, D., *Chem. Rev.* **1988**, 88, 747.
- [2] For example, Sartori, G.; Savage, D. W., *Ind. Eng. Chem. Fundam.* **1983**, 22, 239.
- [3] Peppel, W. J., *Ind. Eng. Chem.* **1958**, 50, 767.
- [4] For the synthesis of **MTHP**, see: Seckin, T.; Alici, B.; Cetinkaya, E.; Ozdemir, I. *J. Polym. Sci., Part A: Polym. Chem.* **1997**, 35, 2411.
- [5] Endo, T.; Nagai, D.; Tomohiro, M.; Hiroshi, Y.; Bungo, O. *Macromolecules* **2003**, submitted.
- [6] Kihara, N.; Hara, N.; Endo, T., *J. Org. Chem.* **1993**, 58, 6198.
- [7] (a) Kihara, N.; Endo, T., *Makromol. Chem.* **1992**, 193, 1481. (b) Kihara, N.; Endo, T., *Macromolecules* **1992**, 25, 4824. (c) Kihara, N.; Endo, T., *J. Chem. Soc. Chem. Commun.* **1994**, 937. (d) Kihara, N.; Endo, T., *Macromolecules* **1994**, 27, 6239.
- [8] Kihara, N., Endo, T., *J. Polym. Sci. Part A: Polym. Chem.* **1993**, 31, 2765.

NOVEL PROCESS FOR STYRENE FROM ETHYLBENZENE WITH CARBON DIOXIDE

Sang-Eon Park^a and Jong-San Chang^b

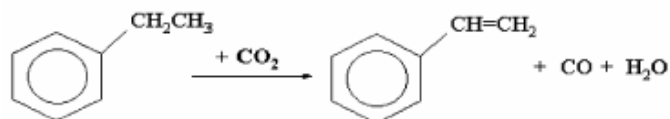
^aDepartment of Chemistry, Inha University, Incheon 402-751, Korea

^bCatalysis Center for Molecular Engineering, Korea Research Institute of Chemical Technology (KRICT), Taejeon 305-600, Korea

Introduction

The utilization of carbon dioxide, which is known as a main contributor to the greenhouse effect, has been of global interest from both fundamental and practical viewpoints in green chemistry.¹ The application of supercritical CO₂ is one of the most exciting ideas to replace volatile organic solvents in green chemistry approach.² As another way of the utilization, it is worthwhile to note that carbon dioxide can be used as an oxygen source or oxidant. It has been proposed that carbon dioxide plays a role as the soft oxidant to abstract hydrogen from simple or functionalized hydrocarbons through the catalytic activation of carbon dioxide to form CO and oxygen species.³⁻⁷

Vapor-phase dehydrogenation of ethylbenzene (EBDH) is a representative process to produce styrene (SM), an important monomer for synthetic polymers. This is one of the ten most important industrial processes. However, it is thermodynamically limited and, moreover, very energy-consuming process. As an alternative way, the oxidative dehydrogenation of ethylbenzene (EB) has been proposed to be free from thermodynamic limitation regarding conversion, operating at lower temperatures with an exothermic reaction.⁸ However, this process with use of strong oxidant, oxygen, suffers from loss of selectivity for styrene due to the production of carbon oxides and oxygenates. Recently, the utilization of carbon dioxide as an oxidant for the EBDH has been attempted to explore new technology for producing styrene selectively. We have recently developed a novel process for dehydrogenation of ethylbenzene to produce styrene using carbon dioxide as soft oxidant, so-called SODECO₂ (Styrene Production via Oxidative Dehydrogenation of Ethylbenzene with Carbon Dioxide as Soft Oxidant) process. This work deals with characteristics of this novel process.



Results and Discussion

The EBDH reaction is generally carried out in vapor phase at 600 - 650°C under steam. The important roles of steam in the industrial dehydrogenation of EB are classified as follows: providing heat to the endothermic dehydrogenation, diluting EB in order to increase equilibrium conversion, and preventing coke deposition on the catalyst.¹¹ Although steam is widely used in the EB dehydrogenation due to these beneficial roles, the use of steam has a drawback of losing latent heat of condensation during subsequent separation particularly in a mass process.^{11,12} Characteristics of steam and carbon dioxide are summarized in Table 1. It is easily presumable that carbon dioxide can play the same beneficial roles of steam mentioned above.

Table 1. Comparison of Carrier Gases for Dehydrogenation of Hydrocarbons

Characteristics	Steam	Carbon Dioxide
Function	Not oxidant Diluent	Soft oxidant Diluent
Heat capacity	Medium (37.0 J/mol·K at 673K)	High (49.1 J/mol·K at 673K)
Advantage	High selectivity Catalyst stability Coke resistance Keeping oxidation state	High selectivity Activity enhancement Equilibrium shift Cheap carrier gas
Disadvantage	Expensive diluent Highly endothermic High latent heat High operation cost	Not commercialized Endothermic Catalyst deactivation

In the case of steam as diluent, it has been pointed out that the present commercial processes require an excess of superheated steam (steam/EB = 7 - 12 mol/mol), so that they consume a large amount of latent heat of steam upon condensation at a liquid-gas separator following a reactor.⁹ Moreover, in conventional dehydrogenation units, selectivity and conversion are linked so that high conversion and high selectivity cannot be achieved simultaneously. To achieve high selectivity, conventional plants are limited to less than 70 % conversion. For overcoming these drawbacks, the ABB/UOP SMARTTM (Styrene Monomer Advanced Reheat Technology) process has been recently proposed (See http://www.uop.com/petrochemicals/processes_products/smart_sm_intro.htm). The major reactions in the process are the EBDH to styrene and the subsequent oxidation of the hydrogen produced in the first reaction. This hydrogen is reacted with oxygen over a highly selective catalyst. In the process, the removal of hydrogen from the process substantially increases single-pass EB conversions while maintaining high SM selectivity.

We propose here another process using carbon dioxide in order to solve the problems due to use of steam such as high-energy consumption and thermodynamic limitation. The main concept of this new technology is started from the utilization of carbon dioxide as the soft oxidant in oxidative catalysis. We pay attention to the possibility to utilize oxygen atoms of a carbon dioxide molecule as the oxidant to abstract hydrogen atom in dehydrogenation of hydrocarbons because the C-H bond dissociation through the hydrogen abstraction with oxygen species is generally accepted to be the rate-determining step in dehydrogenation of hydrocarbons. Thus, the main role of CO₂ in the process is illustrated to play the function of hydrogen abstraction from ethyl group of ethylbenzene, leading to the enhanced activity as well as selectivity over the catalysts that are capable of activating CO₂ to generate atomic surface oxygen.

Besides the role of CO₂, another important thing to consider for the CO₂ utilization is how to and where to bring a large amount of CO₂ with high concentration. Fortunately, there are many processes to produce CO₂ by-product with relatively high concentration in petrochemical industry, for example, gas-phase partial oxidation, reforming, etc. Based on these ideas, we propose the new process for producing styrene, so-called the SODECO₂. In addition to the above advantages, it is advantageous in the SODECO₂ process that very cheap carbon dioxide thus obtained from by-product of petrochemical oxidation or reforming process is utilized without further purification instead of using expensive steam diluent. Subsequent advantages of the process are: (1) energy saving by the replacement of steam which

SIMULTANEOUS CARBON DIOXIDE FIXATION IN THE PROCESS OF NATURAL ASTAXANTHIN PRODUCTION BY A MIXED CULTURE OF *HAEMATOCOCCUS PLUVIALIS* AND *PHAFFIA RHODOZYMA*

Qing-lin Dong; Xue-ming Zhao*

Department of Biochemical Engineering, School of Chemical Engineering & Technology, Tianjin University, Tianjin 300072, People's Republic of China. Email: xmzhao@tju.edu.cn,

Introduction

Carbon dioxide is considered as a major greenhouse gas causing the global warming problem. To find a solution, many attempts have been made through out the world, among which, biological CO₂ fixation (BCF) is thought to be an environment friendly way to remove CO₂ using microalgal photosynthesis. Up to now, microalgae biotechnologies have been practiced to convert CO₂ emitted from power plant [1] and lime production plant [2] into algal biomass. However, there still exist some problems remaining unsolved, such as lower CO₂ conversion rate, high concentration O₂ evolved in photosynthesis, which cause inhibitory effects on cell growth.

Astaxanthin is a kind of high value carotenoid (US\$2500/kg) possessing strong biological antioxidation. *Haematococcus pluvialis* and *Phaffia rhodozyma* are the two main different species of microorganisms used in the production of astaxanthin through biotechnology. *H. pluvialis* is a green alga that absorbs CO₂ and evolves O₂ in photosynthesis; While, *P. rhodozyma* is a sort of red yeast which can use a variety of organic materials as fermenting substrates, generating CO₂ and carboxylic acids[3-4], which restrain both cell growth and astaxanthin formation of the red yeast. On the contrary, O₂ is required for astaxanthin synthesis in *P. rhodozyma* fermentation [5]. However, at present, both of the two species are all cultured purely, and under this culture regime, astaxanthin production declines due to the changes of pH, CO₂ and O₂ concentrations in the media through out the culture process. In this study, the mixed culture method for *H. pluvialis* with *P. rhodozyma* was used trying to fix CO₂ released in red yeast fermentation simultaneously and also to stimulate astaxanthin production.

Materials and Methods

Microorganisms. *H. pluvialis* and *P. rhodozyma*(AS2-1557) were obtained from Institute of Hydrobiology and Institute of Microbiology, Chinese Academy of Science respectively. *H. pluvialis* was maintained at 4 °C in a liquid BBM medium; *P. rhodozyma* was maintained on a slant of yeast malt agar (YM agar, Difco) at 4 °C.

Culture Media and Conditions. The seed culture of *H. pluvialis* was prepared by transferring 5ml of the alga liquid culture into a 500ml-flask containing 100ml BBM medium (supplemented with 0.25g/l acetate). The seed culture of *P. rhodozyma* was prepared by inoculating the yeast from the fresh slant into a 500ml flask containing 100ml YM medium. Both cultures were shaken at 110 rpm in an orbital shaker (with top cool white fluorescent lamps) at 23.8 °C under light intensity 15 μmol photons/m².s for 48h. Pure cultures of *H. pluvialis* and *P. rhodozyma* were conducted by transferring 3ml seed cultures into 250ml-flasks containing 30ml culture media respectively. Mixed cultures were conducted in the same way except that the inoculum contained 1.5ml of each seed culture. The flasks were incubated under 12 μmol photons/m².s constant light intensity (adjusted to 30 μmol photons/m².s after

48h) provided by top cool white fluorescent lamps at 23.8 °C, 110rpm in a rotary shaker for 120h. Culture media were prepared from BBM by supplementing it with glucose, the glucose concentrations (g/l) were as follows: 3, 5, 10, 15, 20, 25 respectively.

Biomass Measurement (dry cell weight). 5ml samples of each culture were centrifuged at 5000rpm for 10 min, the supernatants were transferred into 50ml tubes for residual sugar and nitrogen analysis, the cell pellets were rinsed with distilled water twice, then dried in a electrical oven at 105 °C for 2h to constant weight.

Determination of Residual Sugar. Residual sugar in the culture media was quantified by DNS method.

Astaxanthin Extraction and Quantification. *H. pluvialis* pure culture and mixed culture: cells were harvested by centrifuging 5ml samples at 5000 rpm for 10 min. The supernatant was discarded, the cell pellets were re-suspended in 3ml 30%(v/v) methanol containing 5% KOH (w/v) and heated at 70 °C in a water bath for 5 min to destroy the chlorophyll. The mixture was centrifuged and the supernatant discarded, the remaining cell pellets were extracted with 2ml dimethyl sulphoxide and 5 ml acetone. All the steps were carried out in the dark. For *P. rhodozyma* pure culture, the extraction process was conducted in the same way with an exception of chlorophyll destroying step. Astaxanthin was quantified by HPLC using a 250×4.6 mm Ultrasphere C₁₈ column, the eluting solvent was ethyl acetate: methanol: water=5:18:2 (v/v/v) with a flow rate of 1 ml/min, peaks were measured at 480 nm.

Results and Discussion

Mixed cultures were compared with pure cultures of *H. pluvialis* and *P. rhodozyma* on four aspects: biomass, glucose utilization efficiency, glucose conversion rate, and astaxanthin production, just trying to find out the feasibility of combining CO₂ fixation with astaxanthin production.

Table 1. shows that the biomass concentrations of mixed cultures of *H. pluvialis* and *P. rhodozyma* were much higher than those of the two pure cultures, which were nearly the sum of the two pure cultures when glucose concentration was in the range of 3-5g/l, and increased as the glucose concentration rose. On contrast, biomass concentrations of pure cultures of *H. pluvialis* and *P. rhodozyma* decreased when glucose concentrations were higher than 10g/l and 15g/l respectively.

The reason for higher biomass production of mixed cultures may be as follow: CO₂ released through *P. rhodozyma* fermentation could be absorbed by *H. pluvialis* for photosynthesis, since the dissolved CO₂ in the culture medium is very low and could not meet the need of *H. pluvialis*, so supplementing CO₂ or sodium acetate are required. To deal with this problem, usually air or pure CO₂ were pumped into the high-cell-density microalgal cultures. In this way, however, CO₂ conversion rate is not high. While, in the mixed cultures of *H. pluvialis* and *P. rhodozyma*, CO₂ releasing and uptaking, both processes took place in the same medium, gas exchanged much easily and more efficiently. This conclusion is also confirmed by the results of glucose utilization efficiencies, as shown in Figure 1. For mixed culture and *P. rhodozyma* pure culture, glucose could be utilized totally when its concentration was below 20 g/l, but for *H. pluvialis*, glucose could not be used efficiently when the concentration was higher than 5g/l. Taking biomass concentrations and glucose conversion rates of the three cultures into account, the glucose conversion rates of mixed cultures were higher than both of the pure cultures of the two species, and lower glucose concentrations resulted in higher utilization efficiencies and conversion rates, especially when glucose concentration was between 3-5g/l (Figure 2), this is

because higher glucose concentration inhibits both *H. pluvialis* and *P. rhodozyma* growth. Therefore we can conclude that CO₂ evolved from the red yeast *P. rhodozyma* fermentation was absorbed or fixed rapidly by the green alga *H. pluvialis* in the process of photosynthesis, the highest glucose conversion rate (52.0%) was obtained by mixed culture when glucose concentration was 3g/l, which indicates, for CO₂ fixation purpose, lower glucose concentration is more favorable and fed-batch culture techniques should be employed

Table 1. Biomass production of Different Cultures.

Glucose (g/l)	Biomass production (DCW g/l)		
	Mixed culture	<i>H. pluvialis</i>	<i>P. rhodozyma</i>
3	1.56±0.01	0.54±0.04	1.12±0.13
5	2.45±0.02	0.61±0.12	1.42±0.08
10	3.32±0.35	0.69±0.47	3.22±0.07
15	4.82±0.19	0.68±0.22	5.11±0.11
20	5.32±0.31	0.65±0.11	5.08±0.02
25	5.70±0.28	0.62±0.13	5.02±0.01

Data are expressed as mean ± standard deviation of three replicates

Table 2. Astaxanthin Production of Different Cultures.

Glucose (g/l)	Volumetric astaxanthin content (mg/l)		
	Mixed culture	<i>H. pluvialis</i>	<i>P. rhodozyma</i>
3	12.95±0.11	3.68±0.16	1.09±0.03
5	8.86±0.09	2.99±0.12	1.61±0.13
10	6.50±0.15	2.34±0.17	1.95±0.11
15	5.62±0.12	2.02±0.13	2.05±0.07
20	2.15±0.08	1.96±0.04	1.51±0.02
25	2.10±0.10	1.71±0.03	1.36±0.04

Data are expressed as mean ± standard deviation of three replicates

Table 2. summarizes the astaxanthin production of different cultures. Mixed culture could remarkably promote astaxanthin production comparing with the two pure cultures, which are more than the sum of the two single cultures when glucose concentration was in the range of 3-15g/l. Maximum volumetric astaxanthin production 12.95 mg/l was obtained by mixed culture when glucose concentration was 3mg/l, which was 3.5 and 11 times that of *H. pluvialis* and *P. rhodozyma* pure cultures respectively.

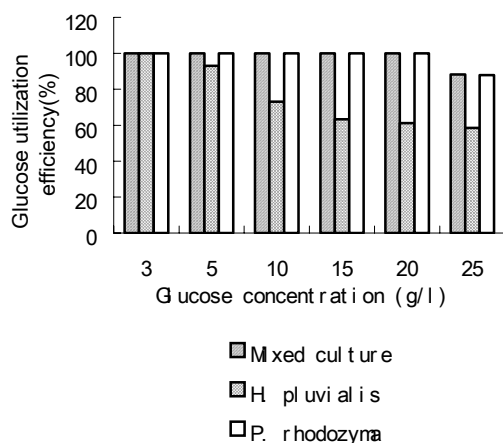


Figure 1. Glucose utilization efficiency of cultures at different glucose concentrations

The reasons for this may come from three aspects: (1) O₂ released by *H. pluvialis* in photosynthesis enhances the astaxanthin production of *P. rhodozyma*, because the conversion of carotene to astaxanthin catalyzed by β-carotene hydroxylase and β-carotene ketolase is oxygen-required, if O₂ supplying rate is under 30mmol/h, cell growth and astaxanthin production decline evidently, and astaxanthin production increases as O₂ concentration in the medium rises. (2) Considering biomass, nitrogen and glucose utilization efficiencies, under mixed culture regime, glucose and nitrogen were utilized efficiently, and higher biomass concentration was obtained so as to increase astaxanthin production. Furthermore, higher nitrogen utilization efficiency resulted in lower nitrogen concentration in the media, which is beneficial to astaxanthin formation both for *H. pluvialis* and *P. rhodozyma*. (3) pH in mixed culture keeps constant at 7.0 due to the interaction between *H. pluvialis* and *P. rhodozyma* which is more favorable for astaxanthin synthesis than pHs are 6.0, 8.0, and 9.0 for *H. pluvialis*.

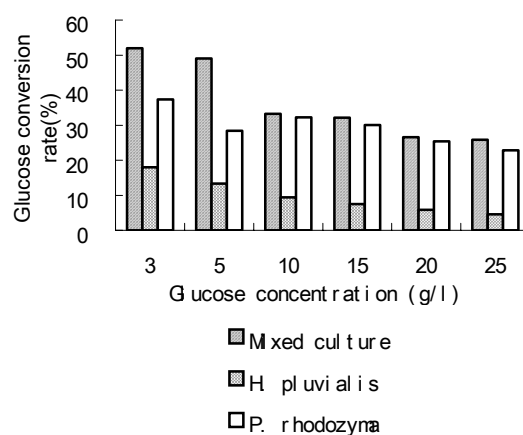


Figure 2. Glucose conversion rate of cultures at different glucose concentrations

Conclusions

Mixed culture of *H. pluvialis* and *P. rhodozyma* presents a new way for combining CO₂ fixation with high value co-product (astaxanthin) formation, promoting glucose utilization efficiency and conversion rate, keeping pH constant as well as increasing astaxanthin production. This culture regime lays a foundation for developing a new technique to put yeast or bacterium fermentation together with algae cultivation.

Acknowledgement. This project was supported by the National Natural Science Foundation of China (Grant No. 20036010).

References

- Benemann, J. R. Microalgae for greenhouse gas abatement: An international R&D opportunity. *Ambiente (Tpoint)*, **2003**, 1, 24-28
- Pulz, O. Photobioreactors: production systems for phototrophic microorganisms. *Appl. Microbiol. Biotechnol.*, **2001**, 57(3), 287-293
- Johnson, E. A.; An, G. Astaxanthin from microbial. Sources. *Crit. Rev. Biotechnol.*, **1991**, 11, 297-326
- Endang, K.; Philippe, G. Growth kinetics and astaxanthin production of *Phaffia rhodozyma* on glycerol as carbon source during batch fermentation. *Biotechnol. Lett.*, **1998**, 20(10), 929-934
- Johnson, E. A.; Lewis, M. J. Astaxanthin formation by the yeast *Phaffia rhodozyma*. *J. Gen. Microbiol.*, **1979**, 115, 173-183

COMPARATIVE STUDIES ON THE PERFORMANCE OF IMMOBILIZED QUATERNARY AMMONIUM SALT CATALYSTS FOR THE ADDITION OF CARBON DIOXIDE TO GLYCIDYL METHACRYLATE

Dae-Won Park, Eun-Seon Jeong, Byung-Soo Yu, Il Kim,
Kwang-Joong Oh, Sang-Wook Park

Division of Chemical Engineering, Pusan National University, Pusan
609-735, Korea

Introduction

Quaternary onium salts are widely used as phase transfer catalysts in the field of organic synthesis [1]. The quaternary onium salts bounded to polymer resins have been reported by several authors [2]. Most published works on resin-bound quaternary onium salts use styrene-divinylbenzene related resins because large amount of technology is available on these resins due to their use as ion-exchange resin support. The polymer-supported catalysts can be easily separated from reaction mixtures and can be reused, or they can be used in flow systems such as fixed-bed and fluidized-bed reactors. However, the polymer-supported catalysts have yet some drawbacks such as diffusion limitations, high cost, tendency to swell, mechanical and thermal instability. Several inorganic supports, involving metal oxides, zeolites and clays have been substituted for polymers. Clay material has high physical strength and chemical resistance towards acid and alkali treatment [3]. Montmorillonite is one of the most widely used support for immobilized and anchored catalysts [4]. It is naturally abundant material and available as inexpensive material. Since the discovery of ordered mesoporous silica [5], there have been continuous efforts to improve their stability and catalytic performance. Recently, the incorporation of 3-chloro propyl methyl substituents on MCM-41 was reported [6].

In our previous work [7], we reported the synthesis of 4-(phenoxymethyl)-1,3-dioxane-2-one (PMEC) from CO₂ and phenyl glycidyl ether (PGE) using immobilized quaternary salt catalysts. In the present study, we studied the addition of carbon dioxide to glycidyl methacrylate (GMA). We prepared five differently supported quaternary ammonium salt catalysts to facilitate their separation after reaction. The different supports are (1) soluble poly(ST-co-VBC), C1 (2) insoluble poly(ST-DVB-VBC), C2 (3) macroporous poly(ST-DVB-VBC), C3 (4) poly(ST-co-VBC)-MMT, C4 (5) MCM-41, C5. A kinetic study on the reaction with the supported catalysts was also carried out in a semi-batch reactor with a continuous supply of carbon dioxide into the reactor.

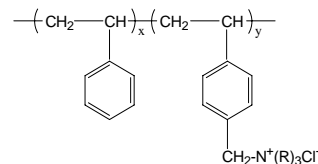
Experimentals

The soluble polymer-supported quaternary ammonium catalysts were prepared as shown in Scheme 1. The synthesis of poly(ST-co-VBC) was carried out by the radical copolymerization of vinylbenzyl chloride(VBC) with styrene(ST) using 2,2'-azobis(isobutyronitrile) [AIBN] as an initiator in toluene at 60 °C for 5 h and then at 80 °C for 2 h under nitrogen, followed by precipitation into methanol and two reprecipitations from tetrahydrofuran(THF) solution into methanol. The addition of the obtained polymer(10mmol) with 15mmol of trialkylamine was performed in 15 mL of dimethylformamide(DMF) at 80 °C for 48 h. The resulting polymer was purified by reprecipitating twice from methanol solution into ethyl ether, and dried at 50 °C under vacuum.

Insoluble poly(ST-DVB-VBC) catalyst were prepared as shown in Scheme 2. A solution of gelatin(1.0 g) and 0.6 mL of 0.1% methylene blue in 100 g of water was added to a 500 mL four-neck

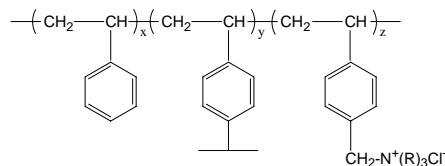
flask fitted with a reflux condenser. A mixture of 14.6 g of ST, 0.4 g of DVB, and 0.1 g of AIBN was added dropwise to the aqueous solution. The solution was partially polymerized at 70 °C for 4 h. Then 5.0 g of VBC was added slowly with vigorous stirring (600rpm). The mixture charged with VBC was polymerized again for 17 h at 70 °C. The obtained polymer support was washed 3 times by stirring in refluxing methanol. After vacuum drying, the polymer support was placed in toluene, and trialkylamine was added to the solution.

The macroporous polystyrene beads were prepared using the same method of synthesis poly(ST-DVB-VBC). Isooctylalcohol was just added to the mixture of ST and DVB solution. The obtained polymer support was extracted by methanol to remove isooctylalcohol. After vacuum drying, trialkylamine was attached to the polymer support.



R : trialkylamine

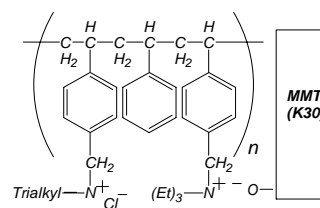
Scheme 1



R : trialkylamine

Scheme 2

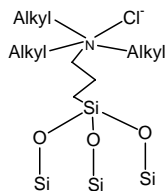
Insoluble poly(ST-co-VBC)-MMT supported catalysts are prepared as shown in Scheme 3. Poly(ST-co-VBC) was dissolved in acetone and treated with 2% trialkylamine by stirring overnight at room temperature to obtain a polymeric ammonium salt. A suspension of MMT in water was stirred overnight, and then a solution of the polymeric ammonium salt in acetone was added dropwise and stirring was continued for 24 h at room temperature. The white precipitate product was filtered, washed with acetone several times and dried at 100 °C under vacuum to give the ST-VBC-MMT intercalate. The quaternization was carried out with tributylamine to produce the final poly(ST-co-VBC)-MMT supported catalyst.



Scheme 3

Organically modified MCM-41 materials were synthesized according to a previous report[6] using a mixture of 3-chloropropyl-dimethoxymethyl silane (CIPDMS, Shin-etsu Chemicals) and tetraethyl orthosilicate (TEOS, TCI) as Si sources.

Cetyltrimethylammonium bromide (CTMABr, TCI) was used as a template and tetra-methylammonium hydroxide (25% aqueous TMAOH, Aldrich) was used to provide alkalinity of the medium. A typical molar ratio of the various constituents in the synthesis mixture was: 4.0 TEOS : 1.5 CIPDMMS : 1.25 C₁₆TMABr : 2.5 TMA-OH : 300 H₂O. The quaternization of the 3-chloropropyl methyl modified MCM-41 was performed by the same procedure used for the other supported catalysts.



Scheme 4

Results and Discussion

The amount of quaternary ammonium salt bound to the different supports was analyzed by an elemental analyzer (Vario EL), and the results are shown in Table 1.

Table 1. The attached amount of benzyltributylammonium chloride to the supports.

Support	C1 ⁽¹⁾	C2 ⁽²⁾	C3 ⁽³⁾	C4 ⁽⁴⁾	C5 ⁽⁵⁾
Attached amount (mmol/g)	0.894	1.087	1.326	2.200	1.720

(1) mole ratio of ST/VBC = 90/10

(2) weight ratio of ST/DVB/VBC = 73/2/25

(3) isooctylalcohol 30wt%

(4) mole ratio of ST/VBC = 30/70

(5) mole ratio of TEOS/CIPDMMS = 4/1.5

In order to study the catalytic activity of the different types of supported catalysts, the addition reaction of GMA and CO₂ was performed with the catalysts of equal amount of attached quaternary ammonium salts. Therefore, 0.2 mmol of pendant benzyltributylammonium bromide residues was used with 20 mmol of GMA. We can consider time variant conversion of GMA with different types of catalysts. The soluble poly(ST-co-VBC) supported catalyst, showed the highest conversion of GMA. However, this catalyst has a drawback of separation after reaction, since it needs another precipitation step for the reuse of the catalyst. Macroporous poly(ST-DVB-VBC) catalyst showed higher GMA conversion than poly(ST-DVB-VBC). Macroporous structure seems to favor the diffusion of GMA to the active site. And poly(ST-co-VBC)-MMT supported catalyst showed higher GMA conversion than Cl-propylmethyl-MCM-41 catalyst

For the addition reaction of CO₂ with GMA using immobilized catalysts, the following elementary reaction steps can be proposed, where we set R=GMA, P=DOMA, and QX=supported quaternary ammonium salt catalyst.



k₁, k₂ and k₃ are reaction rate constants. The rate of formation of P can be written as

$$dP/dt = k_3[CO_2][RQX^*] \quad (3)$$

The active intermediate RQX* has a very short lifetime because of its high reactivity, therefore, pseudo steady state approximation can be applied. Since the addition reaction of CO₂ with GMA is carried out in a semi-batch reactor with a constant flow of CO₂, the concentration of GMA varies only because the concentration of dissolved CO₂ in solvent can be assumed constant.

$$dP/dt = k'[R][QX] \quad (4)$$

where k' is k₁k₃[CO₂] / (k₂ + k₃[CO₂]). Since the catalyst concentration does not change during the reaction, the pseudo first-order rate equation can be applied.

$$\ln([GMA]_0/[GMA]) = kt \quad (5)$$

From the slope of the linear plot between ln([GMA]₀/[GMA]) vs. time, one can estimate the pseudo first-order rate constant k. The results are summarized in Table 2. Soluble poly(ST-co-VBC) supported quaternary ammonium salt showed the highest reaction rate constants and the lowest activation energy.

The stability of the catalysts was tested by reusing them four successive times after separation from the reaction mixture at each experimental run. Insoluble catalysts were easily separated. However, the soluble poly(ST-co-VBC) was separated by precipitation in diethylether. All the catalysts maintained their catalytic activities showing less than 12 % loss of initial activity after 4th runs. Surface analysis of the used catalysts by energy dispersive spectroscopy (EDS, Jeol JXA-8600) confirmed the maintenance of chloride group bound to the polymer support after 4th run.

Table 2. First-order reaction rate constant(k) and activation energy(E) for different catalysts

Temp. (°C)	Rate constant k (h ⁻¹)				
	C1	C2	C3	C4	C5
80	0.383	0.111	0.137	0.067	0.051
90	0.410	0.150	0.179	0.113	0.094
100	0.485	0.210	0.208	0.169	0.144
110	0.504	0.235	0.245	0.218	0.196
E (kJ/mol)	10.31	28.14	20.79	44.09	50.56

Acknowledgement

This work was supported by the Korea Science and Engineering Foundation (R01-2003-000-10020-0), and by the Brain Korea 21 and Brain Busan 21 project.

References

1. Starks, C. M., Liotta, C. L. and Halpern, M. "Phase Transfer Catalysis", Chapman & Hall, New York (1994).
2. Akelah, A. and Moet, A. "Functionalized Polymers and Their Applications", Chapman & Hall, London (1990).
3. Akelah, A., Rehab, A., Selim, A. and Agag, T. *J. Mol. Catal.* 94 (1994) 311.
4. Moronta, A., Ferrer, V., Quero, J., Arteaga, G. and Choren, E. *Appl. Catal. A: Gen.* 230 (2002) 127.
5. Kresge, C. T., Leonowicz, M. E., Roth, W. J., Vartuli, J. C. and Beck, J. S. *Nature* 359 (1992) 710.
6. Bhaumik, A. and Tatsumi, T. *Catal. Lett.* 66 (2000) 181.
7. Yu, B. S., Shin, D. H., Lee, H. S., Park, S. W. and Park, D. W. *ACS Symp.* 226, Preprint of Div. Environ. Chem. 43(2) (2003) 159.

ENZYMATIC CONVERSION OF CO₂ TO METHANOL: EFFECTS OF MODIFICATION OF SILICA GEL AND ADH ON ENZYME ACTIVITY

Hong Wu, Shufang Huang, and Zhongyi Jiang

School of Chemical Engineering and Technology
Tianjin University
Tianjin 300072
P.R.China

Introduction

CO₂ can be converted to methanol through an enzymatic approach in the following three steps:



F_{ate}DH, F_{ald}DH and ADH are formate dehydrogenase, formaldehyde dehydrogenase and alcohol dehydrogenase respectively and are co-encapsulated in a silica gel formed by sol-gel process. Reduced nicotinamide adenine dinucleotide (NADH) is used as a terminal electron donor for each reduction step.^{1,2} To understand the whole process more clearly and get the optimized results, the above three reactions are studied separately. In this paper, we concentrate on the third one.

Immobilized enzyme has advantages over free enzyme such as easy separation and reusability. However, most immobilized enzymes show lower activities than that of the free enzymes. Lower productions were also found in our study where the enzymes were immobilized in silica matrix by sol-gel process.¹ This may be due to the diffusion hindrance of the substrate from bulk solution to the gel, the accessibility hindrance of the immobilized enzyme in the three-dimensional silicate network and the microenvironment for the enzymes.

Herein, an improved sol-gel method using polyethylene glycol (PEG) as a multifunctional agent and an enzyme modification method using methoxypolyethylene glycol (mPEG) as a modifier are reported. Larger pore size and more flexible structure of the gel are expected by using the first method while more suitable microenvironment for enzyme is expected by using the second method. Mainly due to their hydrophilicity, linear structure and biocompatibility, PEG and mPEG are selected as modifiers. Modified gel properties were characterized by BET and IR and were compared with unmodified gel. Enzyme (ADH) activities after modification were investigated and compared with unmodified ones by kinetic studies of the conversion reaction of HCHO to CH₃OH.

Experimental

Synthesis of mPEG-modified ADH. 3.5 mg ADH and 10.5 mg activated mPEG were dissolved in 5 mL of 0.1 M phosphate buffer (pH7.0) and the solution was kept gently stirring for 2 h under room temperature. The degree of modification was 90% determined by using trinitrobenzene sulphonic acid (TNBS) to react with the unPEGylated amino groups and measuring the amount of the product that has a characteristic adsorption at 420nm detected by an UV-visible spectrophotometer (U-2800, Hitachi).

Preparation of gel and immobilization of ADH. The improved sol-gel immobilization processes are illustrated in **Figure 1**. It involves two ways: (1) immobilization of enzyme in modified gels and (2) immobilization of chemical modified enzymes in typical gels. For (1), mix tetraethylorthosilicate (TEOS), the precursor, with HCl, the catalyst, and PEG600 (MW=600), the gel-modifier, together first, then regulate the pH of the solution to 7.0 by adding NaOH solution

to form the modified sol, and finally add a certain amount of enzyme-containing (3.5 mg/ml) 0.01 M phosphate buffer solution (pH7.0) to the sol. A transparent enzyme-containing gel was formed shortly. For (2), mix TEOS with HCl first, then regulate the pH of the solution to 7.0 by adding NaOH solution to form a typical sol, and add a certain amount of mPEG-modified enzyme-containing phosphate buffer solution to the sol. A transparent modified enzyme-containing gel was formed shortly. The gels prepared by the above two ways were aged at 4°C for 7 days. The aged enzyme-containing gel was put into a dialysis membrane bag, dipped into 0.1 M phosphate buffer solution (pH7.0), and kept at 4°C with frequent change of the buffer until there is no alcohol was detected by Gas Chromatographer (HP6890, Agilent). The pore size of the gel and its chemical structure were measured by BET (CHEMBET-3000, QUZNTA CHROME) and IR (Nicolet-560, MAGNA-IR) respectively.

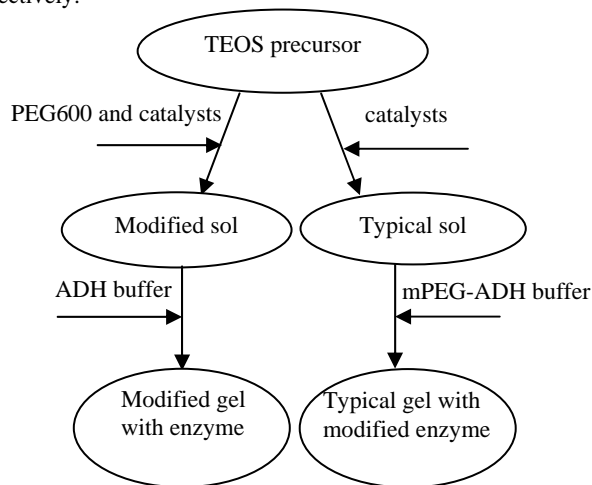


Figure 1. Sol-gel immobilization processes.

Enzymatic reactions. Enzyme activities of ADH were evaluated based on the reaction rates and kinetic Michaelis constants (K_m) of the reduction of HCHO to CH₃OH. Since, during the reaction, the cofactor (NADH), which has a characteristic adsorption at 340 nm, will be converted to NAD⁺ that has no adsorption at 340 nm, the reaction progress can be recorded by the detection of the amount of NADH. A UV-visible spectrophotometer (U-2800, Hitachi) was employed to determine the reduction of the concentration of NADH and the reaction rates were calculated accordingly. At 25 °C and pH7.0, by varying the concentration of NADH from 50 to 250 μM and HCHO from 3 to 30 mM, kinetic parameters were obtained based on the ordered mechanism proposed by Dalziel.³

Results and Discussion

Structure characterization of gels. The pore size distribution of typical gel and PEG-modified gel are given in **Figure 2**. The average pore size of PEG-modified gel (4.67nm) is larger than that of the typical gel (3.88nm). This is due to the linking function of the PEG between sol particles, resulting in a branched structure with larger mesopores. The infrared spectra of the PEG-modified gels (**Figure 3**) show no new bonds formed, indicating that the linkage between PEG and silica sol particles was by molecular forces or hydrogen bonds.

Stability of free ADH and mPEG-modified ADH in alcohol. The sol-gel process using TEOS as the precursor will produce ethanol

that is harmful for enzyme. The alcohol toleration of both native and mPEG-modified ADH were studied by measuring their reacting activities of free enzymes. After being immersed in 1% ethanol solution for 2 minutes, the mPEG-modified ADH maintained 50% of its original activity, while the native ADH retained 36% of its original one. This denotes that such chemical modification of ADH by mPEG is a valid and significant means of stabilizing ADH in alcohol solutions. This may be due to the less flexibility of the enzyme with a long-chain PEG molecule linked to its surface, leading to steric hindrance of protein unfolding. And also, the hydrophilicity of PEG may provide a more hydrophilic microenvironment that is more preferable for enzyme to stay and function.

$$\frac{V_p}{\Delta r_p} \times 10^2 (\text{cm}^3 \cdot \text{nm}^{-1} \cdot \text{g}^{-1})$$

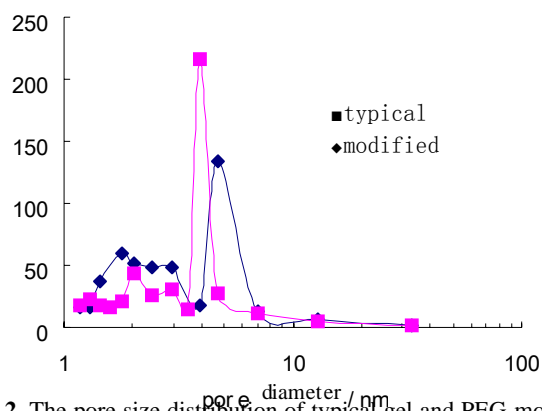


Figure 2. The pore size distribution of typical gel and PEG-modified gel.

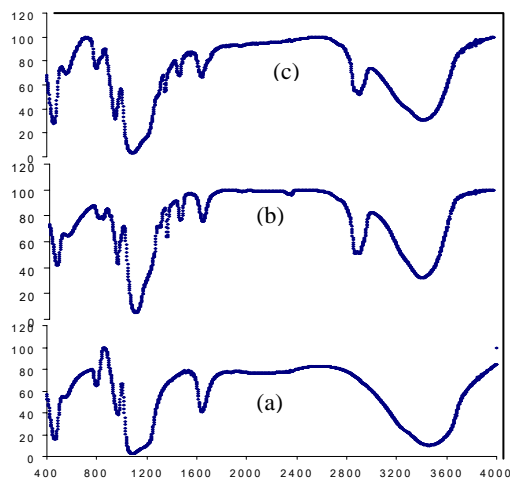


Figure 3. The infrared spectra of (a) typical gel; (b) PEG-modified gel and (c) mPEG-containing gel.

Storage stability of immobilized ADH. As shown in **Figure 4**, the activity of the native ADH encapsulated in typical silica gel was reduced by 17% after 92 days of storage. In contrast, the enzyme activities of ADH in PEG-modified gel and mPEG-modified ADH in typical gel almost showed no decrease after storage for the same period. This may be due to the same reasons mentioned above.

Kinetic parameters. Experimental results showed that all the enzymatic reactions followed Michaelis-Menten kinetics and the kinetic parameters were calculated by Dalziel's double-substrate

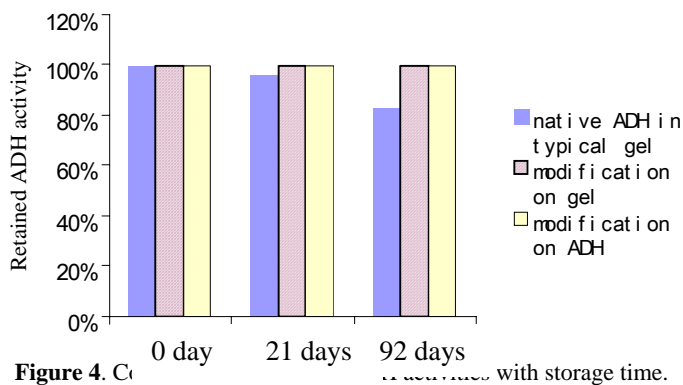


Figure 4. Comparison of retained ADH activity with storage time.

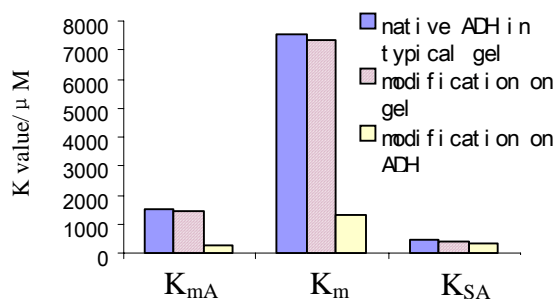


Figure 5. The kinetic Michaelis constants of reactions catalyzed by ADH.

model. Kinetic constants were shown and compared in **Figure 5**. K_{mA} is the Michaelis constant of NADH, while K_{mB} the Michaelis constant of HCHO and K_{SA} the dissociation constant of ADH-NADH pairs. The lower the K_m is, the higher activity the immobilized ADH is. Compared with the unmodified ADH in unmodified gel, both of the two improvement methods work. The mPEG-modified ADH encapsulated in typical gel showed the highest activity among the three cases, indicating that the modification on ADH (improvement method (2)) seems to have a greater effect than the modification on gel (improvement method (1)).

The catalytic activity of ADH immobilized in PEG-modified gel is higher than that in typical gel. This may mainly be attributed to the easier diffusion resulted from the enlarged pore size. These enlarged pores are considered to be more “comfortable” for enzymes to stay and also easier for substrate to diffuse through the pore channel and access to the enzymes. In addition, the improved gel properties such as hydrophilicity and mechanical strength may also provide higher biocompatibility for enzymes.

Acknowledgment

This work was supported by the National Natural Science Foundation of China (No.20176039).

References

1. Obert, R., Dave, B. C., *J. Am. Chem. Soc.*, **1999**, *121*, 12192-3.
2. Wu, H., Jiang, Z. Y., Xu, S. W., Huang, S. F., *Chinese Chemical Letters*, **2003**, *14*(4): p. 423-5.
3. Dalziel, K., *The Journal of Biological Chemical*, **1963**, *238*(8), 2850-3.

SELECTIVE FORMATION OF ETHYLENE FROM CO₂ BY CATALYTIC ELECTROLYSIS AT A THREE-PHASE INTERFACE

Kotaro Ogura, Hiroshi Yano, and Takayasu Tanaka

Department of Applied Chemistry, Yamaguchi University,
Tokiwadai, Ube 755-8611, Japan

Introduction

Chemical conversion of CO₂ to fuels or chemicals is a challenging subject for chemists in connection with the mitigation of greenhouse effect and the carbon resource after the exhaustion of petroleum. Several methods for chemically converting CO₂ have been proposed: e.g., hydrogenation over heterogeneous catalyst at high temperature or in supercritical conditions, electrochemical and photochemical reduction. CO₂ conversion should be achieved with the aid of low input energy and products be highly valuable so that the conversion process may be feasible without accompanying the secondary generation of CO₂. Hence, the most desirable process is an artificial photosynthesis in which CO₂ is convertible to valuable substances with a solar cell as the energy source at room temperature. To attain such a process, we have developed the catalytic electrolysis process in which CO₂ is converted selectively to ethylene at room temperature.¹⁻⁴ The conversion reaction takes place at the three-phase (gas/liquid/solid) interface on a Cu(I) halide-confined Cu-mesh electrode.

Experimental

The electrolysis cell used is described elsewhere.¹ The three-phase interface was constructed on a pure copper-mesh (purity 99.99%, 50 mesh, Nilaco Co.) which was fixed along with a glass filter (average pore size, 20 μm) at the bottom of a cathode compartment. The electrolytic solution was prevented from dropping by the glass filter. The solution surface was forced up by the pressure of CO₂ blown up from the lower part, and the electrolyte meniscus was extended on the copper mesh. Thus, the three-phase zone consisting of gas, liquid and solid was built, and electrochemical reactions took place predominantly in this zone. The copper-mesh put on the glass filter was bound to a Teflon cylinder tightened with a Teflon cap. The cylinder with the copper-mesh was attached to the cathode compartment via an O-ring, which was separated from an anode compartment by a cation-exchange membrane (Selemion CMV 10, Asahi Glass Co.). The purified CO₂ gas was circulated via the cathode compartment with a circulating pump. The three-phase provided on the Cu-mesh electrode was sustained during the electrolysis by adjusting the rate of CO₂. The net surface area of the Cu-mesh was 10.2 cm².

Copper-mesh electrode was modified by CuCl, CuBr and CuI. Before this work, the Cu-mesh electrode was immersed in a concentrated HCl solution to remove Cu oxide, and washed with doubly distilled water. The modification of copper(I) halides was done by the application of electric charge of 220C at a constant potential of +0.4V vs Ag/AgCl in a 0.1M HCl and a 0.5M KBr solution (pH 3) or by passing the electric charge of 20C at +0.2V in a 0.5M KI solution of pH 3. The thickness of CuCl, CuBr and CuI films thus obtained were 7.8, 9.5 and 7.5 μm, respectively. The film thickness was measured with a field emission scanning electron microscope (FE-SEM, Horiba EMAX-7000). The electrolysis of CO₂ was performed by the galvanostatic method. Various amounts of electric charge were applied with a constant current (usually 250mA) by changing the electrolysis time. Platinum or copper gauze with a

large surface area and an Ag/AgCl/saturated KCl electrode were used as the anode and reference electrodes, respectively. The electrolytes mainly used were 3M or 4M KCl, KBr and KI solutions of pH 3. The change in pH of catholyte during the electrolysis was monitored with a pH controller (NPH-660NDE, Nissin Co.). The electrolyte in the anode compartment was a 0.5M KHSO₄ solution of pH 0. In some experiments, a concentrated solution of sulfuric acid was added to the anode compartment between times during the electrolysis in order to indirectly lower the pH of the catholyte.

A Shimadzu GC-8AIT and a GC-8AIF gas chromatograph with a Porapak N column and an active carbon or alumina column were used for the determination of gaseous samples. Aqueous samples were analyzed with a Shimadzu organic analyzer (LS-10AD type) and a Shimadzu GC-MS spectrometer. The electrochemically deposited copper halides were characterized with an X-ray diffractometer (Shimadzu XD-D1), and the XRD patterns were recorded with X-ray line of Cu-Kα (30kV, 30mA).

Results and Discussion

The electrolysis of CO₂ was performed at the three-phase interface on a copper(I) halides-confined Cu-mesh electrode in a potassium halide solution. In **Figure 1**, the conversion percentage of CO₂ obtained with a CuBr-confined Cu-mesh electrode in a KBr solution of pH 3 is shown versus the applied amount of electric charge. The CO₂ conversion increases with increasing the amount of electric charge until about 4500C, but beyond this amount the conversion percentage approximates a constant value of 68%. As seen from this figure, however, the conversion continues to increase when the pH of the catholyte was lowered by adding a concentrated solution of sulfuric acid to the anolyte between times during the electrolysis, and the conversion percentage reached 88% at the electric charge of 8928C. Hence, it is suggested that the approach of the conversion percentage to the constant value in the electrolysis charged with more than 4500C is attributed to the deficiency of proton concentration for the CO₂ reduction, which is discussed below.

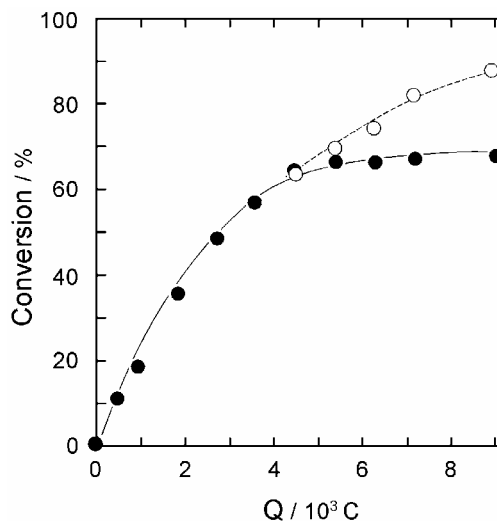


Figure 1. Plot of the conversion percentage of CO₂ versus the applied amount of electric charge in a 4 M KBr solution. The reduction of CO₂ was performed with a CuBr-confined Cu-mesh electrode at a constant current of 250 mA. The pH of the catholyte was lowered by adding a H₂SO₄ solution between times to the anolyte: ---○---, and such a pH-controlling was not given: —●—. The area of a copper-mesh substrate, 10.2 cm²; initial volume of CO₂, 577 cm³.

Table 1 Current efficiencies for the products obtained with a CuBr-confined Cu-mesh electrode in the galvanostatic reduction of CO₂^{a)}

Run	Q ^{b)}	Potential ^{c)}	pH ^{d)}	Current efficiency / %									Conv. ^{e)}	Selec. ^{f)}	η ^{g)}
	C	V	-	Ethylene	Methane	CO	Ethane	Ethanol	Formic ^{h)}	Acetic ⁱ⁾	Lactic ^{j)}	H ₂	%	%	%
1	453	-2.08 ~ -1.98	2.93	72.4	6.2	5.9	0.6	2.1	1.8	1.7	0.3	15.9	11.5	68.6	107
2	903	-2.10 ~ -1.93	2.69	62.5	5.9	4.6	0.6	1.1	1.3	1.2	0.1	21.0	19.0	71.0	98
3	2699	-2.10 ~ -1.92	2.75	48.2	2.2	5.2	0.5	1.0	2.0	1.1	0.2	13.4	48.9	64.3	74
4	4483	-2.08 ~ -1.89	3.78	39.2	1.0	4.0	0.4	0.6	2.9	0.3	0.0	10.6	66.3	63.2	59
4 ^{k)}	4500	-2.12 ~ -1.87	2.09	40.7	1.2	2.7	0.3	0.3	2.8	0.3	0.0	10.6	63.3	68.8	59
5	7157	-2.18 ~ -1.89	5.01	25.9	0.8	1.9	0.2	0.3	2.3	0.3	0.0	7.3	67.9	64.1	39
5 ^{k)}	7160	-2.13 ~ -1.89	2.32	33.3	0.9	2.8	0.2	0.3	2.1	0.4	0.0	7.1	81.9	69.1	47
6	8981	-2.15 ~ -1.88	6.14	21.0	0.4	1.5	0.6	0.2	1.7	0.2	0.0	9.9	68.6	65.6	36
6 ^{k)}	8928	-2.12 ~ -1.91	2.17	30.4	0.7	1.5	0.3	0.3	1.5	0.5	0.0	6.1	87.7	74.0	41

a) Electrolyte, 4M KBr, initial pH, 3.0; the apparent area of a copper-mesh surface, 10.2 cm²; the thickness of confined CuBr film, 7.9 μm; applied current, 250 mA; initial volume of CO₂, 577 cm³; catholyte, 232 cm³; Anode, copper net; anolyte, a 0.5M KHSO₄ solution of pH 0. Cathode and anode compartments were separated by a cation-exchange membrane.

b) Amount of the electric charge applied in the electrolysis. This value was varied by changing the electrolysis time under the galvanostatic condition. C: coulomb (=ampere×sec)

c) Change in electrode potential (vs. Ag/AgCl) during the galvanostatic reduction.

d) Final pH of the catholyte. e) Conversion percentage of CO₂.

f) Selectivity for the formation of ethylene on the basis of carbon content.

g) Total current efficiency in the reduction. h) formic acid. i) acetic acid. j) lactic acid.

k) A concentrated solution of sulfuric acid was added to the KHSO₄ solution in the anode compartment between times during the electrolysis in order to indirectly lower the pH of the catholyte.

The major gases generated in the electroreduction of CO₂ were C₂H₄, CO and H₂, and their current efficiencies are plotted versus the applied amount of electric charge in **Figure 2**. The current efficiency for C₂H₄ decreases with an increase of amount of electric charge, but it still maintains more than 20% even at the electric care of 8900C. This current efficiency was risen to be 30% at the same electric charge when the pH of the catholyte was lowered by controlling the pH of the anolyte.

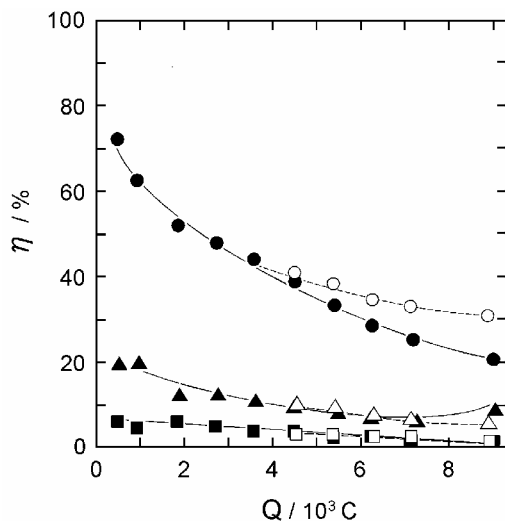


Figure 2. Plot of the current efficiencies for C₂H₄ (○, ●), CO (□, ■), and H₂ (△, ▲) versus the applied amount of electric charge. A H₂SO₄ solution was added to the anolyte: ---○---, ---△---, ---□---, and not: —●—, —▲—, —■—. The experimental conditions were the same as those given in Figure 1.

The detailed distribution of the products is exhibited in **Table 1**. The electrolysis was performed for a given period of time by applying a constant current of 250mA, and the electrode potential was -2.1V~-1.9V vs Ag/AgCl. The major gaseous products were C₂H₄ and CO, the formation of CH₄ was negligible, and the current efficiencies of liquid products were very low except that of formic acid in the prolonged electrolysis. In the electrolysis of Run

1~6 without adjusting the pH of the catholyte, the pH rose as the amount of electric charge was increased, and it became 6.14 after the electrolysis charged with 8981C (Run 6). On the other hand, in Run 4^k~6^k, the pH of the catholyte was adjusted to around 2.2 by adding a H₂SO₄ solution to the anolyte. As compared with the former results, the conversion percentage of CO₂ and the current efficiency for C₂H₄ were always enhanced, i.e., compare between the results of Run 4 and 4^k, 5 and 5^k, and 6 and 6^k. This means obviously that the concentration of protons in the catholyte is insufficient for the efficient reduction of CO₂ in the former case. It is noted that such a high current efficiency and a conversion percentage were brought about by adjusting the pH of the catholyte not directly but through the proton transport from the anode compartment. The current efficiency and conversion percentage were both considerably decreased when the pH of the catholyte was directly controlled by adding strong acid. This is probably caused by the transformation of an interfacial structure of the three-phase zone including adsorbed intermediates. Interestingly, the current efficiency for hydrogen evolution was smaller in the catholyte of which pH was suppressed low compared to that in the catholyte without pH-controlling. The selectivity for the formation of C₂H₄ estimated on the basis of carbon content was 74% at the applied electric charge of 8928C. The selective conversion of CO₂ to C₂H₄ is attributed to the immobilized CuX which operates as a heterogeneous catalyst by offering adsorption sites for reduction intermediates such as CO and methylene radicals.³ A part of CuX is reduced to Cu (CuX + e⁻ → Cu + X⁻) simultaneously with the reduction of CO₂, but new copper(I) halide is always formed on the Cu-mesh electrode by the reduction (Cu²⁺ + X⁻ + e⁻ → CuX) of Cu²⁺ ions which are afforded through the cation-exchange membrane from the anode compartment. Therefore, the electrochemical conversion of CO₂ continue to proceed via the catalysis reactions involving CuX.

References

- 1) H. Yano, F. Shirai, M. Nakayama, and K. Ogura, *J. Electroanal. Chem.*, 519, 93 (2002).
- 2) K. Ogura, *Electrochemistry*, 71, 676 (2003).
- 3) K. Ogura, H. Yano, and F. Shirai, *J. Electrochem. Soc.*, 150, D163 (2003).
- 4) H. Yano, T. Tanaka, M. Nakayama, and K. Ogura, *J. Electroanal. Chem.*, in press.

USE OF IMIDAZOLIUM TRANSITION METAL HALIDES IN THE SYNTHESIS OF CYCLIC CARBONATES FROM THE COUPLING REACTION OF EPOXIDE AND CO₂

Hoon Sik Kim, O-Sung Kwon, Hyunjoon Lee and Jelliarko Palgunadi

Reaction Media Research Center
Korea Institute of Science and Technology
39-1, Hawolgokdong, Seongbukgu,
Seoul, 136-791, Korea

Introduction

The synthesis of cyclic carbonates by the coupling reactions of epoxides with carbon dioxide has attracted much attention with regard to the utilization of CO₂, which is a responsible for global warming.¹ The importance of cyclic carbonates is increased due to their versatile utilization in many application areas. For instance, they can be used as aprotic polar solvents, electrolytes in secondary and fuel-cell batteries, and valuable raw materials in a wide range of chemical reactions.^{2,3} Accordingly, much efforts have been made on the catalyst development for the synthesis of cyclic carbonates *via* coupling reactions has been reported.⁴ While the advances have been significant, there still remain many subjects to be improved in terms of catalytic activity, stability, and recovery of catalyst.

Recently, there have been a considerable number of articles regarding the use of ionic liquids as environmentally benign media in separation, extractions, electrochemistry, and immobilization of homogeneous catalysts.⁵ Imidazolium-based ionic liquids have also been introduced as effective catalysts for the synthesis of propylene carbonate from the coupling reaction of propylene oxide and CO₂, but their catalytic activities were not high enough for the industrial purpose.⁶

With a hope to develop highly active catalysts for the coupling reactions, we have imidazolium metal halide complexes and tested their activities for the production of cyclic carbonates from the coupling reactions of epoxides and CO₂. Herein, we report the synthesis and reactivity of a series of ionic liquid-derived imidazolium metal halide complexes consisting of 1-alkyl-3-methylimidazolium cations and metal halide anion.

Experimental

Synthesis of (1,3-dimethylimidazolium)₂ZnBr₂Cl₂. A solution of (1,3-dimethylimidazolium)Cl⁷ (2.10 g, 15.83 mmol) in methylene chloride (25 mL) was mixed with a solution of ZnBr₂ (1.78 g, 7.90 mmol) in tetrahydrofuran (25 mL) and heated to reflux for 3 h. After cooling to room temperature, the white precipitate was collected by filtration. Yield: 93.9 %; elemental analysis calcd.(%) for C₁₀H₁₈Br₂Cl₂N₄Zn: C 24.49, H 3.70, Br 32.59, Cl 14.46, N 11.43, Zn 13.33; found: C 24.23, H 3.75, Br 31.83, Cl 14.18, N 11.18, Zn 13.43;

All other imidazolium metal halides were similarly prepared.

Coupling reactions of epoxide and CO₂. The coupling reactions were conducted in a 200 mL stainless-steel bomb reactor equipped with a magnetic stir bar and an electrical heater. The reactor was charged with an appropriate catalyst and an epoxide and pressurized with CO₂. The bomb was then heated to a specified reaction temperature with the addition of CO₂ from a reservoir tank to maintain a constant pressure. After the reaction, the bomb was cooled down to room temperature, and the product mixture was analyzed by Hewlett Packard 6890 gas chromatography equipped with a flame ionized detector and a DB-wax column, and Hewlett Packard 6890-5973 MSD GC-mass spectrometry.

Results and Discussion

As shown in equation (1), a series of imidazolium metal halides, (1-R-3-methylimidazolium)_bMX_aY_b (M = Zn, Fe, Mn, In; R = CH₃, C₂H₅, *n*-C₄H₉, CH₂C₆H₅; X, Y = Cl, Br; a, b = 2, 3) were prepared by reacting MX_a (X = Cl, Br) with (1-R-3-methylimidazolium)Y (R = CH₃, C₂H₅, *n*-C₄H₉, CH₂C₆H₅; Y = Cl, Br) at an ambient temperature or at reflux depending on the nature of halide groups.



R = CH₃, C₂H₅, *n*-C₄H₉, CH₂C₆H₅; X, Y = Cl, Br; a, b = 2, 3
M = Zn, Fe, Mn, In

Interestingly, (1-R-3-methylimidazolium)_bMX_aY_b was also obtained when MX_a and (1-R-3-methylimidazolium)X were reacted. For example, (1-butyl-3-methylimidazolium)₂ZnBr₂Cl₂ can be obtained either from the reaction of ZnCl₂ and (1-butyl-3-methylimidazolium)Br or from the reaction of ZnBr₂ and (1-butyl-3-methylimidazolium)Cl.

The catalytic activities of various imidazolium metal halides were evaluated for the coupling reactions of CO₂ and ethylene oxide (EO) or propylene oxide (PO) at 100 °C for 1 h.

As shown in Table 1, imidazolium halides and metal halides were hardly able to catalyze the coupling reactions when they were used alone. However, the combination of metal halide with imidazolium halide exhibited much higher activity for the coupling reactions (entry 1-3). Among (1-R-3-methylimidazolium)_bMX_aY_b tested, imidazolium zinc tetrahalide exhibited the highest activities. Such enhanced activities are most likely to be attributed to the in situ formation of new active complexes, bis(1-butyl-3-methylimidazolium) zinc tetrahalides from 1-butyl-3-methylimidazolium halide and ZnBr₂. This is supported by the fact that (1-butyl-3-methylimidazolium)₂ZnBr₂Cl₂ and (1-butyl-3-methylimidazolium)₂ZnBr₄ show similar activities to the corresponding catalytic systems of 1-butyl-3-methylimidazolium chloride-ZnBr₂ and 1-butyl-3-methylimidazolium bromide-ZnBr₂ (entry 9-10). By-products such as polyalkylene oxides and halogenated compounds were not detected by GC and GPC analysis.

The catalytic activities of imidazolium metal halides were greatly influenced by the nature of halide ions bonded to metal atom. The order of reactivity was found to be in the following order: [ZnBr₄]²⁻ > [ZnBr₂Cl₂]²⁻ >> [ZnCl₄]²⁻, suggesting the importance of the nucleophilicity of halide ions. The nucleophilicity of halide ions is likely to be enhanced by the presence of imidazolium cations.

The dissociation of a halide ion and the following attack of the dissociated halide ion on the carbon atom of the coordinated ethylene oxide would take place more easily for more nucleophilic bromide ion.⁸ Interestingly, the effect of the alkyl groups on the imidazolium cations is relatively small and can be negligible.

Table 1. Catalytic activities of imidazolium metal halides for the coupling reactions of CO₂ and epoxides^a

Entry	Catalyst	TOF(h ⁻¹) ^b	
		EO	PO
1	(1-butyl-3-methylimidazolium)Br	78	37
2 ^c	MX _a	n.r. ^d	n.r. ^d
3	(1-butyl-3-methylimidazolium) ₂ ZnBr ₂ Cl ₂	2112	1295
4	(1,3-dimethylimidazolium) ₂ ZnBr ₂ Cl ₂	2697	1001
5	(1-ethyl-3-methylimidazolium) ₂ ZnBr ₂ Cl ₂	2137	1335
6	(1-ethyl-3-methylimidazolium) ₂ ZnBr ₄	3588	1617
7	(1-ethyl-3-methylimidazolium) ₂ ZnCl ₄	2538	1352
8	(1-ethyl-3-methylimidazolium) ₂ MnBr ₂ Cl ₂	210	79
9	(1-benzyl-3-methylimidazolium) ₂ MnBr ₄	2527	1201
10 ^e	(1-butyl-3-methylimidazolium) ₃ FeBr ₃ Cl ₃	697	410
11 ^e	(1-ethyl-3-methylimidazolium) ₂ FeBr ₄	923	439
12 ^e	(1-benzyl-3-methylimidazolium) ₃ InBr ₃ Cl ₃	790	359

^a Reactions were carried out at 100 °C and 3.5 MPa of CO₂ for 1 h. Molar ratios of epoxide to imidazolium metal halide complex were set at EO/catalyst = 5,000 and PO/catalyst = 2,000. ^b TOF(h⁻¹): moles of alkylene carbonate/moles of catalyst/hour. ^c MX_a = ZnBr₂, FeBr₃, InBr₃. ^d No reaction. ^e Molar ratios of EO/catalyst = 1,000, PO/catalyst = 500.

The coupling reactions of various epoxides with CO₂ were also conducted in the presence of an imidazolium metal halide, (1-ethyl-3-methylimidazolium)₂ZnBr₂Cl₂. As shown in Table 2, corresponding carbonates were produced in high yields and selectivities except for tert-butyl glycidyl ether and glycidyl isopropyl ether. The lower reactivity of tert-butyl glycidyl ether and glycidyl isopropyl ether is likely due to the crowding around epoxide, which might prevent the attack of CO₂ on the coordinated epoxide.⁹ In fact, the yields of cyclic carbonates decreased with increasing bulkiness of the substituent on the epoxide group (entry 1, 2 and 4).

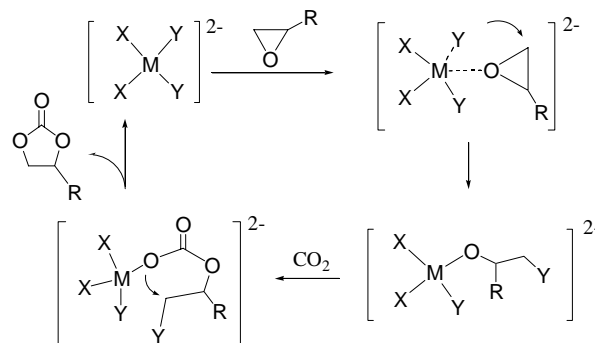
Table 2. Results of catalytic formations of alkylene carbonates from various epoxides by (1-ethyl-3-methylimidazolium)₂ZnBr₂Cl₂^a

Entry	Substrate	yield(%)	Selectivity(%)	TOF(h ⁻¹)
1	1,2-epoxybutane	98	100	490
2	Tert-butyl glycidyl ether	11	97	55
3	Epichlorohydrin	77	100	385
4	Glycidyl isopropyl ether	23	98	115
5	Styrene oxide	77	99	385
6	Glycidyl methacrylate	98	100	490

^a Reactions were carried out at 100°C and 500 psig of CO₂ for 1 h. Molar ratio of epoxide to zinc was set at 500. ^b TOF(h⁻¹): moles of cyclic carbonate/moles of catalyst/hour.

Previous reports by Kisch on the synthesis of cyclic carbonates from CO₂ and epoxide suggested the parallel requirement of both Lewis acid-activation of epoxide and Lewis base-activation of CO₂.⁹ In the case of imidazolium metal halide-catalyzed reaction, metal center is expected to act as a Lewis acid for the coordination of an epoxide and halide ion is expected to act as a Lewis base to ring-

open the coordinated epoxide. The plausible mechanism for the coupling reaction catalyzed by an imidazolium metal halide [MX₂Y₂] is depicted in scheme 1.



Scheme 1. Proposed reaction mechanism for the coupling reaction of ethylene oxide with CO₂ catalyzed by (1-R-3-ethylimidazolium)₂-MX₂Y₂.

Conclusions

A series of ionic liquid-based imidazolium metal halide, (1-R-3-methylimidazolium)_bMX_aY_b (M = Zn, Fe, Mn, In; R = CH₃, C₂H₅, *n*-C₄H₉, CH₂C₆H₅; X, Y = Cl, Br; a, b = 2, 3), prepared from the reaction of MX_a with (1-R-3-methylimidazolium)Y were effective for the coupling reaction of epoxides and CO₂. The catalytic activity of (1-R-3-methylimidazolium)_bMX_aY_b was found to increase with increasing nucleophilicity of halide ion. But, the substitution on the imidazolium cation showed a negligible effect on the catalytic activity.

Acknowledgement

This work was financially supported by the Ministry of Environment of Korea and Honam Petrochemical Co.

References

- (1) Darensberg, D. J.; Holtcamp, M. W. *Coord. Chem. Rev.* **1996**, *153*, 155.
- (2) Shaikh, S. *Chem. Rev.* **1996**, *96*, 951.
- (3) Inaba, M.; Siroma, Z.; Funabiki, A.; Asano, M. *Langmuir* **1996**, *12*, 1535.
- (4) (a) Kim, H. S.; Kim, J. J.; Kwon, H. N.; Chung, M. J.; Lee, B. G.; Jang, H. G. *J. Catal.* **2002**, *205*, 226. (b) Paddock, R.; Nguyen, S. *J. Am. Chem. Soc.* **2001**, *123*, 11498. (c) Kim, H. S.; Kim, J. J.; Lee, B. G.; Jung, O. S.; Jang, H. G.; Jang, Kang, S. O. *Angew. Chem. Int. Ed.*, **2002**, *39*, 4096. (d) Yamaguchi, K.; Ebitani, K.; Yoshida, T.; Yoshida, H.; Kaneda, K. *J. Am. Chem. Soc.* **1999**, *121*, 4526.
- (5) Rogers, R. D.; Seddon, K. R. "Ionic liquid: Industrial Applications to Green Chemistry", ACS symposium series 818, American Chemical Society, Washington DC, **2002**.
- (6) Peng, J.; Deng, Y. *New J. Chem.* **2001**, *25*, 639.
- (7) Hasan, M.; Kozhevnikov, I. V.; Siddiqui, M. R. H.; Steiner, A.; Winterton, N. *Inorg. Chem.* **1999**, *38*, 5637.
- (8) Calo, V.; Nacci, A.; Monopoli, A.; Fanizzi A. *Org. Lett.* **2002**, *4*, 2561.
- (9) Kim, M. R.; Jeon, S. R.; Park, D. W.; Lee, J. K. *J. Ind. Eng. Chem.* **1998**, *4*, 122.
- (10) (a) Dümmler, W.; Kisch, H. *Chem. Ber.* **1990**, *123*, 277. (b) Kisch, H.; Millini, R.; Wang, I. *J. Chem. Ber.* **1986**, *119*, 1090. (c) Ratzenhofer, M.; Kisch, H. *Angew. Chem. Int. Ed. Engl.*, **1980**, *19*, 317.

The Co-activation of CH₄ and CO₂ To Syngas and Ethylene Simultaneously

Changwei Hu, Haili Zhang, Jingjing Wu

Sichuan Key Laboratory of Green Chemistry and Technology, College of Chemistry, Sichuan University, Chengdu 610064, China

Introduction

Recently, the activation and co-activation of CH₄ and CO₂ have received much attention for environmental and industrial reasons¹⁻³. Previous studies focused either on the production of syngas or ethylene. Syngas could be produced either from the partial oxidation or CO₂ reforming of CH₄ over several kinds of catalyst, and ethylene could also be fabricated from the partial oxidation of CH₄ by both O₂ and CO₂. However, in CO₂ reforming of CH₄, the deactivation of the catalyst by coke formation reserves a great challenge in the development of a practical catalyst, and in the partial oxidation of CH₄ to produce ethylene, the deep oxidation forming carbon oxides is inevitable. In order to activate the two green house gases simultaneously and make effective use of both of them, a new process, that is, activating the two gases simultaneously to produce ethylene and syngas, is proposed in present work. The overall reaction could be written as: $5\text{CH}_4 + \text{CO}_2 + 2\text{O}_2 \rightarrow 2\text{CO} + 2\text{H}_2 + 2\text{C}_2\text{H}_4 + 4\text{H}_2\text{O}$. This path has the following advantages: (1) The reforming of methane with CO₂ is an endothermic reaction, and in contrast, the partial oxidation of methane by O₂ is exothermic. While the proposed process combines the partial oxidation and CO₂ reforming of methane together, resulting in a compensation of heat required and even achieving a thermo-neutral reaction by manipulating the CH₄:CO₂:O₂ ratio⁴. (2) The products (the mixture of CO, H₂ and C₂H₄ with proper ratio) formed from the reaction mentioned above could be used to the synthesis of propanal, and the atom utilization of the later reaction is 100% and the commercial value of natural gas and carbon dioxide could then be elevated. (3) The presence of O₂ in the combination process decreases coke formation⁵, though it is a serious and general problem in CO₂ reforming of methane.

Experiment

Catalysts preparation

(1) Grind catalysts. TiO₂ and CeO₂ are ground to 20-40 mesh and impregnated with aqueous solution of the corresponding metal nitrate for 24h. The pastes were dried in vacuum and calcined in air flow for 3h at 500°C before use.

(2) Monolithic catalysts. Various supports mentioned above were ground to >80 mesh, and treated in a similar way as the preparation of conventional grind catalysts before coating. Cordierite support was cut into small column (length 25mm, diameter 12mm) and impregnated by the paste of the above sample by a special process to coat the catalytic components on the cordierite, and then the sample is dried and calcined at 500°C. A thin surface layer was formed on cordierite

The catalytic reaction

The reaction was carried out in a tubular fixed-bed quartz reactor (15mm o.d., 12.5mm i.d.) under atmospheric pressure. The mole ratio of CH₄, CO₂ and O₂ was controlled to be 1:1:1 with a GHSV of 10⁴h⁻¹. The analysis of the effluents mixture was performed by a 1790 gas chromatograph with a plot-C2000 capillary column on line, and a microcomputer was used to quantify the composition.

Results and discussion

It is observed that CO, H₂ and C₂H₄ formed simultaneously on the catalysts investigated in present work. The catalytic activity and C₂H₄ selectivity on the catalysts over the temperature range of 650°C-800°C are shown in Figure 1 and Figure 2. It is seen that both CH₄ conversion and C₂H₄ selectivity are improved with increasing reaction temperature. On the catalyst Ca-Ni/TiO₂(Ca, 21wt%; Ni, 0.15wt%), CH₄ conversion increases monotonically with increasing temperature over the temperature range tested, while C₂H₄ selectivity increases initially and reaches its maximum value at 770 °C. Nevertheless, on the catalyst Ca-Ni*/TiO₂ (Ca, 14wt%; Ni, 0.1wt%), the C₂H₄ selectivity increases monotonically with increasing temperature while CH₄ conversion shows its maximum value at 750 °C. Higher surface area TiO₂ is also used to prepare Ca-Ni/TiO₂

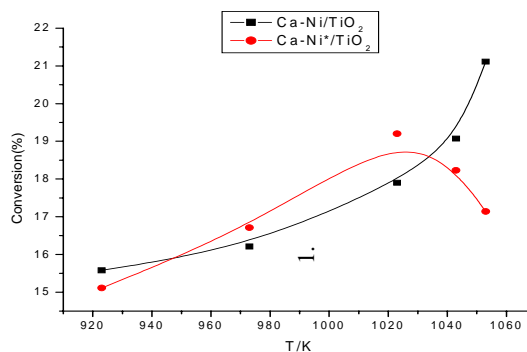


Figure 1 The variation of CH₄ conversion with increasing

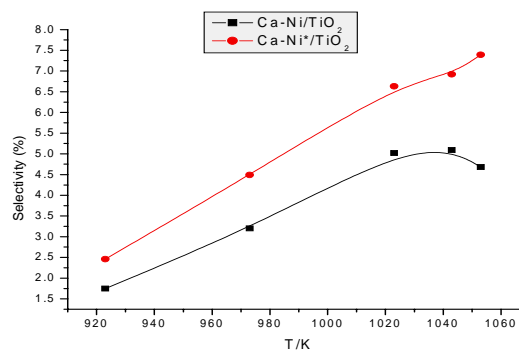


Figure 2 The variation of C₂H₄ selectivity with increasing temperature

catalyst, and it is found that CH₄ conversion and C₂H₄ selectivity are obviously improved and C₂H₄ yield could reach 3.7%. NaWO₄ is considered to be an effective promoter in the partial oxidation of CH₄ to ethylene⁶, it is used to modified Ca-Ni/TiO₂* system in present work, the resulting catalyst exhibit higher C₂H₄ selectivity, but C₂H₆ is also detected in the effluent. Monolithic cordierite show better mechanical intensity and thermal stability than conventional grind supports, and monolithic catalysts were widely used in the purification of vehicle's exhaust gas and methane combustion, but there are few reports in partial oxidation of methane.⁷ In present work, monolithic supported catalysts containing Ni/CeO₂ and Ca/TiO₂ is prepared and used to co-activate methane and CO₂. It is interesting

that the grind forms of Ni/CeO₂ and Ca/TiO₂ show no activity to the target reaction, but they become active when prepared into monolithic catalysts, CO, H₂ and C₂H₄ are obtained at the same time indicating a process intensification effect. Monolithic supported Ca-Ni/TiO₂ catalyst shows activity at about 750°C, and at 770°C, C₂H₄ selectivity reaches 4.3%, and the mole ratio of CO, H₂ and C₂H₄ is 88.5:7.15:4.3.

Conclusions

The simultaneous production of ethylene and syngas from the co-activation of CH₄ and CO₂ is realized over conventional grind Ca-Ni/TiO₂ catalyst. The composition of the catalyst affects the activity and selectivity. The optimal temperature for higher ethylene selectivity over the catalyst Ca-Ni/TiO₂(Ca, 21wt%; Ni, 0.15wt%) is about 770 °C. High surface area TiO₂ and NaWO₄ promoter is beneficial for the formation of ethylene. Monolithic supported Ni/CeO₂ and Ca/TiO₂ catalysts are also effective in the co-activation of methane and CO₂ simultaneously to ethylene and syngas. Process intensification may be important for the co-activation of methane and carbon dioxide.

Acknowledgement

The authors are grateful for the financial support by the NNSFC (No.20243006), The Special Research Foundation of Doctoral Education of China (No. 2000061028) and the TRAPOYT (2002)

References

- (1) Wang Y., Yoshimoto, Takahashi, Ohtsuka Y., *J. Catal.* **1999**, *128*, 160
- (2) Cheng Z. X., Zhao X. G., Li J. L., Zhu Q.M., *Appl. Catal.* **2001**, *205*, 31
- (3) Kus S., Otremba M., Torz A., Wski M. T. *Appl. Catal. A* **2002**, *230*, 263
- (4) Vernon P. D. F., Green M. L. H., Cheetham A. K., Ashcroft A. T., *Catal. Today* **1992**, *13*, 417
- (5) Choudhary V.R., Rajput A.M., Prabhakar B., *Catal. Lett.* **1995**, *32*, 391
- (6) Jia S. F., Xiao T. C., Li S. B., Xu C. Z., Hou R. L., Coleman K. S., Green M.L.H., *Appl.Catal.A* **2002**, *225*, 271
- (7) Tang X. L., Zhang X., Chen Y. Q., Gong M. C., Zhou S. R., Zheng L., Li X. W., *Tian Ran Qi Hua Gong (Chinese)* **2000**, *25*, 4

SYNTHESIS AND ALTERNATING COPOLYMERIZATIONS OF CARBON DIOXIDE WITH CYCLOHEXENE OXIDE OVER (6-Me-pyCAR₂O)Zn(OAc) COMPLEXES CONTAINING BIDENTATE PYRIDINE-ALKOXIDE LIGANDS

Il Kim*, Sang Mook Kim, Jae Sung Kim, Gi Wan Son, Dae Won Park, Chang-Sik Ha

Division of Chemical Engineering, Pusan National University, Jangjeon-dong, Geumjeong-gu, Busan, 609-735, Korea; e-mail:ilkim@pnu.edu

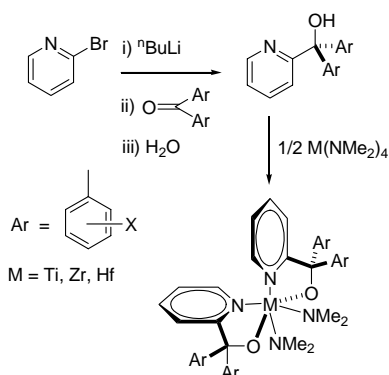
Abstract

The reaction of 2-lithio-6-methylpyridine or 2-lithiopyridine and the appropriated diarylketone followed by hydrolysis yields 6-Me-pyCAR₂OH pyridine alcohols (**1a**, Ar = -C₆H₅; **1b** = 4-Me-C₆H₄; **1c** = 4-Cl-C₆H₄; **1d** = 4-Me₂N-C₆H₄) or pyCAR₂OH pyridine alcohols (**2a**, Ar = -C₆H₅; **2b** = 4-Me-C₆H₄; **2c** = 4-Cl-C₆H₄; **2d** = 4-Me₂N-C₆H₄). The reactions of zinc acetate with 1 equiv of lithiated products of **1a-d** and **2a-d** proceed rapidly to afford LiOAc salt and mono(ligand) complexes (6-Me-pyCAR₂O)Zn(OAc) (**3a-d**) and (pyCAR₂O)Zn(OAc) (**4a-d**), respectively, in high yield. The copolymerizations of carbon dioxide with cyclohexene oxide using **3a-d** complexes were investigated. The (6-Me-pyCAR₂O)Zn(OAc) showed comparable yield and CO₂ incorporation with the β-diiminate zinc complexes. **3c** complex gave high polymers with high carbonate linkage (> 60%) and narrow polydispersity (< 2.0), indicating single active sites.

Introduction

Jordan and coworkers¹ described the synthesis of new group 4 metal alkyl complexes of the general form (Ox)₂MR₂ and (pyCR₂O)₂MR₂ which contain quinolato or pyridine-alkoxide ancillary ligands. The reaction of 2-lithiopyridine and the appropriated diarylketone followed by hydrolysis yields pyCAR₂OH pyridine alcohols. The reaction of M(NMe₂)₄ (M = Ti, Zr, Hf) with 2 equiv of pyCAR₂OH yielded (pyCAR₂O)₂M(NMe₂)₂ complexes (**Chart 1**) which adopt distorted octahedral structure with *trans*-O, *cis*-py, *cis*-amide arrangement of ligands and are active for the ethylene polymerizations.¹

Chart 1



Coates developed β-diiminate zinc complexes for preparation of aliphatic polycarbonate (PC).² The β-diiminate zinc complex showed significantly higher activity than previous catalysts and produced aliphatic PC with very narrow polydispersity. These homogeneous single-site zinc complexes can give different activity

and structure of the resulting copolymer according to β-diimine ligand structure. The specific objectives of this study were to develop efficient synthetic routes to (pyCAR₂O)Zn(OAc) complexes for the preparation aliphatic polycarbonate. Initial efforts to activate these complexes for the alternating copolymerization of carbon dioxide with cyclohexene oxide (CHO) are also described.

Experimental

General procedure. All reactions with air and/or moisture sensitive compounds were carried out under dry nitrogen using standard Schlenk line techniques. ¹H NMR spectra were measured on a Varian Gemini 2000 & HP5P with CDCl₃ as a solvent. Gel permeation chromatography (GPC) analyses were carried out using a Waters-400 spectrometer using polystyrene as a standard and dimethyl formamide as a solvent. All materials such as zinc(II) acetate [Zn(OCOCH₃)₂] and n-butyl lithium were purchased from Aldrich and used without further purification. Cyclohexene oxide (CHO, Aldrich) was distilled for 6 hours over sodium metal and stored over Linde type 4 Å molecular sieves. Tetrahydrofuran (THF) and methylene chloride were refluxed over sodium and stored over 4 Å molecular sieves under dry nitrogen.

Preparation of ligands and catalysts. Pyridine alcohol ligands were prepared according to literature procedures.¹ To a solution of ligand (1.28 mmol) in THF (10 mL), n-BuLi (1.6M in hexane, 0.88 mL, 1.41 mmol) was added dropwise at 0 °C.

Reacting the mixture for 5 min at 0 °C, the solution was cannulated to a solution of zinc acetate (0.24 g, 1.41 mmol) dissolved in THF (10 mL). After stirring overnight at room temperature, the suspension was filtered and the clear solution was dried in vacuum. The resulting metal complexes were recrystallized in toluene and hexane and then characterized by ¹H NMR spectra.

(6-Me-pyCAR₂O)Zn(OAc) (**3a**, Ar = -C₆H₅); light yellow solid (57 % yield). ¹H NMR (CDCl₃, 300 MHz) δ 7.58 – 6.62 (13H, m, ArH), 2.50 (3H, s, Py-Me), 1.49 (3H, s, OAc).

(6-Me-pyCAR₂O)Zn(OAc) (**3b**, Ar = 4-Me-C₆H₄); pale yellow solid (63 % yield). ¹H NMR (CDCl₃, 300 MHz) δ 7.54 – 6.60 (11H, m, ArH), 2.59 (3H, s, Py-Me), 2.33 (3H, s, Ph-Me), 2.23 (3H, s, OAc).

(6-Me-pyCAR₂O)Zn(OAc) (**3c**, Ar = 4-Cl-C₆H₄); light yellow oil (21 % yield). ¹H NMR (CDCl₃, 300 MHz) δ 7.52 – 6.79 (11H, m, ArH), 2.50 (3H, s, Py-Me), 1.19 (3H, s, OAc).

(6-Me-pyCAR₂O)Zn(OAc) (**3d**, Ar = 4-Me₂N-C₆H₄); yellow solid (49 % yield). ¹H NMR (CDCl₃, 300 MHz) δ 7.43 – 6.57 (11H, m, ArH), 2.85 (12H, s, NMe), 2.48 (3H, s, Py-Me), 1.51 (3H, s, OAc).

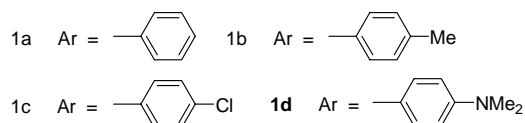
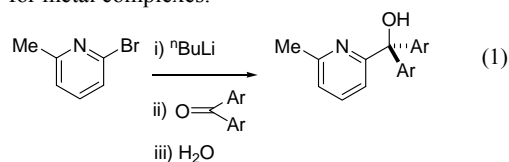
(pyCAR₂O)Zn(OAc) (**4a**, Ar = 4-Me-C₆H₄); pale yellow solid (52 % yield). ¹H NMR (CDCl₃, 300 MHz) δ 7.57 – 6.77 (11H, m, ArH), 2.17 (3H, s, Ph-Me), 2.09 (3H, s, OAc).

Copolymerization of CO₂ with cyclohexene oxide. The copolymerizations were performed in a 10 mL high-pressure reactor equipped with a thermometer and a magnetic stirrer. The reactor was charged with catalyst (3.7 × 10⁻⁵ mol) and CHO (3.7 × 10⁻² mol) in a dry box, and then transferred to a bath controlled at a desired temperature. The vessel was pressurized to 6.8 bar with CO₂ and allowed to stir. After 2 h of polymerization, the copolymer was dissolve in minimum amount of methylene chloride and precipitate from excess methanol. The product was then dried in vacuum.

Results and Discussion

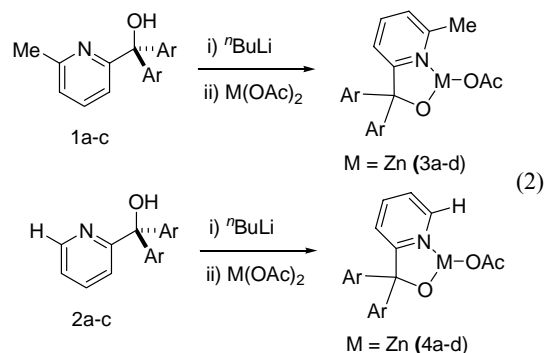
Ligand Synthesis. Pyridine-alcohols **1a-c** were prepared by addition of 2-lithio-6-methylpyridine to the appropriate ketone,

followed by aqueous workup (eq 1), using the approach developed originally by Holm.³ These compounds are isolated as sharp-melting white to tan crystalline solids following recrystallization. The use of symmetric ketones yields symmetric 6-Me-pyCR₂OH alcohols, which in turn simplifies the stereochemical possibilities for metal complexes.⁴

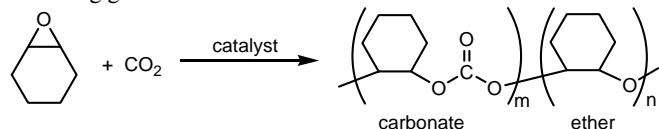


Similar ligands pyCAR₂OH pyridine alcohols (**2a**, Ar = -C₆H₅; **2b** = 4-Me-C₆H₄; **2c** = 4-Cl-C₆H₄; **2d** = 4-Me₂N-C₆H₄) without methyl substituent in 6-position of the pyridine ring were also successfully synthesized according to the similar procedures.

Synthesis of (6-Me-pyCAR₂O)M(OAc) (M = Zn, Mn) complexes. The reactions of zinc acetate or manganese acetate with 1 equiv of lithiated products of **1a-c** proceed rapidly to afford LiOAc salt and mono(ligand) complexes (6-Me-pyCAR₂O)M(OAc) [M = Zn (**2a-c**), Mn (**3a-c**)] in high yield (eq 2).



Alternating copolymerization of CO₂ with cyclohexene oxide. Semi-batch copolymerizations of CHO and CO₂ using Zn complexes have been carried out at the temperature range between 30 and 70 °C at a constant pressure of CO₂ (6.8 bar). Copolymerization of CHO and CO₂ leads to the copolymers of the following general structure:



If the alternating copolymerization is perfect, only carbonate groups should be generated. However, homopolymerization of CHO results in ether linkage. The typical IR spectrum of the resultant copolymers obtained from 3b catalyst system is shown in **Figure 1**. It was found that the IR spectrum showed the strong absorption band at 1745 and 1238 cm⁻¹ characteristic of stretching vibration of C=O bond and C-O-C bond of the carbonate group, respectively. The content of carbonate and ether linkages can be estimated exactly by assigning ¹H NMR spectrum of methine hydride (3.3 – 4.0 ppm) in cyclohexane backbone. Zinc complexes

bearing ligands (**1a-c**) with 6-methyl substituted pyridyl produced aliphatic PCs which have high carbonate contents (≥ 60 %) as shown in Table 1. It is interesting to note that the **3d** catalyst bearing ligand with electron donating NMe₂ group on the aryl ring showed only negligible activity, while **3c** catalyst with electron withdrawing Cl group showed highest activities. Copolymers obtained by **3c** catalyst recorded highest molecular weight, demonstrating the electron withdraw group retards chain termination reaction. In addition the methyl group on the pyridyl ring influences both catalytic activity and CO₂ reactivity (compare **3b** and **4b** in Table 1). The Mn acetate complexes bearing **1b** and **2b** ligands were also prepared and utilized for the copolymerization of CO₂ and CHO, resulting in negligible activities. All Zn complexes bearing pyridine alcohol ligand can produce aliphatic PC with high molecular weight and narrow PDI at mild conditions.

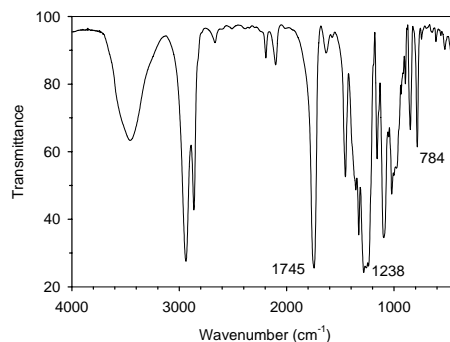


Figure 1. The typical IR spectra of CO₂/CHO copolymer obtained by 3b at 30 °C.

Table 1. Results of CO₂/CHO copolymerizations

No.	Cat.	Temp.	Yield (%)	M _n	MWD	Carbonate (%)
1	3a	30	22.8	4660	1.38	74.5
2		50	19.6	3830	1.10	72.2
3		70	19.2	3610	1.14	69.9
4	3b	30	15.4	4250	1.06	72.9
5		50	10.4	3890	1.04	56.4
6		70	11.6	3620	1.05	50.6
7	3c	30	26.8	6820	2.05	61.5
8		50	30.6	9540	2.55	62.6
9		70	26.0	5590	1.96	51.5
10	3d	30	nil	-	-	-
11		50	0.8	-	-	0.2
12		70	1.4	-	-	0.2
13	4b	30	13.6	3500	1.04	43.6
14		50	12.2	3560	1.03	47.3
15		70	11.2	3370	1.03	35.5

Acknowledgment

This work was supported by grant No. R01-2003-000-10020-0 from the Basic Research Program of the Korea Science & Engineering Foundation. IK is also grateful to the Brain Korea 21 Project in 2003.

References

- Kim, I., Nishihara, Y., Jordan, R.F., Rogers, R.D., Rheingold, A.L., Yap, G.P.A., *Organometallics*, **1997**, *16*, 3314.
- Chen, M., Lobkovsky, E.B., Coates, G.W., *J. Am. Chem. Soc.*, **1998**, *120*, 11018.
- Schultz, B.E., Gheller, S.F., Muetterties, M.C., Scott, M.J., Holm, R.H., *J. Am. Chem. Soc.* **1993**, *115*, 2714.
- Tsukahara, T., Swenson, D.C., Jordan, R.F. *Organometallics*, **1997**, *16*, 3303.

HYDROGENATION OF NITROBENZENE WITH SUPPORTED TRANSITION METAL CATALYSTS IN SUPERCRITICAL CARBON DIOXIDE

Fengyu. Zhao^{a,b,c}, Rong Zhang^b, Maya Chatterjee^b, Yutaka Ikushima^{b,c}, and Masahiko Arai^{c,d}

a, Japan Society for the Promotion of Science, Domestic Research Fellow. b, Supercritical Fluid Research Center, National Institute of Advanced Industrial Science and Technology, Sendai 983-8551, Japan. c, CREST, Japan Science and Technology Corporation (JST), Japan. d, Division of Materials Science and Engineering, Graduate School of Engineering, Hokkaido University, Sapporo 060-8628, Japan.

Introduction

The selective hydrogenation of nitro-compounds is commonly used to manufacture amines, which are important intermediates for dyes, urethanes, agro-chemicals and pharmaceuticals. Hydrogenation of nitrobenzene is used to produce aniline, which can be carried out in gas or liquid phase by using supported metal catalysts and organic solvents such as alcohols, acetone, benzene, ethyl acetate, or aqueous acidic solutions.^{1,2} The use of these solvents has some drawbacks owing to their toxicity, flammability, or environmental hazards. In addition, the solvent may play a crucial role in the stabilization of reactive intermediates and have a decisive influence on chemical reactions. Therefore, the choice of solvent is important and a green solvent should be considered for contemporary chemical processes. Supercritical carbon dioxide (scCO₂) is an environmentally acceptable replacement for conventional organic solvents, due to its environmentally benign, non-toxic, and non-flammable nature, low cost, and wide tuning ability of solvent properties.^{3,4} Moreover, the rate of catalytic hydrogenation in a gas-liquid system is not so high because of a low solubility of gaseous hydrogen in common solvents. In contrast, hydrogen is completely miscible with scCO₂, and this is beneficial for enhancement of hydrogenation reactions.⁵

The present work has been undertaken to study the catalytic hydrogenation of nitrobenzene in scCO₂ and in ethanol at a low temperature of 35 °C using several supported transition metal catalysts. The influence of metals (Pt, Pd, Ru, and Rh), supports (C, SiO₂, and Al₂O₃), and solvents (scCO₂ and ethanol) on the catalytic activity and selectivity has been investigated.

Experimental

Materials. All the chemicals were purchased from Wako Pure Chemicals Industries and used without further purification. Carbon- and alumina-supported Pd, Rh, Pt and Ru catalysts were also purchased from Wako. Silica-supported Pd and Pt catalysts were prepared using ion-exchange method. All the catalysts were reduced by hydrogen at 300 °C for 2 h before activity measurements.

Activity measurement. The activity of those catalysts was tested for the hydrogenation of nitrobenzene, which was carried out in a 50 mL high-pressure autoclave. Nitrobenzene (2.0 g (16.2 mmol)) and catalyst (0.01 g) were charged into the reactor and the reactor was flushed with 2.0 MPa CO₂ for three times. The reactor was then heated up to the desired temperature of 35 °C and then H₂ and compressed liquid CO₂ were introduced up to the desired pressure with a high-pressure liquid pump. The hydrogenation reaction was conducted while stirring with a magnetic stirrer. After the reaction, the reactor was cooled to room temperature and the reaction mixture was analyzed with a gas chromatograph (HP 5890, HP5 capillary column

with 0.53 mm in diameter, 0.25 μm in film, and 15 m in length) using a flame ionization detector.

Catalyst characterization. X-ray diffraction (XRD) patterns of catalysts were measured on Rigaku RINT 220VK/PC powder diffractometer operated at 40 kV and 20 mA, using CuKα monochromatized radiation (λ = 0.154178 nm). The crystallite size of supported metals was calculated using the Scherrer equation, $D = K\lambda / (\beta \cos\theta)$, where K is a constant taken as 0.9, λ is the wavelength of the X-ray radiation, β is the peak width at half maximum.

Results and Discussion

Hydrogenation of nitrobenzene in organic solvents was reported to produce aniline along with several intermediate products such as nitrosobenzene (NSB), phenylhydroxylamine (PHA), azoxybenzene (AOB), azobenzene (AB) and hydrazobenzene (HOB), which are formed in several parallel and consecutive reactions. It has been observed in the present work that all the catalysts show 100% selectivity towards aniline in scCO₂ at 50 °C. In order to compare the influence of metal and support on both activity and selectivity, the reaction has been carried out at a lower temperature of 35 °C. At this temperature as well, PHA and HOB were not detected to form.

The influence of metals has been examined using C-supported catalysts (Table 1). In scCO₂, the highest conversion of 71% was obtained with Pt/C catalyst; however, the selectivity to aniline was lower compared to those obtained with the other catalysts. The Pd/C, Ru/C, and Rh/C catalysts exhibit 100% selectivity to aniline in scCO₂. In a conventional organic solvent of ethanol, Pt/C also shows a higher conversion compared with the other catalysts. With Ph/C and Ru/C catalysts, no products were detected in ethanol. For all the catalysts used, both the conversion and selectivity to aniline obtained in scCO₂ are higher than those obtained in ethanol. The order of activity is Pt > Pd > Rh, Ru in scCO₂ as well as in ethanol. The solubility of H₂ in ethanol and CO₂ calculated according to Henry's law and equation state for ideal gases, indicated that the concentration of H₂ in CO₂ is 15 times higher than that in ethanol.

Table 1 Results of hydrogenation of nitrobenzene in scCO₂ and in ethanol with different carbon supported metal catalysts at 35 °C

Solvent	Catalyst	Time (min)	Conversion (%)	Selectivity (%)			
				AN	NSB	AB	AOB
CO ₂ 14.0 MPa	5% Pd/C	10	52	100	--	--	--
	5% Pd/C	50	100	100	--	--	--
	5% Pt/C	10	71	79	4	12	5
	5% Pt/C	50	100	100	--	--	--
	5% Ru/C	10	4	100	--	--	--
	5% Rh/C	10	12	100	--	--	--
Ethanol	5% Pd/C	10	21	68	16	--	16
	5% Pt/C	10	63	58	4	26	12
	5% Ru/C	10	0	--	--	--	--
	5% Rh/C	10	0	--	--	--	--

Next, the total conversion and the selectivity to aniline obtained with various supported metal catalysts in scCO₂ and ethanol were shown in figure 1. In scCO₂, all the Pd catalysts indicate 100%

selectivity to aniline, while the Pt catalysts have lower selectivity to aniline. With the Pt catalysts, some amounts of NSB, AOB, and AB were produced. In ethanol, the same byproducts were also detected with all the Pt and Pd catalysts. Higher aniline selectivity values were obtained in scCO₂ than these obtained in ethanol for all the catalysts used. The order of the total conversion with respect to the supports is C > Al₂O₃, SiO₂ in scCO₂ for both Pt and Pd. It is interesting to see that the total conversion in ethanol is higher than that obtained in scCO₂ for Al₂O₃ and SiO₂ supported Pt and Pd catalysts; on the contrary, the conversion in scCO₂ is higher than that in ethanol for Pd/C and Pt/C catalysts.

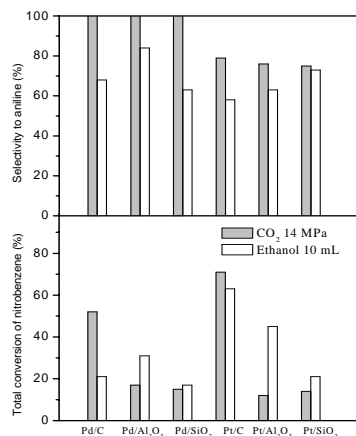


Figure 1. Nitrobenzene hydrogenation in scCO₂ and in ethanol at 35°C. Reaction conditions: nitrobenzene 2.0 g (16.2 mmol), catalyst 0.01g, H₂ 4.0 MPa, temperature 35°C, reaction time 10 min.

These results can be explained with metal particle size and the interaction between reaction medium and metal particle. The metal particle size on the supports were quite different and a larger metal particle presented on the C-supported Pd and Pt catalysts as calculated by Scherrer equation. The nitrobenzene hydrogenation proceeded on the surface of metal particles, the higher activity presented in scCO₂ for Pd/C and Pt/C catalysts indicates a significant interaction existed between scCO₂ molecular and the larger Pt and Pd metal particle, which benefits the formation of aniline, thus, the higher selectivities to aniline have been obtained in scCO₂ than these obtained in ethanol for all the catalysts used.

The CO₂ pressure presents a significant effect on the reaction conversion and product selectivity in Figure 2. The conversion increases with increasing CO₂ pressure up to 12 MPa, which can be explained by the phase behavior and the concentration of nitrobenzene distributed in liquid and CO₂ phases. The concentration of nitrobenzene in CO₂ increases with increasing CO₂ pressure; when CO₂ pressure was raised to 12 MPa, a completely miscible mixture (NB, H₂ and CO₂) was formed. In this case the mass transfer resistance between gas (H₂) and liquid (NB) was decreased with increasing CO₂ pressure and then it disappeared at 12 MPa as a result of the phase changes to a homogeneous phase. This is a reason for that the conversion increases with increasing CO₂ pressure. The selectivity to aniline increases and has a maximum at 8.0 MPa, and then it decreases with increasing CO₂ pressure for both Pd/C and Pt/C catalysts. It was supposed that density variation around the critical point would cause a change in chemical or physical properties and affects the activity and selectivity of a reaction. The density of scCO₂

is highly pressure dependent, for instance, to change CO₂ pressure from 6.0 MPa to 8.0 MPa, the density changes from 160.0 to 520.8 kg/m³ [6].

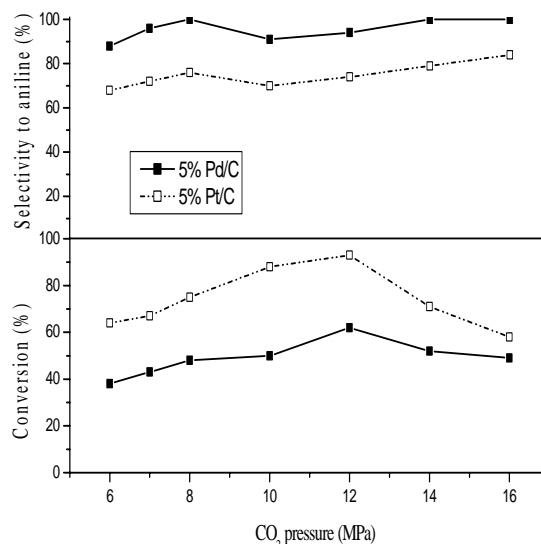


Figure 2 Influence of CO₂ pressure on the total conversion and selectivity to aniline. Reaction conditions: nitrobenzene 2.0 g (16.2 mmol), 0.324 mmol/ml in the reactor), catalyst 0.01g, H₂ 4.0 MPa, temperature 35°C, reaction time 10 min.

The transition metal catalysts of Pd, Pt, Ru, and Rh supported on carbon presented a similar active order of Pt > Pd > Ru, Rh in scCO₂ as well as in ethanol. An active order of supports is C > Al₂O₃, SiO₂ in scCO₂ for both Pd and Pt catalysts. Higher selectivity to aniline has been obtained in scCO₂ compared with that in ethanol. the hydrogenation of nitrobenzene catalyzed with Pd/C and Pt/C catalysts was successfully conducted in scCO₂ with a 100% yield to aniline at a lower temperature of 35°C for 50 min. Clearly, scCO₂ is a suitable replacement for organic solvent in the hydrogenation of nitrobenzene and the present hydrogenation is an environmentally benign and “green” process as it is free of harmful organic solvents. In addition, it is easy to separate the organic phase (the desired product, aniline), aqueous phase (the only byproduct, water), gas phase (CO₂, H₂).

Acknowledgements

The authors would like to thank Dr. M. Shirai for fruitful discussions, and thanks also to Dr. Y. Hakuta for measurement of TEM images.

References

- Figueras, F.; Coq, B., *J. Mol. Catal. A Chem.* **2001**, 173, 223.
- Torres, C. C.; Jablonski, E. L.; baronetti, G. T.; Castro, A. A.; de Miguel, S. R.; Scelza, O. A.; Blanco, M. D.; Pena Jimenez, M. A.; Fierro, L. G., *J. Appl. Catal. Gen.* **1997**, 161, 213.
- Leitner, W., *Acc. Chem. Res.* **2002**, 35, 746.
- Baiker, A., *Chem. Rev.* **1999**, 99, 453.
- Zhao, F.Y.; Ikushima, Y.; Chatterjee, M.; Sato, O.; Arai, M., *J. Supercrit. Fluids*, **2003**, 27, 65.
- Arai, M.; Nishiyama, Y.; Ikushima, Y., *J. Supercrit. Fluids*, **1998**, 13, 149.

Challenges and Progress in the Conversion of Natural Gas to Fuels and Chemicals

Enrique Iglesia

Department of Chemical Engineering, University of California at Berkeley and Chemical Sciences Division, E.O. Lawrence Berkeley National Laboratory, Berkeley, CA 94720
iglesia@cchem.berkeley.edu

Low heteroatom and high hydrogen contents make natural gas an attractive feedstock for the synthesis of fuels and chemicals currently derived from petroleum. This keynote lecture describes recent progress in concept demonstrations and technological applications as well as in the fundamental understanding of the kinetic and thermodynamic constraints prevalent in direct and indirect methane conversion routes to fuels and chemicals. These recent advances combine catalyst improvements with the design and implementation of novel chemical reactors and separation schemes. These topics are discussed also in the context of their thermal efficiency and of their impact on potential strategies to minimize CO₂ formation and the economic viability of CO₂ sequestration.

Gas conversion processes will produce predominately liquid fuels in remote locations, because the prevalent economies of scale and the required field depletion rates will require large process throughputs. These throughputs are too large for chemical markets, with the possible exception of the ethylene and methanol markets. Depletion strategies based on methane conversion to liquid fuels will ultimately be replaced by the direct use of natural gas as a fuel, as pipelines and liquefied natural gas facilities develop together with the local economies and the required distribution infrastructures. Concurrent production of commodity and intermediate chemicals in large natural gas conversion complexes will increase economic incentives for first-of-a-kind technologies and possibly lead to their earlier deployment. The significant market penetration of wax, lubricants, and linear α -olefins from initial coal and gas conversion deployments by Sasol attests to the potential for co-production of chemicals, but also to their significant impact on relatively small chemical markets. The use of natural gas for chemicals syntheses will continue, using both remote and local fields, well beyond the remote gas-to-liquids commercialization time window, because natural gas provides clean and economical routes to methanol and ammonia, as well as to other chemicals currently derived from crude oil.

The conversion of natural gas to useful products is discussed here in the context of a methane refinery, possibly located far from markets, and designed to produce fuels, chemicals, and intermediates currently derived from crude oil. Process simplicity, minimal cycling of process and reaction conditions, and high conversions per pass lead to higher practical thermal efficiencies and lower capital costs for both direct and indirect processes for converting natural gas to fuels and chemicals. Direct conversion routes, however, provide paths to only a few desired products, and the high reactivity of these products typically requires their kinetic protection or selective extraction, both of which increase process complexity and costs. Indirect routes via synthesis gas provide broader options for final products or intermediates. They require less toxic and expensive oxidants than indirect functionalization routes involving bisulfate or halogenated methane derivatives. Direct paths involve C-H bond activation and the conversion of the resulting CH_x or CH_yO species to desired products within a single vessel. Pyrolysis, oxidative coupling, selective oxidation (to methanol or formaldehyde), partial oxidation (to synthesis gas; H₂/CO) and reforming with either steam or carbon dioxide are direct (one-step) methane conversion routes.

Direct processes can produce only a few products (H₂/CO, acetylene, ethylene, benzene, methanol, formaldehyde). In many cases, these reaction products are much more reactive than the CH₄ reactant, either because of their weaker C-H bonds or their unsaturated character. Thus, they progress along reaction paths that ultimately lead to thermodynamically more stable carbon or CO₂ products. Only H₂/CO mixtures, useful only as intermediates to more useful products, reach equilibrium yields without significant formation of carbon or CO₂, and only as a result of the thermodynamic preference for H₂ and CO at conditions used for partial oxidation and reforming reactions.

High product yields in most direct routes therefore require continuous removal of desired products from the reaction zone or the thermodynamic or kinetic protection of these products against subsequent reactions. These approaches increase process complexity and second-law inefficiencies. In general, maximum attainable yields depend on the thermodynamic tendency of a given product to oxidize to CO₂ or to dehydrogenate to solid carbon. Weaker C-H bonds in products tend to favor their activation at lower reaction temperatures in the absence of thermodynamic or kinetic protection. Thus, low temperatures actually disfavor desired products in such cases, because subsequent reactions of such desired products have much lower activation energies than CH₄ activation steps leading to the desired initial products.

Direct paths become indirect when desired products are made via the initial formation of chemically-protected intermediates, which must be subsequently converted to the desired products. In such cases, the first step forms a protected form of methane, which resists further conversion to CO₂ or carbon because of its low reactivity, while a second step in a downstream vessel "de-protects" this intermediate and forms the desired products in higher yields than by the corresponding direct routes. For example, synthesis gas (H₂/CO) is in effect a thermodynamically protected, but quite reactive, form of "activated" methane, useful to form a broad range of hydrocarbons and oxygenates. High-temperature CH₄ reactions with H₂O, CO₂, or even O₂ form minor amounts of CO₂ because of thermodynamic constraints imposed by high reaction temperatures at typical reactant stoichiometries.

Synthesis gas conversion processes are significantly more advanced in development than direct processes and than other two-step conversion schemes using methane bisulfate or halogen derivatives. Indirect gas conversion processes via synthesis gas are currently practiced for methanol synthesis and for hydrocarbon formation via the Fischer-Tropsch synthesis. Diesel-range hydrocarbons (via Fischer-Tropsch synthesis) and gasoline (via methanol to gasoline) can be produced with thermal efficiencies as high as 80% of their respective theoretical values (78% and 75%). These indirect processes have continuously evolved with advances in synthesis gas generation, in the design and deployment of three-phase bubble columns for synthesis gas conversion, and in the development of improved catalytic materials for the selective synthesis of paraffins, intermediate size α -olefins, and higher alcohols. Small modular gas conversion plants using catalytic partial oxidation in monolith reactors and CO hydrogenation in bubble columns may also create future opportunities for combining H₂ and power generation and the synthesis of commodity petrochemicals, and even of liquid fuels, in smaller scales than for remote fuels-based gas to liquid plants.

Clean diesel products and intermediate range α -olefins can be efficiently produced via Fischer-Tropsch synthesis pathways, but lighter olefins, such as ethene and propene, and gasoline-type hydrocarbons require an additional process step, in which methanol derived from synthesis gas reacts on shape-selective catalysts.

Attractive routes for the synthesis of oxygenates with C-C bonds will require new approaches involving bifunctional dehydrogenation-condensation pathways. Multifunctional reactors combining membrane separations with chemical reactions and cyclic reactors for temporal separation of reactants and products hold significant promise for increasing the efficiency of synthesis gas generation and direct conversion steps, but their ultimate impact on capital costs and thermal efficiencies remain unclear.

Acknowledgement.

The author acknowledges the financial support from BP through the Methane Conversion Cooperative for the contributions of his own group mentioned in this manuscript. The specific technical contributions of many members of his research group are also acknowledged with thanks, specifically those of Drs. Junmei Wei, Haichao Liu, and Jeffrey Zalc, and of Ms. Patricia Cheung and Mr. Howard Lacheen. The guidance and technical input of Drs. Theo Fleisch and Graham Butler and of other BP technical staff are also gratefully acknowledged.

NOVEL ZERO-CO₂ EMISSION TECHNOLOGY OF CATALYTIC PRODUCTION OF HYDROGEN AND AROMATICS FROM METHANE AND BIOGAS FOR FUEL CELL SOCIETY

Masaru Ichikawa

Catalysis Research Center, Hokkaido University
Sapporo 001-0021 Japan

Introduction

Since a decade ago, we have developed a novel zero-CO₂ emission technology with Mo/Re based zeolite catalysts for catalytic dehydrocondensation of methane to produce hydrogen and benzene/naphthalene as aromatic products. We have constructed a fixed bed demonstration plant of this direct methane reforming process at Muroran, Hokkaido, and succeeded to operate in 2001-2003 a stable and feasible performance with kg-scale Mo/HZSM-5 catalysts. This sustainable technology is available to produce hydrogen and aromatics such as benzene and naphthalene from biogas(60%CH₄+40%CO₂) derived from cows excrements, sewage and biomass. Benzene (cyclohexane) and naphthalene(decalin) as liquid organic hydrides are good for efficient and safe storage, transportation and supply of hydrogen to fuel cell systems. We have developed the organic hydride technology using a cyclic conversion of cyclohexane-benzene (or decalin-naphthalene) which is conducted by pulse-spray technique with a heated Pt-based catalysts at 250-300°C for an efficient, safety and feasible storage and supply to PEM fuel cell car, home electric generator and non-wiring (cable) transportation of electricity generated by solar cells, windmills and other renewable sources. A "Cyclohexane/decalin Hi-way" concept is discussed for 21st century sustainable hydrogen energy from methane and biogas for fuel cell society.

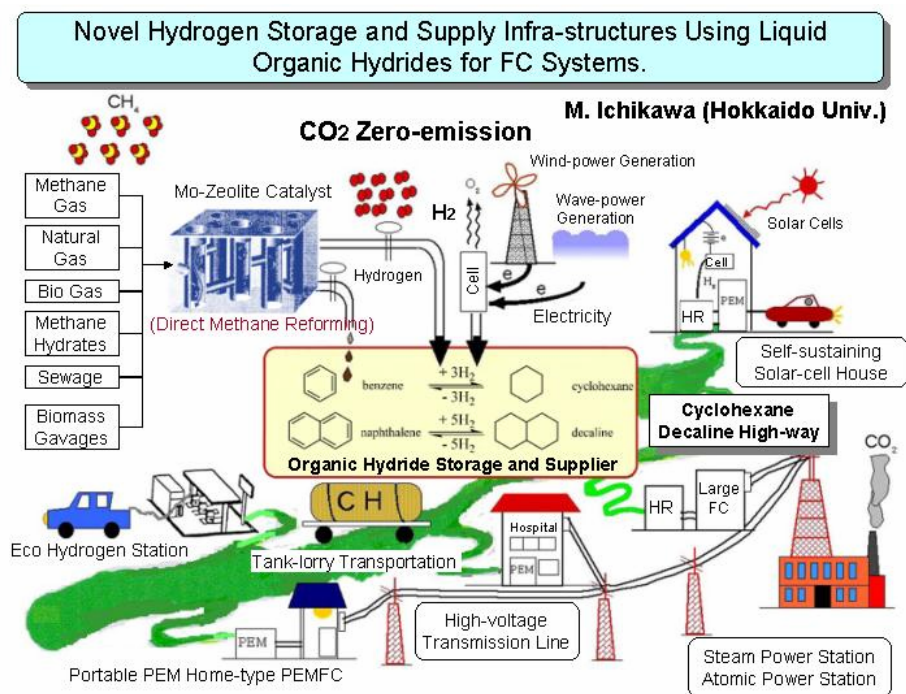
Novel Catalytic Technology of Direct Methane(Biogas) Reforming towards Hydrogen and organic hydrides for Chemical Industry and Fuel Cell Society

We have developed in 1996-2000 the novel Mo carbide and Re based zeolite (HZSM-5, MCM-22) catalysts which exhibit the practically efficient performances (20% conv, over 90%selectivity) for dehydrocondensation of methane(natural gas and biogas) to simultaneously produce benzene and naphthalene with a bulky hydrogen, and the feasible catalyst stability by addition of a few percents CO/CO₂ or hydrogen to methane feed has been demonstrated due to an effective removal of coke formed on the catalysts. We have constructed the 1 Kg catalyst-scale demonstration plant of this direct reforming process at Muroran, Hokkaido, and proceeded the operation with kg-scale catalysts of Mo supported zeolites to produce benzene/naphthalene and hydrogen with a low coke formation at 700-750 °C and 3-5 bar. This catalytic technology of methane direct reforming is evaluated as non-CO₂ emission and eco-feasible process to produce hydrogen and benzene (cyclohexane) and naphthalene(decalin)as efficient storage and supply of hydrogen for fuel cells.

New Technology of Hydrogen Storage and Supply to Fuel Cell Systems Using Organic Hydrides for Fuel Cell Society

The novel technology of hydrogen supply infra-structures using liquid organic hydrides such as cyclohexane and decalin recently emerge for 21st century hydrogen eco energy society connected with reliable PEM fuel cell. A novel catalytic converter of cyclohexane(or decalin) are developed with carbon-based Pt catalysts to efficiently supply pure hydrogen at moderate temperatures of 250-350 °C. A cyclic conversion of cyclohexane-benzene (or decalin-naphthalene) system is available for efficient, safety and feasible storage and supply (50-500 l/min) by hydrogen station for hydrogen fuel car, home electric generator and non-wiring (cable) transportation of electricity generated by solar cells, windmills and other renewable sources.

This is promising sustainable technology of zero-CO₂ emission hydrogen supply from methane and biogas using organic hydrides connected with reliable PEM fuel-cell systems, as follows.



Towards an efficient process for small-scale, decentralized conversion of methane to synthesis gas or hydrogen

Dirk Neumann, Mark Kirchhoff, and Götz Vesper*

Department of Chemical Engineering
1249 Benedum Hall, University of Pittsburgh
Pittsburgh, PA 15261, USA

Introduction

Methane is one of the major contributing gases to global warming. According to a recent study by the IPCC [1], about 70% of all atmospheric methane is of anthropogenic origin, and this value has shown a particularly strong growth rate through the 1990s with an average increase of about 7 ppt/yr. However, since methane has a very short atmospheric lifetime of about 8 – 12 years, it also appears to be one of the most promising greenhouse gases for short-term measures to counter global warming trends with (almost) immediate impact [2].

In the US, more than a third of all methane emissions result from landfills [3]. These emissions not only represent a significant environmental problem, but at the same time also are a waste of a valuable and renewable natural resource. However, these sources are too small and often too remote to be exploited with existing industrial technology for methane utilization (other than combustion). With current trends towards a more sustainable economic growth and a clean, hydrogen-based economy, however, it seems necessary to develop technologies for efficient, small-scale and decentralized utilization of these and similar methane resources.

Direct 'valorization' of methane, i.e. the direct conversion of methane to higher value products via process routes such as methane coupling, is currently neither efficient nor economical. The only available route for methane valorization is therefore the indirect route via the production of synthesis gas, a mixture of CO and hydrogen, followed by secondary processes such as methanol or Fischer-Tropsch syntheses. In these indirect processes, the syngas production step is currently the limiting factor particularly for small-scale processes, with about 60% of overall investment costs.

Catalytic partial oxidation (CPO) of methane to synthesis gas has recently found much attention as alternative to the industrially dominant, highly endothermic steam reforming route ($\text{CH}_4 + \text{H}_2\text{O} \rightarrow \text{CO} + 3 \text{H}_2$, $\Delta H_R = 206 \text{ kJ/mol}$). CPO is a mildly exothermic reaction and has thus the potential to be run autothermally ($\text{CH}_4 + 0.5 \text{O}_2 \rightarrow \text{CO} + 2 \text{H}_2$, $\Delta H_R = -36 \text{ kJ/mol}$). This independence on external heat sources is quintessential for an efficient small-scale, decentralized process. Furthermore, the reaction is characterized by the extremely high reaction rates typical for catalytic oxidation processes at high temperatures ($T > 800^\circ\text{C}$). This allows for catalytic contact times in the order of about 10 ms and thus for extremely compact reactors with large through-puts.

However, for all its advantages over the conventional steam-reforming route, adiabatic CPO of methane is far from optimal. Simple thermodynamic calculations demonstrate that adiabatic temperatures are too low to achieve optimal methane conversions and syngas selectivities, and even these adiabatic temperatures are only achieved via internal combustion of some of the methane feed, hence intrinsically capping the maximum attainable yields at autothermal process conditions [4].

However, combining the CPO reaction route with an efficient heat-integrated reactor concept, a very efficient overall process can be attained. In this report, we briefly present some of our recent results on CPO of methane in a catalytic reactor with integrated regenerative heat-exchange via reverse-flow operation.

Experimental Set-up

The experimental set-up has been described in more detail in a previous publication [4]. The reactor consists of a stainless steel – quartz glass double tube, in which the catalyst is positioned between two extruded cordierite monoliths which serve as heat reservoirs. Four valves are positioned pair-wise on either end of the reactor to allow switching of the flow direction at reverse-flow operation. If the flow direction is reversed periodically at an appropriate frequency, the heat of the exothermic oxidation reaction is "integrated" and reactor temperatures are increased well beyond the adiabatic limit.

Moveable thermocouples allow measurement of temperature profiles, while reactant and product concentrations are measured via mass spectrometry and gas chromatography.

The catalysts used are platinum precipitated from a salt solution on an alumina foam monolith, and a novel nanocomposite catalyst, in which platinum nanoparticles are anchored in a high-temperature stabilized ceramic matrix [5].

Results and Discussion

Pt-Alumina Catalyst. Figure 1 shows results from CPO of methane with air over a platinum-coated alumina foam monolith at stationary reactor operation ('SS') and at reverse-flow operation ('RFR') versus methane/oxygen ratio. One can see that the regenerative heat-integration in the RFR leads to a significant improvement in methane conversion of about 20% over the whole range of conditions (left graph), as well as drastic improvements in hydrogen selectivity of up to 40% (right graph).

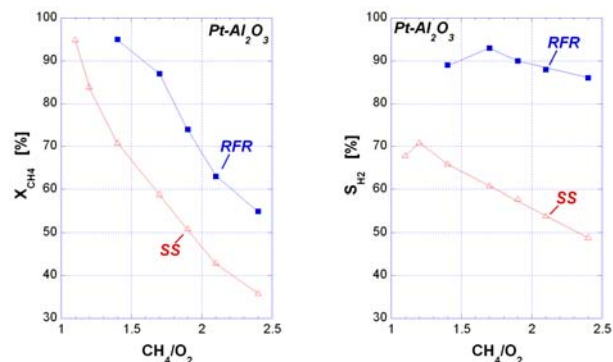


Figure 1. Experimental results for CPO of methane over an alumina supported Pt catalyst in a comparison between steady-state (SS) and reverse-flow operation (RFR). Methane conversions (left graph) and hydrogen selectivities (right graph) are shown versus methane/oxygen-ratio at a reactor feed of 4 slm methane/air. The duration of one half-period at RFR operation was 15 s.

While methane conversion increases continuously with decreasing methane/oxygen ratio due to the increasing amount of oxygen available for methane oxidation, hydrogen selectivity shows a maximum near $\text{CH}_4/\text{O}_2 = 1.2$ at SS which shifts to about $\text{CH}_4/\text{O}_2 = 1.7$ at reverse-flow operation. This maximum can be explained by the superposition of two effects: The overstoichiometric supply of oxygen for $\text{CH}_4/\text{O}_2 < 2.0$ leads to some total oxidation, hence reducing selectivities. At the same time, the exothermicity of the total oxidation reaction also increases temperatures and hence thermodynamically attainable selectivities, thus helping process selectivities. The observed shift in the maximum therefore indicates that less total oxidation is needed to achieve high reaction temperatures, as reactor temperatures are already increased due to the heat-integration. Heat-integration thus leads to an effective conversion of thermal energy (heat) into chemical energy (process yields).

Reactor Simulations. The experimental investigations were complemented by a detailed simulation study of the reaction behavior at reverse-flow operation of the reactor in order to obtain a better understanding for the reaction kinetics at high-temperature unsteady-state conditions. A heterogeneous one-dimensional reaction-diffusion reactor model was coupled with detailed reaction kinetics for the catalytic surface reaction which had previously been validated against experimental results at stationary reactor operation [6]. Figure 2 shows results from one simulation: catalyst temperatures (left graph) and water concentrations (mass fractions, right graph) in the catalyst zone are shown for one half period immediately after flow reversal.

The reactor model confirms the (qualitative) experimental observation that maximum catalyst temperatures are kept below 1500°C and thus maintain within a range. Furthermore, one can see that a strong (spatial) temperature maximum develops near the catalyst entrance which matches with the maximum in water concentration in this location. This indicates that some total combustion of methane is occurring near the catalyst entrance, the exothermicity of which results in strong temperature maxima.

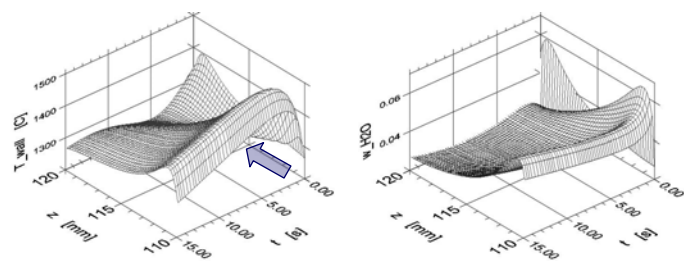


Figure 2. Simulation results for CPO of methane over a Pt catalyst at reverse-flow reactor operation. Temperature profiles in the catalyst bed (top graph) and water concentrations (mass fractions, bottom graph) are shown versus catalyst length (z) and time after flow reversal (t). Flow direction is from right to left as indicated by the arrow in the top graph. Reactor feed is methane/air at room temperature with $\text{CH}_4/\text{O}_2 = 2.0$ and RFR periodicity is 15 s.

At the same time, one can also see that the *temporal* temperature maximum in the catalyst zone corresponds to a *minimum* in water concentration. This is due to the (transient) increase in reaction temperature due to heat-integration which leads to an improvement in selectivity and hence to a decrease in the amount of water formed in the reaction.

This results again highlights the above mentioned complex interplay between reactor temperatures and reaction selectivity: while low selectivity results in high reactor temperatures, these high temperatures in turn improve reaction selectivity and hence counter the increasing temperatures.

Pt-BHA Nanocomposite Catalyst. As seen above, heat-integrated reactor concepts alone are not sufficient to achieve optimal reaction temperatures. Development of an efficient process should always involve reactor engineering in combination with the design of adapted catalyst systems. We recently developed novel nanocomposite catalyst systems, in which well-defined noble metal nanoparticles are embedded in a ceramic matrix, yielding highly active, selective and high-temperature stable catalyst systems [5].

Figure 3 shows experimental results in CPO of methane over a Pt-barium hexa-aluminate (Pt-BHA) nanocatalyst at stationary reactor operation ('SS') and reverse-flow operation ('RFR') with varying methane/oxygen ratio. One can see that the results both at SS

and RFR are significantly improved in comparison to the conventional supported platinum catalyst (see fig. 1). Furthermore, heat-integration again leads to a strong improvement in conversions and selectivities for this catalyst, raising methane conversion at stoichiometric conditions to about 80% with hydrogen selectivities of about 95%. While this is still far from the thermodynamically allowed complete conversion at perfect selectivity, it is a drastic improvement in comparison to the values of less than 50% conversion and about 55% H_2 selectivity at conventional stationary reactor operation with a conventional catalyst.

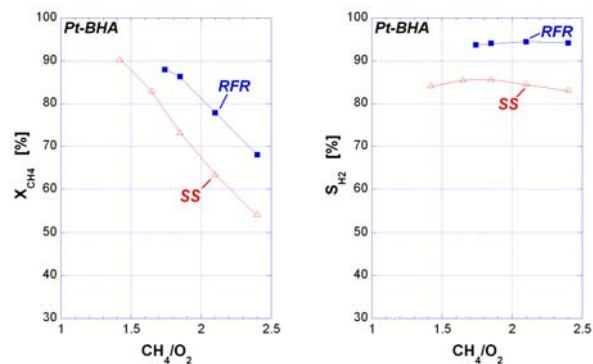


Figure 3. Experimental results for CPO of methane over a novel nanocomposite Pt-BHA catalyst in a comparison between steady-state (SS) and reverse-flow operation (RFR). Methane conversions (right graph) and hydrogen selectivities (left graph) are shown versus methane/oxygen-ratio at a reactor feed of 4 slm methane/air. The duration of one half-period at RFR operation was 15 s.

Conclusions

We presented some recent results from our ongoing studies towards the development of a flexible and efficient process for methane valorization via direct catalytic partial oxidation to synthesis gas or hydrogen.

The combination of reactor engineering with catalyst development, and of experimental investigations with numerical simulation is essential for the development of such processes which we see as critical enabling technologies for a more efficient and sustainable utilization in particular of small-scale, decentralized and remote methane resources.

Acknowledgement. Financial support by the German Science Foundation (DFG), the Funds of the Chemical Industry (VCI), and the Max-Planck-Society (MPG) are gratefully acknowledged.

References

- (1) Climate Change 2001: The Scientific Basis, IPCC, **2001**, http://www.grida.no/climate/ipcc_tar/wg1/index.htm.
- (2) EPA Report on US Methane Emissions, **1999**, <http://www.epa.gov/ghginfo/pdfs/07-complete.pdf>
- (3) Hansen, J.; Sato, M.; Ruedy, R.; Lacis, A.; Oinas, V; *Proc. Natl Acad. Sci.* **2000**, *97*, 9875.
- (4) Neumann, D.; Vesper, G. *AIChE Journal*, **2003**, accepted.
- (5) Schicks, J.; Neumann, D.; Specht, U.; Vesper, G., *Catal. Today* **2003**, *81*, 287
- (6) Frauhammer, J.; Vesper, G., *Chem. Eng. Sci.* **2000**, *55*, 2271

STRUCTURAL REQUIREMENTS AND ACTIVATION PATHWAYS IN REACTIONS OF METHANE CATALYZED BY SUPPORTED METALS

Junmei Wei and Enrique Iglesia

Department of Chemical Engineering, University of California at Berkeley,
Berkeley, CA, 94720, USA

CH₄ reactions with CO₂ or H₂O lead to synthesis gas mixtures, which are used to produce valuable fuels and chemicals. Rigorous assessments of the relevant elementary steps and of the effects of metal dispersion and support on reaction rates and selectivities have remained elusive. Here, we report isotopic tracer and kinetic studies that provide a simple mechanistic picture and a unifying kinetic treatment of CH₄/CO₂, CH₄/H₂O, and CH₄ decomposition reactions on supported Rh, Ni, Pt, Ru, and Ir catalysts. The required kinetic processes are exclusively limited by the first activation of a C-H bond in CH₄ and the relevant rate constant is unaffected by the presence or the concentration of co-reactants (H₂O, CO₂) or by the identity of the support. The elementary steps proposed and confirmed by kinetic and isotopic evidence provide a rigorous basis for treating the dynamics of carbon formation during CH₄ reforming. On all metals, turnover rates increased with increasing metal dispersion. This reflects the higher reactivity of coordinatively unsaturated surface atoms for C-H bond activation reactions.

The kinetic effects of CH₄, H₂O, and CO₂ pressures on CH₄ reaction rates were measured at 850-1000 K and 0.1-1.5 MPa total pressure over a wide range of reactant ratios. Transport artifacts were excluded using dilution strategies. Measured reaction rates were corrected for the distance of the overall reaction from thermodynamic equilibrium in order to obtain rigorous values of the forward kinetic rates. On all catalysts, CH₄ reactions rates were proportional to CH₄ pressure, independent of co-reactant pressure, and identical for CH₄/CO₂, CH₄/H₂O, and CH₄ decomposition reactions, indicating that these reactions are mechanistic equivalent and that C-H bond activation is the sole kinetically-relevant step in all three reactions. These conclusions were confirmed by identical CH₄/CD₄ kinetic isotope effects for reforming and decomposition reactions and by undetectable H₂O/D₂O isotopic effects. The kinetic relevance of C-H bond activation is consistent with the relative rates of chemical conversion and isotopic mixing in CH₄/CD₄/CO₂ mixture and with the isotopic evidence for the quasi-equilibrated nature of co-reactant activation and H₂ and H₂O desorption obtained from reactions of CH₄/CO₂/D₂ and ¹²CH₄/¹²CO₂/¹³CO mixtures. Taken together, these quasi-equilibrated steps involved in H₂O, H₂, and CO formation lead to equilibrated water-gas shift reactions. These elementary steps provide also a rigorous basis for a kinetic treatment of carbon formation processes during CH₄ reactions at high temperatures on metal surfaces and for the assembly of carbon filaments as specific side products of these reactions [1].

Turnover rates were obtained from forward reaction rates and metal dispersions. Turnover rates and metal dispersions are based on strongly chemisorbed H₂ or on H₂-O₂ titration measurements. Turnover rates for CH₄-H₂O reaction increase with increasing dispersion and decreasing size of Rh, Ir, Pt, Ru and Ni clusters supported on various oxides (Figure 1). Identical turnover rates and dispersion effects rates were observed CH₄-CO₂ reactions, as expected from the rigorous kinetic equivalence of CH₄-CO₂ and CH₄-H₂O reactions. On all metals, turnover rates increased monotonically with increasing metal dispersion, suggesting that the coordinatively unsaturated surface atoms prevalent in small crystallites are significantly more active than those in the low-index planes

predominately exposed on larger metal crystallites. Similar effects have been measured and predicted theoretically for model metal surfaces [2,3]. These low-coordination surface atoms appear to provide more stable binding sites for CH_x and H products and for the relevant activated complexes. Similar CO oxidation rates were measured before and after CH₄ reactions on all of the noble metals, indicating that metal dispersion is not affected by unreactive deposits or sintering during catalysis. The identity of the support does not influence turnover rates, and previous literature claims for support effects, attributed to co-reactant activation on the supports, are inconsistent with these data and with the kinetic irrelevance of co-reactant activation steps. Supports, however, influence metal dispersion, and in this manner, they can affect turnover rates.

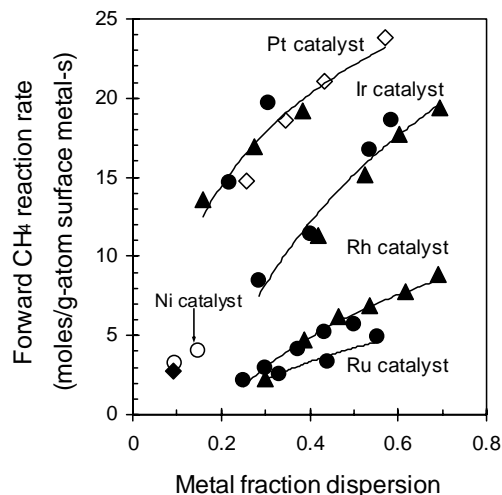


Figure 1. Forward CH₄ turnover rates for H₂O reforming of CH₄ on different metal clusters as a function of metal dispersion on various supports (873 K, 20 kPa CH₄, (▲) ZrO₂, (●) γ -Al₂O₃, (◇) ZrO₂-CeO₂ as support, (○) MgO-A (◆) MgO-B).

This study was supported by BP as part of the Methane Conversion Cooperative Research Program at the University of California at Berkeley.

References

- (1) Wei, J.; and Iglesia, E. submitted to *J. Catal.*
- (2) Beebe, T.P.; Goodman, D.W.; and Kay, B.D. *J. Chem. Phys.*, **1987**, 87, 2305.
- (3) Watwe, R.M.; Bengaard, H.S.; Rostrup-Nielsen, J.R.; Dumesic, J.A.; and Nørskov, J.K. *J. Catal.*, **2000**, 189, 16.

C₁ Coupling via Bromine Activation and Tandem Catalytic Condensation and Neutralization over CaO/Zeolite Composites.

Ivan M. Lorkovic,^{a,*} Maria L. Noy,^a Walter A. Schenck,^a Mike Weiss,^b Jeffrey H. Sherman,^b Eric W. McFarland,^{b,c} Galen D. Stucky,^a and Peter C. Ford^a

^aDepartment of Chemistry and Biochemistry, University of California, Santa Barbara, CA 93106.

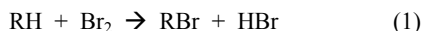
^bGas Reaction Technologies, Inc., 301B S. Wimbrow Dr. Sebastian, FL 32958

^cDepartment of Chemical Engineering, University of California, Santa Barbara, CA 93106

Introduction

Although much of the world's methane is stranded, utilization of available methane as a chemical feedstock begins in practice with its conversion to methanol by partial oxidation to syn gas followed by recondensation. Subsequent conversion of CH₃OH to olefins was made possible by discoveries in the early seventies by Mobil scientists,¹⁻⁴ and later generalized by other workers to CH₃X (X = halide, SH, NH₂, OCH₃) condensation.⁵⁻¹⁴ The proposed mechanism^{15, 16} is an initial dehydrative coupling to form the actual catalyst, a relatively ill-defined adsorbed cyclic hydrocarbocation (carbon pool). The technology has been widely developed for multiple product outputs, and may be considered an alternative to the reliable but extreme steam cracking method of olefin production from low and middle petroleum distillates. For CH₃Cl, formed from CH₄ oxychlorination, the product in most cases is an aromatic-rich liquid together with HCl and water,⁸⁻⁹ with some variation depending on the promoters used.¹⁰⁻¹⁴ While this chloromethane chemistry has been well characterized and the kinetics are favorable, the process has not been commercialized.

Above, we demonstrated a two step technique for partial oxidation of alkanes by oxygen in which a two electron oxidation of a C-H bond is effected by bromine, giving HBr and bromoalkane (Equation 1).¹⁷⁻²⁰



These intermediates were further converted either to unsaturated hydrocarbons (for C₂+) or to oxygenates by reaction with a metal oxide solid reactant. The metal oxide served to remove HBr actively, and to direct the output to specific partial oxidation products dependent upon the metal oxide composition and reaction conditions. Complete recovery of bromine and regeneration of the metal oxide was accomplished by reaction of the spent solid with O₂.

During the course of development of active and regenerable metathesis materials, oxides of calcium were investigated because of their lack of facile redox activity (leading to deep oxidation), stoichiometric HBr neutralization capacity, and the nearly thermoneutral regeneration of CaBr₂ with O₂ to give CaO and Br₂ ($\Delta G^\circ = 14.9$ kcal/mol). We observed that while activated HZSM-5 (Si:Al = 80) rapidly lost catalytic CH₃Br coupling activity over the course of 10 minutes, calcium oxide zeolite composites[#] quantitatively neutralized HBr and effected the presumably superacidic condensation of methyl bromide to higher olefins (Eq. 2).



Figure 1 shows the time dependent product output from two serial continuous flow reactors for methane bromination (1) at 525° C. followed by reaction over a bed of CaO-ZSM-5 at 400° C. (2). Retention of bromine within the second packed bed under these conditions is better than 99.9%, while the product output is very similar to that observed for CH₃OH coupling over Ca/ZSM-5.²¹

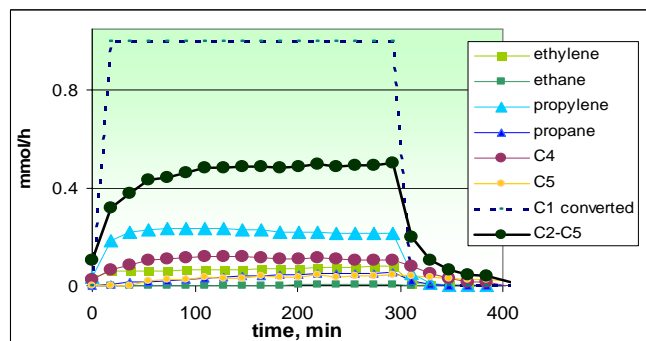
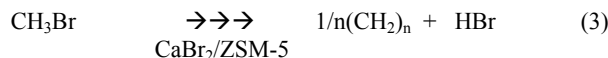


Fig. 1. Output of dual stage reactor with a feed of CH₄:Br₂ (5:0.5 cc/min). First Stage: Plug flow reactor (1 x 100 mm glass tube, 500° C. space time = 0.3 s. Br₂ conversion = 100%, CH₄ conversion = 8.2%). Second Stage: Fixed bed: (10 x 100 mm plug of 5 g. Ca-ZSM-5, 400 C, space time = 20 s, WHSV = 0.04 h⁻¹).

The reaction in Figure 1 represents HBr sequestration to 50-75% of neutralization capacity (5 hours, 5cc/min CH₄, 0.5 cc/min Br₂(g)) of the solid. After more than 10 runs and regenerations (525 C, 5 hours, 5 cc/min O₂, quantitative Br₂ recovery), the coupling/neutralization reactivity and product distribution of the regenerated solid (50% selectivity to C₂-C₅) remained unchanged within experimental error. Furthermore, these materials are also catalytic (Eq. 3) in that even after HBr breakthrough due to metal



oxide depletion, the conversion of bromomethanes under the conditions shown in Figure 1 continues (Figure 2). This catalytic reactivity allows use of more specialized auxiliary metal oxides for HBr sequestration and Br₂ recovery.

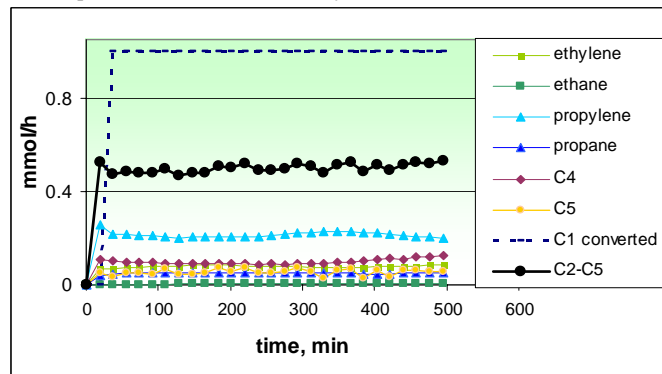


Figure 2. Continued methane bromination and condensation over the same Ca/ZSM-5 bed (5.0 g) used in Figure 1 past the HBr saturation limit (reached at ~100 min) of the bed. Feed: CH₄:Br₂ (5:0.5 cc/min). First Stage: Plug flow reactor (1 x 100 mm glass tube, 500° C. space time = 0.3 s. Br₂ conversion = 100%, CH₄ conversion = 8.2%). Second Stage: Fixed bed: (10 x 100 mm plug of 5 g. Ca-ZSM-5, 400 C, space time = 20 s, WHSV = 0.04 h⁻¹).

Methane partial oxidation by free radical bromination leads to significant buildup of CH_2Br_2 as well as some CHBr_3 at appreciable methane conversion. Over CaO/ZSM-5, CH_2Br_2 condenses predominantly to adsorbed carbon in the absence of CH_3Br while cross coupling between CH_2Br_2 and CH_3Br is manifest in the higher output of aromatics (best represented as mesitylene C_9H_{12}), when both species are present (Figure 3).

Notably, with pure CH_3Br feed, the yield of $\text{C}_2\text{-C}_5$ is significantly higher, and that of adsorbed carbon and aromatics significantly lower than observed for a mixed bromomethane feed, Figure 3.

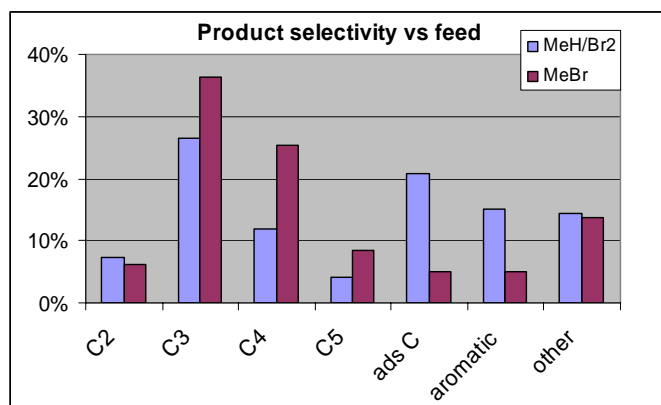


Fig. 3 Comparison of product selectivity for methane/bromine reaction product feed vs pure CH_3Br feed (conditions as in Fig. 1).

The advantage of Br_2 over other halogens in this partial oxidation scheme may be understood in terms of the reduction potential of Br_2 to Br^- (1.07 V vs NHE), which in comparison with Cl_2 (1.36 V) and I_2 (0.54 V), makes alkane bromination significantly less exothermic, yet spontaneous enough to go to completion. Bromine also allows for utilization of a wider range of metal oxides as bromide metathesis reagents because the reoxidation of metal bromides by O_2 (1.23 V) can be accomplished under relatively mild conditions. Despite the slightly lower selectivity for monobromination versus monochlorination for comparable methane conversion, a higher degree of reversibility is expected for the weaker C-Br bonds²² than exists for C-Cl bonds for corresponding C_1 species. In addition, CH_3Br and CH_2Br_2 are expected to be significantly easier to separate from each other than are CH_3Cl and CH_2Cl_2 . Hence polybrominated methanes are not necessarily lost from a methane conversion process and may be induced to compropionate with CH_4 feed, raising overall CH_3Br , and ultimately olefin, yield.²³

We direct further work towards establishing the generality of the condensation reactivity of CH_3Br over microporous solids to give olefins or other products and draw on analogies to CH_3OH coupling.²¹ Ultimately our goal is to utilize the three step low temperature route -- bromination, coupling, regeneration -- to streamline the production of higher hydrocarbons from methane, technology which is presently dominated by processes involving CH_3OH or synthesis gas as intermediates. Selective bromination and reactor configurations favoring compropionate of methane and CH_2Br_2 or CHBr_3 to CH_3Br are potential routes to improved carbon utilization.

Acknowledgements: This research was funded by Gas Reaction Technologies, Inc., through a sponsored research agreement with the University of California.

Notes

CaO/ZSM-5 composites were prepared by wet impregnation of 1 part $\text{Ca}(\text{NO}_3)_2$ to 4 parts H-ZSM-5, (Si:Al = 80:1, obtained from Zeolyst Corp.), drying at 125° C. overnight, followed by calcination at 500° C. overnight. Catalytic coupling reactivity was not evident until after the first $\text{CH}_3\text{Br}/\text{HBr}$ metathesis/regeneration cycle.

References

- C. D. Chang and A. J. Silvestri, *J. Catal.* 1977, **47**, 249.
- C. D. Chang, W. H. Lang, and A. J. Silvestri, *US Pat.* 3 998 898, 1976.
- C. D. Chang and W. H. Lang, in *US Pat.* 3 899 544, 1975
- S. A. Butter, A. T. Jurewicz, and W. W. Kaeding, *US Pat.* 3 894 107, 1975.
- J. F. Haw, W. Song, D. M. Marcus, and J. B. Nicholas, *Acc. Chem Res.* 2003, **36**, 317.
- S. Svelle, S. Kolboe, U. Olsbye, and O. Swang, *J. Phys. Chem. B*, 2003, **107**, 5251.
- V. N. Romannikov and K. G. Ione, *Kinet. Katal.*, 1984, **25**, 75.
- R. P. Noceti and C. E. Taylor, *US Pat.* 4 769 504, 1988.
- C. E. Taylor, R. P. Noceti, and R. R. Schehl, in 'Direct Conversion of Methane to Liquid Hydrocarbons through Chlorocarbon Intermediates', ed. D. M. Bibby, C. D. Chang, R. F. Howe, and S. Yurchak, Amsterdam, 1988.
- G. A. Olah, H. Doggweiler, J. D. Felberg, S. Frohlich, M. J. Grdina, R. Karpeles, T. Keumi, S.-I. Inaba, W. M. Ip, K. Lammertsma, G. Salem, and D. C. Tabor, *J. Am. Chem. Soc.* 1984, **106**, 2143.
- C. M. White, L. J. Douglas, J. P. Hackett, and R. R. Anderson, *Energy and Fuels*, 1992, **6**, 76.
- Y. Sun, S. M. Campbell, J. H. Lunsford, G. E. Lewis, D. Palke, and L.-M. Tau, *J. Catal.* 1993, **143**, 32.
- D. K. Murray, T. Howard, P. W. Goguen, T. R. Krawietz, and J. F. Haw, *J. Am. Chem. Soc.* 1994, **116**, 6354.
- K.-J. Jens, in 'Methane Conversion via Methyl Chloride: Condensation of Methyl Chloride to Light Hydrocarbons', ed. D. M. Bibby, C. D. Chang, R. F. Howe, and S. Yurchak, Amsterdam, 1988.
- J. R. Anderson, *Appl. Catal.*, 1989, **47**, 177.
- F. Banderman and P. Lersch, *Appl. Catal.* 1991, **75**, 133.
- X.-P. Zhou, A. Yilmaz, G. A. Yilmaz, I. M. Lorkovic, L. E. Laverman, M. J. Weiss, J. H. Sherman, E. W. Mcfarland, G. D. Stucky, and P. C. Ford, *Chem. Commun.* 2003, 2294.
- X.-P. Zhou, I. M. Lorkovic, G. D. Stucky, P. C. Ford, J. H. Sherman, and P. Grosso, *US Pat.* 6 462 243, 2002.
- X.-P. Zhou, I. M. Lorkovic, G. D. Stucky, P. C. Ford, J. H. Sherman, and P. Grosso, *US Pat.* 6 472 572, 2002.
- X.-P. Zhou, I. M. Lorkovic, and J. H. Sherman, *US Pat.* 6 486 368, 2002.
- M. Stoecker, *Microporous Mesoporous Mat.* 1999, **29**, 3.
- D. R. Lide, 'CRC Handbook of Chemistry and Physics 1999-2000: A Ready-Reference Book of Chemical and Physical Data', CRC Press, 2000.
- I. M. Lorkovic, P. Grosso, J. H. Sherman, E. M. Mcfarland, P. C. Ford, and G. D. Stucky. *Manuscript in Preparation.*

DIRECT SYNTHESIS OF ACETIC ACID FROM METHANE AND CARBON DIOXIDE OVER SiO₂ AND TiO₂ SUPPORTED Pd AND Rh CATALYSTS

Yihui Ding, Wei Huang, Ping Jin, and Kechang Xie

Key laboratory of Coal Science and Technology, Ministry of Education and Shanxi Province; Institute of Coal Chemistry and Engineering, Taiyuan University of Technology, Taiyuan 030024, Shanxi, China

Introduction

Based on the beneficial experience in synthesis of acetic acid from CO₂ and H₂, the pioneer noticed of two pieces of information in support of this research. One was the level 435.43 kJ/mol of bond energy of H-H bond in H₂, which is equivalent to that of C-H in CH₄; the other was the same intermediate CH_x involved in both CH₄ activation and CO₂ hydrogenation. And this led to a novel and interesting route to conversion of greenhouse gases, CH₄ and CO₂, directly to acetic acid by a two-step sequence employing heterogeneous catalysts like Cu-Co oxides¹. In this work, we have investigated the supported transition metal catalysts and found that Pd and Rh catalysts exhibited a better performance.

Experimental

The catalysts were prepared by incipient wetness impregnation of silica from an aqueous solution of their chlorides. The slurry was dried at 110 °C for 16 h and then calcined at 500 °C for another 5 h. The reaction was implemented in a micro-reactor at atmospheric pressure with 400 mg catalyst (sized 40-60 mesh). A flowing argon (at a flow rate of 100 cm³/min) was first used for 10 min to purge out the impurity gases in the reactor. The catalyst was then reduced from the room temperature to 400 °C. The reactor was maintained at this temperature for 2.5 h. The catalyst was then cooled in argon (or nitrogen) stream to the desired temperature. After that, a two-step sequence began with exposing the catalyst to a flow of CH₄ (85 cm³/min) for 5 min and CO₂ (85 cm³/min) for 10 min in turn. More CO₂ was fed to increase the yields on the basis of the consumed CH₄. The products were collected at ice-water mixture temperature by a bubbling absorber filled with caustic soda solution (50 ml). After reaction for 20 turns around 5 h, the products were analyzed by IC20 gas chromatography.

Results and Discussion

Figure 1 shows the yield of acetic acid synthesized directly from CH₄ and CO₂ over Pd/SiO₂ catalysts, while Figure 2 presents the results obtained from Rh/SiO₂ catalysts.

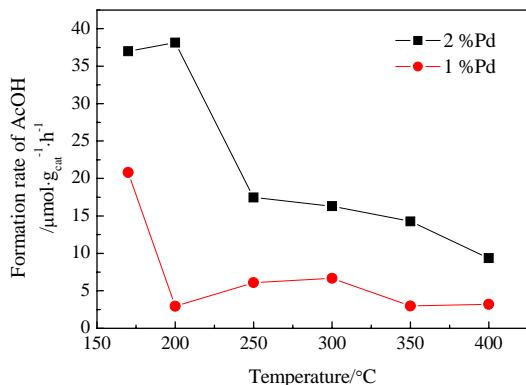


Figure 1. The formation rate of AcOH over Pd/SiO₂ at different temperatures

One can observe an apparent decline and a slight decline vibrated in acetic acid yield along with the temperature rises from 170 to 400 °C in the presence of catalyst 2%Pd/SiO₂ and 1%Pd/SiO₂. The maximum yield of acetic acid is 37.0 and 38.2 μmol/g_{cat}·h at 170 °C and 200 °C of the former, and the latter is 20.8 μmol/g_{cat}·h. An interesting point we noticed is that some formic acid was also formed for reaction carried out at 300 °C over both 2%Pd/SiO₂ and 1%Pd/SiO₂.

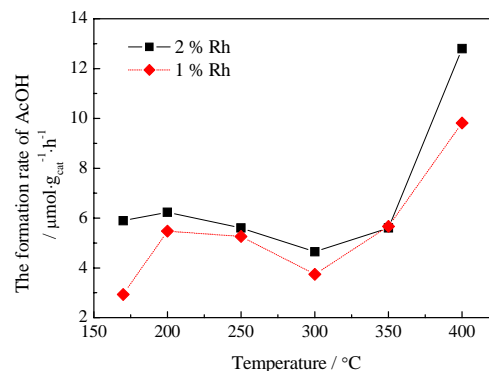


Figure 2. The formation rate of HCOOH over Rh/SiO₂ at different temperatures

The catalysts Rh/SiO₂ can also give to acetic acid. However, its catalytic activity was not as good as we expected. As represented in Figure 2, the yield of acetic acid does not exhibit a marked decline, but ascend as the temperature rises. The best results we obtained in our experiments are 12.8 μmol/g_{cat}·h for 2%Rh/SiO₂ and 9.8 μmol/g_{cat}·h for 1%Rh/SiO₂ at 400 °C. And no formic acid was observed. Unsurprisingly, a higher yield can be achieved by using more supported amount of metal.

TiO₂-supported Rh, Pd catalysts give results similar to SiO₂. The yield of acetic acid over Pd catalyst is higher than Rh catalyst, as shown in Figure 3. And, only Pd catalyst can lead to a formation of formic acid too. The yield of formic acid is shown in Figure 4.

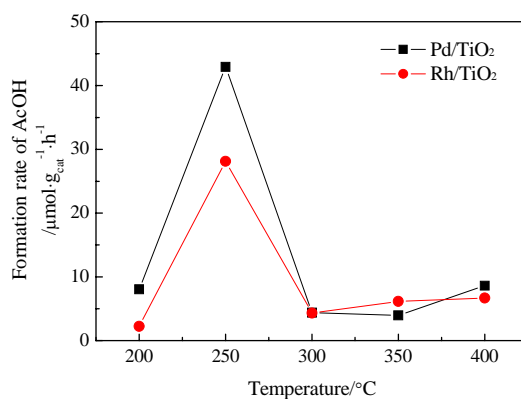


Figure 3. The formation rate of AcOH over Pd, Rh/TiO₂ at different temperatures

The present investigation has confirmed the effectiveness of the direct synthesis of acetic acid directly from methane and carbon dioxide. This route provides a potentially valuable means to convert directly greenhouse gases, CH₄ and CO₂, to acetic acid, a useful target molecule for methane conversion². Further study is being conducted.

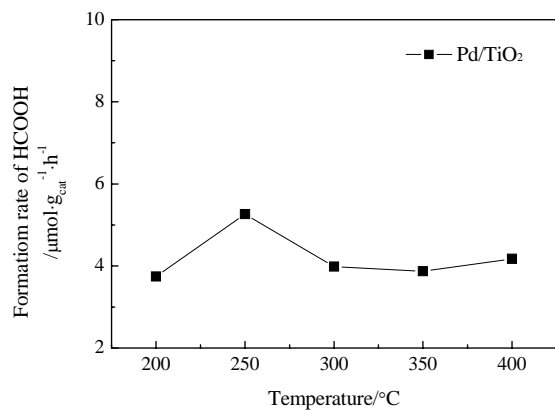


Figure 4. The formation rate of HCOOH over Pd/TiO₂ at different temperatures

Acknowledgement

The authors are grateful to the support from both the National Natural Science Foundation and the Research Foundation to Returned Scholars of Shanxi Province, China.

References

- (1) Huang, W.; Xie, K.C.; Wang, J.P. *J. Catal.*, **2001**, *201*, 100.
- (2) Lin, M.; Sen, A. *Nature*, **1994**, *368*, 613.

PARTIAL OXIDATION OF METHANE TO SYNGAS OVER $\text{BaTi}_{1-x}\text{Ni}_x\text{O}_3$ CATALYSTS

Cuili Guo, Jinli Zhang, Wei Li, Pingfan Zhang and Yiping Wang

School of Chemical Engineering, Tianjin University, Tianjin 300072, China

Introduction

Catalytic partial oxidation of methane to syngas is a slightly exothermic, highly selective, and energy efficient process. It gives syngas with H_2 to CO ratio of 2:1 that is suitable for F-T and methanol syntheses. Hence, much effort has been devoted to partial oxidation of methane to syngas in the presence of catalysts. Perovskite catalysts have attracted much attention for more than two decades due to their potential commercial applications as catalysts [1-3]. Lago et al[4] observed that a series of cobalt-containing perovskites LnCoO_3 ($\text{Ln}=\text{La, Pr, Nd, Sm, and Gd}$) have high activity and selectivity for the partial oxidation of methane to syngas. Slagtern and Olsbye[5] and Provendier[6] concluded that the addition of a third metal into the perovskite structure is necessary to stabilize the catalytic system. Supported Ni catalysts on CaTiO_3 , SrTiO_3 and BaTiO_3 oxides have been investigated[7]. Ni/SrTiO₃ and Ni/BaTiO₃ showed that high activity for POM.

In this study, partial oxidation of methane was investigated over $\text{BaTi}_{1-x}\text{Ni}_x\text{O}_3$ catalysts. We evaluated the catalysts prepared with different Ni loading amount and with different calcination temperatures. The reaction mechanism and activity are discussed.

Experimental

A series of $\text{BaTi}_{1-x}\text{Ni}_x\text{O}_3$ catalysts were prepared by the sol-gel method with x values ranged from 0 to 0.3. The calculated amounts of tetrabutyl titanate, citric acid and glycol were mixed and stirred to solution under reflux. The calculated amounts of $\text{Ba}(\text{NO}_3)_2$ and $\text{Ni}(\text{NO}_3)_2 \cdot 6\text{H}_2\text{O}$ were added to the hot solution with stirring and to make nitrate decomposition. A gel was obtained by adding triethanolamine. The nanometer powders of $\text{BaTi}_{1-x}\text{Ni}_x\text{O}_3$ were made by calcining the dried gel for 2h at different temperature (600, 700 and 800 °C).

X-ray diffraction (XRD) patterns were obtained with a Rigaku 2038 diffractometer using $\text{CuK}\alpha$ radiation at a rate of 4°/min. The XRD patterns of $\text{BaTi}_{1-x}\text{Ni}_x\text{O}_3$ shows that the pure perovskite structure is formed. The particle textures of the samples were investigated using a JEOL TEM-100X II transmission electron microscope. The TEM images of $\text{BaTi}_{1-x}\text{Ni}_x\text{O}_3$ indicate that the mean sizes of the particles are 13 to 21 nm and particles distributions are uniform. Specific surface areas were derived from N_2 adsorption isotherms that were determined with a Chem BET-3000 instrument. The values of the BET specific surface area of $\text{BaTi}_{1-x}\text{Ni}_x\text{O}_3$ are in the 10-16 m^2/g .

The methane oxidation reaction was carried out in a fixed bed quartz reactor (8 mm in i.d.) filled with 300 mg catalyst at atmospheric pressure. The feed gas mixture were composed of CH_4 , O_2 and N_2 with a space velocity of $3 \times 10^5 \text{ h}^{-1} \text{ g}^{-1}$. The products were analyzed on-line by a SP3420 gas chromatograph equipped with TCD.

Results and Discussion

Table 1 lists the results of activity and selectivity of $\text{BaTi}_{1-x}\text{Ni}_x\text{O}_3$ with different x values (Ni content) in POM reaction at 950 °C, which indicate that the activity of BaTiO_3 is very low and the activity of $\text{BaTi}_{1-x}\text{Ni}_x\text{O}_3$ increase significantly with the addition of

Ni into the perovskite. The activity of $\text{BaTi}_{0.8}\text{Ni}_{0.2}\text{O}_3$ is the highest with CH_4 conversion of 95% and CO selectivity of 98%.

Table 1. Effect of x Value in $\text{BaTi}_{1-x}\text{Ni}_x\text{O}_3$ on the Activity at 950 °C

X value	CH_4 conversion (%)	CO selectivity (%)
0 (BaTiO_3)	40	75
0.1 ($\text{BaTi}_{0.9}\text{Ni}_{0.1}\text{O}_3$)	89	97
0.2 ($\text{BaTi}_{0.8}\text{Ni}_{0.2}\text{O}_3$)	95	98
0.3 ($\text{BaTi}_{0.7}\text{Ni}_{0.3}\text{O}_3$)	86	96

Figure 1 shows the catalytic activity for partial oxidation of CH_4 at CH_4/O_2 mole ratio of 2:1 with a space velocity of $4.4 \times 10^5 \text{ h}^{-1} \text{ g}^{-1}$ over $\text{BaTi}_{0.8}\text{Ni}_{0.2}\text{O}_3$ calcined at different temperatures. From Figure 1, we can see that with the increase of calcination temperature, the activation temperature of $\text{BaTi}_{0.8}\text{Ni}_{0.2}\text{O}_3$ decrease and the optimum reaction temperature scarcely change. It is suggested that the perovskite catalysts should be calcined at low temperatures, since the activity of $\text{BaTi}_{0.8}\text{Ni}_{0.2}\text{O}_3$ was significantly reduced with an increase of calcination temperature from 600 to 800 °C.

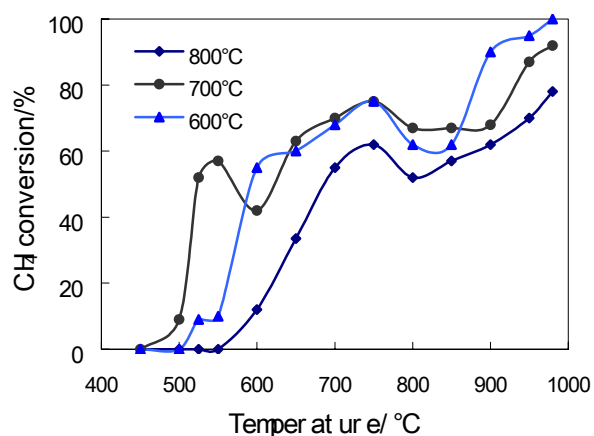


Figure 1. CH_4 conversion versus temperature

The results reveal that the calcination temperature of the $\text{BaTi}_{1-x}\text{Ni}_x\text{O}_3$ has a close relation with activity. The increase of calcination temperature can lead to a decrease in surface area and an increase in crystal size, which make concentration of active oxygen decrease. Thereby the catalytic activity of $\text{BaTi}_{1-x}\text{Ni}_x\text{O}_3$ decreases.

Figure 1 shows CH_4 conversion increase with the increase of reaction temperature. It is found from experiments that the temperature difference between reaction temperature and control temperature changed from 24°C to -4°C with the increase of reaction temperature, which indicate the heat of reaction gradually decrease. These results suggest that the combustion of a part of CH_4 to H_2O and CO_2 (exothermic reaction) first took place in the lower temperature and reforming reaction of CH_4 with H_2O and CO_2 (endothermic reaction) was followed in the higher temperature for POM over $\text{BaTi}_{1-x}\text{Ni}_x\text{O}_3$. This result is agreement with the results in literature [7].

Figure 2 shows the catalytic activity for partial oxidation of methane at CH₄/O₂ mole ratio of 2:1 with a space velocity of $4.4 \times 10^5 \text{ h}^{-1} \text{ g}^{-1}$ over BaTi_{0.8}Ni_{0.2}O₃ at different reaction time. The results show that the catalytic activity of BaTi_{0.8}Ni_{0.2}O₃ increases with the increase of the reaction time. When the reaction time is over 3h, the catalytic activity of BaTi_{0.8}Ni_{0.2}O₃ remained unchanged after 40h of operation at 950 °C. This indicates that the activation stage of the catalyst is needed at the initiation stage of reaction and that catalyst is stable under the POM reaction at 950°C for 40h.

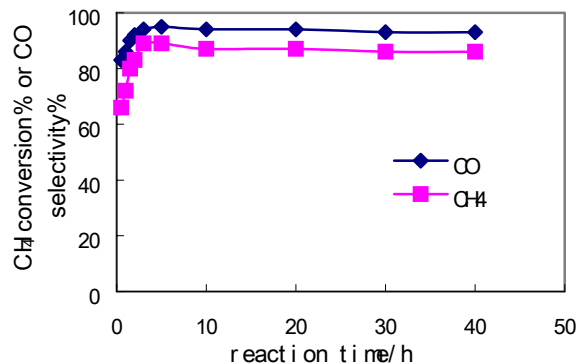


Figure 2. CH₄ conversion and CO selectivity versus reaction time

Conclusions

From the results above, we can conclude that perovskite BaTi_{1-x}Ni_xO₃ are highly efficient catalysts for POM. The calcination temperature of the BaTi_{1-x}Ni_xO₃ can affect the activation temperature. The addition of Ni into the perovskite structure makes activity increase significantly. The most active system BaTi_{0.8}Ni_{0.2}O₃ presents a stable activity, with no deactivation at 950°C during 40h test.

References

- (1) Ferri, D.; Forni, L. *Appl. Catal. B.* **1998**, *16*, 119.
- (2) Cimino, S.; Lisi, L.; Pirone, R.; Russo, G.; Turco, M. *Catal. Today* **2000**, *59*, 19.
- (3) Shu, J.; Kaliaguine, S. *Appl. Catal. B.* **1998**, *16*, L303.
- (4) Lago, R.; Bini, G.; Pena, M.A.; Fierro, J.L.G. *J. Catal.* **1997**, *167*, 198.
- (5) Slagtern, A.; Olsbye, U. *Appl. Catal. A.* **1994**, *110*, 99.
- (6) Provendier, H.; Petit, C.; Estournes, C.; Libs, S.; Kiennemann, A. *Appl. Catal. A.* **1999**, *180*, 163.
- (7) Takehira, K.; Shishido, T.; Kondo, M. *J. Catal.*, **2002**, *207*, 307.

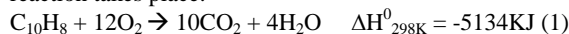
The Potential of the CO₂ reforming of CH₄ as a method of CO₂ mitigation. A thermodynamic study.

Damien Treacy, Julian R.H. Ross

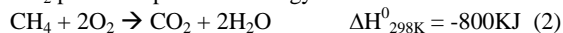
Centre for Environmental Research,
University of Limerick,
Ireland.

1. Introduction.

Carbon dioxide (CO₂) has been identified as the most significant greenhouse gas arising from anthropogenic activities. Presently, atmospheric levels of CO₂ are thought to be about 25% higher than in pre-industrial times [1]. It is of great importance to reduce anthropogenic CO₂ emissions in order to counteract global warming. In many countries (7 in the EU) a tax related to CO₂ emissions has been introduced in order to encourage better plant efficiency and/or create increased investment in CO₂ mitigation. One method of accomplishing a reduction in CO₂ emissions is fuel switching. As an example, if naphtha is used as a fuel, the following combustion reaction takes place:

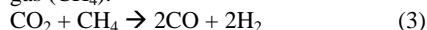


and 0.085g of CO₂ is released per KJ of energy produced. If the naphtha is replaced with a low-carbon containing fuel such as natural gas the energy:CO₂ ratio becomes more favourable with 0.055g of CO₂ produced per KJ of energy released.



In the long term one must consider more innovative options for anthropogenic CO₂ reduction. One such method, which is presently being extensively investigated, is the sequestration of CO₂ produced by concentrated sources (such as industry and power stations) and the subsequent disposal of the trapped CO₂ in reservoirs such as the deep sea or in aquifers [3,4]. Ocean disposal is seen as the method with the greatest long-term application possibilities. However there are a number of relevant concerns about this method of CO₂ disposal: how much of the sequestered CO₂ will be returned to the atmosphere and when will it be returned? According to Adams *et al.* [5] the atmosphere and the ocean eventually equilibrate on a timescale of about 1000 years regardless of where the CO₂ is originally discharged. Wong *et al.* [4] estimated that the disposal of CO₂ in to the intermediate waters of the North Pacific would buy only 20-50 years of CO₂ reduction. Another option which may aid in the reduction of CO₂ emissions is the fixation of CO₂ as a chemical. The advantage of CO₂ utilisation (fixation) over CO₂ disposal is that the production of chemicals with an economic value is possible. Aresta *et al.* [6,7] have done extensive research in this area. They have shown that the production of materials such as carbamic esters, urea and methylamines can be produced from CO₂ feedstocks.

Another reaction which consumes CO₂ is the dry reforming of natural gas (CH₄).

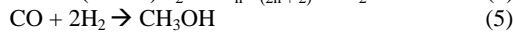
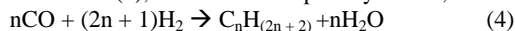


This paper assesses whether dry reforming can be viably used as a method of CO₂ mitigation. We have calculated all-over energy balances for a number of all over process scenarios involving the production of synthesis gas followed by the production of some other product (methanol, sulphur-free diesel and carbon).

2. Methods of Analysis.

Much of the work carried out on dry reforming of CH₄ has been justified by the argument that the reaction offers a route for the conversion of large amounts of CO₂. The product of reaction (3), synthesis gas, is an equimolar mixture of CO and H₂. Synthesis gas

can be used to produce higher value products, most notably sulphur free diesel (4), via Fischer-Tropsch synthesis, and methanol (5).



Both of these reactions ((4) and (5)) require H₂ to be added to the reactant synthesis gas feed in order to establish the correct reactant ratio. This hydrogen would usually be supplied by the steam reforming of CH₄ (6).



CO₂ and CH₄ are both relatively stable compounds with low potential energies. As a result the dry reforming reaction is highly endothermic and so energy has to be provided in order to drive it in the forward direction. Similarly, the steam reforming of CH₄ is also an endothermic reaction. The most likely energy source to drive these reactions will be the combustion of natural gas (2) and this process, in itself, produces CO₂.

In these calculations we assume CO₂ and steam reforming operate in parallel to form the necessary ratio of synthesis gas to produce; (i) methanol, (ii) sulphur free diesel, represented simply as C₆H₁₂, and (iii) carbon.

In the case of carbon production the process could occur directly via reaction (8);



or more likely by the production of synthesis gas (3) followed by the reduction of CO (9).

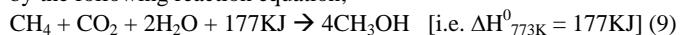


The carbon all-over process does not require additional steam reforming, as the synthesis gas ratio required for reaction (8) is 1.

In these calculations we assumed an all-over energy efficiency of 80%, i.e. 80% of the energy released from the exothermic final reaction step (e.g methanol synthesis) can be recycled to drive the endothermic reforming steps. The remainder of the energy required can be attained from the combustion of natural gas (also at an 80% energy efficiency). For simplicity, we have calculated the enthalpies for the processes involved at a single temperature of 773K. This temperature represents a compromise between the low and high temperature steps (the final reaction and the reforming steps respectively) likely to be involved in the all-over process. For example, methanol is produced by the Syntex (formerly ICI) process in the temperature range 473-573K [7], while reforming reactions are usually carried out in the temperature range 973-1223K [8].

(i) Methanol Synthesis.

In this study methanol is assumed to be produced in two steps. The first step involves the formation of synthesis gas via the combined steam and CO₂ reforming of CH₄ (reactions (3) and (6)). Following the reforming step, methanol is synthesised by reacting the resultant synthesis gas (CO and H₂). This all-over process can be summarised by the following reaction equation;



When the heat efficiency of the system is assumed to be 80%, the heat required to drive the reaction increases to 221KJ. This means for 1 mole of CO₂ to be consumed by reaction (9), a heat input of 221KJ is required from an external source. This usually is obtained by combusting natural gas;



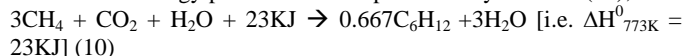
This implies that 0.34 moles of CO₂ will be released so as to provide the required energy to drive the all-over methanol synthesis reaction (9).

Therefore the all-over amount of CO₂ consumed in methanol synthesis process is 0.66 moles per mole of CO₂ consumed by the initial reforming of CH₄.

(ii) Sulphur Free Diesel (Fischer-Tropsch Synthesis).

Again this reaction occurs in two steps; the first being the reforming of CH₄ to produce synthesis gas while in the second step the resultant synthesis gas is reacted to produce higher hydrocarbons (C₆H₁₂).

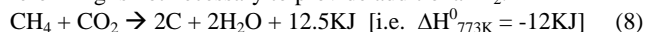
This all over energy process can be represented by reaction (10);



At an energy efficiency of 80%, the amount of energy required to drive reaction (10) is 28.8KJ. This energy is supplied by combusting CH₄ at the expense of 0.05 moles of CO₂ per mole of CO₂ consumed in the Fischer-Tropsch process. Therefore 0.95 moles of CO₂ are mitigated in this process per mole of CO₂ consumed in the initial reforming step.

(iii) Carbon production

This all-over reaction scheme differs from the previous two, as steam reforming is not necessary to provide additional H₂.



$\Delta H^0 < 0$ at the reaction temperature examined (indeed $\Delta H^0 < 0$ for all temperatures) and as a result there is no need for additional CH₄ combustion. For every mole of CO₂ consumed in reaction (11) one mole of CO₂ is mitigated.

3. Discussion.

Although there were a number of gross approximations made in calculating the all-over energy results presented in this paper, the results are very informative and may inevitably lead to one gaining a greater understanding of the environmental benefits, if any, of CO₂ reforming.

3.1 Methanol Synthesis.

CO₂ reforming when used in parallel with steam reforming can produce synthesis gas with a CO/H₂ ratio suitable for methanol synthesis or in Fischer-Tropsch synthesis. The all-over methanol synthesis process enables, theoretically, 0.66 moles of CO₂ to be mitigated per mole of CO₂ consumed in the initial reforming stage. A 66% reduction of CO₂ per mole of CO₂ reacted seems a favourable result in terms of CO₂ mitigation. Methanol is a very useful commodity, with a worldwide annual production of approximately 30 million tonnes [7,9]. Industrially methanol is synthesised in a process where synthesis gas is produced solely by the steam reforming of CH₄ [7]. If all the methanol production in the world were to be shifted to a process which combined CO₂ and steam reforming, 10 million tonnes of CO₂ could be consumed in this process. This would correspond to the mitigation of 6.6 million tonnes of CO₂ annually. However this amount of CO₂ is rather insignificant in comparison to global CO₂ emissions; excluding deforestation and land use change CO₂ emissions amounted to 23.9 giga tonnes in 1996 [10]. Therefore an equivalent reduction in global CO₂ emissions of 0.0027% is possible by producing methanol via the CO₂ reforming of natural gas. Unless vast new markets are created for methanol, this method does not constitute a viable potential method of CO₂ mitigation.

3.2 Fischer-Tropsch Synthesis.

Fischer-Tropsch synthesis date back to the nineteen twenties when Fischer and Tropsch first published results concerning the reaction of H₂ and CO over Co, Ni and Fe catalysts to produce paraffins, olefins, waxes and oxygenates. The present and, most likely long term, application of the Fischer-Tropsch (FT) process concerns the conversion of natural gas to liquid transportation fuels (green diesel). The advantage of green diesel fuel over more conventional diesel is that green diesel has a higher cetane rating. Green diesel also contains virtually no sulphur compounds and is low in aromatics, thus greatly reducing soot and particulate emissions. The FT process is highly exothermic: the heat released per mole of CO is approximately 1000 KJ (if one assumes the composition of the end product is primarily

C₆H₁₂). From an engineering aspect this highly exothermic reaction causes a number of problems in the design of an effective FT reactor [11]. However, if this heat can be rapidly transported from the reactor to heat exchangers it can be used to provide energy the endothermic CH₄ reforming reactions (3 and 6). The calculations carried out in this study show that the all-over reforming and FT process is slightly endothermic ($\Delta H = 23$ KJ). A small quantity of CH₄ combustion is therefore required to drive the all-over process. This occurs at the expense of 0.05 moles of CO₂ per mole of CO₂ consumed in the reforming-FT all-over process. Therefore, for every mole of CO₂ which is consumed in these all-over process, 0.95 moles of CO₂ can be mitigated. This method however only offers an effective method of short-term CO₂ mitigation (or fixation), as the green diesel will eventually be burnt in an engine consequently releasing the "fixed" CO₂ back into the atmosphere.

3.3 Carbon Production.

The all-over process of CO₂ reforming followed by carbon production is an energy efficient process at 773K. The production of carbon enables 1 mole of CO₂ to be mitigated per mole of CO₂ reacted initially in the reforming reaction. The carbon formed, in principle, can be used for a number of purposes; for example as an adsorbent or as a catalyst support. The carbon could also be used, in theory, in the production of synthetic diamonds. Ni/Fe alloys, which catalyse the diamond synthesis reaction, are also active for reaction (9) (i.e. carbon production from syngas) [12,13]. However, if the aim is solely to remove CO₂ from a flue gas and the cost of CH₄ required is not a serious factor, the carbon formed can be disposed of easily. If we consider this all-over process as a suitable potential method of CO₂ mitigation it becomes interesting to consider types of catalyst which can be used to carry out the CO₂ reforming and C production reaction steps.

3.4 CO₂ reforming.

The CO₂ reforming of CH₄ has been extensively studied in the literature. The most active catalysts contain either the active phase Ni, Co, noble metals or Mo₂C. A review of these catalysts is carried out elsewhere [8]. One of the main problems with CO₂ reforming is the risk of catalyst deactivation due to coke deposition. This will also be discussed [8].

Acknowledgement. This study was funded by the EU RUCADI project (BRRT-CT98-5098).

References.

- [1] H.H. Lamb, (eds.) 1972 Climate Change, Past Present and Future, Fundamentals and Climate Now, London Methuen, vol. 1, London 1974.
- [2] P. Reimer, Energy Convers. Mgt., 37 (1996) 665
- [3] C.S. Wong and R.J. Matear, Waste Mgt., 17 (1997) 329
- [4] E.E. Adams, D.S. Golomb, H.J. Herzog, Energy Convers. Mgt., 36 (1995) 447
- [5] M. Aresta (eds.) Carbon Dioxide Recovery and Utilisation, Kluwer Academic Publishers, London (2003).
- [6] M. Aresta and I. Tommasi, Energy Convers Mgt., 38 (1997) S373
- [7] P.J.A. Tijm, F.J. Waller, D.M. Brown, Appl. Catal. A: Gen., 221 (2001) 275
- [8] D. Treacy, J.R.H. Ross, *full paper in preparation.*
- [9] A. Baiker, Appl. Organometal. Chem., 14 (2000) 751
- [10] D. Gielen, Energy Convers Mgt., 44 (2003) 1027
- [11] H. Schulz, Appl. Catal. A: Gen., 186 (1999) 3
- [12] Y.V. Babich, B.N. Feigelson, D. Fisher, A.P. Yelliseyev, V.A. Nadolinny, J.M. Baker, Diamond Rel. Mat., 99 (2000) 893
- [13] C. Park, N.M. Rodriguez, R.T.K. Baker, J. Catal., 169 (1997) 212.

TRI-REFORMING OF METHANE: A NOVEL CONCEPT FOR SYNTHESIS OF INDUSTRIALLY USEFUL SYNTHESIS GAS WITH DESIRED H₂/CO RATIOS USING CO₂ IN FLUE GAS OF POWER PLANTS WITHOUT CO₂ SEPARATION

Chunshan Song and Wei Pan

Clean Fuels and Catalysis Program, The Energy Institute, and Department of Energy & Geo-Environmental Engineering, Pennsylvania State University, 209 Academic Projects Building, University Park, PA 16802

Introduction

CO₂ conversion and utilization are an important element in chemical research on sustainable development, because CO₂ also represents an important source of carbon for fuels and chemical feedstock in the future [1-3]. The prevailing thinking for CO₂ conversion and utilization begins with the use of pure CO₂, which can be obtained by separation. In general, CO₂ can be separated, recovered and purified from concentrated CO₂ sources by two or more steps based on either absorption or adsorption or membrane separation. Even the recovery of CO₂ from concentrated sources requires substantial energy input [4,5]. According to US DOE, current CO₂ separation processes alone require significant amount of energy which reduces a power plant's net electricity output by as much as 20% [6].

This paper discusses a new process concept that has been recently proposed [7-9] for effective conversion of CO₂ in the flue gases from electric power plants without CO₂ pre-separation, which can be used for the production of synthesis gas (CO + H₂) with desired H₂/CO ratios for synthesizing clean fuels and chemicals. The tri-reforming concept represents a new way of thinking both for conversion and utilization of CO₂ in flue gas without CO₂ separation, and for production of industrially useful synthesis gas with desired H₂/CO ratios using flue gas and natural gas. Experimental results with Ni catalysts will be reported.

Why Using Flue Gas?

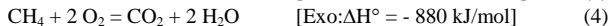
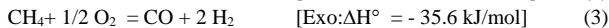
Flue gases from fossil fuel-based electricity-generating units are the major concentrated CO₂ sources in the US. If CO₂ is to be separated, as much as 100 megawatts of a typical 500-megawatt coal-fired power plant would be necessary for today's CO₂ capture processes based on the alkanolamines [4-6]. Therefore, it would be highly desirable if the flue gas mixtures can be used for CO₂ conversion but without pre-separation of CO₂. CO₂ conversion and utilization should be an integral part of CO₂ management, although the amount of CO₂ that can be used for making industrial chemicals is small compared to the quantity of flue gas.

Based on our research, there appears to be a unique advantage of directly using flue gases, rather than using pre-separated and purified CO₂ from flue gases, for the proposed tri-reforming process. Typical flue gases from natural gas-fired power plants may contain 8-10% CO₂, 18-20% H₂O, 2-3% O₂, and 67-72% N₂; typical flue gases from coal-fired boilers may contain 12-14 vol% CO₂, 8-10 vol% H₂O, 3-5 vol% O₂ and 72-77% N₂. The typical furnace outlet temperature of flue gases is usually around 1200°C which will decrease gradually along the pathway of heat transfer, while the temperature of the flue gases going to stack is around 150°C. Pollution control technologies can remove the SO_x, NO_x and particulate matter effectively, but CO₂ and H₂O as well as O₂ remain largely unchanged.

Concept of Tri-reforming

Tri-reforming is a synergetic combination of endothermic CO₂ reforming (eq. 1) and steam reforming (eq. 2) and exothermic partial oxidation of methane (eq. 3, eq. 4). CO₂, H₂O and O₂ in the waste flue gas from fossil-fuel-based power plants will be utilized as co-reactants for tri-reforming of natural gas for the production of synthesis gas.

Tri-reforming of Natural Gas:



Reactions for Coke Formation and Destruction:

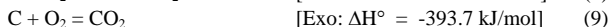
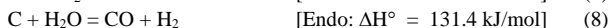
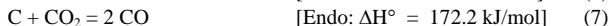
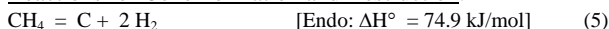


Fig. 1 illustrates the tri-reforming concept as a new approach to CO₂ conversion using flue gases for syngas production. The tri-reforming is a synergetic combination of three catalytic reforming reaction processes. Coupling CO₂ reforming and steam reforming can give syngas with desired H₂/CO ratios for methanol (MeOH) and Fischer-Tropsch (F-T) synthesis. Synthesis gas (syngas) can be made using natural gas, coal, naphtha, and other carbon-based feedstocks by various processes. Steam reforming of methane, partial oxidation of methane, CO₂ reforming of methane, and autothermal reforming of methane are the representative reaction processes for syngas production from natural gas.

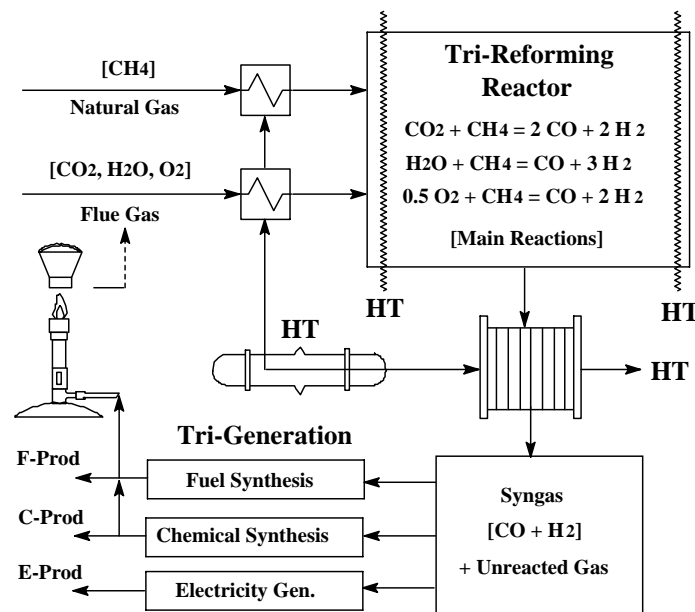


Fig. 1. Process concept for tri-reforming of natural gas using flue gas from fossil fuel-based power plants. HT represents heat transfer or heat exchange including reactor heat up and waste heat utilization.

The combination of dry reforming with steam reforming can accomplish two important missions: to produce syngas with desired H₂/CO ratios and to mitigate the carbon formation problem that is significant for dry reforming. Integrating steam reforming and partial

oxidation with CO₂ reforming could dramatically reduce or eliminate carbon formation on reforming catalyst thus increase catalyst life and process efficiency. Therefore, the proposed tri-reforming can solve two important problems that are encountered in individual processing. The incorporation of O₂ in the reaction generates heat in situ that can be used to increase energy efficiency and O₂ also reduces or eliminates the carbon formation on the reforming catalyst. The tri-reforming can thus be achieved with natural gas and flue gases using the 'waste heat' in the power plant and the heat generated in situ from oxidation with the O₂ that is already present in flue gas.

Thermodynamics of Tri-reforming Reactions

Table 1 shows the equilibrium conversions and the product H₂/CO molar ratios calculated using HSC program [10,11] for tri-reforming under atmospheric pressure. It is possible to perform tri-reforming with over 95% CH₄ conversion and over 80% CO₂ conversion at 800-850 °C when the ratio of CO₂ and H₂O is close to 1.0, O₂/CH₄= 0.1, and the ratio of (CO₂+H₂O+O₂)/CH₄ = 1.05. This is close to the cases with compositions of flue gases.

Table 1. Equilibrium CO₂ and CH₄ conversions and product H₂/CO molar ratios for tri-reforming of CH₄ with CH₄:CO₂:H₂O:O₂ =1:0.475:0.475:0.1 at 850C under 1 atm.

Reaction Temperature °C	Equilibrium		
	CH ₄ Conv. (%)	CO ₂ conv. (%)	H ₂ /CO Mol Ratio
850	98.54	84.50	1.71
800	96.00	81.10	1.72
750	90.70	73.33	1.77
700	86.00	55.60	2.14

Is Tri-reforming Feasible?

We have not found any previous publications or reports on reforming using flue gases for CO₂ conversion related to the concept proposed [7-9]. Our computational analysis shows there are benefits of incorporating steam (H₂O) and oxygen (O₂) simultaneously in CO₂ reforming of CH₄ [10,11]. Prior work established that CO₂ reforming encounters carbon formation problem, even with noble metal catalysts, particularly under elevated pressure [11-13]. Some recent laboratory studies with pure gases have shown that the addition of oxygen to CO₂ reforming [14-17] or the addition of oxygen to steam reforming of CH₄ [18] can have some beneficial effects in terms of improved energy efficiency or synergetic effects in processing and in mitigation of coking. Inui and coworkers have studied energy-efficient H₂ production by simultaneous catalytic combustion and catalytic CO₂-H₂O reforming of methane using mixture of pure gases including CH₄, CO₂, H₂O and O₂ [19]. Choudhary et al. reported their experimental study on simultaneous steam and CO₂ reforming of methane in the presence of O₂ at atmospheric pressure over Ni/CaO [20,21] or Ni/MgO-SA [22]; they have shown that it is possible to convert methane into syngas with high conversion and high selectivity for both CO and H₂. Ross and coworkers have shown that a Pt/ZrO₂ catalyst is active for steam and CO₂ reforming combined with partial oxidation of methane [23]. Therefore, tri-reforming seems feasible, and we also conducted laboratory studies [7-10].

Catalytic Tri-reforming Reactions

We also conducted catalytic tri-reforming experiments in a fixed-bed reactor using various catalysts prepared at Penn State University (by wet impregnation onto MgO, ZrO₂, CeO₂-ZrO₂, and Mg-CeO₂-ZrO₂ supports) [10]. Figs. 2, 3 and 4 show the CH₄

conversion, CO₂ conversion, and H₂/CO ratio in the products, respectively, for tri-reforming over Ni/MgO, Ni/ZrO₂, Ni/CeO₂, Ni/CeZrO and Ni/MgO/CeZrO catalysts prepared in our laboratory as well as commercial Ni/Al₂O₃ (ICI Syntex 23-4) catalyst. The feed for tri-reforming had the composition of CH₄:CO₂:H₂O:O₂ (mol ratio) = 1:0.48:0.54:0.1. Almost equal amounts of CO₂ and H₂O in the feed were intentionally selected for the convenience of comparing CO₂ conversions in the presence of an equal amount of H₂O in tri-reforming. The tri-reforming reactions were conducted at 700°C – 850°C and 1 atm at the space velocity of ca. 32,000 ml/(h.g cat.). Under all these reaction conditions, CH₄ and CO₂ conversions are very dependent on the type of catalysts used, but O₂ conversion is always 100%. Ni/MgO and Ni/MgO/CeZrO show the highest CO₂ conversion in general (Fig. 3). Ni/MgO/CeZrO, Ni/ZrO₂, and Ni/Al₂O₃ (ICI catalyst) give almost the same CH₄ conversions at 800°C – 850°C, while Ni/CeO₂ and Ni/CeZrO have relatively lower CH₄ conversions (Fig. 2).. With the reaction temperature decreasing, CH₄ conversion over Ni/MgO declines much faster than that over other catalysts. At 700°C, the CH₄ conversion over Ni/MgO is the lowest among all the tested catalysts. We speculate that the deactivation of Ni/MgO at lower temperatures cause the fast decline of CH₄ conversion over Ni/MgO and the deactivation is caused by the re-oxidation of Ni. This speculation is justified by the facts that NiO in the NiO/MgO catalyst is not reducible at temperature below 750°C and no carbon formation is observed on the used Ni/MgO catalyst. In addition, metal sintering may not be the reason for deactivation because all the catalytic performance tests were first carried out at 850°C. Then the reaction temperatures were gradually decreased to 700°C.

Among all the catalysts tested, Ni/CeO₂ has the second lowest CH₄ conversion at reaction temperatures above 750°C. The low CH₄ conversion over Ni/CeO₂ is probably related to the larger Ni particles over Ni-CeO₂ or the occurring of strong metal-support interaction (SMSI) due to the partial reduction of CeO₂ at high temperatures. Surprisingly, Ni/CeZrO has the lowest CH₄ conversion. Although Ni/MgO, Ni/MgO/CeZrO, Ni/Al₂O₃ (ICI catalyst), and Ni/ZrO₂ have similar CH₄ conversions, their CO₂ conversions are quite different. Ni/MgO shows the highest CO₂ conversion at temperatures above 750°C, followed by Ni/MgO/CeZrO. Ni/CeO₂ and Ni/CeZrO again show the lowest CO₂ conversion.

The H₂/CO ratio in the products depends mainly on the CO₂ and H₂O conversions in tri-reforming. If more H₂O is converted than CO₂, then the H₂/CO ratio in the product would be higher. Similarly, if less H₂O is converted than CO₂, the H₂/CO ratio would be lower. Therefore, the H₂/CO ratio is a good indicator for comparing the ability to convert CO₂ in the presence of H₂O over different catalysts. Ni/MgO gives the lowest H₂/CO ratio, followed by Ni/MgO/CeZrO (shown in Fig. 4). The H₂/CO ratios over Ni/CeO₂, Ni/ZrO₂, and Ni/Al₂O₃ (ICI catalyst) are similar and slightly higher than Ni/MgO/CeZrO. Ni/CeZrO gives the highest H₂/CO ratio. These results strongly suggest that Ni/MgO enhance the CO₂ conversion most in the presence of H₂O and O₂. Among all the tested catalysts, their ability to enhance the conversion of CO₂ follows the order of Ni/MgO > Ni/MgO/CeZrO > Ni/CeO₂ ≈ Ni/ZrO₂ ≈ Ni/Al₂O₃ (ICI) > Ni/CeZrO.

The different ability to convert CO₂ over different catalysts in tri-reforming is related to the properties of the catalysts. The enhancement of CO₂ conversion over Ni/MgO might be related to its enhanced CO₂ adsorption ability as evidenced by the CO₂-TPD results (not shown here). However, catalysts supported on CeZrO (e.g., Ni/MgO/CeZrO and Ni/CeZrO) do not show more enhancement of CO₂ conversion than Ni/MgO even though these catalysts demonstrate more and stronger CO₂ adsorption than

Ni/MgO as indicated by the large CO₂ desorption peaks at 710-717°C. To further elucidate the enhancement of CO₂ conversion over Ni/MgO in tri-reforming, a kinetic study was carried out, the result of which will be reported in the future.

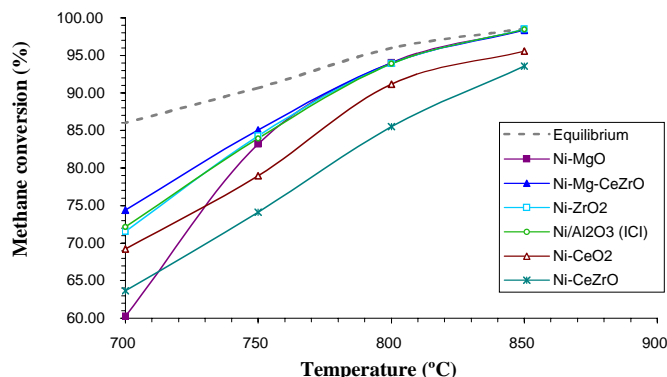


Fig. 2. CH₄ conversions in the tri-reforming reaction over 100 mg supported Ni catalysts at 1 atm and feed composition of CH₄ : CO₂ : H₂O : O₂ = 1 : 0.48 : 0.54 : 0.1 (CH₄ flow rate = 25 ml/min)

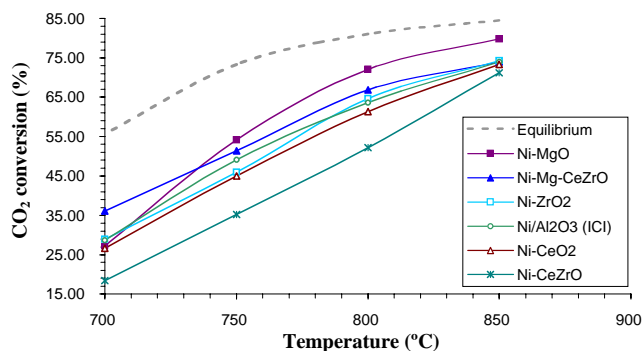


Fig. 3. CO₂ conversions in the tri-reforming reaction over 100 mg supported Ni catalysts at 1 atm and feed composition of CH₄ : CO₂ : H₂O : O₂ = 1 : 0.48 : 0.54 : 0.1 (CH₄ flow rate = 25 ml/min)

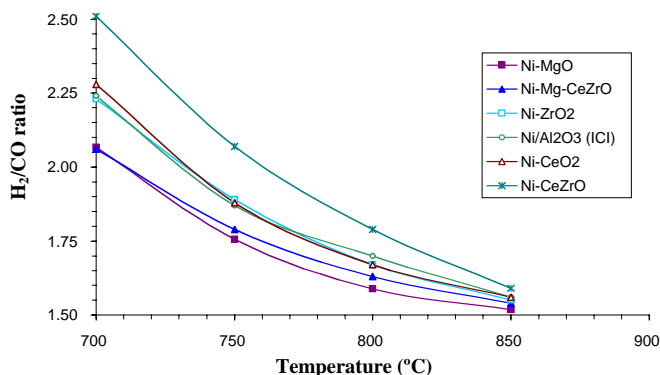


Fig. 4. H₂/CO ratios in the tri-reforming reaction over 100 mg supported Ni catalysts at 1 atm and feed composition of CH₄ : CO₂ : H₂O : O₂ = 1 : 0.48 : 0.54 : 0.1 (CH₄ flow rate = 25 ml/min)

Elimination of Carbon Formation by Tri-reforming Compared to CO₂ Reforming

We conducted temperature-programmed oxidation of the used catalysts from the above tri-reforming experiments and found that except for Ni/ZrO₂ catalyst, all the other catalysts (corresponding to the experiments shown in Figs. 2 and 3) showed no sign of carbon formation after the tri-reforming experiments. We have also tested a commercially available Haldor-Topsoe R67 Ni-based catalyst for tri-reforming in a fixed-bed flow reactor using gas mixtures that simulate the cases with flue gases from coal-fired power plants (CO₂:H₂O:CH₄:O₂ = 1:1:1:0.1, mol ratio) and from natural gas-fired power plants (CO₂:H₂O:CH₄:O₂ = 1:2:1:0.1, mol ratio) [28]. For CO₂ reforming of CH₄, carbon formation is an important problem [12,13,24-27]. Temperature-programmed oxidation (TPO) results show that the used Haldor-Topsoe R67 catalyst after 300 min time-on-stream for CO₂ reforming at 850 °C and 1 atm contained 21.8 wt% carbon [28]. On the other hand, the same catalyst employed in tri-reforming showed no sign of carbon formation after 300 min TOS, as the used catalyst appears to be greenish powder (versus the black sample from CO₂ reforming). Fig. 5 shows the photographs of the used catalysts after CO₂ reforming and tri-reforming. Therefore, our results show that tri-reforming can be performed with stable operation, and no carbon formation and no appreciable deactivation of catalyst were observed under the tri-reforming conditions.

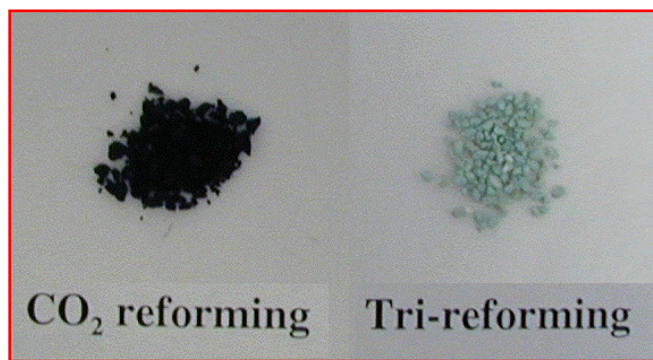


Fig. 5. Appearance of Haldor-Topsoe R67 Ni-based catalyst after 300 min TOS of CO₂-reforming (CO₂:CH₄ = 1:1, used catalyst particles are black in color) and tri-reforming (CO₂:H₂O:O₂:CH₄ = 1:1:0.1:1, used catalyst particles are green in color) at 850 °C.

Does Tri-reforming Consume More Energy Than Steam or CO₂ Reforming ?

A comparative energy analysis by calculation indicated that tri-reforming is more desired for producing syngas with H₂/CO ratios of 1.5-2.0 compared to CO₂ reforming and steam reforming of methane, in terms of less amount of energy required and less net amount of CO₂ emitted in the whole process for producing synthesis gas with H₂/CO ratio of 2.0 [8]. The tri-reforming process could be applied, in principle, to the natural gas-based power plants and coal-based power plants.

Conclusions

Catalytic tri-reforming of methane can be achieved successfully with high CH₄ conversion (>97%) and high CO₂ conversion (>80%) for producing syngas with desired H₂/CO ratios of 1.5-2.0 over supported nickel catalysts at 800-850 °C under atmospheric pressure

without the problem of carbon formation on the catalyst.

The CO₂ and CH₄ conversion as well as H₂/CO ratios of the products from tri-reforming also depend on the type and nature of catalysts.

An important observation is that CO₂ conversion can be maximized by tailoring catalyst composition and preparation method. In other words, certain catalysts with proper feature can give much higher CO₂ conversion than other catalysts under the same reaction conditions with the same reactants feed.

Among all the catalysts tested for tri-reforming, their ability to enhance the conversion of CO₂ follows the order of Ni/MgO > Ni/MgO/CeZrO > Ni/CeO₂ ≈ Ni/ZrO₂ ≈ Ni/Al₂O₃ (ICI) > Ni/CeZrO. The different ability to convert CO₂ over different catalysts in tri-reforming is related to the properties of the catalysts.

Results of catalytic performance tests over Ni/MgO/CeZrO catalysts at 850°C and 1 atm at different feed compositions confirm the predictions based on the thermodynamic analysis for equilibrium conversions in tri-reforming of methane.

Further studies on improving catalysts are necessary for understanding the factors affecting CO₂ conversion and CH₄ in the presence of steam and oxygen during tri-reforming.

Acknowledgments

We are grateful to US DOE (UCR Innovative Concepts Program) for supporting this work, to Prof. H.H. Schobert and Prof. A.W. Scaroni of PSU for their encouragement of CS's efforts on CO₂ conversion, to Mr. B. Miller and Dr. S. Pisupati of PSU for helpful discussions on flue gas, and to Haldor-Topsoe and ICI for the catalysts. CS thanks Dr. J. Armor of Air Products and Chemicals for helpful discussions on CO₂ reforming.

References

- 1). Halmann, M. M.; Steinberg, M. Greenhouse Gas Carbon Dioxide Mitigation: Science and Technology. Lewis Publishers, Boca Raton, FL, 1999, 568 pp.
- 2). Song, C., A. M. Gaffney, and K. Fujimoto. CO₂ Conversion and Utilization. American Chemical Society, Washington DC, ACS Symposium Series, Vol. 809, 2002, 420 pp.
- 3). Maroto-Valer, M. M., C. Song, and Y. Soong. Environmental Challenges and Greenhouse Gas Control for Fossil Fuel Utilization in the 21st Century. Kluwer Academic/Plenum Publishers, New York, 2002, 447 pp.
- 4). DOE/OS-FE. Carbon Sequestration. State of the Science. Office of Science and Office of Fossil Energy, U.S. DOE, 1999.
- 5). Weimer, T., Schaber, K., Specht, M. and Bandi, A. Comparison of CO₂-Sources for Fuel Synthesis. Am. Chem. Soc. Div. Fuel Chem. Prepr., 1996, 41 (4), 1337-1340.
- 6). DOE/FE. Capturing Carbon Dioxide. Office of Fossil Energy, U.S. DOE, 1999.
- 7). Song, C. Chemical Innovation (formerly Chemtech, ACS), 2001, 31, 21-26.
- 8). Song, C., W. Pan and S. T. Srimat. In "Environmental Challenges and Greenhouse Gas Control for Fossil Fuel Utilization in the 21st Century". Edited by M. M. Maroto-Valer, C. Song, and Y. Soong. Kluwer Academic/Plenum Publishers, New York, 2002, Chapter 18, pp. 247-267.
- 9). Song, C. CO₂ Conversion and Utilization. Am. Chem. Soc. Symp. Ser., 2002, 809, 2-30.
- 10). Pan, W. *Tri-reforming and Combined Reforming of Methane for producing Syngas with Desired H₂/CO Ratios. PhD Thesis, Pennsylvania State University, 2002.*
- 11). Pan W. and C. Song. Am. Chem. Soc. Symp. Ser., 2002, 809, 316-329.
- 12). Song, C., S. T. Srimat, S. Murata, W. Pan, L. Sun, A. W. Scaroni and J. N. Armor. Am. Chem. Soc. Symp. Ser., 2002, 809, 258-274.
- 13). Srimat S. T. and C. Song. Am. Chem. Soc. Symp. Ser., 2002, 809, 289-302.
- 14). O'Connor A.M. and Ross J.R.H. The Effect of O₂ Addition on the Carbon Dioxide Reforming of Methane over Pt/ZrO₂ Catalysts. Catal. Today, 1998, 46 (2-3), 203-210.
- 15). Ruckenstein E. and Hu Y. H. Combination of CO₂ reforming and partial oxidation of methane over NiO/MgO solid solution catalysts. Ind. Eng. Chem. Res., 1998, 37 (5), 1744-1747.
- 16). Vernon, P.D.F., Green, M.L.H., Cheetham, A.K., Ashcroft, A.T. Partial Oxidation of Methane to Synthesis Gas, and Carbon-Dioxide as an Oxidizing-Agent for Methane Conversion. Catal. Today, 1992, 13 (2-3), 417-426.
- 17). Choudhary V.R., Rajput A.M., and Prabhakar B. Energy-Efficient Methane-to-Syngas Conversion with Low H₂/CO Ratio by Simultaneous Catalytic Reactions of Methane with Carbon-Dioxide and Oxygen. Catal. Lett., 1995, 32 (3-4), 391-396.
- 18). Choudhary, V.R.; Mamman, A. S. Simultaneous Oxidative Conversion and CO₂ or Steam Reforming of Methane to Syngas over CoO-NiO-MgO Catalyst. J. Chem. Technol. Biotechnol., 1998, 73 (4), 345-350.
- 19). Inui T., Saigo K., Fujii Y., and Fujioka K. *Catalytic Combustion of Natural Gas as the Role of On-site Heat Supply in Rapid Catalytic CO₂-H₂O Reforming of Methane. Catal. Today, 1995, 26 (3-4), 295-302.*
- 20). Choudhary V.R., Rajput A.M., and Prabhakar B. NiO/CaO-Catalyzed Formation of Syngas by Coupled Exothermic Oxidation Conversion and Endothermic CO₂ and Steam Reforming of Methane, Angew. Chem. Int. Ed. Engl., 1994, 33 (20), 2104-2106.
- 21). Choudhary, V. R., and Rajput A.M. Simultaneous Carbon Dioxide and Steam Reforming of Methane to Syngas over NiO-CaO Catalyst. Ind. Eng. Chem. Res., 1996, 35, 3934-3939.
- 22). Choudhary, V.R.; Uphade, B.S., Mamman, A. S. Simultaneous Steam and CO₂ or Reforming of Methane to Syngas over NiO/MgO/SA-5205 in Presence and Absence of Oxygen. Appl. Catal. A: Gen., 1998, 168, 33-46.
- 23). Hegarty M.E.S., O'Connor A.M. and Ross J.R.H. Syngas Production from Natural Gas using ZrO₂-Supported metals. Catal. Today, 1998, 42 (3), 225-232.
- 24). Xu BQ, Wei JM, Wang HY, Sun KQ, Zhu QM. Nano-MgO: Novel Preparation and Application as Support of Ni Catalyst for CO₂ Reforming of Methane. Catal Today, 2001, 68 (1-3): 217-225.
- 25). Wei JM, Xu BQ, Li JL, Cheng ZX, Wang YQ, Zhu QM. CO₂ Reforming of CH₄ over Ni Supported on Nano-ZrO₂(I) - Comparison with Conventional Oxide Supported Nickel. Chem. J. Chinese Univ., 2002, 23 (1), 92-97.
- 26). Wei JM, Xu BQ, Sun KQ, Li JL, Zhu QM. CO₂ reforming of CH₄ over Ni supported on Nano-ZrO₂(II) Effect of catalyst composition and reaction conditions on catalytic reactivity. Chem. J. Chinese Univ., 2002, 23 (11), 2106-2111.
- 27). Wei JM, Xu BQ, Li JL, Chen ZX, Zhu QM. Nano-g-Al₂O₃ supported Ni catalysts for CO₂ reforming of CH₄ to syngas. Am. Chem. Soc. Div. Fuel Chem. Prepr., 2001, 46 (1), 97-98.
- 28). Song, C., Srinivas, S.T., Pan, W. and Sun, L. Technical Program, 17th North American Catalysis Society Meeting, Toronto, Canada, June 3-8, 2001.

Partial Oxidation and Combined Reforming of Methane on Ce-promoted Catalysts

Wei Wang, Susan M. Stagg-Williams, Fabio B. Noronha*, Lisiane V. Mattos*, Fabio B. Passos

Chemical and Petroleum Engineering Department,
University of Kansas, Lawrence KS, 66045

*Laboratório de Catálise, Instituto Nacional de Tecnologia, Brasil

Introduction

Significant attention has been given to the partial oxidation and reforming of various hydrocarbon sources for the production of synthesis gas. This work has stemmed from the concern about the world dependence on petroleum oil. Many hydrocarbon sources are currently being investigated including bio-based feedstocks, such as ethanol, sunflower oil, and biomass derived oils. However, the most common feedstock is still methane due to its abundance and inexpensive nature.

Many of the natural gas reservoirs are located in remote regions making the recovery and transportation cost prohibitive. The conversion of natural gas into transportation fuels such as gasoline and diesel helps top overcome these costs. The so-called gas-to-liquids technology (GTL) is based on the conversion of natural gas to a synthesis gas prior to the liquid production through the Fischer-Tropsch Synthesis (1). The syngas generation is the most capital and energy intensive part of the production plant (2). Therefore, the economic viability of GTL technology depends on optimizing the process for syngas production. Autothermal reforming (ATR) fulfills the requirements to a syngas with H₂/CO ratio of 2, the ratio necessary for GTL plants. ATR combines non catalytic partial oxidation with steam reforming in one reactor. The ATR technology requires the addition of CO₂ or CO₂-rich gas, in order to adjust the syngas composition to the desired H₂/CO ratio (3).

Catalyst stability in the presence of O₂, CO₂, and H₂O can be a significant issue. It is well established that mixed oxide supports result in improved catalytic performance for the dry reforming reaction due to the ability of the support to participate in the reaction (4). Similar studies for the partial oxidation reaction have shown that the addition of Ce to ZrO₂ results in a catalyst which exhibits minimal deactivation compared to Pt/Al₂O₃ and Pt/ZrO₂ catalysts (5). The mechanism of reaction was shown to proceed through combustion of methane followed by combined steam and CO₂ reforming.

Several studies have been performed on the dry reforming reaction in the presence of oxygen (6,7). The results showed that the conversion of methane increased as the amount of oxygen in the feed increased, but the selectivity towards H₂ decreased. The decrease in H₂ selectivity was more pronounced at lower temperatures where the formation of CO₂ and H₂O were favored. Minimal deactivation was observed on the Pt/ZrO₂ catalyst at low space velocities and with a significant amount of diluent in the feed (6).

This paper focuses on the partial oxidation and combined partial oxidation and reforming reactions over Pt supported on ZrO₂ and CeZrO₂. Specifically, we have investigated the effect of the metal loading and effect of the addition of oxygen and water on the activity, stability, and syngas ratio produced. A general reaction mechanism is discussed.

Experimental

ZrO₂ and cerium (18 wt%)-doped ZrO₂ were all obtained from Magnesium Elektron, Inc. Prior to the addition of the metal the supports were calcined at 800°C in stagnant air for 4 hours. Pt was added to the supports using incipient wetness impregnation of an

aqueous solution of H₂PtCl₆•6H₂O. The metal loading was 0.5 wt% and 1.5 wt%. All of the catalysts were dried overnight at 110°C, and then reduced *in-situ* in H₂ (30 cm³/min) at 500°C for 1.5 h, prior to reaction.

Partial oxidation experiments were carried out in a quartz flow reactor at 800°C using a CH₄:O₂ ratio of 2:1 and a total flow rate of 100 cc/min. The catalysts were diluted with a 3:1 ratio of SiC to catalyst to help reduce any heat effects. 20 milligrams of catalyst was used for the reaction on the 1.5 wt% catalysts while 60 mg was used for the runs with the 0.5 wt% catalyst, in order to maintain the same metal content in the reactor. For the experiments in the presence of oxygen, the composition of the feedstock was such that the C:O ratio was 1:1. The reactions were performed at 800°C with a total flow rate of 100 cc/min.

Results and Discussion

The surface area of the Ce promoted ZrO₂ support was 48 m²/g while that of the ZrO₂ was 29 m²/g. Transmission Electron Microscopy (TEM) was used to determine the dispersion of the 0.5 wt% catalysts. The catalysts were reduced at 500°C and then heated to 800°C in He. The dispersion of the 0.5 wt% Pt/ZrO₂ catalyst was approximately 21% while the dispersion of the 0.5 wt% Pt/CeZrO₂ catalyst was near 30%. The dispersion of the 1.5 wt% catalysts was measured using dehydrogenation of cyclohexane after reduction at 500°C. The dispersion after reduction at 500°C before heating to 800°C was measured to be 29% for the 1.5 wt% Pt/ZrO₂ catalyst and 34% for the 1.5 wt% Pt/CeZrO₂. TEM of a 1.5 wt% Pt/ZrO₂ catalyst after heating to 800°C showed that the dispersion was closer to 15%. These results are in agreement with previous studies which have shown that the sintering of the Pt/ZrO₂ catalyst during the heating from 500°C to 800°C is much greater than the sintering on the Pt/CeZrO₂ catalyst. Based on the dispersion results, it appears as if the metal particle sizes for the 0.5 wt% and the 1.5 wt% catalysts are similar after heating to 800°C.

Table 1. Methane Conversion During the Partial Oxidation Reaction at 800°C and a 2:1 CH₄:O₂ Feed Ratio

Catalyst	% Methane Conversion		
	After 1 hour	After 12 hours	After 24 hours
0.5 wt % Pt/ZrO ₂	49	26	13
0.5 wt % Pt/CeZrO ₂	39	40	37
1.5 wt % Pt/ZrO ₂	51	34	13
1.5 wt % Pt/CeZrO ₂	49	46	37

Table 1 shows the methane conversion during the partial oxidation reaction at 800°C and a 2:1 ratio of CH₄:O₂. The 0.5 wt% Pt/CeZrO₂ catalyst had an initial activity that was approximately 10% less than the 1.5 wt% Pt/CeZrO₂ and both of the unpromoted ZrO₂ catalysts. However, this material was the most stable of the 4 catalysts studied. Both of the ZrO₂ catalysts exhibited significant deactivation during the reaction which has been ascribed to carbon deposition. The loading of the metal was found not to have any effect on the long term activity of the catalyst which is most likely due to the similarity in the metal particle size after heating to 800°C and reaction for 24 hours.

Figure 1 shows the CO and CO₂ selectivity for the same 24 hour experiment for the CeZrO₂ and ZrO₂ catalysts containing 0.5 wt% Pt. Similar profiles were obtained for the 1.5 wt% samples. The CO selectivity for the ZrO₂ catalyst decreased significantly during the 24

hour experiment while the CO₂ selectivity increased. After approximately 10 hours of reaction the CO₂ selectivity became greater than the CO selectivity. In contrast, the CO and CO₂ selectivities of the CeZrO₂ catalyst were very stable with CO always being greater than CO₂. Similarly, the H₂:CO ratio remained at 2.6 during the 24 hour reaction for the Ce containing catalysts, while it was initially 2.6 for the ZrO₂ samples, but decreased to 0.8 by the end of the reaction.

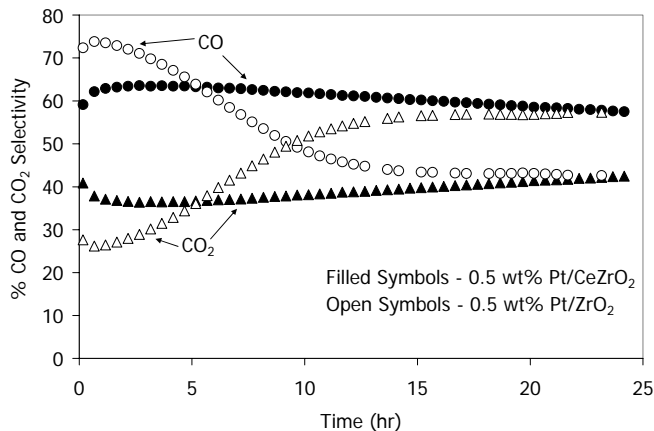


Figure 1. CO and CO₂ selectivity for the 0.5 wt% Pt/CeZrO₂ and the 0.5 wt% Pt/ZrO₂ during the partial oxidation reaction at 800°C and a 2:1 CH₄:O₂ feed ratio.

Previous studies (5) on a Pt/Ce_{0.75}Zr_{0.25}O₂ catalyst have suggested that the reaction mechanism proceeds via the combustion of methane followed by the combined steam and dry reforming. The observed initial H₂:CO ratio greater than 2 is evidence for the occurrence of the steam reforming reaction and the two step mechanism. The decrease in the CO selectivity and the H₂:CO ratio with the simultaneous increase in CO₂ selectivity is attributed to carbon formation inhibiting the second step of the reaction mechanism. The stability of the Ce-promoted materials is ascribed to the ability of the support to minimize carbon deposition on the Pt particle due to increased oxygen release capability.

The catalysts were exposed to reactions with both CO₂ and O₂ at 800°C with a CH₄:CO₂:O₂ feed ratio of 4:2:1. Reactions were performed such that the C:O ratio remained at 1:1. Figure 2 shows the conversion for the 0.5 wt% catalysts for 10 hours of reaction. The conversion of methane and the deactivation observed on the 0.5 wt% Pt/ZrO₂ is almost identical to that observed for the partial oxidation reaction. The H₂:CO product ratio was initially 1.18 but decreased to 0.95 during the experiment. A significant amount of water was collected using a condenser placed after the reactor. The formation of water could be due to the occurrence of the reverse water gas shift reaction, which also explains the H₂:CO ratio being less than 1. The water could also be formed by the combustion reaction. The partial oxidation studies demonstrated that combustion does occur in the presence of O₂ and that the ZrO₂ catalysts are prone to carbon deposition which can decrease the ability to do combined CO₂ and steam reforming. In order to determine the relative importance of each reaction, combustion and reverse water gas shift, in the overall process a complete mechanistic study is currently being performed.

The 0.5 wt% Pt/CeZrO₂ catalyst was very stable in the presence of oxygen and the H₂:CO ratio produced was constant throughout the experiment at 1.25. Higher oxygen contents resulted in an increase in the product ratio and the formation of water.

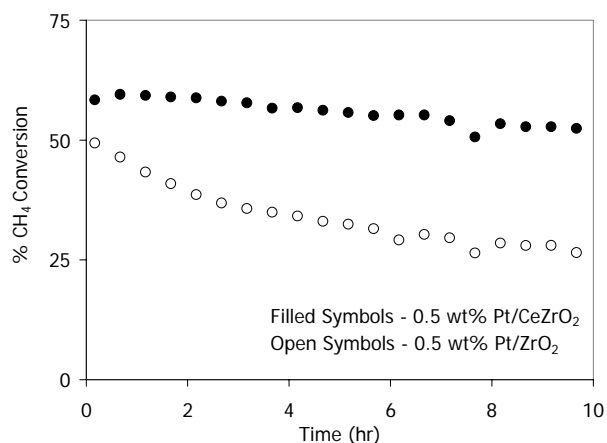


Figure 2. CH₄ conversion for the 0.5 wt% Pt/CeZrO₂ and the 0.5 wt% Pt/ZrO₂ during the combined dry reforming and partial oxidation reaction at 800°C and a CH₄:CO₂:O₂ feed ratio at 4:2:1.

Additional reaction studies on the 0.5 wt% and 1.5 wt% Pt/CeZrO₂ catalysts have shown that the catalysts are very stable in the presence of water. Switching the feed composition while the reactor was online resulted in the same conversion and product ratio as would be obtained by the individual reactions. Thus, the product ratio can be accurately predicted prior to switching the feed and a variety of syngas ratios can be generated without altering the catalyst performance.

Conclusions

The studies reported here have shown that increasing the Pt metal loading did not have any effect on the long term activity of the catalyst. The initial activity of the 1.5 wt% Pt/CeZrO₂ was higher than the 0.5 wt% Pt/CeZrO₂ catalyst. However, the deactivation on the 1.5 wt% catalyst was more pronounced resulting in the same activity after 24 hours. The similar long term activity is most likely due to the similar particle size after heating to 800°C. Significant deactivation is observed in the presence of O₂ and water on the Pt/ZrO₂ catalysts which is ascribed to the formation of carbon deposits that hinder the reforming reaction. In the presence of oxygen, the reaction mechanism is believed to proceed through combustion followed by combined dry and steam reforming as opposed to through direct partial oxidation. The Ce-promoted catalysts are very stable in the presence of oxygen and water and are promising for the ATR reaction. Detailed mechanistic studies in the presence of oxygen and water are currently underway.

Acknowledgements. The authors gratefully acknowledge funding from the KU Energy Research Center.

References

- (1) M. Prettre, C. Eichner, and M. Perrin, Transactions of the Faraday Society, **1946**, 43, 335.
- (2) D. Dissanayake, M. P. Rosynek, and J. H. Lunsford, Journal of Physical Chemistry, **1993**, 97, 3644.
- (3) V.R. Choudhary, A.M. Rajput, B. Probhaker, Journal of Catalysis, **1993**, 139, 326.
- (4) Stagg-Williams S, M; Noronha, F. B; and Resasco, D. E., *J. Catal.*, **2000**, 194(2), 240.
- (5) L.V. Mattos, E.R. de Oliveira, P.D. Resende, F.B. Noronha, F.B. Passos, Catalysis Today, **2002**, 77(3), 245.
- (6) A. M. O'Connor, and J. R. H. Ross, Catalysis Today, **1998**, 46, 203.
- (7) Venkatesh Phadnavis, Bakul Pant, and Susan M. Stagg-Williams, *Fuel Chem. Div. Preprints*, **2002**, Vol. 41(1).

CO₂ REFORMING OF METHANE ON LaA'Ru_{0.8}Ni_{0.2}O₃ (A'= Sm, Nd, Ca) PEROVSKITES AS CATALYSTS PRECURSORS IN PRESENCE AND ABSENCE OF O₂

E. Pietri^{1*}, M. E. Rivas¹, M. R. Goldwasser¹, M. J. Pérez-Zurita¹, M. L. Cubeiro¹, L. Leclercq² and G. Leclercq²

1. Centro de Catálisis, Petróleo y Petroquímica, Escuela de Química, Fac. Ciencias, UCV, Apartado 47102, Los Chaguaramos, Caracas, Venezuela; 2. Université des Sciences ET Technologies de Lille, Laboratoire de Catalyse Hétérogène et Homogène, 59655 Villeneuve D'Ascq, Cedex, Francia

Introduction

Over the past years, the CO₂ reforming of methane yielding synthesis gas has been the subject of numerous studies. The objective is to find a suitable material that allows the reaction to proceed at low temperature with a minimum of carbon production. Among these material, the perovskites like oxides ABO₃, in which A-site cation is a rare earth and/or alkaline earth and B-site cation is a transition metal has drawn a lot of attention. The reason for this is because by a careful reduction of the perovskites, the B-site cations will remain distributed in the structure, producing a well dispersed and stable metal particle inhibiting coke formation. Although many previous investigations of the CO₂ reforming of methane were performed over transition metals supported on alumina, silica and magnesia, the use of perovskite has been less studied. The performance of these solids for the CO₂ reforming of CH₄ in the presence (combine) and absence (dry) of O₂ was investigated. The use of oxygen as co-reactant could allow the reaction to proceed at lower temperatures due to its exothermic character.

Experimental

Four Ru-Ni based perovskite type oxides were synthesized by the citrate sol gel method based on the Pechini type reaction route. La in the A-site position was partially replaced by Sm, Nd and Ca to produce LaRu_{0.8}Ni_{0.2}O₃, La_{0.8}Sm_{0.2}Ru_{0.8}Ni_{0.2}O₃, La_{0.8}Nd_{0.2}Ru_{0.8}Ni_{0.2}O₃, and La_{0.8}Ca_{0.2}Ru_{0.8}Ni_{0.2}O₃. The procedure has been published elsewhere [1]. The homogeneity and structure of the obtained powders have been investigated before and after reduction and after reaction by ICP, IR, BET surface areas, XRD, TPR and XPS analysis. Catalytic tests were performed in a continuous flow system an integral reactor at atmospheric pressure.

Results and Discussion

The XRD patterns of the as synthesized solids at room temperature revealed that the perovskite structure was the main phase detected for all solids. All perovskites could be indexed with an orthorhombic or cubic symmetry of the ABO₃ type. The ICP analysis showed a close agreement between experimental and theoretical

values corroborating the advantage of the sol-gel method. The TPR shows that the perovskite reduction proceeds in two steps. The XRD in situ reduction results seems to indicate, that the first peak of reduction at ~ 400 °C could be attributed to weakly bound Ru-Ni cations and to residues of the precursors. The second peak could be attributed to a simultaneously Ru and Ni reduction to produces Ru⁰ and Ni⁰ probably with an alloy formation. For all solids, the observed phases after reduction at 700°C were: Ru metal (alone or allied with Ni), La₂O₃ and CaO, Sm₂O₃ and Nd₂O₃ depending on the composition of the starting perovskite. However, changes in the reducibility pattern were introduced due to the difference in ionic radii of the substituting cations. XRD analysis was also used to determine the metal particles size of the reducible species. It is interesting to point out that the metallic particle sizes were in the order of 10-34 nm as determined by the Scherrer equation [2]. Peaks correspond mainly to Ru (44,37°, 2θ) slightly shifted, due to the presence of Ni.

The experimental results of the methane reforming show high methane conversions both in presence and absence of O₂ (Table 1). However, higher ratios H₂/CO were obtained for the combined reaction. For this reaction, CO₂ conversion was also lower (30%) than that of methane due to the fact that the CO₂ is being generated as a product of the methane combustion in the presence of O₂ [3].

On Sm and Nd containing solids, a great improvement on the H₂/CO ratios was observed for the combine reaction compared to the dry reaction, while the substitution of La by Ca increases the activity and selectivity, as shown in table 1. On this solid, for the dry reaction, the CO₂ conversion is higher than that of CH₄ due to the reverse water gas shift reaction.

The simultaneous oxidative and CO₂ reforming reaction of methane notably diminished coke formation, increasing the syngas production. The addition of oxygen to the CH₄ + CO₂ system decreases the reaction temperature and energy consumption, indicating that the partial oxidation (exothermic) reaction promotes the dry (endothermic) reaction, in agreement with Tomishige et al. result for Ni/Al₂O₃ and Pt/ Al₂O₃ catalysts [4].

Acknowledgement. The authors thank Venezuelan FONACIT for its financial support through Agenda Petroleum Project N° 97-003739.

References

- (1) Pietri, E.; Barrios, A.; Gonzalez, O.; Goldwasser, M.R.; Pérez-Zurita, M.J.; Cubeiro, M.L.; Goldwasser, J.; Leclercq, L.; Leclercq, G. *Stud. Surf. Sci. Catal.*, **2001**, *136*, 381.
- (2) Bradford, M.C.J. and Vannice, M.A. *Appl. Catal. A: Gen.* **1996**, *142*, 73.
- (3) Ruckenstein, E. and Wang, H.Y. *Catal. Lett.* **2001**, *73*, 2.
- (4) Tomishige, K.; Kanazawa, S.; Suzuki, K.; Asadullah, M.; Sato, M.; Ikushima, K. and Kunimori, K. *Appl. Catal. A: Gen.* **2002**, *233*, 35.

Table 1. CO₂ Reforming of Methane in the Presence and Absence of O₂

SOLIDS	DRY			COMBINE		
	XCH ₄	XCO ₂	H ₂ /CO	XCH ₄	XCO ₂	H ₂ /CO
LaRu _{0.8} Ni _{0.2} O ₃	79.0	81.0	0.94	87.0	47.0	1.18
La _{0.8} Sm _{0.2} Ru _{0.8} Ni _{0.2} O ₃	84.4	67.4	0.75	89.7	39.7	1.04
La _{0.8} Nd _{0.2} Ru _{0.8} Ni _{0.2} O ₃	83.5	63.8	0.66	81.3	32.3	1.02
La _{0.8} Ca _{0.2} Ru _{0.8} Ni _{0.2} O ₃	67.9	85.3	0.86	85.0	50.0	1.18

tr =24 h, WHSV =24L/ h.g, CH₄/CO₂ =1, CH₄/O₂=2, W = 200 mg, Tred =700°C/ 8h, Treac. = 700°C

DRY REFORMING OF METHANE ON NANO-ZIRCONIA SUPPORTED NICKEL CATALYST

Yajun Zhao, Xinmei Liu and Zifeng Yan

State Key Laboratory of Heavy Oil Processing, Key Laboratory of Catalysis, CNPC, University of Petroleum, Dongying 257061, China

Introduction

Catalytic reforming of carbon dioxide with methane to synthesis gas has been proposed as one of the most promising technologies for the utilization of these two greenhouse gases. Moreover, this route produces synthesis gas with a suitable CO/H₂ ratio for the production of hydrocarbons and oxygenated derivatives. Supported noble metals catalysts have characteristic of high activity, selectivity and resistance to coke formation. Nevertheless, consideration of high cost and limited availability of noble metals makes the development of a nickel-based catalyst more feasible for industrial practice, but it is rapidly deactivated by carbon deposition.

Nanosized catalysts possess more edges, corners, defects, small-sized particles, large surface area and high metal dispersion, as a result exhibit the good catalytic performance. In this work, we synthesized nano-zirconia and used it as the support of Ni-based catalyst for dry reforming of methane.

Experimental

Preparation of Nano-zirconia Support and Catalysts. The nano-zirconia was synthesized by solid state reaction method. Zirconyl chloride, sodium hydroxide, CTMABr were milled respectively and mixed together. The reaction product was then transferred to the autoclave to age. Finally, the sample was washed and dried.

The nano-zirconia supported nickel catalyst, denoted as NZ, was prepared by incipient wet impregnation method using nickel nitrate as the precursor. For comparison, the catalyst of the same component was prepared by conventional co-precipitation method, denoted as CZ.

Catalytic evaluation. The catalysts behavior was carried out in the continuous flow quartz-fixed-bed reactor under atmospheric pressure. The catalyst was reduced in situ at 673K during 5h with H₂, then the reaction was performed at 973K with CH₄:CO₂ ratio (mol) of 1:1 and space velocity of 5000cm³/g·h.

Results and Discussion

Characterization of the Support. Figure 1 exhibits the XRD pattern of nano-zirconia. Evidently, the four peaks appearing at high degrees show that the synthesized zirconia is of tetragonal structure, and the particle size calculated by Sherrer equation is about 3.5 nm.

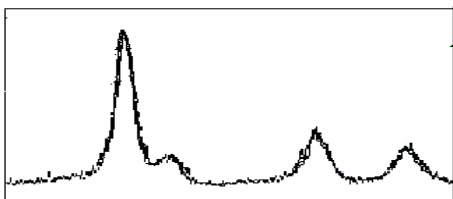


Figure 1. The XRD pattern of nano-zirconia

Figure 2 shows that nano-zirconia possesses mesopore of about 3.6 nm and large specific surface area of about 381.8 m²/g. Moreover, it is seen that the isotherm exhibits a shape of type IV with a hysteresis of type H3. It is thought that the mesopore formed by aggregates of plate-like nanosized particles is slit-like.

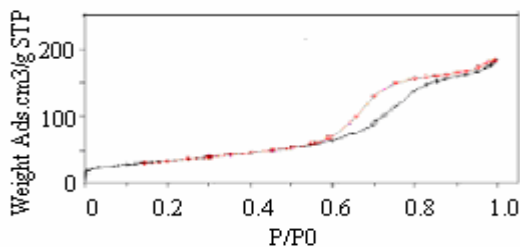


Figure 2. N₂ adsorption / desorption isotherm of nano-zirconia

Two weight loss stages are observed in the TG profile of nano-zirconia as shown in Figure 3. The first one, before 373K, corresponds to desorption of water physically adsorbed in the sample. The second one, after 473K, corresponds to loss of hydroxyl groups bonded on the surface of zirconia. No further weight loss is observed after 773K.

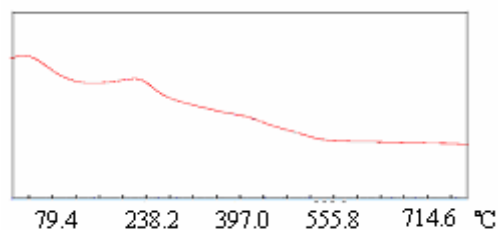


Figure 3. TG profile of nano-zirconia

Characterization of the Catalysts

Figure 4 shows that the pattern of NZ catalyst is the characteristic peaks of nano-zirconia and has no that of NiO, which indicates the dispersion of NiO on the support of nano-zirconia is uniform. However, NZ catalyst is amorphous. At the same time, the surface area, above 125.4 m²/g, of NZ catalyst is about 2 times higher than that of CZ catalyst.

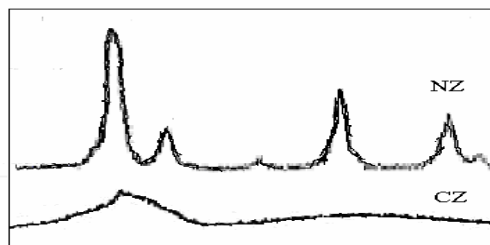


Figure 4. XRD patterns of the catalysts prepared with different method

Figure 5 shows that the weight loss of NP is slow, has no obvious exothermic spectra, and the reduction temperature is relatively low, which indicate that NiO dispersion is uniform and the interaction of NiO and support is relatively weak. However, the weight loss of CP is fast, has no obvious exothermic spectra, and the reduction temperature is relatively high, which indicate that the interaction between NiO and ZrO₂ is strong and NiO is not easily reduced, this is in accordance with the amorphous phase shown in XRD pattern.

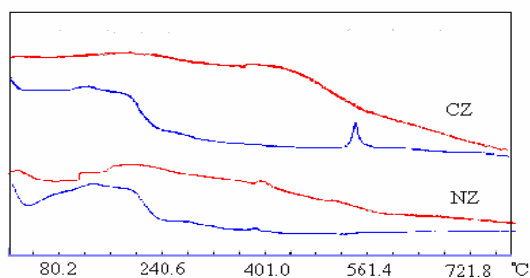


Figure 5. TG profiles of the catalysts prepared with different method in the atmosphere of H₂

Figure 6 shows that the particles of NZ catalyst are small and uniform, have no conglomeration, so the catalyst is considered as the compound of nanosized nickel oxide and zirconia. However, CN catalyst has obvious aggregates.

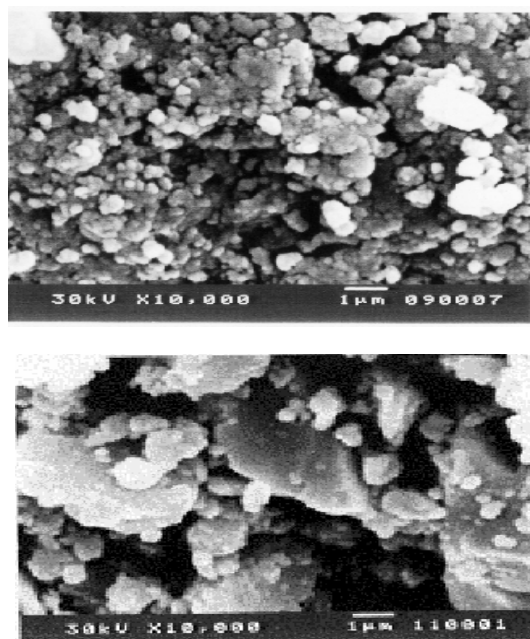


Figure 6. SEM images of the catalysts prepared with different method

Catalytic activity and stability

Figure 7 shows that the conversion of CH₄ on NZ catalyst is much higher than that of CZ catalyst. NZ catalyst exhibits high stability, the conversion of CH₄ is 77.8% at the beginning and decreases by about 8% after reacting 170h., however, the conversion of CH₄ is 59.22 on average over CZ catalyst. This indicates that the nano-sized catalyst with small-sized particles, large specific surface area and high metal dispersion possesses good catalytic property.

Conclusion

The results of catalytic activity and stability on dry reforming of methane reveals the important role of nano-zirconia to the catalyst. It makes the catalyst possess the characteristic of nano-particles such as more edges, corners, defects and abundant exposed atoms and so on. So nano-zirconia is the promising support of reforming catalysts.

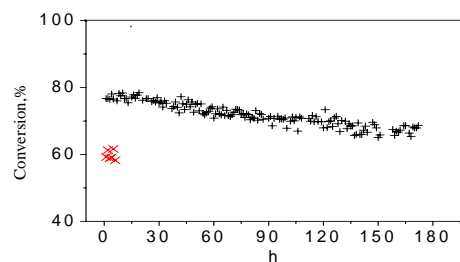


Figure 7. The variation of CH₄ conversion on the catalysts prepared with different method as a function of time

References

- (1) Yan, Z.F.; Ding, R.G.; Song, L.H. and Qian, L. *Energy & Fuels* **1998**, *12*, 1114.
- (2) Ding, R.G. and Yan, Z.F. *Catal. Today* **2001**, *68*, 135.
- (3) Ding, R.G.; Yan, Z.F.; Song, L.H. and Liu, X.M. *J. Natural Gas Chem.*, **2001**, *10*, 273.
- (4) Mattos, L.V.; Roino, E.; and Noronha, F.B. *Fuel Processing Technol.* **2003**, *83*, 147.
- (5) Mariana, M.V.M. Souza; Donato, A.G. Aranda and Martin, Schmal. *J. Catal.*, **2001**, *204*, 498.

Reforming of Methane and Coalbed Methane over Nanocomposite Ni/ZrO₂

Qin-Hui Zhang, Yan Li, Bo-Qing Xu*

Innovative Catalysis Program, Department of Chemistry, Tsinghua University, Beijing 100084, China (Email: [bxu@tsinghua.edu.cn](mailto:bqxu@tsinghua.edu.cn))

Introduction

One of the most attractive chemical approaches for the utilization of CO₂ and methane resources, e.g. coalbed gases, could be the catalytic CO₂ reforming of methane (CRM) to produce syngas (a mixture of H₂ and CO). CO₂ molecules in this CRM reaction function as a clean oxidant for the methane molecules. We have discovered recently that nanocomposite Ni/ZrO₂ catalysts, which consists of comparably sized Ni-metal (10-15 nm) and zirconia (7-25 nm) nanocrystals, are highly active and extremely stable for the CRM reaction at 700-800°C with a stoichiometric CO₂/CH₄ = 1.0 mixture [1,2]. However, in some other resources, the molecular CO₂/CH₄ ratio can be below the stoichiometry of the CRM reaction. A simple and convenient technological solution for the utilization of such resources is to add water (steam) as a compensation since catalytic steam reforming of methane (SRM) produces the same kind of products. In the present work, we demonstrate first that the nanocomposite Ni/ZrO₂-AN catalyst [1,2] also exhibits superior catalytic performance than the conventional oxide-supported Ni catalysts (Ni/ZrO₂-CP and Ni/Al₂O₃) for the SRM reaction. Our further study on combined steam and CO₂ reforming of methane (CSCRM) over the nanocomposite Ni/ZrO₂-AN catalyst will show that the extremely stable nanocomposite catalyst could make the CCSRM viable for producing syngas with flexible H₂/CO ratios.

Experimental

Preparation and catalytic testing of Ni/ZrO₂ catalyst
Conventional 12.9 wt% Ni/ZrO₂-CP (the BET surface area: 18 m²/g, reducibility of Ni: 98.5% and Ni-dispersion: 5.8) and nanocomposite 12.1 wt% Ni/ZrO₂-AN (the BET surface area: 38 m²/g, reducibility of Ni: 95.2% and Ni-dispersion: 9.4) catalysts were prepared according to our previous methods [1-4]. Z107 (13.0 wt% Ni/Al₂O₃-C) sample is a commercial catalyst for the industrial SRM reaction. The catalytic reaction was conducted at 800°C, measured by a thermal couple in a quartz-well inserted into the catalyst bed, in a vertical fixed-bed U-shape quartz reactor (i.d.10mm) under atmospheric pressure as described previously [1-4]. A specially designed chamber was placed ahead of the reactor inlet and used to make the stoichiometric mixture of CH₄ and steam (H₂O/CH₄=1.0). This chamber was heated to 300°C to ensure no condensation of the water reactant. For the combined steam and CO₂ reforming reaction, CO₂ is also mixed with other reactants in the chamber. Unless otherwise specified, the space velocity by the methane reactant was GHSV_{CH₄} = 1.2 × 10⁴ ml/(h·g_{cat}). Before the reaction, the catalyst was reduced in situ with H₂ (40ml/min) at 700°C for 3 h. Products from the reactor were analyzed on line by a gas chromatograph (SQ206) equipped with TCD and a carbon molecular sieve (80~100 mesh) column.

Results and Discussion

Figure 1 shows the TEM micrograms of the reduced Ni/ZrO₂-AN and Ni/ZrO₂-CP samples. It is remarkable that the structure of nanocomposite Ni/ZrO₂-AN catalyst is distinctive compared with the conventional Ni/ZrO₂-CP catalyst.

The catalytic data of SRM reaction at conditions of P=0.1MPa, T=800°C, GHSV_{CH₄} = 12,000 ml/(h·g_{cat}), H₂O/CH₄=1.0 are given in

Figure 2 by plotting CH₄ conversion against the reaction time on-stream over the different catalysts.

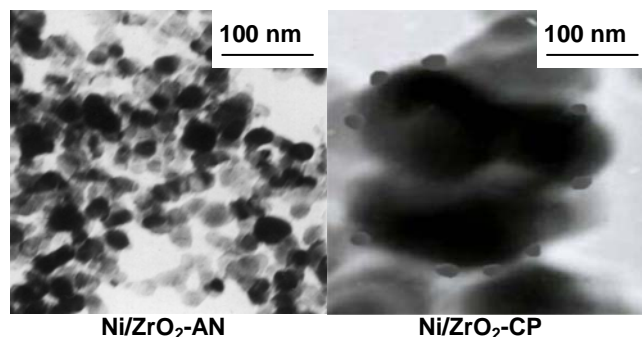


Fig. 1. TEM micrograms of the reduced Ni/ZrO₂ catalysts

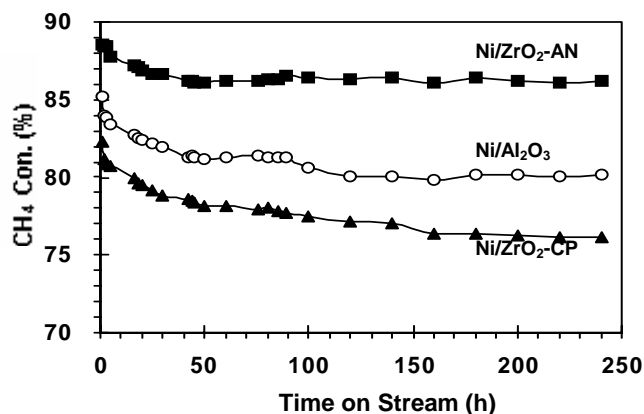


Fig. 2. Catalytic activity and stability during SRM process (P=0.1MPa, T=800°C GHSV_{CH₄}=12,000 ml/(h·g_{cat}), H₂O/CH₄=1.0

Although all the three catalysts showed high and stable catalytic activities in the SRM process for 240 hrs reaction time on stream with CH₄ conversions of 87-88%, 81-84% and 76-83% respectively which are close to the thermodynamic equilibrium values (90%) at 800°C, the nanocomposite Ni/ZrO₂-AN catalyst is apparently more active as well as more stable than the commercial Z107 and the conventional Ni/ZrO₂-CP catalyst at this space velocity.

To further demonstrate the catalyst stability at methane conversion far below its thermodynamic equilibrium value, all the catalysts were tested with stepwise increasing the space velocity of methane from GHSV_{CH₄} = 12, 000 to 96, 000 ml/(h·g_{cat}) and the results are shown in **Figure 3**. The data for the first 150 hrs reaction time on stream, which were the same as those at reaction TOS=150~200 hrs, were not shown in **Figure 3**.

It is evident that the nanocomposite Ni/ZrO₂-AN catalyst showed extremely stable catalysis for the SRM reaction since the observed catalytic methane conversions were stable every time after changing the reaction GHSVs from GHSV_{CH₄} = 12, 000 to 96, 000 ml/(h·g_{cat}), and surprisingly, the conversion at every specific GHSV was kept constant after switching between several different GHSVs during 400 hrs reaction time on stream; In contrast, the conventional Ni/ZrO₂-CP and commercial Z107 catalyst began deactivating at high space velocity of GHSV_{CH₄} = 48, 000 ml/(h·g_{cat}) and this deactivation is severely irreversible and by the end of 400 hrs they almost had no activity.

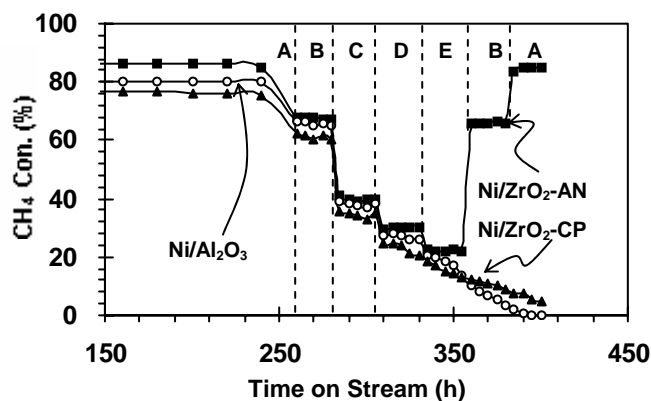


Fig. 3. Catalytic stability test at different methane space velocities of $GHSV_{CH_4} = 12,000$ (A), 24,000(B), 36,000(C), 48,000(D), and 96,000(E) $ml/(h \cdot g_{cat})$ ($P=0.1MPa$, $T=800^\circ C$, $H_2O/CH_4=1.0$)

It should be mentioned that we operated SRM reaction with rather lower H_2O/CH_4 molar ratio=1.0 and high space velocity as compared with most SRM process conducted under an H_2O/CH_4 molar ratio between 2.0-5.0 [6] to avoid the deactivation caused by severe carbon deposition under an H_2O/CH_4 molar ratio below 2.0 at atmospheric pressure [7]. However, with high H_2O/CH_4 molar ratios (>2.0), the following drawbacks exist: (a) the equilibrium of water-gas shift reaction ($H_2O + CO = H_2 + CO_2$) will become favorable, as a result, the H_2/CO_2 mole ratio in product will be high, which is not preferable for the downstream process such as methanol and Fischer-Tropsch synthesis; (b) an enormous amount of energy will be consumed in the production of steam thus the energy efficiency and process economy will decrease. Therefore, the development of nanocomposite Ni/ZrO₂-AN catalyst with high activity and stability under low H_2O/CH_4 molar ratio is promising for commercial utilization in the future SRM process.

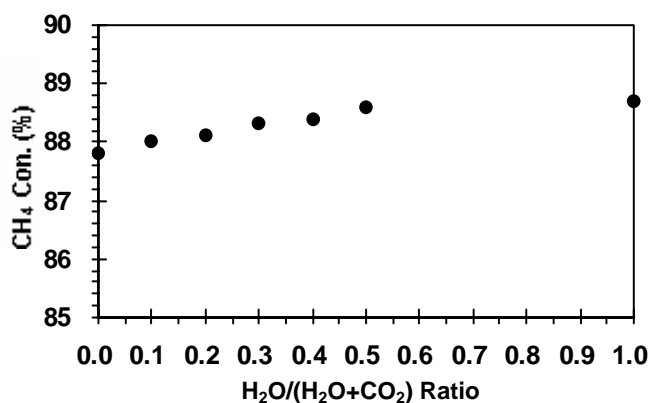


Fig. 4. Effect of the feed $H_2O/(H_2O+CO_2)$ ratio on methane conversion ($P=0.1MPa$, $T=800^\circ C$, $GHSV_{CH_4}=12,000$ $ml/(h \cdot g_{cat})$, $(H_2O+CO_2)/CH_4=1.0$)

We further applied the nanocomposite Ni/ZrO₂-AN catalyst in the CSCRM reaction since its remarkable catalytic activity and stability both in CRM [1-4] and SRM reactions. **Figure 4** shows the effect of the feed $H_2O/(H_2O+CO_2)$ ratio on methane conversion. With different H_2O/CO_2 ratios, the CH_4 conversion was stable and

maintained between 87.8%-88.8%. **Figure 5** shows the effect of the feed $H_2O/(H_2O+CO_2)$ ratio on the H_2/CO ratios of the products. It is clear that, with the increase of steam content in the feed, the H_2/CO ratios of the products increased from 1.0~3.0. Thus on the nanocomposite Ni/ZrO₂-AN catalyst, we could achieve syngas with flexible H_2/CO ratios of 1.0~3.0 by CSCRM reaction for different downstream synthesis, and could eliminate carbon formation which is a serious problem in the methane CO_2 reforming process [7].

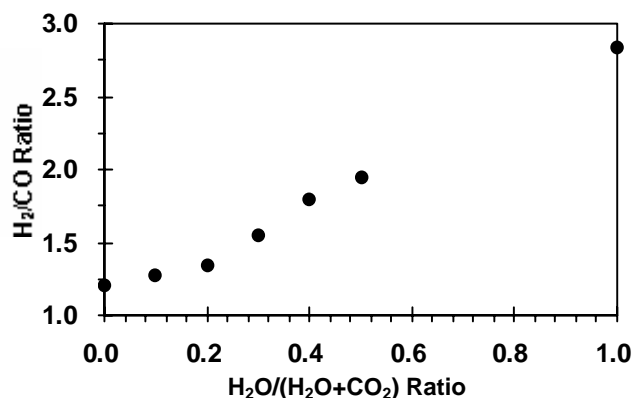


Fig. 5. Effect of the feed $H_2O/(H_2O+CO_2)$ ratio on H_2/CO ratio ($P=0.1MPa$, $T=800^\circ C$, $GHSV_{CH_4}=12,000$ $ml/(h \cdot g_{cat})$, $(H_2O+CO_2)/CH_4=1.0$)

Conclusions

This work proves that the nanocomposite Ni/ZrO₂-AN catalyst is highly active and extremely stable for both the steam reforming and the combined steam and CO_2 reforming of methane. In comparison with commercial Ni/Al₂O₃ catalyst, the nanocomposite Ni/ZrO₂-AN catalyst allows the use of a much higher space velocity of the reaction feed and a stoichiometric H_2O/CH_4 and $H_2O/(H_2O+CO_2)$ ratios, which could meet requirements for the commercial utilization of different methane and CO_2 resources.

References

- [1] Xu, B. -Q., Wei, J. -M. *et al.*, *J. Phys. Chem. B*: **2003**, 107, 5203
- [2] Xu, B. -Q., Wei, J. -M. *et al.*, *Top. Catal.* **2003**, 22, 77
- [3] Y. Li, Q. Ye, Wei, J. -M., Xu, B. -Q., *Chin. J. Catal.*, in the press
- [4] Wei, J. -M., Xu, B. -Q. *et al.*, *Chem. J. Chin. Univ.* **2002**, 23, 2106; *Catal. Today*, **2001**, 68, 217
- [5] G. Ertl, H. Knoezinger and J. Weitkamp, Eds., *Handbook of heterogeneous catalysis, Part B: Catalytic process*, (Wiley-VCH, **1997**), Vols. 4 and 5, 1819
- [6] J. P. Van Hook, *Catal. Rev. - Sci. Eng.*, **1980**, 21, 1

PLAMSAS FOR GREENHOUSE GAS UTILIZATION

Huy Le, L. L. Lobban and R. G. Mallinson

School of Chemical Engineering and Materials Science
University of Oklahoma
100E. Boyd Street, Room T335
Norman, OK 73019
mallinson@ou.edu

Introduction

Natural gas is considered the energy source of the future, because it is environmentally friendly with clean and low carbon emissions. However, it is not an easy-to-transport fuel. Unfortunately, many of the large proven reserves are located far away from the major markets, and it is not economical to transport the gas to the markets.

Methane, the major component of natural gas, is currently used primarily for its heating value. However, methane has a tremendous potential to be used as a building block to form other more valuable fuels and chemical feedstock. In indirect methane conversion processes, methane is first converted to synthesis gas, a mixture of CO and hydrogen, either via partial oxidation or steam reforming of methane. From synthesis gas, chemicals can be produced via many routes, or hydrogen can be extracted and used as a clean fuel used to power fuel cells. These indirect methane conversion processes are energy-intensive and less feasible at small capacity due to the high operating cost of the syngas generation unit.

Different advanced gas conversion technologies are desired to utilize and monetize the natural gas resources, whether it is stranded gas or not. From methane, different chemicals such as oxygenates, unsaturated C₂ hydrocarbons, and heavier hydrocarbons could be directly produced via different routes. The gas conversion technology using the non-equilibrium plasma generated by the AC corona discharge is such a technology, which can be used to convert methane to hydrogen and C₂ hydrocarbons under atmospheric pressure and room temperature.

The applications of indirect gas conversion technologies can be dated back before the 1950s. These technologies were based on the Fischer-Tropsch reaction (FT), discovered in the 1920s by the German scientists Franz Fischer and Hans Tropsch. They heated coal to produce synthesis gas, which when passed over a metal catalyst produced liquid hydrocarbons. Since synthesis gas can also be produced from natural gas, several processes have been designed and built to make liquid hydrocarbons from natural gas (GTL process). SASOL, the South Africa's state-owned oil company, is the most experienced in GTL processes. They have built GTL plants since the 1950s. Exxon-Mobil also has a 10 thousand barrel per day plant in Bintulu, Malaysia, in which synthesis gas was produced using pure oxygen. Other major energy companies such as Coconophillips are developing similar GTL processes, which would be built on large scale.

Non-equilibrium Plasmas

Non-equilibrium plasma technology has been used to convert methane to various products. It can be non-catalytic or catalytic.³⁻²⁵ Methane is converted to other products, such as C₂s and synthesis gas, under the temperature and pressure conditions that traditional chemistry cannot.

The non-equilibrium plasma is a type of plasma, in which the electron has much higher energy or temperature than the neutral gas species.^{2, 3} In the non-equilibrium plasma, total number density of the charged particles is much less than the total number density of

the neutral particles. When a potential difference is imposed across a gaseous mixture, the electric field acts upon the charged particles such as the electron but not the neutral species. The interaction transfers energy from the field to those charged particles in terms of kinetic energy. The electron, due to its light weight, is accelerated to higher velocity in the time between collisions. The electron has higher kinetic energy than the energy of gas molecules in random motion, if the applied field is high enough. Then, the non-equilibrium plasma is generated.

There are five common types of non-equilibrium discharges: glow discharge, silent (dielectric barrier) discharge, radio frequency discharge, microwave discharge, and corona discharge. The corona discharge is not homogenous, while the silent discharge is considered homogeneous and both can occur at atmospheric pressure conditions. This is the plasma type used in most recent work when a high voltage AC or pulsed waveform on the order of several KV is applied across two metal electrodes. In the case of the silent discharge, a dielectric barrier such as glass electrically isolates one or both electrodes. The average electron energy in these discharges is in the range of 1-10 eV and both cause only a small degree of ionization.²

The only commonly known industrial application using plasmas to produce chemicals is ozone production using the silent (DBD) discharge. However, plasmas have been used in large screen plasma televisions. The electron in the traditional CRT TV, emitted by an electron gun and accelerated via a strong electric field, is replaced by the electron initiated inside the plasma. The plasma TV can be as thin as 4 inches and as large as 72 inches.

Equilibrium Plasmas

The non-equilibrium plasma is different from the thermal plasma, or equilibrium plasma, in which all particles have approximately the same high temperature or kinetic energy. Thermal plasmas will not be discussed here as they may be generally regarded in many respects as conventional high temperature homogenous processes, with some exceptions. Also, these plasmas typically have prohibitively large energy input that is unsuitable to cost effective methane and CO₂ utilization. An intermediate category might be considered for plasmas that are nearly thermal, but of more moderate temperature. An example would be what might be called an igniting plasma in which the primary purpose of the plasma is to provide a rapid preheating of the gas where once the plasma has initiated the reactions they become thermally self sustaining.

Partial Oxidation of Methane

Many efforts have been concentrated on the partial oxidation of methane using the AC plasmas. Liu⁴ introduced helium into the methane-oxygen feed as a diluting species. The frequency was in the range of 10 Hz to 60 Hz. With methane to oxygen ratio varying from 2 to 10, it was reported that as the oxygen mole fraction increased, the methane conversion and the carbon monoxide selectivity increased, however, the ethane selectivity decreased. The ethylene selectivity did not change much. Theoretically, it is expected that hydrogen and acetylene be present in the product. However, these two species were not reported in this work.

The partial oxidation of methane using helium as a diluting species was also conducted in a higher frequency range from 150 Hz to 300 Hz.⁸ It was reported that increasing the oxygen mole fraction up to 20% increased the methane conversion and decreased the C₂ selectivities. Hydrogen and acetylene were not reported, as in Liu's case. This could be due to the limitation of the GC analysis. Even though the C₂ yield was said to reach a maximum at 0.6 atm helium

partial pressure, the major C₂ product was ethane, which is not a very useful product. The CO_x selectivity did not change noticeably. This implies that helium does not help the partial oxidation of methane.

The partial oxidation of methane using the AC plasma was also studied by Caldwell.⁹ The operating frequency was between 100 Hz and 800 Hz, covering the higher frequency range that previous works left. Increasing the oxygen mole fractions from 5% to 33% was reported to increase the methane conversion and energy efficiency. The CO₂ selectivity varied from 1% to 6%, suggesting that over-oxidation of methane was not excessive. The methane throughput compared to Liu and Hill's could be eight times higher, while the obtained methane conversions were in similar range, confirming that it was more energy efficient not to use any diluting species such as helium in the feed. The hydrogen selectivity was as high as 55%. All C₂ hydrocarbons and CO_x were reported in the products as expected. At 33% oxygen mole fraction in the feed, the carbon monoxide selectivity reached 55%. The lowest energy consumption was 6 eV per methane molecule converted. In addition to pure oxygen, air was used as the oxygen source. The energy consumption when using air was higher than the energy consumption when using pure oxygen. The lowest energy consumption reported in the air-methane system was ~15 eV/molecule of methane converted, higher than that in the methane-oxygen system, suggesting that nitrogen dilutes the feed and decreases the reaction rates. This result is consistent with the results from the methane-oxygen-helium system.

In Liu's work, it was reported that under a constant applied voltage, the methane conversion reached a maximum at 30 Hz. The maximum C₂ yield, obtained at 60% conversion of methane, was around 20%. It was explained that as the frequency was reduced to 30 Hz, the discharge changed from the corona discharge to the spark discharge. According to Eliason,² this change occurs when the applied voltage has exceeded a threshold. This implies that as the frequency was reduced the actual applied voltage to the electrodes increased. Therefore, at 10 Hz and 20 Hz frequencies, the discharge should also be the spark discharge. The authors did not give an explanation why the methane conversion at 10 Hz (~5%) was much lower than that at 30 Hz (~58%). The change in the input power with varying the frequency was not reported. Thus, there was no reported conclusion if the frequency influenced the energy efficiency of the system.

Hill⁸ also studied the effect of frequency with the same approach as Liu. It was reported that the methane conversion decreased when the frequency was increased from 150 Hz to 300 Hz, and the applied voltage was kept constant. The input power decreased from 15 W to 10 W, and the methane conversion decreased from 32% to 17%. Therefore, the energy efficiency did not change much within this frequency range.

Similarly, Caldwell⁹ studied the effect of the frequency with a different approach. Instead of keeping the applied voltage constant, the input power was kept constant. It was reported that the methane conversions were similar at the frequencies between 100 Hz to 800 Hz. The experimental data, such as flow rate, power, and oxygen ratio, were not reported.

Supat⁷ and Caldwell⁹ reported that increasing the input power by changing the frequency or increasing the applied voltage resulted in increasing the methane conversion. However, as the input power reached a certain threshold, excessive coke formation started. It could be because the heating of the bulk gas led to thermal dehydrogenation of methane to form coke.⁹ A higher input power would allow more energy to form more CH and CH₂, which are less stable than CH₃. Therefore, there were more CO, unsaturated C₂s as well as coke produced, when the input power increased.

Hill⁸ reported that at a constant feed flow rate and applied voltage, increasing the gas gap between the two electrodes increased the methane conversion. It could be explained that increasing the gas gap increased the residence time, therefore, increased the methane conversion.

The Steam Reforming and the Combined Steam Reforming with Partial Oxidation of Methane

The conventional steam reforming normally involves high temperature and catalysts. However, plasma technology allows it to be carried out at much lower temperatures. Hammer¹⁰ used the silent discharge in a Dielectric Barrier Discharge (DBD) reactor to study the steam reforming of methane. The steam mole fraction was varied from 50% to 75% at temperatures in the range of 200°C to 600°C. The products included CO_x, C₂s, C₃s, and butane. Based on the author's data, the energy consumption per methane molecule converted was in the range of 50 eV to 100 eV, an order of magnitude higher than the energy consumption in the partial oxidation of methane. High energy consumption has been the main disadvantage of the DBD system.

Supat⁷ studied the combined steam reforming and partial oxidation at the steam mole fractions less than 50%. The methane to oxygen ratio (MTOR) was in the range of 2:1 to 5:1. The CO selectivity was as high as 62%. The estimated H₂ selectivity (not reported by the author) was 80%, about 20% higher than that in the partial oxidation of methane. The lowest energy consumption per molecule of methane converted was 9 eV, much higher than that in the partial oxidation of methane.

Also using the combined steam reforming and partial oxidation with air as the oxygen source, Bromberg¹¹ reported a high efficiency plasmatron producing hydrogen from natural gas using the catalytic DC plasma. The feed conversions were as high as 100%. Most of the methane was converted to carbon monoxide. There was only a small amount of ethylene reported. Even though the input power was high (270 W), the high feed conversions as well as high methane throughput led to a low energy consumption: ~0.24 eV/molecule of methane converted. This is the lowest energy consumption ever reported and may reflect more of an ignition phenomena than an initiation phenomena. Since the partial oxidation and steam reforming of methane is thermodynamically favored at high temperatures, the use of catalysts at high operating temperatures helps increase the feed conversions. The plasma source could be considered as an ignition stage providing heat to preheat the gas and the catalysts. As a result, the plasmas could be replaced by a conventional heater without impacting the results.

Dry reforming of methane has been studied using the AC Dielectric Barrier Discharge²², the AC arc discharge²⁴, and the pulsed discharge.²¹ The CO selectivity above 82% was obtained in the AC DBD²² and the AC arc discharge.²⁴ The ethylene selectivity was not reported²² or was very low (2.3%).²⁴ On the other hand, the ethylene selectivity, as high as 64%, was obtained in the pulse discharge.²¹ The lowest energy consumption per molecule of carbon (including CH₄ and CO₂) converted was 15 eV.²⁴ This seemed to be more efficient than the steam reforming of methane. However, the energy consumption was still much higher than that in the partial oxidation of methane.

Conclusions and Prospects

Methane as a greenhouse gas is misleading in the context of GHG utilization in that methane that is consumed is produced for its utilization (or might be recovered for that purpose in relatively small quantities). Thus it seems that the primary impact of plasma

based processes on GHG utilization when converting methane would be to reduce CO₂ emitted as a result of its consumption, e.g. to be more energy efficient than conventional processes. As a crude comparison, methane has an energy content of about 8 eV/molecule and conventional steam reforming is about 70 percent efficient, using direct fired combustion for the input heat, thus approximately 5.6 eV/molecule is retained in the products (hydrogen and CO). For a plasma, the allowable energy “cost” is then about 2.4 eV/molecule. However if this is supplied by electricity, generated with an efficiency of about 35 % (single cycle fossil energy), then the maximum electrical energy that can be supplied competitively is about 0.8 eV/molecule of methane converted. No plasma system has yet achieved this. The silent discharge systems appear to be sufficiently inefficient that this will be difficult to conceive, however some corona discharge results are certainly within an order of magnitude and perhaps substantially closer to this. So there seems to be some promise that improvements may make this achievable and may also apply to steam combined with CO₂ reforming to some extent. This could be particularly valuable where CO₂ is a significant contaminant of the natural gas resource. (Note that CO₂ reforming as a net sink for CO₂, say recovered from power production, is not a net sink for CO₂!).

In the case of partial oxidation, no net energy input is required for convention conversion due to its exothermicity, and therefore even for an ignition type plasma system, the net greenhouse gas “consumption” for a plasma will always be less. Fortunately, oxygen is the most efficient initiator for methane conversion in low temperature plasmas and energy consumption can be quite low under the best conditions, approximately 1eV/molecule. So even here, other factors, such as the ability to operate on a much smaller scale, with less need and cost, for heat recovery, may allow application of low temperature corona type plasma methane conversion even with some loss in net energy efficiency (and therefore greenhouse gas consumption) compared to conventional processes.

References

- Strategic Plan for DOE Hydrogen Program, US Department of Energy, Jan **1998**
- Eliasson, B.; Kogelschatz, U.; “Nonequilibrium Volume Plasma Chemical Processing”. *IEEE Trans. Plasma Sci.* **1991**, 19 (6), 1063-1077
- Chang, J.-S.; Lawless, P. A.; Yamamoto, T.; “Corona Discharge Process”. *IEEE Trans. on Plasma Sci.* **1991**, 19 (6), 1152-1166
- Liu, C.; Marafee, A.; Hill, B.; Xu, G.; Mallinson, R.; Lobban, L.; “Oxidative Coupling of Methane with ac and dc Corona Discharges.” *Ind. Eng. Chem. Res.* **1996**, 35, 3295- 3301
- Larkin, D.W.; Caldwell, T.A.; Lobban, L.L.; Mallinson, R.G.; “Oxygen Pathways and Carbon Dioxide Utilization in Methane Partial Oxidation in Ambient Temperature Electric Discharges.” *Energy and Fuels* **1998**, 12, 740-762
- Fan, W. Y.; Knewstubb, P. F.; Kaening, M.; Mechold, L.; Roepcke, J.; Davies, P. B.; “A Diode Laser and Modeling Study of Mixed (CH₄-H₂-O₂) AC Plasmas.” *Journal of Physical Chemistry A* **1999**, 103(20), 4118-4128
- Supat K, Chavadej S., Lobban, L. L., Mallinson, R. G.; “Combined Steam Reforming and Partial Oxidation of Methane to Synthesis Gas Under Electrical Discharge.” *Ind. Eng. Chem. Res.* **2003**, 42 (8), 1654-1661
- Hill, J. B.; “The Oxidative Coupling of Methane Using an AC Electric Gas Discharge.” A Thesis for Master of Science, University of Oklahoma, **1997**
- Caldwell, T.A.; Le, H.; Lobban, L. L.; and Mallinson, R. G.; “Partial Oxidation of Methane to Form Synthesis Gas in a tubular AC Plasma Reactor.” *Studies in Surface Science and Catalysis* **2001**, 136, 265-270
- Hammer, T.; Kappes, T.; Schience, W.; “Plasma Catalytic Hybrid Reforming of Methane.” *Preprints of Symposia - American Chemical Society, Division of Fuel Chemistry*, **2002**, 47(1), 278-279.
- Bromberg, L.; Cohn, R. D.; Rabinovich, A.; Heywood, J.; “Emissions Reductions Using Hydrogen from Plasmatron Fuel Converters.” *Diesel Engine Emission Reduction Workshop*, San Diego, CA August **2000**
- Mallinson, R.G.; Braun, R.L., Westbrook; C.K., Burnham, A.K., “Detailed Chemical Kinetics Study of the Role of Pressure in Butane Pyrolysis.” *Ind. Eng. Chem. Res.*, **1992**, 31 (1), 37-
- Larkin, D.W.; Lobban, L.L.; Mallinson, R.G.; “Production of Organic Oxygenates in the Partial Oxidation of Methane in a Silent Electric Discharge Reactor.” *Ind. Eng. Chem. Res.* **2001**, 40, 1594-1601
- Larkin, D.W.; Zhou, L.; Lobban, L.L.; Mallinson, R.G.; “Product Selectivity Control and Organic Oxygenate Pathways from Partial Oxidation of Methane in a Silent Electric Discharge Reactor.” *Ind. Eng. Chem. Res.* **2001**, 40, 5496-5506
- Liu, C.; Marafee, A.; Mallinson, R. G.; Lobban, L. L.; “Methane Conversion to Higher Hydrocarbons in a Corona Discharge over Metal Oxide Catalysts with OH Groups.” *Appl. Catal. A.*, **1997**, 164 (1-2) 21-33
- Liu, C.; Mallinson, R.G.; Lobban, L.L.; “Nonoxidative Methane Conversion to Acetylene over Zeolite in a Low Temperature Plasma.” *J. Catal.* **1998**, 179, 326-334
- Marchionna, M.; Lami, M.; Anna, M.; Raspolli G.; “Synthesizing Methanol at Lower Temperature.” *Chemtech* **1997**, 15, 27-31
- Thanyachotpaiboon, K.; Chavadej, S.; Caldwell, T. A.; Lobban, L.L.; Mallinson, R. G.; “Conversion of Methane to Higher Hydrocarbons in AC Nonequilibrium Plasmas.” *AIChE J.* **1998**, 44 (10), 2252-2257
- Savinov, S. Y.; Lee, H.; Song, H. K. Na, B.-H. “Decomposition of Methane and Carbon Dioxide in a Radio-frequency Discharge.” *Ind. Eng. Chem. Res.* 1999, 38 (7), 2540-2547
- Yao, S. L.; Takemoto, T.; Ouyang, F.; Nakayama, A.; Suzuki, E.; “Selective Oxidation of Methane Using a Non-Thermal Pulsed Plasma.” *Energy and Fuels* **2000**, 14 (2), 459-463
- Yao, S.; Nakayama, A., Suzuki, E.; “Methane Conversion Using a High-Frequency Pulsed Plasma: Important Factors.” *AIChE Journal* **2001**, 47 (2), 413-425
- Zhou, L. M.; Xue, B.; Kogelschatz, U.; Eliasson, B.; “Nonequilibrium Plasma Reforming of Greenhouse Gases to Synthesis gas.” *Energy & Fuels* **1998a**, 12 (6), 1191-1199
- Zhou, L. M.; Xue, B.; Kogelschatz, U.; Eliasson, B.; “Partial Oxidation of Methane to Methanol with Oxygen of Air in a Nonequilibrium Discharge Plasma.” *Plasma Chemistry and Plasma Processing* **1998b**, 18(3), 375-393
- Huang, Aimin; Xia, Guangang; Wang, Jinyun; Suib, Steven L.; Hayashi, Yuji; Matsumoto, Hiroshige. “CO₂ Reforming of CH₄ by Atmospheric Pressure ac Discharge Plasmas.” *Journal of Catalysis*, **2000**, 189(2), 349-359
- Sorensen, S. L.; Karawajczyk, A.; Stromholm, C.; Kirm, M.; “Dissociative Photoexcitation of CH₄ and CD₄.” *Chem. Phys. Lett.*, **1995**, 232, 554

RF Plasma Modification of Supported Pt Catalysts for CO₂-CH₄ Reforming

Jason Zhan¹, Praveen Boopalachandran¹, Ben W.-L. Jang¹,
Jai Choi², Richard B. Timmons²

¹Department of Chemistry, Texas A&M University-Commerce,
Commerce, TX 75429-3011

²Department of Chemistry & Biochemistry, U. of Texas-Arlington,
Arlington, TX 76019

Introduction

Numerous studies dealing with CO₂/CH₄ reforming have been recently published. Edwards and Maitra (1), in a detailed review, have suggested that further catalyst development is the major hurdle before this reforming can be widely commercialized. Literature shows that the supported Group VIII elements in their reduced forms, especially Ni, Co, Ru, Rh, Pd, Ir and Pt, are active for CO₂/CH₄ reforming. Among these metals, Ni, Pt, Ru and Rh are the most studied elements.

Many different support materials, such as SiO₂, Al₂O₃, ZrO₂, TiO₂ and mixed oxides, have been studied for CO₂/CH₄ reforming. Results suggest that supports have a strong effect on the activity and the stability of CO₂ reforming catalysts. For example, replacing γ -Al₂O₃ by single crystal MgO as support material for Ni results in low coking and high catalytic activity (2). The support materials apparently influence the growth of carbon by controlling the type of metallic clusters that are sites for carbon formation (1). The acid/base properties of the support material are also important to the activity and stability of the catalysts. Tang et al. report that the increase in base strength of catalysts decreased the coke deposition rate on both SiO₂ and Al₂O₃ supported Ni catalysts (3). Ferreira-Aparicio et al have suggested that surface hydroxyl groups are involved with the reaction mechanism (4).

Strong support-metal interactions can result in changes in catalytic activity, selectivity, and stability. For example, Ni/Al₂O₃ forms NiAl₂O₄ (which is inactive for CO₂ reforming with CH₄) at high temperatures. Modifiers such as La₂O₃ and CeO₂ promote the activity of alumina supported Ni catalysts for CO₂ reforming. It is reported, by Bitter et al., that the available perimeter around Pt-ZrO₂ interfaces is critical for the reforming activity in that CO₂ reduction occurs close to the metal-support boundary (5). Verykios also proposed that active carbon containing species on Rh/Al₂O₃ are in the reaction pathway of CO formation during CO₂/CH₄ reforming (6). These results confirm the importance of metal-support interactions.

Recently, non-thermal plasma based techniques for catalyst preparation have attracted significant attention (7,8). Materials with unusual and highly advantageous catalytic properties, including high metal dispersion and enhanced metal-support interaction resulting in better catalyst stability, have been achieved via the plasma route. These advances have been documented in symposia and detailed in recent reviews (9-11). For example, Zhang et al. reported plasma activation of a Ni/ α -Al₂O₃ catalyst for methane conversion to synthesis gas using a radio-frequency (RF) argon plasma for the decomposition of Ni(NO₃)₂. The resulting catalyst exhibited improved activity and catalytic lifetime compared to material obtained using conventional high temperature methods (12). More recently, a Ni-Fe/Al₂O₃ catalyst, prepared first by glow discharge plasma treatment followed by calcination, was studied for partial

oxidation of methane by Wang et al. (13). The resultant catalyst exhibited overall improved performance compared to a catalyst of identical composition prepared via calcination. In addition, the plasma treated Ni-Fe/Al₂O₃ catalyst also exhibited better resistance to carbon deposition (13).

The present study examines further the utility of plasma processing in developing improved catalysts for eventual use in CO₂/CH₄ reforming operations. Specifically, we report plasma modification effects on metal-support interactions of 1%Pt/Al₂O₃ catalysts. By substituting plasma treatment for the conventional high temperature calcination step, both higher metal dispersions and improved sintering resistance are observed with the resultant catalysts. Additionally, the distribution of CO₂ adsorption sites on the catalyst is observed to be strongly regulated by various plasma treatments.

Experimental

Catalyst Synthesis. Alumina pellets, 1/8 in., (from Alfa Aesar) with 1.14 ml/g pore volume and a 255 m²/g surface area were crushed and screened to 20-40 mesh. The 20-40 mesh alumina particles were dried at 200°C for one hour then cooled in a desiccator to room temperature. The resultant alumina particles were then impregnated with H₂PtCl₆ solution based on the incipient wetness technique to provide 1% Pt loading. The materials were dried at 120°C for 2 hours and are designated as 1%Pt/Al₂O₃(A). Powder aluminum hydroxide (from Aldrich) was used as the alumina precursor to prepare impregnated Pt catalysts for acid/base studies. Aluminum hydroxide and the Pt precursor were mixed in water and heated until dry. The dried sample was then calcined at 500°C in air for 3 hours and it is designated as 1%Pt/Al₂O₃(H).

Plasma Treatment. Plasma treatments were carried out in a custom-designed 360° rotating RF plasma system. The system consists of three major components: power supply, reaction chamber, and a gas delivery and pumping system. The power supply includes an ENI A-300 amplifier, Tetrionix pulse generation (Model 2101), and a Wavetech function generation (Model 166). A custom designed matching network was employed to minimize the reflected power. Power wattage is measured by the combination of a Bird watt meter (Model 4412), and a Leader oscilloscope (Model LS1020). This system is operable from milli-torr to a few torrs, with a base pressure of 10 mtorr. For O₂ plasma, 150W peak power and a 10ms/10ms plasma on/off cycle was used. For H₂ plasma, 200W and 10ms/10ms on/off cycle was employed. Typically, one gram of catalyst was loaded into the plasma chamber for treatment. The times for plasma treatment ranged from 1 to 3 hours. Both O₂ and H₂ gases were UHP grade.

H₂-Chemisorption. H₂-Chemisorption tests were performed with the automatic catalyst characterization system, AMI-200 (Altamira Instruments). Approximately 70mg samples were heated in H₂ with a 5°/min ramping rate, to 450°C or 600°C before cool down in argon to 35°C. Hydrogen-chemisorption was carried out by pulsing H₂ over clean metal surfaces until saturation. The consumption of H₂ due to chemisorption is measured by TCD for metal dispersion determination.

CO₂/NH₃-TPD. Catalyst samples (~70 mg) were heated in UHP helium at 20°C/min to 500°C before cooling down to 50°C for adsorption with 10% CO₂/NH₃ in helium for an hour. CO₂/NH₃-TPD is recorded with TCD using a ramp rate of 10°C/min from 50°C to 500°C in helium.

Results and Discussion

Pt Dispersion. Pt metal dispersions of 1%Pt/Al₂O₃(A), determined by H₂-chemisorption after reduction at different temperatures, are summarized in Table 1. After hydrogen reduction at 450°C, both O₂ and H₂ plasma treated samples show higher dispersions than the plasma untreated control sample. The O₂ plasma is more effective than the H₂ plasma in promoting the dispersion with 39.5% (O₂) vs 34.1% (H₂) compared to 31.1% for the untreated sample. After 600°C reduction for 5 hours, both O₂ and H₂ plasma treated samples show much higher dispersions than the untreated sample. The Pt dispersions are 34.1%, 34.7% and 24.4% for O₂ plasma, H₂ plasma and untreated samples, respectively. These results suggest that the sintering resistance of these catalysts is improved by the plasma treatments. The relative improved resistance is even more prominent after extended reductions at 600°C. After reduction at 600°C for 12 hours, H₂ plasma treated sample shows superior sintering resistance over O₂ plasma treated and untreated samples. As shown in Table 1, no apparent decrease in Pt dispersion is detected for the H₂ plasma treated sample while metal dispersion on the O₂ plasma treated sample decreased by 22% while the untreated one decreased by 34.7%. These results demonstrate that both O₂ and H₂ plasmas are effective in promoting increased metal dispersion, with the H₂ treated materials also exhibiting improved sintering resistance.

NH₃-TPD. The NH₃-TPD results of calcined, H₂ plasma treated and O₂ plasma treated 1%Pt/Al₂O₃(H) are shown in Figure 1. Both H₂ and O₂ plasmas modify the acidic sites for NH₃ adsorption. The O₂ plasma shows a stronger effect on 1%Pt/Al₂O₃(H) increasing strongly the surface density of weak, medium and strong sites for NH₃ adsorption. In contrast, the H₂ plasma treatment apparently results in a more selective increase in the concentration of the weakly acidic sites, relative to smaller increases in the medium and strong NH₃ adsorption sites.

CO₂-TPD. CO₂-TPD results of calcined, H₂ plasma treated and O₂ plasma treated 1%Pt/Al₂O₃(H) are listed in Figure 2. As shown in Figure 2, H₂ plasma has little effect on the population and the distribution of CO₂ adsorption sites. O₂ plasma, on the other hand, is highly effective in the generation of strong and medium CO₂ adsorption sites on 1%Pt/Al₂O₃(H). Oxygen plasmas are well known for etching ability and are used extensively for that purpose. It is likely that O₂ plasma creates vacancies which serve as new sites for CO₂ adsorption. H₂ plasma, on the other hand, is known for passivation effects (14) and is less efficient for site generation. However, after site generation by O₂ plasma, a subsequent H₂ plasma treatment alters the properties of generated sites, as shown in Figure 3. Figure 3 lists the CO₂-TPD results of samples with the 3-h O₂ plasma treatment followed by H₂ plasma treatments of 1 to 6 hours. As shown in Figure 3, one hour of H₂ plasma treatment largely reduces the strong sites generated by the 3-h O₂ plasma treatment and simultaneously increases the sites with less strength (mainly weak sites) for CO₂ adsorption. As the H₂ plasma time increases from 1 hour to 3 hours, the strong site population further decreases and, simultaneously, both weak and medium sites decrease. Further increase of the H₂ plasma treatment time to 6 hours results in further decrease of the weak sites, with relatively no changes of medium sites. These results indicate that H₂ plasma is effective in reducing the strength of CO₂ adsorption sites while O₂ plasma generates CO₂ adsorption sites with medium to high strengths. Thus, it appears the combination of O₂ and H₂ plasma treatments, especially an initial O₂ plasma followed a subsequent H₂ plasma, can manipulate the population and distribution of CO₂ adsorption sites. It is anticipated

that regulation of the nature and surface density of active sites should affect the activity and stability of catalysts employed in CO₂/CH₄ reforming. Present studies involve a continuation of this work and they include examination of the effect of similar plasma treatments on CH₄ adsorption site densities. The RF plasma treatment approach described offers a viable route to evaluation of the role of active surface site densities on the CO₂/CH₄ reforming process, and thus a potentially important route to synthesis of improved catalysts for this purpose.

Conclusions

Both O₂ and H₂ plasmas are effective in promoting increased metal dispersion. Additionally, H₂ plasma treatments results in catalysts having improved resistance to sintering. The CO₂-TPD study indicates that the combination of O₂ and H₂ plasma treatments, especially the O₂ plasma first followed by H₂ plasma, can manipulate the population and distribution of CO₂ adsorption sites. Further studies of these effects are currently in progress in our labs.

Acknowledgement. Authors wish to acknowledge the financial support of an Organized Research Grant and an equipment grant from the College of Arts and Sciences at TAMU-Commerce.

Table 1. Metal dispersion results of 1%Pt/Al₂O₃(A).

Catalyst	Reduction at 450°C for 2 hr	Reduction at 600°C for 5 hr	Reduction at 600°C for 12 hr
Uncalcined	31.1	24.5	20.3(-34.7%)
H ₂ plasma, 1 hr	34.1	34.7	35.1(~0)
O ₂ plasma, 1 hr	39.5	34.1	30.8(-22.0%)

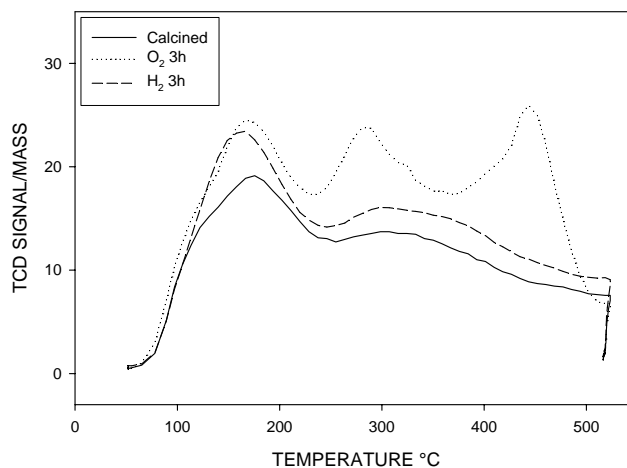


Figure 1. NH₃-TPD of calcined, O₂ treated and H₂ plasma treated 1%Pt/Al₂O₃(H).

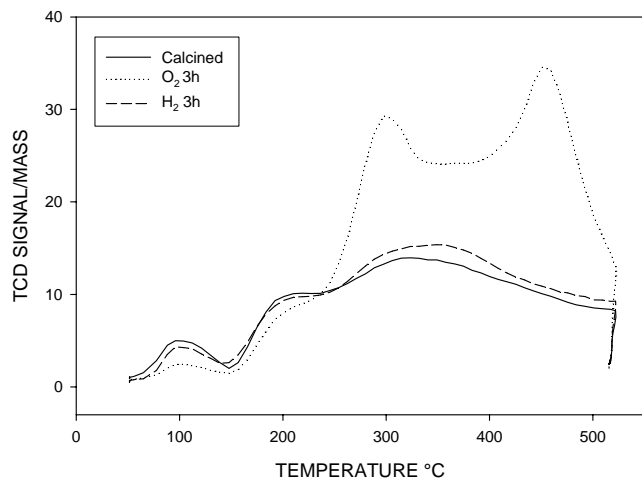


Figure 2. CO₂-TPD of calcined, O₂ treated and H₂ plasma treated 1%Pt/Al₂O₃(H).

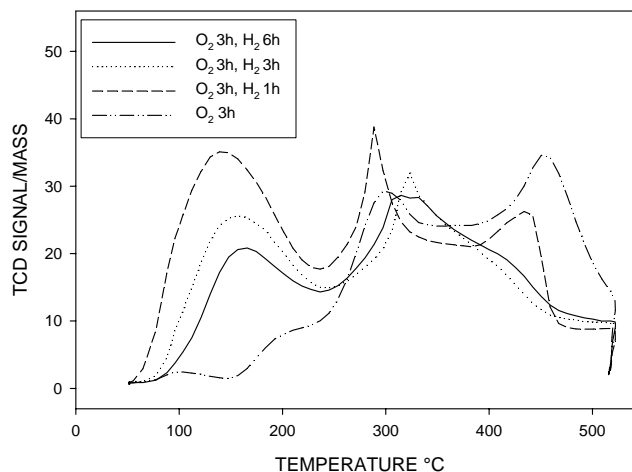


Figure 3. CO₂-TPD of calcined 1%Pt/Al₂O₃(H) with combinations of O₂ plasma and H₂ plasma treatments.

References

- [1] Edwards, J.H.; Maitra, A.M. *Fuel Processing Technology* **1995**, *42*, 269.
- [2] Gadalla, A.M.; Sommer, M.E. *Chemical Engineering Science* **1989**, *44*(12), 2825.
- [3] Tang, S.-B.; Qiu, F.-L.; Lu., S.-J. *Catal. Today* **1995**, *24*, 253.
- [4] Ferreira-Aparicio, P.; Rodriguez-Ramos, I.; Anderson; Guerrero-Ruiz, A. *Appl. Catal. A*, **2000**, *202*, 183.
- [5] Bitter, J.H.; Seshan, K.; Lercher, J.A. *J. Catal.* **1998**, *176*, 93.
- [6] Verykios, X.E. *Appl. Catal. A*, **2003**, *255*, 101.
- [7] "Catalysis and Plasma Technology" symposium organized by B.W.-L. Jang, J.G. Reynolds, M. Boutonnet and J.J. Spivey, the 220th ACS National Meeting at Washington DC in August, **2000**.
- [8] "Plasma Technology and Catalysis" symposium organized by B.W.-L. Jang, C.-J. Liu and T. Hammer, the 225th ACS National Meeting at New Orleans, LA in March, **2003**.
- [9] Liu, C.-J.; Vissokov, G.P.; Jang, B.W.-L. *Catal. Today*, **2002**, *72*, 173.
- [10] Kizling, M.B.; Jaras, S.G. *Appl. Catal., A*. **1996**, *147*, 1.
- [11] Vissokov, G.P. *J. Material Sci.*, **1998**, *33*, 3711.
- [12] Zhang, Y.; Chu, W.; Cao, W.; Luo, C.; Wen, X.; and Zhou, K. *Plasma Chem. Plasma Processing*, **2000**, *20*, 137.
- [13] Wang, Jian-guo; Liu, Chang-jun; Zhang, Yue-ping; Yu, Kai-lu; Zhu, Xin-li; He, Fei *Catal. Today*, in press.
- [14] Luo, B.; Ren, F.; Lee, K.P.; Pearton, S.J.; Wu, C.-S.; Kopf, R.F.; Johnson, D.; Sasserah, J. N. *Solid-State Electronics* **2001**, *45*(9), 1613.

MINIMUM ENERGY REQUIREMENT FOR METHANE STEAM REFORMING IN PLASMA-CATALYST REACTOR

Tomohiro Nozaki, Nahoko Muto, Shigeru Kado, Ken Okazaki

2-12-1 O-okayama, Meguro, Tokyo Japan 152-8552
TN: tnozaki@mech.titech.ac.jp

1. Introduction

This paper describes advanced steam reforming of methane in plasma-catalyst hybrid reactor. Synergistic effect between non-thermal plasma (DBD) and Ni-catalyst was observed at lower reaction temperature (400°C-600°C). Methane conversion exceeded far beyond equilibrium conversion, while product selectivity tended to follow equilibrium composition at given conditions: energy cost and energy efficiency were improved by 134 MJ/kg_{H₂} and 69%. According to numerical simulation of streamer propagation in pure methane, production of large number of vibrationally excited methane seems to contribute significant increase in methane conversion since vibrational species promoted dissociative chemisorption on nickel surface at lower temperature. Based on those experimental and numerical evidences, minimum energy required in plasma-catalyst hybrid reactor for methane steam reforming was estimated. The energy consumption might be reduced by one-quarter of experimental result, which also means that hybrid reactor might be able to regenerate low temperature thermal energy during low temperature plasma catalysis of methane (400°C-600°C).

2. Methane steam reforming by plasma-catalyst hybrid reactor

Experimental. Authors developed Barrier-discharge Enhanced Catalytic-bed (BEC) reactor for methane steam reforming (1-5). The wire-to-tube (I.D. 6 mm) reactor packed with 3wt%Ni/SiO₂ catalyst pellets (1.2 mm and 0.9 mm) was situated in a constant temperature bath (120°C). High voltage sine wave (76 kHz) was applied between wire and external electrodes. Methane and water-vapor mixture was fed into the reactor at various mixture ratio and flow rate. Three different conditions were investigated: (1) 3wt%Ni/SiO₂, (2) plasma and 3wt%Ni/SiO₂, and (3) plasma with SiO₂. Detailed description of reactor and experimental conditions are presented elsewhere (1).

Synergistic effect between plasma and catalyst. Figure 1 (a) compares methane conversion characteristics for three different reaction systems, and (b), (c) show product selectivity. Barrier discharge is able to decompose methane at lower temperature, and 25% conversion was achieved at 200°C. However, methane conversion falls far short of equilibrium at higher temperature since methane activation by electron impact is basically independent of gas temperature (within 25°C -700°C). On the other hand, nickel catalyst does not show catalytic activity below 400°C, and methane conversion was half of the equilibrium at 600°C. If the temperature reached 700°C, methane conversion abruptly increased and attained equilibrium. We didn't observe major changes in methane conversion and product selectivity with respect to pellet diameter.

When barrier discharge and catalyst was combined, methane conversion exceeded equilibrium over the tested temperature range. The strong synergistic effect of barrier discharge and nickel catalyst was observed between 400°C and 600°C: methane conversion exceeded combined result of barrier discharge and nickel catalyst. On the other hand, catalytic reaction predominated over barrier discharge above 700°C, and synergistic effect was not observed below 200°C. Methane conversion curve for Ni/SiO₂ shifted 200°C towards lower temperature region in the presence of barrier discharge: the apparent activation temperature for nickel catalyst seemed to be lowered due to the existence of barrier discharge.

Figure 1 (b) and (c) show product selectivity obtained by BEC reactor. When the temperature was 200°C, reaction characteristics were very similar to those obtained by DBD reactor: 50% of carbonaceous products were C₂ (mainly ethane) and C₃ (propane) hydrocarbons. Product selectivity approaches equilibrium curve (dotted line) with increasing reaction temperature, and perfectly follows equilibrium curve over 600°C. It is interesting to note that methane conversion largely exceeded equilibrium value, but product selectivity follow equilibrium. This means that electron impact process plays an important role during gas phase methane activation: not only ground state methane molecule, but also excited molecule can be decomposed on nickel catalyst, leading to apparent low temperature activation of methane.

3. Radical formation by electron impact

Model. We performed numerical simulation on streamer development in pure methane for better understanding of elementary

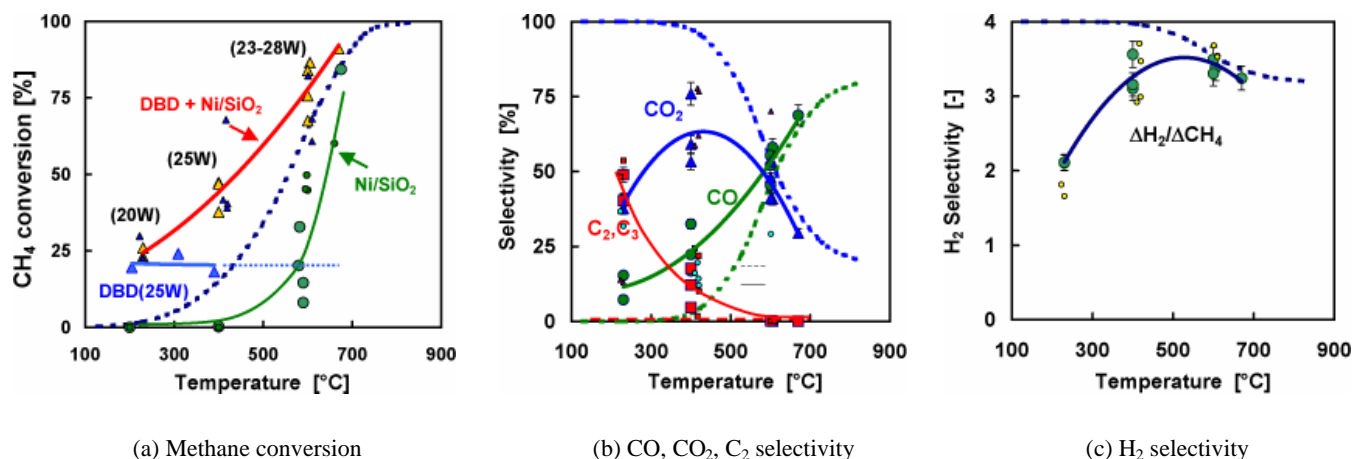
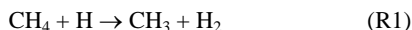


Fig. 1 Methane conversion and product selectivity at different temperatures, showing synergistic effect of plasma and Ni catalyst on methane decomposition. (--- Equilibrium). Smaller symbols represent results obtained with 0.9 mm Ni/SiO₂ pellet.

electronic and chemical processes. We assumed that streamer was one-dimensional cylinder with 100 μm radius and 2 mm long. We simulated Anode Directed Streamer (ADS) ignited from tiny plasma spot located in front of the cathode. Basic equations were continuity equations for electron, ions, and neutral species, and Poisson's equation. 38 elementary reactions including 8 inelastic collisions were simultaneously solved. During streamer development, electric energy input and radical formation efficiency was analyzed in detail. After the termination of streamer development (~ 5 ns), ionic and free radical chemistry that would last for 10 ms was performed with the reaction scheme proposed by Tachibana et al (6). 16 neutral species, 4 positive ions, and 2 vibrationally excited species were considered in our model. Temperature and pressure were 300 K and 760 Torr, respectively.

Energy branching to radicals. Table 1 shows energy branching and relative radical density during streamer propagation. Excitation threshold for vibrational excitation is of the order of 0.1-0.3 eV; however, 40% of input electrical energy was consumed since rate constants are 10 times larger than that for other reactions. Vibrational population was 150 times larger than electron number density. Density of CH_3 was the highest among other methane fragments due to hydrogen abstraction reaction:



(R1) is obviously independent of electronic processes. In fact, energy branching to CH_3 is the same order as other inelastic collisions. From this point, decomposition of vibrationally excited methane poses significant importance in order to improve energy cost.

4. Minimum energy consumption in BEC reactor

In general, production of vibrational species leads to significant energy loss in many plasma processes since reactivity of vibrational species is generally low. However vibrational methane seems to increase reactivity significantly in hybrid system since it increases dissociative chemisorption on Ni surface at lower temperature. We calculated energy consumption which is necessary to decompose 1 mol of methane by electron impact, and estimated minimum energy required in methane steam reforming. Main assumptions are as follows:

1. Assume stoichiometric mixture of methane and water vapor, i.e. $\text{CH}_4 : \text{H}_2\text{O} = 1 : 2$.
2. One-third of energy spent by single streamer is utilized for

Table 1. Electric processes and energy branching (200 Td, 300 K-760 Torr, $N_e \approx 10^{14} \text{ cc}^{-1}$, 1 μs)

$\text{CH}_4 + e \rightarrow$	ϵ_i [eV]	Density	Energy branch %
$\text{CH}_4(\nu_{24}) + e$	0.162	$150N_e$	11.9
$\text{CH}_4(\nu_{13}) + e$	0.361		24.5
<hr/>			
$\text{CH}_3 + \text{H} + e$	9.0	$10N_e$	17.0
$\text{CH}_2 + \text{H}_2 + e$	10.0		13.2
$\text{CH} + \text{H}_2 + \text{H} + e$	11.0	N_e	10.8
$\text{C} + 2\text{H}_2 + e$	12.0		9.3
<hr/>			
$\text{CH}_4^+ + e + e$	12.6	N_e	9.4
$\text{CH}_3^+ + \text{H} + e + e$	14.3		4.0

methane activation.

3. Ignore reactions related to H_2O and ion lose.
4. All vibrational species react on Ni catalyst to produce hydrogen.
5. Inelastic collision by electron is independent of temperature.

When external field strength is 200 Td, a single streamer spends 0.150 μJ electrical energy during propagation, and vibrationally excited methane in streamer, on space average, is populated by 1000ppm. Assume those vibrational methane is able to fully decompose if Ni catalyst is present, then 0.85×10^{-13} mol of methane is supposed to decompose to produce hydrogen, which corresponds to 0.757 μJ of heating value. That is,

$$N_{\text{methane}} = 2.55 \times 10^{-9} \text{ mol} \times 0.001 \times (1/3) = 8.5 \times 10^{-13} \text{ mol}$$

$$\text{Heating value for } N_{\text{methane}}: 890 \text{ kJ/mol} \times 8.5 \times 10^{-13} [\text{mol}] = 0.757 \mu\text{J}$$

$$\text{Heating value for } N_{\text{hydrogen}} (= 4N_{\text{methane}}): 0.757 \times (1144/890) = 0.973 \mu\text{J}$$

$$\text{Energy absorbed by steam reforming: } 0.973 - 0.757 = 0.216 \mu\text{J}$$

About 70% of endothermic reaction enthalpy (0.15 $\mu\text{J}/0.216 \mu\text{J} = 0.7$) must be supplied through electronic process, while 30% is from low temperature thermal energy source. This relation is schematically expressed in Fig. 2. Although current plasma-catalyst hybrid reactor spends 744 kJ of electrical energy per 1 mol of methane, it might be minimized by 176 kJ if ion current and any other losses could be neglected.

5. Concluding remarks

The result does not necessarily mean that plasma fuels processing must be combined with catalyst. The point is that plasma processing, in principle, accompanies considerable energy losses during inelastic electron impact process. Even though 50% of electrical energy is utilized by radical production, minimum energy requirement incredibly amounts to 6000 kJ per 1 mol of methane without help of vibrational methane since population of those radical is very small (3×10^{-14} mol in a single streamer). Authors strongly recommend plasma hybrid system which promotes decomposition of vibrational species or chain reactions in a given condition.

References

- (1) T Nozaki, Catalysis Today, in print (2003).
- (2) T Nozaki et al, Part 2, Catalysis Today, in print (2003).
- (3) H H Kim et al., IEEE Trans. Ind. Appl., **35**(6) (1999) 1306-1310.
- (4) A Ogata et al., IEEE Trans. Ind. Appl., **37**(4), (2001) 959-964.
- (5) H Kabashima et al., IEEE Trans. Ind. Appl., **39**(2) (2003) 340-345.
- (6) K Tachibana et al., J Phys D: Appl Phys **17** (1984) 1727-1742.

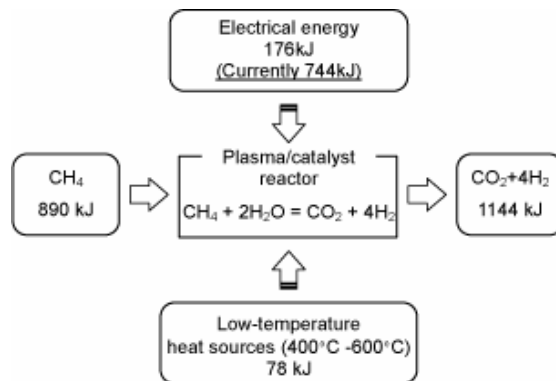


Figure 2. Schematic representation of energy balance

CONVERSION OF NATURAL GAS TO HYDROGEN AND CARBON BLACK BY PLASMA AND APPLICATION OF PLASMA BLACK

Wonihl Cho, Seung-Ho Lee, Woo-Sung Ju and Youngsoon Baek

LNG Technology Research Center, Korea Gas Corporation R&D Division, Incheon, Korea

Introduction

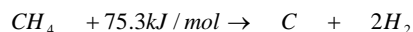
Natural gas is an environment-friendly resource as a clean fuel and a feed-stock for production of synthesis gas and power plant and it has provided the most abundant energy resource in the recent decade. In the future, it will play an important role as raw material for chemical supplies.

Most of natural gas conversion processing is to produce the synthesis gas in accordance with reforming of methane and then it synthesizes liquid fuels as methanol, DME (dimethyl ether) and other higher hydrocarbons (1).

Recently the direct conversion of methane, which is main component of natural gas, using various plasma technologies has widely been studied in order to obtain synthesis gas or hydrogen-rich gas without CO₂ emission (2,3). In general, there are many processes for production of hydrogen-rich gas with CO₂; steam reforming, partial oxidation, auto another reforming and carbon dioxide reforming of methane or natural gas. However, these processes cause the reduced efficiency due to the high cost of energy and device.

Therefore, the attention is being concentrated on the direct process, which makes decomposition of methane into the production hydrogen-rich gas. In this study, we will illustrate our recent research on the development of a microwave plasma-catalytic reaction process to produce hydrogen and carbon black from natural gas (4). In our plasma system of high power discharge, hydrogen and carbon black is produced by the decomposition of methane, which nearly resembles thermal cracking.

It may be assumed that decomposition of methane produces hydrogen and carbon black by the following single reaction:



Methane is a preferred raw material for the production of hydrogen from a hydrocarbon because of its high H to C ratio (H/C = 4), availability and low cost. Furthermore, the C produced can be sold as a co-product into the carbon black market (ink, paints, tires, batteries, etc). Several processes of carbon black production are currently used to produce furnace black, lampblack, channel black, thermal black, and acetylene black, which represent 95% of world production and consume primarily petroleum byproducts (5). In the present study, a plasma black was used as a for lithium ion battery. The carbon black is not only acts as an electron pathway by formation of a conducting network of active material but also improves electrical conductivity of interfacial electrode surface.

According to Fulcheri and Schwob (6), the total enthalpy of methane decomposition at 1600°C is 181.8 kJ/mol, and the energy related to carbon mass varies approximately between 3 and 5 kWh per kg of carbon produced. This paper discussed the decomposition of methane by microwave plasma and possible application to CO₂-free hydrogen production.

Experimental

Figure 1 schematically shows the experimental apparatus for the microwave plasma system. In order to investigate the plasma catalytic reaction, the reactor was designed to be able to insert the catalyst pellet.

Plasma System Reactor In our experiments, microwave plasma (2.45GHz, iplas Co.) was used to produce hydrogen and carbon black from methane. The maximum microwave power is 6 kW. Plasma reactor consists of quartz tube of 6" O.D. that is connected to a microwave waveguide and resonator. It is mainly composed of (Figure 1):

- 6kW magnetron power source and plasma generator (resonance)
- cold plasma reactive zone where methane is introduced
- separation bag filter of hydrogen and carbon
- water and air cooling and gas supply systems

Prior to characterization and plasma-catalytic reactivity measurements, the samples were annealed at 473K in the presence of N₂ and hydrogen gas could be used during reaction as plasma gas.

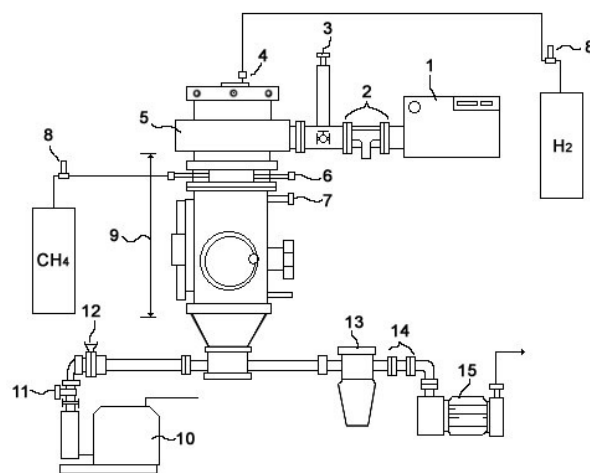


Figure 1. Experimental set for microwave plasma and catalytic reaction process; Magnetron (1), Waveguide (2), E-H tuner (3), microwave quartz tube (4), Plasma Generator (5), Jet inlet nozzle (6), Cooling line inlet, (7) MFC, (8) Microwave plasma reactor, (9) Vacuum pump, (10) Control valve for pressure (11, 12), Cyclone (13), filter (14), Mechanical diaphragm pump (15)

Thermal conductivity analyzer (Teledyne, 2000A-EU) analyzed the reaction product (hydrogen, methane and C₂+ chemicals). Scanning electron microscopy (SEM) was used to observe the nano size of carbon black. SEM observation was conducted using a transmission electron microscopy operation at 15kV.

Plasma Black Characteristics The plasma black was treated at 800°C(PB800), 1300°C(PB1300) and 2100°C(PB2100) at 10⁻³ torr pressure in order to improve its conductivity. To determine the property of plasma black, surface area and porosity analysis, temperature programmed desorption (TPD), volume resistivity measurement experiments were performed.

Results and Discussion

Conversion of methane and yields of hydrogen and carbon black as a function of applied power are exhibited in Figure 2. The conversion of methane obtains up to 96% of a plasma and catalytic reaction at 3kW of applied power. Furthermore, the yield of hydrogen is from 83% to 95% at above condition. The yield with respect to carbon black and hydrogen increases with increasing applied power. When an input of 1 mole of methane was introduced, 0.6 mole of carbon and 1.62 mole of hydrogen were produced. Also, we carried out the microwave heating catalysis in order to improve

the performance of methane conversion. The microwave heating of the catalysts might have an important advantage over conventional thermal heating. The catalyst may play a role of abstracting more hydrogen from methane as improving the reactions of radicals. between catalyst surface and reactant gas. Our observation reveals that hydrogen and carbon black are produced at the rate of almost 2:1.

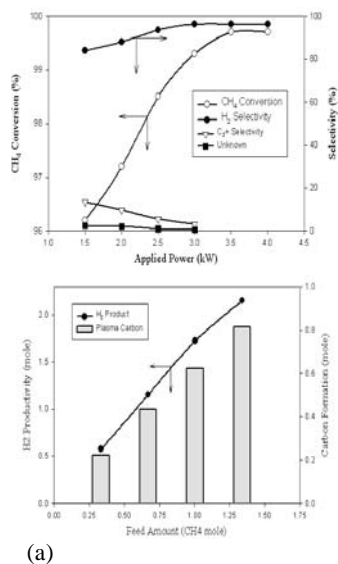


Figure 2. Conversion of methane and yields of hydrogen and carbon black as a function of applied power (a) and the productivity of hydrogen and carbon as a function of feed amount (b).

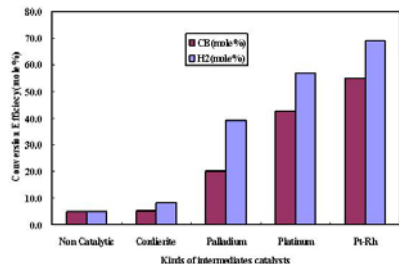


Figure 3. Comparison of various catalysts in the plasma-catalytic reaction; 200ml/min of flow rate, 30 torr of system pressure and applied plasma power is 3.0 kW.

Figure 3 illustrates the comparison of various catalysts in the plasma-catalytic reaction of methane decomposition. Among the novel metals, Pt-Rh catalyst is good for methane decomposition and production H₂/carbon black. Conversion methane to hydrogen is 72% and to carbon black is 54%.

In order to determine the effects of heat treatment on surface area, surface heterogeneity, electrical resistivity and morphology of carbon black, we carried out electrochemical behavior of the carbon black as a conductor of lithium secondary battery electrode. The BET surface area of various carbon black as well as carbon black produced by plasma (plasma black) and average particle size were described as shown in Table 1. In order to compare the size, we determined the acetylene black and the plasma black by TEM as shown Figure 4.

The result of measurement of BET (213.23 m²/g) showed that the carbon black by manufactured under a microwave plasma catalytic reaction system is very similar to classical furnace black.

Table 1. BET surface area of various carbon black

Carbon black	Surface area (BET : m ² /g)	Surface area (Langmuir : m ² /g)	Average particle size (nm)
Thermal black	50-120	75.7-171	40-200
Furnace black	100-ab. 200	150-300	ca. 20-30
Plasma black	213.23	293.05	20-30

Heat-treatment carbon black of produced plasma reaction has highest conductivity and highest purity. Four different samples including raw plasma black were added to LiCoO₂ to investigate effects of properties of plasma black as conductors on electrochemical characteristics as shown Figure 5. Plasma black conductors with low amount of surface functional groups and high electrical conductivity enhanced initial discharge capacity.

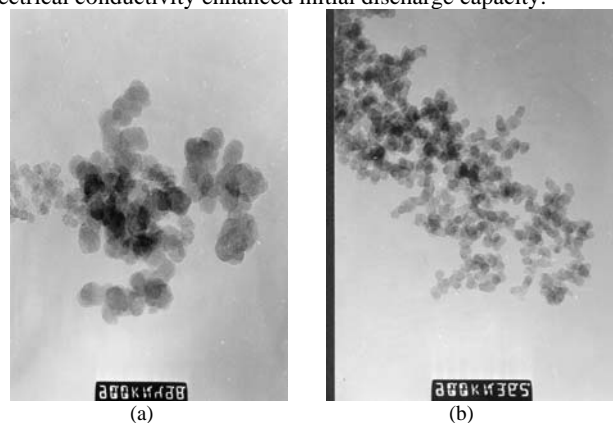


Figure 4. High-resolution TEM photographs (x 900,000) of acetylene black (a) and plasma black (b)

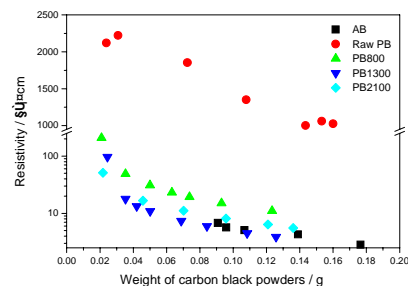


Figure 5. Volume resistivity of packed bed carbon black powders, AB (acetylene black), PB (plasma black) and heat treated samples at 800°C, 1300°C, 2100°C.

Conclusions

An environment-friendly process for hydrogen and carbon black from natural gas was developed by microwave plasma and catalytic reaction. The high frequency discharge is an effective method to decompose methane to hydrogen and carbon black in the present catalyst. The catalytic reaction enhances the decomposition of methane to hydrogen and carbon black due to abstract more hydrogen electron from methane as activating the reaction of radicals. The plasma process appears to have better than conventional hydrogen production processes. And the performance of plasma black has almost the same electronic resistivity with that of acetylene black.

Acknowledgement Supports from MOCIE (Ministry of Commerce, Industry and Energy) and Korea Gas Corporation are very much appreciated.

References

- (1) Lee, S.- H.; Cho, W; Ju, W-. S. Ju; Cho, B-. H.; Lee, Y-.C. and Baek, Y-. S. *Catalysis Today*, **2003**, in press.
- (2) Liu, C.; Mallinson, R. and Lobban, L. *J. Catal.*, **1998**, *179*, 326.
- (3) Cho, W; Baek, Y; Moon, S.-K and Kim, Y. C. *Catalysis Today*, **2002**, *74*, 207.
- (4) Cho, W; Baek, Y; Kim, Y. C. and Anpo, M. *Res. Chem. Intermed.*, **2002**, *28*, 343.
- (5) Gaudernack, B and Lynum, S., *Int. J. Hydrogen Energy*, **1998**, *23*, 1087.
- (6) Fulchri, L. and Schwob, Y., *Int. J. Hydrogen Energy*, **1995**, *20*, 197.

Liquid phase fuel reforming at room temperature using non-thermal plasma

Yoshihiko MATSUI*, Souichirou KAWAKAMI*, Kazutoshi NISHINAKAMURA*, Kazunori TAKASHIMA*, Shinji KATSURA* and Akira MIZUNO**

*Department of Ecological Engineering, Toyohashi Univ. of Tech., 1-1 Tempaku-cho, Hibiyaoka, Toyohashi, Aichi, 441-8580, Japan.

**Okazaki National Research Institutes, Institute for Molecular Science, 38 Nishigo-Naka, Myodaiji, Okazaki, Aichi 444-8585, Japan.

Introduction

Hydrocarbon fuel reforming is a very important technology for a variety of applications. For example in cracking process, it is necessary to get various useful hydrocarbon gases and oils. Hydrogen manufacturing from hydrocarbon fuels is also important and could be used for many applications. These applications introduced the fuel cells used in stationary electric power production and in vehicular propulsion, such as refueling stations for hydrogen-powered vehicles. Hydrogen manufacturing is also needed for many industrial applications. Many catalytic methods were investigated for fuel reforming to get the gas phase hydrocarbons and H₂. However, almost catalysts are composed by valuable metals and materials. Then, catalytic methods require high temperature, around 300°C to 800°C to get the activation for reforming.

Recently, a novel technology of plasma and catalytic processes were studied by many researchers for hydrocarbon reforming^[1-3]. In this study, a new type of plasma reactor was investigated for fuel reforming at room temperature. Positive square pulsed high voltage generates strong plasma in the oils. We expected that liquid oil change to gas and solid.

Experimental setup and procedure

Plasma reactor and a power source. Liquid phase plasma reactor consists of a plastic column vessel, metal plate as both, high voltage and ground electrodes and metal chips. Aluminum or copper plates and chips were investigated as the electrodes. Reactor was filled with 100ml of iso-octane or diesel oil. A magnetic stirrer and a stirring bar to stir the oil and metal chips were placed into the reactor. Spark plasma, including light and heat, was generated by the high voltage in many points of contact between the metal electrodes and chips. It was a spark discharge including light and shock wave.

Gas Sampling for GC and FT-IR

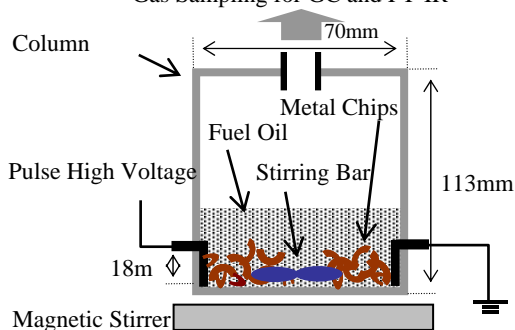


Figure1 Liquid phase plasma reaction

The plasma reactor was driven by positive pulsed square high voltage generated by a rotary spark gap (RSG) switch. The rise time of the pulsed voltage was about 40nsec, and the repetition frequency of the pulse was set at 240Hz. The high voltage applied was about 10kV peak to peak. During the rising time, spark discharges are produced and few amperes of current are flow to reform the hydrocarbon fuels.

Characterization Methods. Much gas and black powder were generated from the oil during plasma operation. H₂, N₂, O₂, CO, CO₂ and many low molecular hydrocarbons were detected and analyzed by GC-FID(Shimazu 14B) equipped with a metanizer(GL Science MT-21), GC-TCD(Shimazu 8A) and FT-IR(Bio-rad FTS3000). The black power was inspected using E-SEM and analyzed by XRD after evaporation of liquid oils.

For the E-SEM and XRD analysis, samples were prepared as follows: carbon powder deposited on the bottom of the reactor was taken, with a pipette, filtered with a quartz fiber filter (Whatman QM-A) and dried during 6h in an oven at 200°C.

Results and Discussion

The reforming process of iso-octane and diesel oil was investigated using plasma reactor at room temperature, in this study.

The generated gas compounds from iso-octane from 5 to 20 minutes are shown in Fig1 (A). Generation of gases was in the following order to H₂> CH₄ >> C₂H₄ >> CO, C₂H₆, C₃, C₄. More than 60% of H₂ gas was generated during high voltage application. Focusing the H₂ and CH₄, 86% of selectivity (H₂+CH₄) was obtained from the gas generate in this case. Fig.1 (B) shows the time elapse change of the gas compounds. The H₂ and CH₄ concentrations gradually decreased with the increment of CO₂ and CO concentrations in this case. Proportionally, the C₂H₆, C₃, and C₄ hydrocarbons gradually increased with time. On the other hand, black powder was rapidly obtained in the liquid phase when starting at high voltages, and this powder also increased with the time. After the plasma application, the temperature of the liquid iso-octane was increased at around 55°C to 65°C

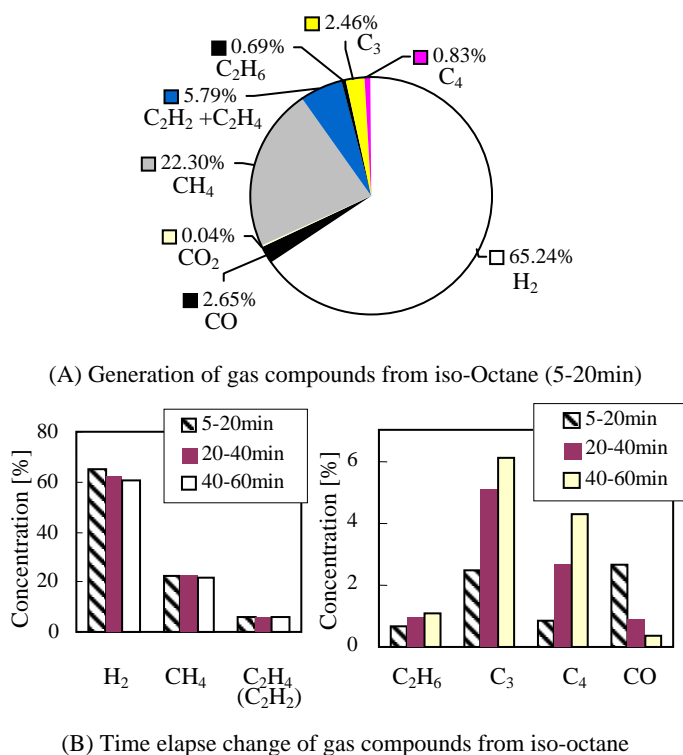


Figure2 Gas compounds generation and time elapse change from liquid phase iso-octane using liquid phase plasma reactor

After the experiments, the surface of both electrodes and the aluminum chips had many black points. These aluminum chips did not have such points before the experiment. Moreover almost all chips decreased their size losing their edges. E-SEM (E-SEM-2700) photograph show aluminum particles around sub-micro meter to several ten micro-meter in diameter. Aluminum and carbon were detected by X-ray micro analyzer (HORIBA EDX). On the other hand, a large aluminum peak was obtained from XRD (RINT 2500) measurements. These results indicated that iso-octane was reformed to gas and solid by high voltage application through electrodes and contact points of aluminum chips. At the same time, aluminum electrodes and chips were melted by the heat generated by the shock wave with spark discharge.

Gas generation rate using plasma reactor with aluminum chips is shown in Fig.3. The total gas flow rate included H₂, CH₄ and other hydrocarbons obtained were 17ml/min and 80ml/min for an applied power of 10W and 32W respectively. In this case, H₂ gas was flowed at 11ml/min and 52ml/min with an energy efficiency of 8.6g/kWh. Gas generated rates were proportional to the input energy in this case.

On the other hand, electrolysis has about 20g/kWh of energy efficiency to get H₂ from water^{[1][4]}. Almost catalytic methods could get very large amount of H₂ compared with the electrolytic method and this method. However, catalysts need a very high temperature of more than 400°C to get high concentration of H₂ gas. Liquid plasma method and electrolysis also could be driven at room temperature. Moreover, plasma method has the possibility of fuel cracking control, producing the various carbon compounds and other many reactions. Focusing only in H₂ generation for industrial application, it requires large amount of H₂ generation efficiency. We must explore the catalytic reactions by combination of plasma and catalysts.

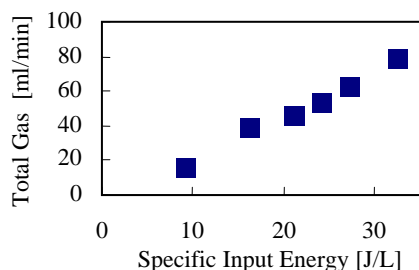


Figure3 Gas generation rate using plasma reactor with aluminum chips

Reforming of diesel oil was also investigated in this study. Fig.4 shows the gas compounds generation and the time-elapse change using the liquid phase plasma reactor. Comparing Fig.4 with Fig.2, it is clearly different the amount of N₂ and O₂ formed during the first 20 minutes as it is shown in Fig.4 (a). On the other hand, N₂ and O₂ disappeared during the next 20min as it is shown in Fig.4 (b). It can be suggested that N₂ and O₂ gas were already present into the diesel oil, and they were rapidly derived to the gas phase when plasma was applied. The amount of gases generated were in the following order: H₂ > C₂H₄ >> CH₄ >> CO, C₂H₆, C₃, C₄ in the case of (b). Ethylene selectivity is very high compared with the iso-octane case.

Fig.5 shows the XRD pattern of black powder from diesel oil using three types of metal chips and electrodes. Type I using aluminum electrodes and chips, type II using copper, and type III using a mixture of aluminum (2g) and copper (9g) chips.

When using aluminum chips, aluminum peaks and Al₄C₃ peaks were obtained. Only when using copper chips, its corresponding peaks appeared. When using aluminum and copper chips mixed type their corresponding peaks appeared. However, many small peaks also

appeared for the copper-aluminum mixed type, which seems to be sulfur and copper compounds (CuS₂ or Cu₈S₅). These results suggested that plasma might transform some compounds into solid crystals in the diesel oil, indicating this, a way for the removal of compounds by plasma treatment at low temperature.

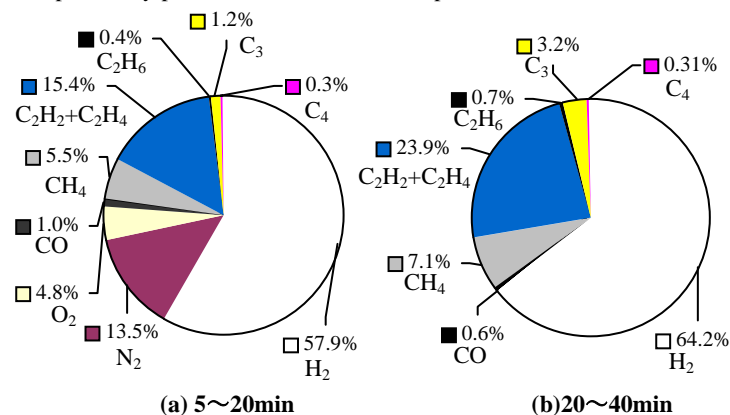


Figure4 Gas compounds generation and time elapse change from diesel oil using liquid phase plasma reactor

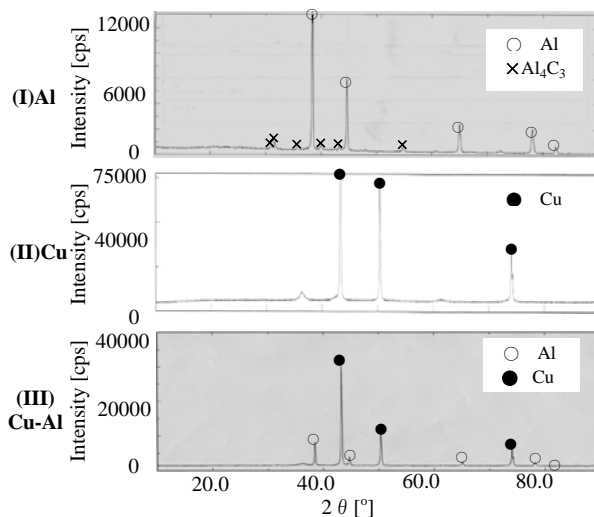


Figure5 XRD patterns of black carbon powder using aluminum, copper and aluminum-copper mixed metallic fragments

Acknowledgment

The authors wish to thank Prof. Graciela Prieto from the National University of Tucuman, Argentine, and Mr. Sigeo Nomura of DENSO Co. for valuable discussions. This work was partially supported by Japan Society for the Promotion of Science Research Fellowship for Young Scientists (8345) from the ministry of Education, Culture, Sports, Science and Technology.

References

- (1) H. Kabashima, H. Einaga and S.Futamara, IEEE, Trans. Ind. Appli. Vol.39, No.2, pp. 340-345, MARCH/APRIL, **2003**
- (2) M. Okumoto, A. Mizuno et al IEEE, Trans. Ind. Appli., Vol.37, No.6, pp.1618-1624, NOV/DEC, **2001**
- (3) M. G. Sobacchi, A. V. Saveliev, A. A. Fridman, L. A. Kennedy, S. Ahmed, and T. Krause, Hydrogen Energy 27, pp.635-642, **2002**
- (4) H. Wendt and V. Plzak, Kerntechnik 56, No.1 pp.22-28, **1991**

SURFACE ANALYSIS OF MO/HZSM5 CATALYST PREPARED BY MICROWAVE HEATING FOR NON-OXIDATIVE AROMATIZATION OF METHANE

Suitao Qi, Bolun Yang and Le Lang

Department of Chemical Engineering,
Xi'an Jiaotong University, Xi'an 710049, China

Introduction

The direct conversion of methane into hydrogen and other high-value-added products such as aromatics has recently attracted considerable attention. It makes the natural gas resource become one attractive feed which produce the aromatic hydrocarbon products following petroleum, and open up the new route to the utilization of natural gas resources.

There has been a general agreement that methane aromatization catalyzed by Mo/HZSM-5 has been recognized as a promising route for producing aromatics in an oxygen-free atmosphere¹⁻². Several factors such as the acid site density, the zeolite channel structure, and the oxidation state and location of the molybdenum species have been recognized to affect the performance of methane conversion into aromatics³⁻⁴. Despite prolific research activity worldwide, progress in this field has been hampered by serious catalyst deactivation, which is responsible for the decrease in conversion into useful products. As the performance of the catalyst often depends on surface status, and the surface status of catalyst is related with the preparation method, it is therefore necessary to seek better preparation method and analyze surface species for improving the catalyst performance.

Nowadays, the impregnation method is the major method for its easier operation and economical cost. The novel method i.e. microwave heating is recently applied in the oxidative coupling of methane. Seen from the results of reaction, the performance of catalysts prepared by microwave heating is better than that of catalysts prepared by impregnation, and this method is also very simple. Here a series of catalysts are prepared by microwave heating, the oxidation state and location of the Mo species were analyzed by XRD, and the surface distribution of catalysts and form of carbon deposit of catalysts after reaction were investigated by TEM.

Experimental

Catalysts preparation The zeolite [HZSM-5, (Si/Al=25), from Nankai chemical reagent factory of China] and the required amount of ammonium heptamolybdate $[(\text{NH}_4)_6\text{Mo}_7\text{O}_{24}\cdot 4\text{H}_2\text{O}]$, from Jinduicheng molybdenum chemical division of china] were mechanically mixed, subsequently, the mixtures were calcined under proper power in the microwave oven for some time, and then the solid samples were pressed, crushed, and sieved to separate catalyst grain in the size range 20-35 mesh for subsequent use in aromatization reactions. In addition, the same Mo loading catalyst is prepared by impregnation so that there is the contrast between two methods on the characterization of catalyst.

Reaction testing Catalysts reaction testing has carried out at atmospheric pressure by a fixed-bed continuous flow system with a quartz reactor of 8-mm-i.d., in which 0.5 g of catalyst was loaded. It was connected to a gas feeding unit and analytical equipment. The reaction temperature 973K was controlled by a sheathed thermocouple embedded in a 35-mm-high catalyst layer. CH_4 was fed to the reactor at mass-flow controlled rates sweeping the methane hourly space velocity range of $3600\text{mL (STP)} \cdot \text{h}^{-1} \cdot \text{g}^{-1}$. The gaseous reaction products were analyzed by means of a HP gas chromatograph equipped with a flame ionization detector (FID)

connected to a PLOT-Q capillary column (30 m long and $50\mu\text{m}$ i.d.) supplied by J&W Scientific Cop.

Catalysts characterization The surface species analysis of catalysts was carried out with the RIGAKUD/MAX-2400 diffract meter by Rigaku Corporation of Japan using $\text{Cu K}\alpha$ radiation at 36kV and 80mA. The spectrums were recorded over a 2θ range of 5° -- 60° at a scanning rate of 5°min^{-1} . The surface states of catalysts before and after reaction were carried out using JEM-200CX Transmission Electron Microscope supplied by Electric Corporation of Japan. The samples were dispersed in ethanol reagent, and then one of them was selected and suspended on the copper web for analysis under different multiple of enlargement.

Results and discussion

XRD analysis Figure 1 showed the XRD spectrum of 6% Mo based catalysts prepared by different methods, in which spectrum 1 is the XRD spectrum of catalyst prepared microwave heating, spectrum 2 is catalyst prepared by impregnation, and spectrum 3 is the used catalysts prepared by microwave heating. Seen from figure 1, all of spectrums have a majority of same peaks with the XRD spectrum of HZSM5 from corresponding literature⁵, but the loading of Mo species makes the characteristic diffraction peaks lower. It reveals that the Mo species on the HZSM5 are dispersive relatively. There are three characteristic diffraction peaks of MoO_3 species when 2θ is about 30° in all spectrums; the MoO_3 species signal in spectrum1 is higher than that in spectrum 2. It's implied that most of MoO_3 species spread the outer surface of the catalyst prepared by microwave method. The main reason of this phenomenon is the difference of calcination mode of catalysts. The microwave heating have the characters of high speed and from inside to outside compared with conventional heating, as the result of it, the shift of Mo species from outer surface to inner channel of zeolite stopped and the blockage of zeolite channel could be avoided. It led to the higher selectivity to benzene of catalysts. Compared with spectrum1, 2 and 3, all of characteristic diffraction peaks sharply decreased in spectrum 3, the new characteristic diffraction peak was found when 2θ is about 39° . That's because the carbon accumulated at a higher rate on the surface of catalyst, blocked active sites and thus caused gradual deactivation. The new characteristic diffraction peaks occurred was thought as Mo_2C species according to literature⁶. It is consist with the statement that Mo occurred as molybdenum carbide (say Mo_2C) under reaction conditions. The Mo_2C is real active species during reaction.

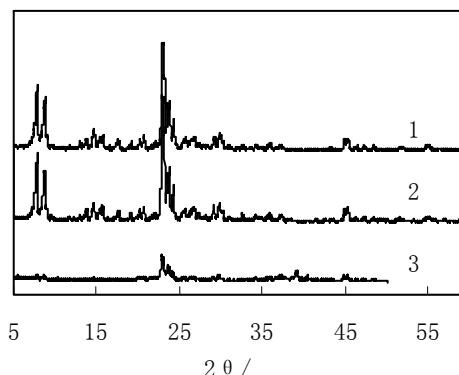


Figure 1. XRD spectrum of a series of 6% Mo/HZSM5 catalysts

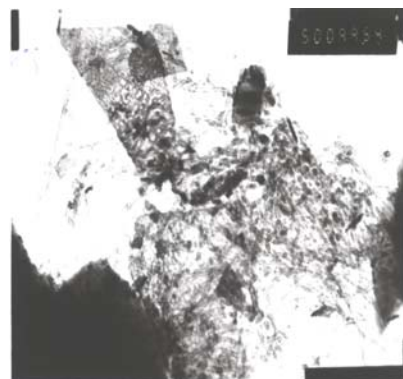
TEM analysis Methane aromatization is an endothermic equilibrium-controlled reaction, and the high temperature is required to yield meaningful conversions into aromatics during the reaction. However, such severe conditions are favorable for carbon deposition.



2a. 27×1000 before reaction



2b. 180×1000 before reaction



2c. 50×1000 after reaction



2d. 100×1000 after reaction

interaction of Mo species and the Brønsted acid site, then stretch out towards outside.

Figure 2. TEM picture of 6% Mo/HZSM5 catalysts before and after reaction

They occurred as the form of carbon nanotube during the reaction. Figure 2 showed the TEM pictures of 6%Mo/HZSM-5 catalyst before and after reaction. Figure 2a and 2b showed the surface state before reaction under different multiple. Seen from figure 2a, the massive material in the right is the HZSM-5 zeolite, and the Mo species are in the middle. The active Mo species was closely attached to carrier. Figure 2b was obtained under 180×1000 multiple. It showed the surface distribution of catalyst clearly. The size of Mo species is 20~30 nm, which is much larger than that of ZSM-5 zeolite channel (0.54nm×0.56nm), so the most of Mo species should be spread the outer surface of carrier, the active species were highly dispersed on zeolite. It is consistent with the results of XRD analysis. No fibriform material can be seen on surface of catalyst in figure2a and 2b.

Figure 2c and 2d are the TEM pictures of catalyst under different multiple. They represent the surface carbon deposit of catalysts after reaction. Seen from figure2c, the fibriform materials are winding on the surface of catalyst, which indicates that the coke occurred. In the figure 2c, the fibriform materials are the carbon deposit and the massive material is carrier. Figure 2d was pictured under 100×1000 multiple. A brunch of tubular material can be seen clearly. They are the carbon nanotubes due to carbon accumulation. One end of each carbon nanotube was attached to catalyst, the other end extended to outside. They are slim and have same size range of 10-20 nm. The similar phenomenon was reported in Ni catalysts⁷. As the Brønsted acid site is the major position of accumulating carbon deposits at high temperature, in addition to the existence of Mo species on the surface of zeolite, the carbon nanotube generate under

Conclusion

The analysis of XRD showed that the Mo species highly dispersed on outer surface of carrier for catalyst prepared by microwave heating method. Mo₂C is the real active species during the reaction, and its characteristic diffraction peaks can be found on surface of catalyst after reaction. Analysis of TEM further proved the high dispersion of Mo species. The size of Mo species is 20-30nm. The form of carbon deposit in methane aromatization is the hollowed carbon nanotube. The size of them is 10-20 nm. They grew up with the carbon accumulation.

References

1. L. Wang, L. Tao, M. Xie, X. Guo, Catal. Lett. **1993**, 21, 35-41.
2. Y. Xu, L. Lin, Appl. Catal. A, **1999**, 188, 53-67.
3. Suitao Qi, Bolun Yang, Modern Chemical Industry. **2002**, 22, 13-17.
4. V. T. T. Ha, L. V. Tiep, P. Meriaudeau, C. Naccache, J. Mol. Catal. A, **2002**, 181, 283-290.
5. Y. Shu, D. Ma, L. Xu, X. Bao, Y. Xu, Chinese J. Catal., **2002**, 23, 24-28.
6. F. Solymosi, A. Szoke, J. Cserenyi, Catal. Lett., **1996**, 39, 157-162.
7. P. Chen, P. Wang, G. Lin, B. Zhang, Q. Cai, Chem. J. Chinese University, **1995**, 16, 1783-178

Carbon Dioxide Reforming of Methane over a Novel Ni/Al₂O₃ Catalysts

Minhua Zhang, Dang-guo Cheng, Yue-ping Zhang*

Key Laboratory of Green Chemical Technology of Ministry of Education, School of Chemical Engineering, Tianjin University, Tianjin 300072, China

Introduction

A lot of attentions have been recently paid to the CO₂ reforming of methane to syngas. A major reason for it is that this reaction can provide us a syngas with a 1/1 ratio of H₂ and CO, which is typically suitable for the synthesis of valuable oxygenated chemicals.¹ Among the catalysts developed, Al₂O₃ supported Ni catalysts were extensively investigated due to their relatively high activity and low cost. The major problem for the further practical application of these nickel catalysts is the deactivation of the catalyst, suffered from carbon deposition on the catalyst during reactions. Many investigators are working on the improvement in this nickel catalyst by using the addition of promoters,²⁻⁵ using novel reactor configurations,^{6,7} and using different supports.³ In this work, we attempt to use a glow discharge plasma treatment following by thermal calcinations to achieve a better catalyst with higher activity at lower temperatures and better stability.

Experimental

The preparation or the plasma treatment of catalyst has been described elsewhere.^{8,9} The principal procedure of the catalyst preparation includes: 1) impregnation conventionally; 2) drying; 3) glow discharge plasma treatment; and 4) calcination thermally. During the plasma treatment, we use argon glow discharge plasma to treat the catalyst. The loading amount of nickel on the alumina support is 9 wt.%. The reaction of CO₂ reforming of methane was carried out at atmospheric pressure in a 6 mm i.d quartz-tube fixed-bed reactor. A thermocouple placed in the center of the catalyst bed was used to measure the reaction temperature. The reaction temperature was maintained at 873 K, 923 K and 973 K, respectively. The reaction time is 48 h for all the temperatures. Argon was used as the dilution gas during the reaction. The ratio of the feeding gases is 1:1:2 of methane/carbon dioxide/argon. The total flow rate is 40 ml/min with a space velocity of 48000 ml/h-gcat. The reactants and products were analyzed with an online gas chromatography (Agilent 4890D) with a Porapak Q column. An ice-cold trap was set between the reactor exit and the GC sampling valve to remove the water formed during the reaction. CO₂, CH₄ conversions and H₂, CO selectivities were calculated according to the following formulas:

$$X(\text{CH}_4)\% = (\text{FCH}_{4,\text{IN}} - \text{FCH}_{4,\text{OUT}}) / \text{FCH}_{4,\text{IN}} \times 100\%$$

$$X(\text{CO}_2)\% = (\text{FCO}_{2,\text{IN}} - \text{FCO}_{2,\text{OUT}}) / \text{FCO}_{2,\text{IN}} \times 100\%$$

$$S(\text{H}_2)\% = \text{FH}_{2,\text{OUT}} / [2 \times (\text{FCH}_{4,\text{IN}} - \text{FCH}_{4,\text{OUT}})] \times 100\%$$

$$S(\text{CO})\% = \text{FCO}_{2,\text{OUT}} / [(\text{FCH}_{4,\text{IN}} - \text{FCH}_{4,\text{OUT}}) + (\text{FCO}_{2,\text{IN}} - \text{FCO}_{2,\text{OUT}})] \times 100\%$$

$$F_i = C_i \cdot F_{\text{total}}$$

where X, S and F are conversion, selectivity and gas flow rate, respectively. F_{total} is the total feed rate or the gas effluent flow rate. C_i is the molar fraction of component i in the feed gas or in the gaseous effluent that is detected by GC.

The morphology of the used catalysts was observed by TEM with a JEOL JEM-100CXII transmission electron microscope.

Results and Discussion

The stability test was investigated at 873K, 923K and 973K, respectively. Figure 1 and Figure 2 present the conversions of methane and carbon dioxide at different reaction temperatures. Evidently, the catalyst prepared with glow discharge plasma treatment following by calcination thermally is very stable, especially, at the reaction temperature of 923 K. At lower temperatures, the stability of the catalyst is also very well but the catalytic activity is lower. At higher temperature, however, the catalytic activity reduces slightly with the reaction time. Compared to the reported results with Ni/Al₂O₃ catalysts,^{2,5} the catalyst reported in this work shows a better low temperature activity.

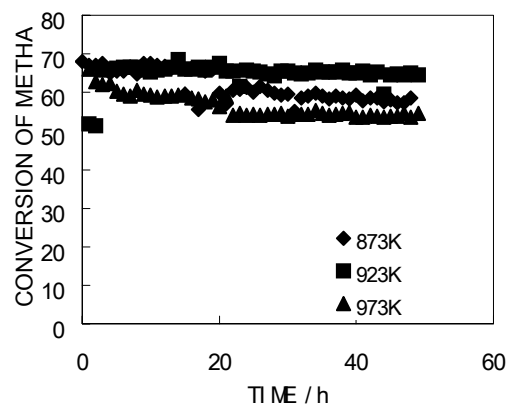


Figure 1. Catalytic activity and stability of Ni/Al₂O₃ catalyst represented by methane conversion (reaction conditions: CH₄:CO₂:Ar=1:1:2, space velocity=48000 ml/h-gcat.)

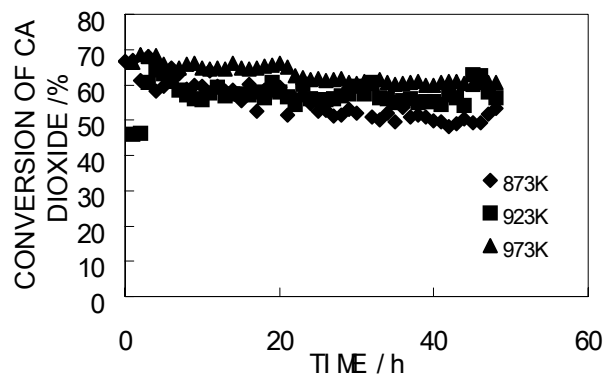


Figure 2. Catalytic activity and stability of Ni/Al₂O₃ catalyst represented by carbon dioxide conversion (reaction conditions: CH₄:CO₂:Ar=1:1:2, space velocity=48000 ml/h-gcat.)

Figure 3 and Figure 4 show the selectivities of hydrogen and carbon monoxide at reaction temperature of 873 K, 923 K and 973 K. With temperature varying from 873 K to 973 K, the selectivities of products increased significantly. Parvery *et al.*⁵ have reported a promoted mixed LaNi_xAl_{1-x}O₃ perovskite catalysts prepared by a sol-gel related method for dry reforming of methane. Compared to their results, both of the two works achieved good activities of catalysts. However, the catalyst prepared with glow discharge plasma in this work showed a better stability. This means that the glow discharge treatment followed by calcinations thermally leads to a plasma-

enhanced catalytic stability. The TEM provides us evidence with this enhanced stability. It is well known that the carbon deposition is the main reason for the deactivation of the conventional catalysts with the dry reforming of methane. However, the glow discharge treated catalysts exhibit an excellent anti-carbon deposit performance, as shown in Figure 5. Figure 5 shows a TEM image of the used plasma-treated catalyst, taken from the stability test at 923 K. Evidently, some well defined facets of Ni can be observed. This suggests that the carbon deposition is not serious under this reaction condition over the plasma-treated catalyst. Further investigation is being conducted for a better understanding of the plasma-enhanced catalytic stability.

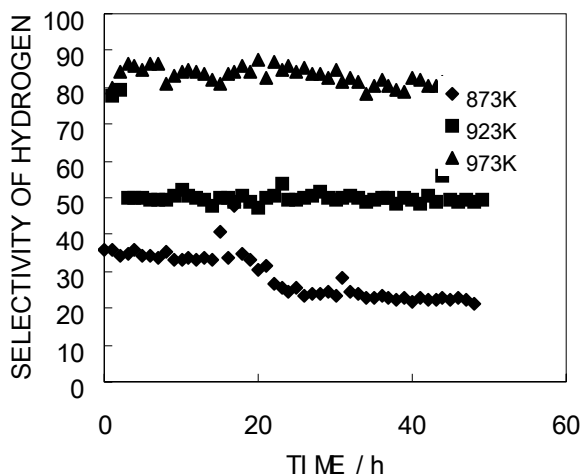


Figure 3. Catalytic activity and stability of Ni/Al₂O₃ catalyst represented by hydrogen selectivity (reaction conditions: CH₄:CO₂:Ar=1:1:2, space velocity=48000 ml/h-gcat.)

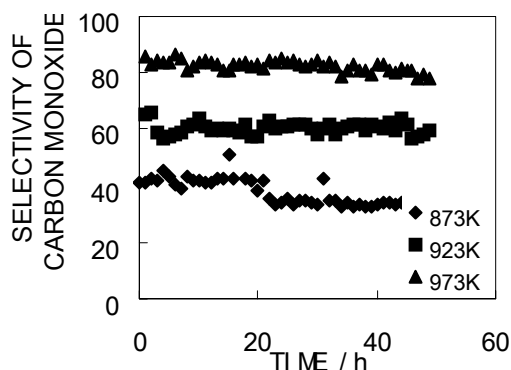


Figure 4. Catalytic activity and stability of Ni/Al₂O₃ catalyst represented by carbon monoxide selectivity (reaction conditions: CH₄:CO₂:Ar=1:1:2, space velocity=48000 ml/h-gcat.).

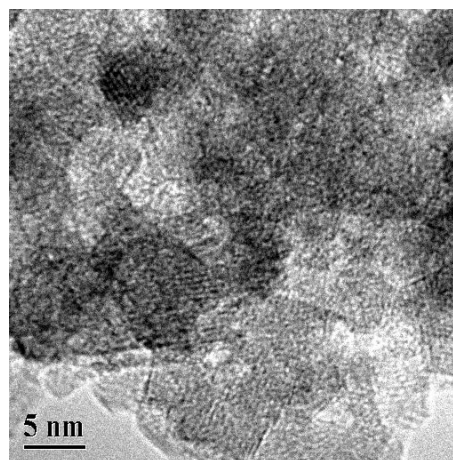


Figure 5. TEM image of used catalyst taken after the stability test (reaction conditions: reaction temperature=923 K, CH₄:CO₂:Ar=1:1:2, space velocity=48000 ml/h-gcat.)

Conclusion

The present investigation confirms that the plasma catalyst preparation described in this work can lead to a production of catalyst with a better low temperature activity and an enhanced catalytic stability for CO₂ reforming of methane. Such prepared catalyst exhibits some well-defined Ni facets after the stability test. This means that the glow discharge plasma treatment would improve the metal-support interaction significantly and induce a better anti-carbon deposit performance.

Acknowledgement

The support from the Major Research Foundation of Ministry of Education of China (under the contract of Major 0212) is very appreciated. Part of equipment and instrument used in this work was donated by ABB Switzerland Ltd., which is also very appreciated.

References

- [1] Lunsford, J.H., *Catal. Today*, **2000**, 63, 165.
- [2] Lemonidou, A.; Vasalos, I.A., *Appl. Catal. A*, **2002**, 228, 227.
- [3] Chang, J.-S.; Park, S.E.; Yoo, Y.W.; Park, J.-N., *J. Catal.*, **2000**, 195, 1.
- [4] Frusteri, F.; Arena, F., *Catal. Commun.*, **2001**, 2, 49.
- [5] Parvary, M.; Jazayeri, S.H., *Catal. Commun.*, **2001**, 2, 357.
- [6] Wang, L.; Murata, K.; Inaba, M., *ACS Symp. Series*, **2003**, 852, 57.
- [7] Supat, K.; Chavadej, S.; Lobban, L.L.; Mallinson, R.G., *ACS Symp. Series*, **2003**, 852, 83.
- [8] Liu, C.-J.; Vissokov, G.P.; Jang, B., *Catal. Today*, **2002**, 72, 173.
- [9] Wang, J.-G.; Liu, C.-J.; Zhang, Y.P.; Zhu, X.L.; Eliasson, B., *Chem. Lett.*, **2002**, 1068.

ENERGY SAVING POTENTIAL FOR NATURAL GAS HYDRATE TRANSPORTATION

Takamichi Daimaru, Minoru Fujii¹, Akihiro Yamasaki², Yukio Yanagisawa

Graduate School of Frontier Sciences, The University of Tokyo
7-3-1 Hongo, Bunkyo-ku, Tokyo 1138656 Japan

¹ National Institute for Environmental Studies
16-2 Onogawa, Tsukuba 3058506 Japan

² National Institute of Advanced Industrial Science and Technology
16-1 Onogawa, Tsukuba 3058569 Japan

Introduction

Gas hydrates are inclusion compounds in which cage-like structures formed by hydrogen-bonded water molecules can hold a variety of guest molecules such as methane, CO₂. Applications of gas hydrates have drawn attentions in the field of energy and environment. Gudmundson et al.¹ proposed a new concept of transportation of natural gas in the form of gas hydrates. Major components of natural gases, methane and ethane, could form gas hydrates. The guest molecules are densely included in the hydrates; the volume per one mole is 1/170 of that of gas at the atmospheric pressure. This is favorable for the storage and transportation of gases in the form of hydrates. In addition, gas hydrates are stable under the conditions of higher temperatures than liquefaction temperature of the natural gas components. This would lead an advantage of the transportation process in the form of gas hydrates over the conventional liquefied natural gas (LNG) transportation, because milder conditions during the transportation are required for the gas hydrates, which will reduce the cost of heat insulation to prevent the dissociation or evaporation.

The reduction of the energy consumption is of primary importance for the implementation of the NGH transport process. Several studies have been conducted on the evaluation of energy consumption by NGH transportation, and the results demonstrated that NGH transportation is advantageous both from energy consumption and cost. For more reduction of the energy consumption for the transport, several options can be considered. One option is a utilization of additives on the hydrate formation to moderate the hydrate equilibrium conditions, which could result in the reduction in the energy consumption for the hydrate formation as well as that during the transportation in a carrier ship of NGH. In this study, the effect of the additives on the energy consumption of NGH transport scenario was examined quantitatively, and energy-saving potential was estimated.

Natural Gas Hydrate Transportation Process

Overview. Natural gas produced from a gas well will be pressurized and cooled to a hydrate formation condition, and converted to natural gas hydrate (NGH) in a stirred tank type reactor. Then, the NGH will be loaded in a hydrate carrier ship, and transported to a consumption site located 6000 km distance from the gas well. In the consumption site, the NGH will be dissociated by heating with seawater flow, and natural gas will be recovered for use.

Assumptions and procedure for energy consumption estimation. The following assumptions were made for the estimation of the energy consumption for the NGH transport scenario.

1. Natural gas production rate

Production rate of natural gas from a natural gas field is assumed at 1.13×10^7 m³/day, which corresponds to a typical natural gas well. Since the heat generation by the combustion of methane is

890 kJ/mol, the total energy potential in the natural gas produced is 4.49×10^{12} J/day. The condition of the produced natural gas is at the atmospheric pressure (0.1 MPa), and at the temperature of 288.15 K. The composition of the natural gas is assumed as pure methane, and no separation or purification process is necessary before hydrate formation.

2. Pre-treatment of natural gas for hydrate production

The feed gas is pressurized by a compressor from 0.1 MPa to a set pressure for the hydrate formation by an adiabatic compression process of ideal gas with the compression efficiency at 0.8. The cooling of the compressed gas is carried out by 2 step; 1st step: cooling to 323.15 K by using seawater flow at 298.15 K; 2nd step: brine refrigeration with the coefficient of performance, COP = 4.

3. Hydrate formation process

Hydrate production is conducted in a stirring vessel type reactor at a given condition of hydrate formation. The pressure and temperature of the hydrate formation conditions are set as operational variables for the energy consumption estimations. The base temperature is assumed at 275.15 K, and the base pressure is assumed at 6.0 MPa.

The feed water is supplied by a pump, and cooled from 298.15 K to the hydrate formation temperature by a brine refrigeration system with COP = 4. The hydration number of the methane hydrate is assumed at 5.75 corresponding fully occupied cages in type I hydrate. Hydrate formation rate is taken from experimental data conducted in a laboratory-scale experimental set-up (volume = 1.2×10^{-3} m³, reaction rate = 3.72×10^{-4} mol/s at 25 rps stirring rate). The power consumption for the stirring process in the model reactor is given by the Nagata's equation, and results on laboratory-scale experiments can be scaled-up under the assumption that the energy consumption for stirring per unit volume of the feed mixture is constant in the scaled-up reactor. The energy consumption for the removal of the heat of formation is considered for the pumping energy of the brine, and cooling for recovery of the brine temperature.

4. Refrigeration of methane hydrate

After removal of the remained water from the natural gas hydrates, the hydrate will be refrigerated to a lower temperature in which the hydrate is stable under the atmospheric pressure. The remained water at the surface of methane hydrate is assumed at 12.0 wt. %. The energy for refrigeration is calculated for a refrigeration process with COP = 4, and specific heat and latent heat of ice are taken from the literatures.

5. Transportation of natural gas hydrate by a NGH carrier ship

The hydrate is transported in an adiabatic tank in the transportation ship. The energy consumption for the transportation is 2.8×10^{-3} kg-Fuel/t/mile (<http://nippon.zaidan.info>), which corresponds to 87.5 J/kg/m. The transportation distance is assumed at 6000 km.

6. Dissociation of natural gas hydrate -recovery of natural gas

The dissociation of the hydrate is carried out by heating the hydrate by a seawater flow of which the temperature is 298.15 K.

Energy Consumption Results

Energy consumption for the base case was shown in Table 1. Since the combustion energy in the natural gas is 5.195×10^3 MW, about 14 % of total energy will be consumed in the NGH transportation scenario. More than half of the energy consumption

could be attributed to the transportation process in a NGH carrier ship, and next major energy consumption sector is pretreatment of the natural gas for hydrate formation including pressurization and cooling. In the following sections, the influences of the operational parameters on the energy consumption were investigated.

Table 1. Breakdown of Energy Consumption for The Transport Scenario of NGH (base case)

Energy consumption sector	Energy consumption [MW]	Percentage [%]
Pretreatment	190.56	25.31
Hydrate formation	130.77	17.34
Refrigeration	14.18	1.88
Transportation	410.35	54.49
Dissociation	7.16	0.95
Total	753.0	100.00

1. Effect of the hydrate formation rate

Hydrate formation rate is a function of a variety of factors such as agitation rate, temperature, and pressure. Some additives such as surfactants can dramatically increase the hydrate formation rate. Figure 1 shows the influence of the hydrate formation rate on the energy consumption of the hydrate formation process.

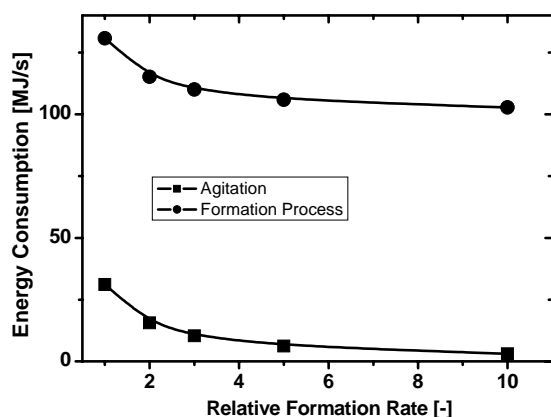


Figure 1 Effect of the hydrate formation rate on the energy consumption in the hydrate formation process

Energy consumption of the agitation for the hydrate formation gradually decreased with an increase in the hydrate formation rate. For the case with 10 times larger hydrate formation rate, the energy consumption for the agitation could be reduced at about 1/10 resulting in about 3.7 % of the total energy consumption.

2. Effect of the temperature for the hydrate transport

NGH is transported in a carrier ship at the temperature under which the hydrate is stable under the atmospheric condition. This temperature could be changed by using hydrate formation helper compounds. Also, some additives used for the promotion of the hydrate formation rates could be used as stabilizer of the hydrate during the transportation. Considering the above effect, effect of the hydrate transport temperature on the energy consumption is calculated and the results are shown in Figure 2. In the present cases,

the energy consumption for the refrigeration is shown. Although energy consumption for the refrigeration decreased linearly with the increase in the transport temperature, but the effect of the reduction on the total energy consumption is less than 1 % at the highest temperature studied, i.e., 273.15 K.

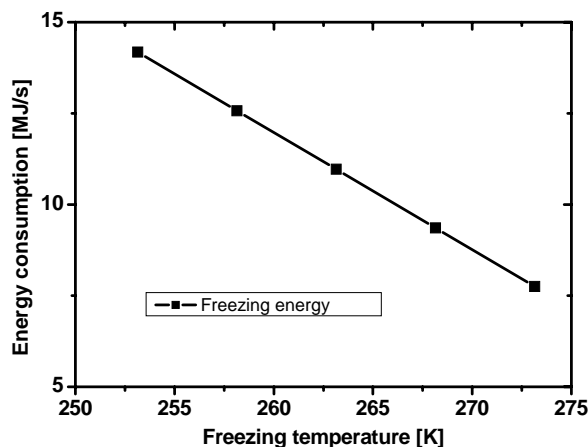


Figure 2 Effect of the hydrate transport temperature on the energy consumption for the refrigeration

3. Effect of the hydrate formation conditions

Hydrate formation conditions could affect the pre-treatment process of natural gas stream before the hydrate formation process. Figure 3 shows the effect of the hydrate formation pressure on the energy consumption for the pre-treatment (pressurization and cooling) process. The energy for the pre-treatment process increased with an increase in the hydrate formation pressure, and the energy saving potential for the case of 3.0 MPa is about 7.7 % compared with the base case at 6.0 MPa.

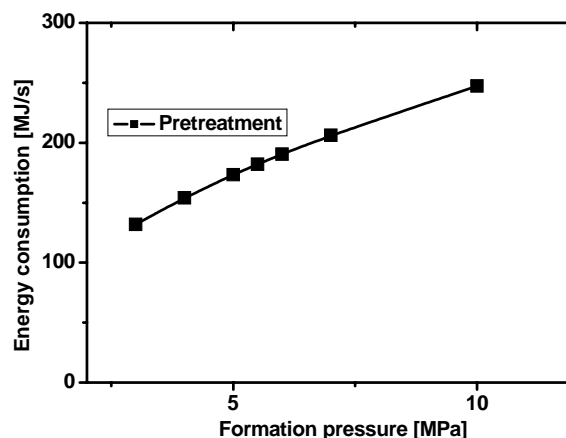


Figure 3 Effect of the hydrate formation pressure on the energy consumption for the pre-treatment process of natural gas stream before hydrate formation

References

[1] Gudmundson, J. S. et al., *Proc. 2nd International Conference on Natural Gas Hydrates (1996)*.

Remarkable Enhancement in the Low-temperature Activity of Catalysts Prepared via Novel Plasma Reduction-Calcination Method for Methane Conversion

Yue-ping Zhang^{1,2}, Pei-sheng Ma², Kai-lu Yu², Xin-li Zhu², Dang-guo Cheng², Jian-guo Wang², Yu-heng Ben², Jijun Zou², You Han² and Chang-jun Liu^{2*}

¹ Department of Chemistry, ² Key Laboratory of Green Chemical Technology and School of Chemical Engineering, Tianjin University, Tianjin 300072, China

Introduction

Methane valorization is very important to the present world. Due to the stability of methane molecule, methane conversion normally requires a high temperature operation, which induces an intense energy input and poor selectivity. We previously reported a novel plasma catalyst preparation, with which the catalyst is first treated by a glow discharge and then the plasma treated catalyst is calcined thermally^[1-8]. During the plasma treatment, the metal ions loaded will be normally reduced. A plasma reduction is thereby occurred. And, during calcination thermally after plasma treatment (no plasma employed in this step), the metal particles will be oxidized again. We nominated this preparation as Plasma Reduction and Calcination method (PR&C). This PR&C preparation can lead to a better catalyst preparation with a high dispersion of metal active species, a significantly enhanced acidity, an improved low-temperature activity and a remarkable promotion of catalyst stability.

The Plasma Reduction and Calcination Method

The catalyst preparation using PR&C method has been reported elsewhere^[1-8]. The procedure for this method includes: the conventional incipient wetness impregnation, drying (sometimes no drying needed), plasma treatment and calcination thermally. For the plasma treatment, several plasma phenomena, e.g., glow discharge, dielectric-barrier discharge and microwave discharge, can be employed. The different discharge plasma treatment would induce a very different catalytic performance. In this work, we focus on the discussion of PR&C method with glow discharge plasma treatment. Glow discharge is a kind of plasma that is created by inserting two electrodes in a cell filled with gas at low pressure (e.g., 1 Torr). During the glow discharge plasma treatment, the catalyst was held in a quartz container and placed in a glow discharge tube. A high-voltage (DC or AC) generator is used to generate the glow discharge plasma. The catalyst powder or particles are usually placed in the "positive column" of glow discharge where it was characterized with highly energetic electrons at low gas temperature^[2]. Argon, helium, nitrogen, hydrogen, carbon dioxide and others can be applied as the plasma-forming gas for PR&C preparation. In the following discussions, we focus the use of argon as the plasma-forming gas. After the plasma treatment, the catalyst is then calcined thermally. The calcination temperature exhibits a significant effect on the dispersion and other catalytic performances that will be discussed in the future.

As mentioned above, during plasma treatment, the catalyst is normally reduced. Figure 1 exhibits XRD patterns of plasma treated catalyst samples. Evidently, some metal species present after the plasma treatment. A plasma reduction is thereby addressed. XPS analysis of the plasma treated catalysts gives us further evidences of the plasma reduction^[2,8]. The reduced metal species would play an important role in the plasma-enhanced dispersion. During the oxidation of the reduced metal species in calcinations thermally, the new-formed metal oxide will induce an intense electric field. The metal species with the same electric properties will therefore exclude each other, which induces a highly dispersion^[8].

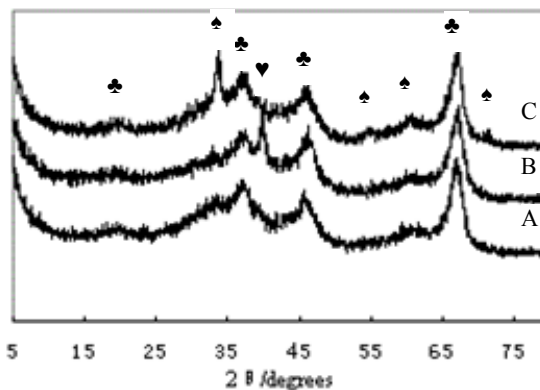


Figure 1. The XRD patterns of Pd/Al₂O₃ catalysts by different preparations A: Pd/Al₂O₃ (conventional catalyst); B: Pd/Al₂O₃ (catalyst after plasma treatment); C: Pd/Al₂O₃ (PR&C prepared)^[8]

Plasma Enhanced Acidity

The catalysts prepared with PR&C method normally show a plasma-enhanced acidity^[2-4]. We used IR-pyridine adsorption to analyze the effect of plasma treatment on the Brønsted and Lewis acidities for further understanding the plasma enhanced catalytic performance. The PR&C preparation normally leads to enhanced Brønsted and Lewis acidities of the supported catalyst. For example, the amount of Brønsted acid sites of the plasma prepared Pd/HZSM-5 catalyst is 1.13 times larger than that of the catalyst prepared thermally, while the amount of Lewis acid sites is 1.21 times higher. Table 1 presents the results obtained over Pt/NaZSM-5 catalyst^[4].

Table 1. Acid site amount of Pt/NaZSM-5 catalysts based on the IR-pyridine adsorption^[4]

	0.1wt%Pt/Na ZSM-5 (conventional)	0.1wt%Pt/Na ZSM-5 (PR&C prepared)	The increased amount of acidic sites
Lewis acid (mmol/g)	1.944	2.147	10%
Brønsted acid (mmol/g)	0.0332	0.0369	11%

Plasma Enhanced Dispersion

Remarkable plasma enhanced dispersion has been achieved from the PR&C preparation. Tables 2 and 3 present some comparisons of the dispersion between Pd/HZSM-5 and Pt/NaZSM-5 catalysts prepared by PR&C and by the conventional way^[3,4]. The results were obtained from hydrogen chemisorption. The calculations from XRD give us further supporting evidence, as shown in Table 4^[2].

Table 2. Results of H₂-chemisorption measurement of

catalysts	Metal dispersion/%	Active particle diameter/nm
Pd/HZSM-5 (conventional)	4.57	24.5
Pd/HZSM-5 (PR&C prepared)	5.92	18.9

2wt%Pd/HZSM-5^[12]

Table 3. The results of H₂-chemisorption for dispersion of 0.1wt%Pt/NaZSM-5^[4]

	0.1wt%Pt/NaZSM-5 (conventional)	0.1wt%Pt/NaZSM-5 (PR&C prepared)
Pt dispersion	4.2	63.3
Surface area of Pt (m ² /g sample)	0.02	0.28
Surface area of Pt (m ² /g metal)	18.5	281.8
Diameter of Pt particle (nm)	27.0	1.8

Table 4. Particle size of PdO obtained by Scherrer formula for 2wt%Pd/HZSM-5^[2]

	Full width at half maximum / rad	Particle size / nm
Pd/HZSM-5 (conventional)	0.00691	21.0
Pd/HZSM-5 (PR&C prepared)	0.00904	16.0

The Ni-supported catalysts prepared via PR&C method exhibit an unusual dispersion characteristic. From hydrogen chemisorption, XRD characterization and TEM analysis, no metal particles can be identified^[5,6]. One possibility is that the metal species is ultra-highly dispersed over the support. Another possibility is that the Ni species changes to amorphous species after the plasma treatment. Further investigation is being conducted to study this unusual dispersion performance.

Plasma Enhanced Low-temperature Activity

All the catalysts prepared by PR&C method and tested by far show a better low-temperature activity, esp., those for methane conversion. We reported a comparison between methane combustion over Pd/HZSM-5 catalysts prepared via PR&C and the conventional catalyst^[2,3]. Obviously, the plasma prepared catalyst presents a better low-temperature activity and an enhanced stability over the catalyst prepared conventionally. The methane conversion over the plasma treated catalyst is close to 100% at 450 °C, but it is only 50% at the same temperature over the conventional catalyst. The alumina supported Pd catalysts exhibit a similar plasma-enhanced low-temperature activity. The light-off temperature of the plasma prepared catalyst is 370 °C, 50 °C lower than that obtained from the conventional catalyst^[7,8].

Ni-Fe/Al₂O₃ catalyst for partial oxidation of methane prepared via PR&C exhibits a better low-temperature activity too over the catalyst prepared thermally^[5]. The conversion of methane and the selectivity of CO and H₂ over the plasma prepared catalyst are 97.44%, 100% and 100% at 875 °C, while, at the same temperature, they are 90.09%, 97.28% and 97.09%, respectively, over the catalyst prepared without plasma treatment. At the same methane conversion, the reaction temperature with the plasma prepared Ni-Fe/Al₂O₃ is at least 80 °C lower.

The PR&C prepared Pt/NaZSM-5 catalyst for NO reduction by CH₄ exhibits a highly dispersion of metal active species and a remarkable improvement in the low-temperature activity, compared to the catalyst prepared conventionally^[4]. The conventional 0.1wt%Pt /NaZSM-5 catalyst shows no activity at temperatures below 673 K, while at 673 K, the NO conversion to nitrogen reaches 61.3% over the plasma prepared 0.1wt%Pt /NaZSM-5 catalyst. The initiated temperature for the plasma prepared 0.1wt%Pt/NaZSM-5 catalyst can be as low as 548 K.

Plasma Enhanced Stability

During our investigation on methane combustion, we have confirmed a remarkable enhanced stability of catalysts from the PR&C preparation. The investigations for partial oxidation of methane to syngas^[5] and carbon dioxide reforming of methane^[6] over Ni supported catalysts give us further evidences for the plasma-enhanced stability. The Ni supported catalyst is active for both reactions but this catalyst suffers from a deactivation, principally due to the carbon deposit. The catalysts prepared via PR&C presents a very different carbon species, compared to the conventional catalyst. A plasma-enhanced stability has also been observed over the Pt/NaZSM-5 catalyst for NO reduction by methane^[4]. It is well known that the catalyst for NO reduction is structure-sensitive. The PR&C preparation would make an improvement too with the structure-sensitive catalyst.

From the present understanding, the plasma-enhanced acidity plays a very important role in the plasma-enhanced dispersion and stability, which makes the catalyst prepared via PR&C method exhibit better low-temperature activity and better thermal stability.

Conclusions

The principal procedure of the catalyst preparation using PR&C method can be summarized: 1) impregnation conventionally; 2) drying or no drying; 3) plasma treatment; and 4) calcination thermally. The PR&C preparation will normally induce a significantly plasma-enhanced acidity and dispersion, which further leads to a low-temperature catalytic activity. A remarkable improved in the stability of catalysts has also obtained with the PR&C catalyst preparation. This improved stability is achieved principally thanks to the plasma-enhanced acidity and the improvement in the interaction between metal species and the support. Further improvement in the PR&C preparation is leading to a development of a novel and practical catalyst preparation technology.

Acknowledgement. This work was supported partly by the National Natural Science Foundation (under the contract #20225618), by the Sino-PEC (under the contract #X501031), by Natural Science Foundation of Tianjin City (under the contract #023606311), by Major Foundation of Ministry of Education of China (under the contract #Major 0212) and by ABB Switzerland Ltd.

References

- (1) Wang, J.G.; Liu, C.-J.; Zhang, Y.P.; Zhu, X.L.; Zou, J.J.; Yu, K.L.; Eliasson, B. *Chem. Lett.* **2002**, 1068.
- (2) Liu, C.-J.; Yu, K.L.; Zhu, X.L.; Zhang, Y.P.; He, F.; Eliasson, B. Characterization of Plasma Treated Pd/HZSM-5 Catalyst for Methane Combustion, *Appl. Catal. B.* (in press).
- (3) Liu, C.-J.; Yu, K.L.; Zhang, Y.P.; Zhu, X.L.; He F.; Eliasson, B. *Catal. Commu.*, **2003**, 4, 303.
- (4) Zhang, Y.P.; Ma, P.S.; Zhu, X.L.; Liu, C.-J.; Shen, Y.T. A Novel Plasma-treated Pt/NaZSM-5 Catalyst for NO reduction by methane, *Catal. Commu.* (in press).
- (5) Wang, J.G.; Liu, C.-J.; Zhang, Y.P.; Yu, K.L.; Zhu, X.L.; He, F. Partial Oxidation of Methane to Syngas over Glow Discharge Plasma Treated Ni-Fe/Al₂O₃ Catalyst, *Catal. Today* (in press).
- (6) Liu, C.-J.; Cheng, D.G. In: *Proc. of the 7th International Conference on Carbon Dioxide Utilization*; Lee, K.W.; Park, S.E., Eds.; Seoul, Korea, Oct. 2003, p.103.
- (7) Han, S.; Yu, K.L.; He, F.; Liu, C.-J. *J. of Chem. Ind. and Eng. (China)*, **2003**, 54, 702.
- (8) Yu, K.L.; Liu, C.-J.; Zhang, Y.P.; He, F.; Zhu, X.L.; Eliasson, B. The Preparation and Characterization of Highly Dispersed PdO over Alumina for Low-temperature Combustion of Methane, *Plasma Chem. Plasma Processing* (accepted)

PLASMACHEMICAL SYNTHESIS AND REGENERATION (ACTIVATION) OF NANOSTRUCTURED CATALYSTS FOR METHANE STEAM CONVERSION

Gheorghy P. Vissokov

Institute of Electronics, Bulgarian Academy of Sciences, 72,
Tsarigradsko Chaussee Bulvd., 1784 Sofia, Bulgaria

There are 2D models of axially symmetric plasma-chemical reactors (PCR) for motion, heating, melting and evaporation (thermal destruction) of micron-sized particles (Ni, NiO, Al, Al₂O₃, CaO, Mg and MgO) developed. By means of these models, profiles of plasma (gas) density; temperature and rate in the plasma generator (plasmatron) in a PCR with "cold" ($T_w = 500$ K) and "warm" ($T_w = 1500$ K) walls are established, as well as the particle diameter changes along the length of the PCR; trajectory of the particles in the PCR, etc. A system of equations that describes the gas motion; equations for particle temperatures depending on the gas temperature; and equations for particle motion are used to model the hydrodynamic and heat-exchange processes in an axially symmetric PCR.

A universal programme is used and the equilibrium parameters of the multicomponent heterogeneous Ni-Al-O-Ca-Mg system are defined at for different initial ingredient compositions at a pressure of 0.1 MPa within the temperature range 1000 - 3700 K, as dependencies of the respective compound concentration in gas or condensed phase at an equilibrium system composition on the temperature are built. We set out to develop a three-dimensional model for the motion, heating, melting and vaporization (thermal destruction) of micron-size particles (Ni, NiO, Al, Al₂O₃, CaO, Mg and MgO) in an axisymmetric plasmachemical reactor (PCR), to determine the equilibrium parameters of the multicomponent heterogeneous Ni-Al-O-Ca-Mg system for the plasma-temperature range, and to carry out experimental studies concerning the plasma-chemical synthesis (PCS) of a catalyst for CH₄ steam conversion.

Considering the results of the model and thermodynamic calculations, we designed and built equipment for PCS and/or regeneration of spent catalyst for CH₄ steam conversion. Under the conditions of an electric-arc low-temperature plasma (LTP), we studied the Ni-O-Al system and performed a comprehensive physicochemical analysis of the ultradispersed product obtained.

It's the first time world-wide when the conditions of plasma-chemical synthesis and/or regeneration of CH₄ steam conversion catalysts under the conditions of electric-arc LTP are investigated, as depending on the plasma-chemical process (PCP) parameters and the plasma-chemical reactor (PCR) type (with CW- "cold walls" $T_w = 500$ K or WW - "warm walls" $T_w = 1500$ K), samples with a specific surface of to 120 m²/g are obtained.

Plasma-chemically synthesised and/or regenerated samples have a homogenous chemical composition similar to that Girdler (USA) the conventional industrial catalyst. It is empirically established that the optimal temperature range in PCR for synthesis of maximum dispersity samples is 2000 - 3000 K. Results from investigation on plasma-chemically synthesised and/or regenerated CH₄ steam conversion catalysts dynamics and kinetics show that under LTP conditions premises for catalyst compositions formation are established. They are reduced 3 to 4 times faster than their industrial analogues.

The heightened catalytic activity of the plasma-chemically synthesised and/or regenerated natural gas reforming catalysts is determined by a whole complex of specific sample properties as follows: defective/faulty crystal structure of catalytically active phases with a lowered crystal lattice parameter; even distribution of the promoting ultra-dispersed components; high porosity, specific surface and dispersity; and appropriate chemical composition of the samples.

High specific surface of the samples, homogenous composition, high rate of active chemical surface forming by reduction, faulty crystal lattice of catalytically active phases and mostly high catalytic activity make them a potential competitor of their industrial analogues upon their probable production in catalyst shops.